

**HASAN KALYONCU UNIVERSITY  
GRADUATE SCHOOL OF  
NATURAL & APPLIED SCIENCES**

**SEISMIC ANALYSIS AND STRENGTHENING OF CYLINDRICAL  
STEEL STORAGE WATER TANKS**

**Ph.D. THESIS  
IN  
CIVIL ENGINEERING**

**BY  
ALİ İHSAN ÇELİK  
AUGUST 2018**

**Seismic Analysis and Strengthening of Cylindrical Steel Storage Water  
Tanks**

**Ph.D. Thesis  
In  
Civil Engineering  
Hasan Kalyoncu University**


**Supervisor**

**Prof.Dr. Ahmet Celal APAY**

**by**

**Ali İhsan ÇELİK**

**AUGUST 2018**



©2018 [Ali İhsan ÇELİK]



**GRADUATE SCHOOL OF NATURAL &  
APPLIED SCIENCES INSTITUTE  
PhD ACCEPTANCE AND APPROVAL FORM**

Civil Engineering Department, Civil Engineering PhD (Philosophy of Doctorate) programme student **Ali İhsan ÇELİK** prepared and submitted the thesis titled “**Seismic Analysis and Strengthening of Cylindrical Steel Storage Water Tanks**” defened successfully at the VIVA on the date of 16/08/2018 and accepted by the jury as a PhD thesis.

<u>Position</u>	<u>Title, Name and Surname</u> <u>Department/University</u>	<u>Signature</u>
<b>PhD Supervisor</b> <b>Chair of the PhD</b> <b>VIVA Board</b>	Prof. Dr. Ahmet Celal APAY Civil Engineering Department/Sakarya University	
<b>Jury Member</b>	Assoc. Prof. Dr. Abdülcelil BUĞUTEKİN Mechanical Engineering Department/ Adiyaman University	
<b>Jury Member</b>	Assist. Prof. Dr. Tahir AKGÜL Civil Engineering Department/Sakarya University	
<b>Jury Member</b>	Assist. Prof. Dr. Hatip TOK Civil Engineering Department/ K.Maras Sutcu Imam University	
<b>Jury Member</b>	Assist. Prof. Dr. Adem YURTSEVER Civil Engineering Department/Hasan Kalyoncu University	

**This thesis is accepted by the jury members selected by the institute management board and approved by the institute management board.**

**Prof. Dr. Mehmet KARPUCU**  
Director



**I declare that the related thesis is written properly according to academic and ethical rules and using all literature information referenced in the related thesis.**

**Ali İhsan ÇELİK**



## **ABSTRACT**

### **SEISMIC ANALYSIS AND STRENGTHENING OF CYLINDRICAL STEEL STORAGE WATER TANKS**

**ÇELİK, Ali İhsan**

**Ph. D. In Civil Engineering**

**Supervisor: Prof. Dr. Ahmet Celal APAY**

**Date:16.08.2018, 179 pages**

Cylindrical steel storage tanks are widely used for the storage of various liquids, industrial chemicals and firefighting waters. Liquid-storage tanks have many different configurations; however, in this study, cylindrical ground-supported liquid steel tanks are preferred due to their simplicity in design and construction as well as their efficiency in resisting hydrostatic and hydrodynamic applied loads, when compared with other configurations. This thesis focuses on the seismic design ground supported cylindrical (vertical) steel liquid storage tanks. Dimensions of cylindrical open-top, flat-closed, conical-closed and torispherical-closed-top tanks were determined for 3D-finite element method (FEM) models in an ANSYS Workbench software. The seismic analyses were conducted under the El-Centro and Kobe earthquake loads at different shell thickness and roof types of cylindrical steel tanks. Directional deformation, Equivalent stress, and buckling results presented for both impulsive and convective masses respectively.

The results show that the directional deformation tanks is seriously reduced in conical and torispherical closed. On the other hand, it is observed that there is no advantage of flat-closing tanks. When shell thickness is increased, it is observed that directional deformation does not decrease in flat-closed tanks and that directional deformation and buckling occur on the flatly roof.

One purpose of this thesis is to strengthen of the cylindrical steel liquid tanks. The tanks were covered with epoxy-carbon composite material. In this study, the directional deformation was observed to reduce in the epoxy-carbon wrapped tanks using the finite element method. Suggestions have been made to strengthen epoxy-carbon tanks, emphasizing that a 4 mm thickness tank may have better performance than an unprotected 6mm thickness tank.

Finally, El-Centro earthquake recording was used as a displacement value for 0.22 seconds in order to be able to see the plastic deformations that took place in the tank walls with the effect analysis carried out under short earthquake load. As a result of this analysis, results similar to those of buckling that occurred in the earthquakes were revealed.

**Keywords:** Cylindrical Storage Tank, Seismic Analysis, Dynamic Analysis, Strengthening

## ÖZET

### SİLİNDİRİK ÇELİK SU DEPOLAMA TANKLARININ SİSMİK ANALİZİ VE GÜÇLENDİRİLMESİ

ÇELİK, Ali İhsan

Doktora Tezi, İnşaat Mühendisliği Bölümü

Danışman: Prof. Dr. Ahmet Celal APAY

Tarih:16.08.2018, 179 sayfa

Silindirik çelik sıvı tankları su, petrol ve endüstriyel kimyasallar gibi çeşitli sıvıları depolamak amacıyla yaygın olarak kullanılmaktadırlar. Sıvı depolama tankları birçok farklı konfigürasyona sahiptirler; ancak bu çalışmada, tasarım ve konstrüksiyondaki sadelikleri ve diğer konfigürasyonlarla karşılaştırıldığında hidrostatik ve hidrodinamik yüklere karşı dayanımlarından dolayı, yerden destekli silindirik sıvı çelik tanklar tercih edilmektedir. Bu tez, yerden destekli silindirik (dikey) çelik su depolama tanklarının sismik tasarımına odaklanmaktadır. Üç boyutlu sonlu elemanlar analizi için, ANSYS Workbench yazılımı ile üstü-açık, düz-kapalı, konik-kapalı ve üstü-kubbe şeklinde kapatılmış tank modelleri tasarlanmıştır. Sismik analiz, El-Centro ve Kobe deprem yükleri altında dört farklı kapak şekline sahip, üç farklı duvar kalınlığındaki tanklar ile gerçekleştirilerek, aksenal deformasyon, eşdeğer gerilme ve burkulma sonuçları sırasıyla hem impulsif hem de konvektif kütleler için sunulmuştur.

Sonuçlar, aksenal deformasyonun, konik ve kubbeli tanklarda ciddi şekilde azaldığını göstermektedir. Öte yandan, düz kapatılmış tankların hiçbir avantajının olmadığı görülmüştür. Duvar kalınlığı artırıldığında, düz kapalı tanklarda aksenal deformasyonun azalmadığı ve düz çatı üzerinde bu deformasyon ve burkulmanın meydana geldiği gözlemlenmiştir.

Bu tezin önemli amaçlarından biri de, silindirik çelik sıvı depolama tanklarının güçlendirilmesidir. Gerilmeleri ve burkulmaları azaltmak için tanklara epoksi-karbon sarılmıştır. Sonlu elemanlar metodu kullanılarak epoksi-karbon ile sarılmış tanklarda aksenal deformasyonun azaldığı görülmüştür. 4 mm kalınlığındaki bir tankın 6 mm kalınlığındaki korunmamış bir tanktan daha iyi bir performansa sahip olabileceği vurgulanarak, epoksi-karbon tankların güçlendirilmesi için öneriler getirilmiştir.

Son olarak, kısa deprem yükü altında gerçekleştirilen etki analizi ile, tank duvarlarında meydana gelen plastik deformasyonları görebilmek için 0,22 saniyelik El-Centro deprem kaydı, deplasman kaydı olarak kullanılmıştır. Bu analiz sonucunda depremlerde meydana gelmiş burkulma şekillerine benzer sonuçlar ortaya çıkarılmıştır.

**Anahtar Kelimeler:** Silindirik Depolama Tankları, Sismik Analiz, Dinamik Analiz, Güçlendirme

## **ACKNOWLEDGEMENT**

I would like to express my deepest respect and most sincere gratitude to my supervisor, Prof. Dr. Ahmet Celal APAY, for his guidance and encouragement at all stages of my work. His constructive criticism and comments from the initial conception to the end of this work is highly appreciated.

I would special thanks to Rector of Hasan Kalyoncu University, Prof.Dr. Tamer YILMAZ and Manager of Graduate School of Natural & Applied Sciences Prof.Dr. Mehmet KARPUZCU for their supports during my academic studies.

I also wish many thanks to Prof.Dr. M.Metin KÖSE for his interprets about the results of ANSYS workbench.

I would also thank to Assist. Prof. Dr. Tahir AKGÜL and Assist. Prof. Dr. Adem YURTSEVER for their support during the writing my thesis.

I am also very thankful to my Wife for her great helps and motivations during my academic education life.

## LIST OF CONTENTS

<b>ABSTRACT</b> .....	<b>VI</b>
<b>ÖZET</b> .....	<b>VII</b>
<b>CONTENTS</b> .....	<b>IX</b>
<b>LIST OF FIGURES</b> .....	<b>XII</b>
<b>LIST OF TABLES</b> .....	<b>XI</b>
<b>LIST OF SYMBOLS</b> .....	<b>XVI</b>
Abbreviations.....	XVI
Scalars.....	XVI
<b>CHAPTER I</b> .....	<b>1</b>
<b>INTRODUCTION</b> .....	<b>1</b>
1.1 Introduction.....	1
1.2 Background of Steel Storage Water Tanks .....	1
1.3 Fem Seismic Analysis.....	4
1.4 The Reason for Seismic Analysis of Cylindrical Storage Tanks .....	4
1.5 Organization of Thesis .....	6
<b>CHAPTER 2</b> .....	<b>9</b>
<b>LITERATURE REVIEW</b> .....	<b>9</b>
2.1 Introduction.....	9
2.2 Damage of CST.....	9
2.3 Previous Study of Cylindrical Water Tanks.....	13
2.3.1 Vibration characteristic of cylindrical water tanks .....	17
2.3.2 Previous investigations on fluid-structure interaction .....	20
2.3.3. Previous investigations on design code .....	24
2.3.4. Analytical and numerical approaches .....	25
<b>CHAPTER 3</b> .....	<b>29</b>
<b>THEORY OF CYLINDRICAL WATER TANK</b> .....	<b>29</b>
3.1 Introduction.....	29
3.2 Theory of Hydrodynamic Fluid .....	29
3.2.1 Lamina fluid method (Housner’s method).....	29
3.2.2 Mechanical model of liquid storage tank.....	30
3.2.3 Hydrostatic and hydrodynamic pressure.....	31
3.2.4 Impulsive pressure components .....	34
3.2.5 Convective pressure components.....	41
3.3 API 650 Guidelines for Cylindrical Steel Tank .....	41
3.3.1 Chose seismic use group .....	42
3.3.2 Vibration structural period .....	42
3.3.3 Impulsive period .....	42
3.3.4 Convective period .....	43
3.3.5 Design spectral response acceleration.....	44
3.3.6. Factors of seismic design .....	45
3.3.6.1. Design forces .....	45
3.3.6.2 Modification factor of response .....	45
3.3.6.3 Importance factor .....	46
3.4 Loads Design .....	46
3.5. Overturning Moment at the Base of Tank .....	47
3.6 Sloshing Effect in the Roof.....	48
3.7 Summary .....	53
<b>CHAPTER 4</b> .....	<b>55</b>
<b>FINITE ELEMENT MODELLING</b> .....	<b>55</b>

4.2 M dof Dynamic System .....	56
4.3 Coupling of Fluid-Structure .....	59
4.4 Derivation of Hydrodynamic Fluid Matrices .....	60
4.5 Fluid Damping .....	65
4.6 Finite Element Modelling .....	67
4.6.1 Finite element geometries .....	69
4.6.2 Fluid Hydrodynamic Bearing .....	71
4.7 Summary .....	72
<b>CHAPTER 5.....</b>	<b>74</b>
<b>SEISMIC ANALYSIS OF CYLINDRICAL STEEL STORAGE WATER TANKS .....</b>	<b>74</b>
5.1 Introduction .....	74
5.2 Seismic Analysis with API 650 .....	75
5.2.1 Impulsive naturel period .....	78
5.2.2 Convective (sloshing) period .....	80
5.2.3 Spectral acceleration and design loads .....	81
5.3 Seismic Analysis with Finite Element Method.....	87
5.3.1 Modal analysis .....	87
5.3.1.1 Verification of model .....	89
5.3.1.2 Modal analysis of open tank model .....	90
5.3.1.3 Modal analysis of flat, conical and torispherical closed top tanks model ...	95
5.4 Analysis of Response Spectrum.....	105
5.5 Time History Analysis .....	108
5.5.1 Directional deformation under El-Centro earthquake.....	108
5.5.2 Impulsive directional deformation under Kobe earthquake.....	117
5.5.3 Convective directional deformation under Kobe earthquake .....	119
5.6 Summary .....	122
<b>CHAPTER 6.....</b>	<b>124</b>
<b>BUCKLING ANALYSIS AND STRENGTHENING OF CYLINDRICAL STEEL TANK</b>	<b>124</b>
6.1 Introduction.....	124
6.2 Buckling Analysis of Cylindrical Steel Tanks .....	124
6.2.1 Equivalent stress and buckling analysis under the El-Centro earthquake ....	125
6.2.2 Buckling analysis under the Kobe earthquake .....	129
6.3 Strengthening of Cylindrical Steel Tanks .....	132
6.3.1 Strengthening of cylindrical steel tank .....	132
6.3.2 Result of strengthening tanks .....	139
6.4 Summary .....	146
<b>CHAPTER 7.....</b>	<b>148</b>
<b>IMPACT ANALYSIS OF CYLINDRICAL STEEL WATER TANK.....</b>	<b>148</b>
7.1 Introduction.....	148
7.2 EXPLICIT DYNAMICS ANALYSIS .....	148
7.2.1 References of Eulerian (virtual) body .....	149
7.2.2 Explicit fluid-structure interaction .....	150
7.3 Setting up Procedure 3d Explicit Dynamic Analysis .....	152
7.4 Performed Explicit Dynamic Analysis and Evaluation of Directional Deformation .....	156
7.4.1.1 Buckling analysis at different thicknesses .....	161
7.5 Summary .....	164
<b>CHAPTER 8.....</b>	<b>166</b>
<b>DISCUSSION AND CONCLUSION .....</b>	<b>166</b>
8.1 Introduction.....	166
8.2 Discussion and Conclusion .....	166
<b>REFERENCES.....</b>	<b>171</b>

## LIST OF TABLES

<b>Table 3. 1</b> Details of the simplified methods developed for the seismic analysis of anchored cylindrical tanks subjected to uniaxial loading .....	38
<b>Table 3. 2</b> Equations for impulsive time period given in tank seismic design codes .....	39
<b>Table 3. 3</b> Response modification factors (API650, 2013) .....	45
<b>Table 3. 4</b> Display importance factor (I) and SUG (seismic use group) (API650, 2013) .....	46
<b>Table 5. 1</b> Dimensions and properties of tanks .....	76
<b>Table 5. 2</b> Recommended design value for the first impulsive and convective modes of vibration as function of liquid-height to tank radius $H/r$ for vertical circular tanks .....	80
<b>Table 5. 3</b> Display response modification factors for ASD methods (API650, 2013) .....	83
<b>Table 5. 4</b> Display importance factor (I) and seismic use group (API650, 2013) .....	84
<b>Table 5. 5</b> Permissible plate materials and allowable stresses (API650, 2013) .....	86
<b>Table 5. 6</b> Results calculated of cylindrical model tank according the API 650 formulation .....	86
<b>Table 5. 7</b> Shell thickness according the API 650 standard (API650, 2013) .....	88
<b>Table 5. 8</b> Modal analysis results of circular steel water tank .....	94

## LIST OF FIGURES

<b>Figure 2.1</b> Elephant foot buckling (Anumod, et al., 2014) .....	10
<b>Figure 2.2</b> Diamond shape buckles (Mohsen and Ali, 2015).....	10
<b>Figure 2.3</b> Damage to the roof of tanks (Mohsen and Ali, 2015) .....	11
<b>Figure 2.4</b> Damage to the anchor bolts and the foundation system (Mohsen and Ali, 2015) .....	11
<b>Figure 2.5</b> Sliding and uplifting of tanks (Mohsen and Ali, 2015) .....	12
<b>Figure 2.6</b> Simulation of all failure modes (Bakalis, et al., 2017) .....	13
<b>Figure 3.1</b> Haroun's spring mass model .....	30
<b>Figure 3.2</b> Mechanical analogue model for cylindrical liquid storage tanks (Malhotra, 1997) .....	31
<b>Figure 3.3</b> Hydrostatic pressure (Sudhir and Kanpur, 2006) .....	31
<b>Figure 3.4</b> Hydrodynamic pressure (Sudhir and Kanpur, 2006) .....	32
<b>Figure 3.5</b> Circular tanks plan viewer (Sudhir and Kanpur, 2006) .....	32
<b>Figure 3.6</b> Represents impulsive and convective liquid.....	33
<b>Figure 3.7</b> Hydrostatic and hydrodynamic pressure on base (Sudhir and Kanpur, 2006) .....	33
<b>Figure 3.8</b> Impulsive base motion (Sudhir and Kanpur, 2006).....	34
<b>Figure 3.9</b> Frequency parameter (Haroun, 1983) .....	35
<b>Figure 3.10</b> Impulsive mass ratios figure (Haroun, 1983) .....	35
<b>Figure 3.11</b> Elevation of impulsive mass ratios (Haroun, 1983) .....	36
<b>Figure 3.12</b> Rigid mass ratios (Haroun, 1983).....	36
<b>Figure 3.13</b> Ratio of the elevation of rigid mass (Haroun, 1983) .....	37
<b>Figure 3.14</b> Convective mass (ms) and elevation (Hs) .....	41
<b>Figure 3.15</b> Coefficient (API 650, 2013) .....	43
<b>Figure 3.16</b> Convective factor, Ks (API650, 2013) .....	44
<b>Figure 3.17</b> Design response spectra (API650, 2013).....	45
<b>Figure 3.18</b> Effective weight of liquid ratio .....	47
<b>Figure 3.19</b> Occurred of overturning moment .....	48
<b>Figure 3.20</b> Sloshing configuration of fixed roof (Nakashima, 2010).....	49
<b>Figure 3.21</b> Impulsive and hydrodynamic pressure (Nakashima, 2010) .....	49
<b>Figure 3.22</b> Sloshing at cone roof with 25 deg slope (Yoshio and Nobuyuki, 1977)..	50
<b>Figure 3.23</b> Sloshing at flat roof (Yoshio and Nobuyuki, 1977) .....	50
<b>Figure 3.24</b> Pressure shape of half-triangle pulse (Yoshio and Nobuyuki, 1977) .....	52
<b>Figure 4.1</b> (a) Classic MDOF system; (b) Free-body diagrams (Moslemi, 2005) .....	56
<b>Figure 4.2</b> Open top tank model a) Empty model b) Filled water model .....	68
<b>Figure 4.3</b> Torispherical-closed tank model.....	68
<b>Figure 4.4</b> Half cross section geometry of tank .....	69
<b>Figure 4.5</b> Geometry of shell element.....	70
<b>Figure 4.6</b> 3D 20-node solid element .....	70



<b>Figure 5. 1</b> Spring mass model of tank & hydrodynamic pressure distribution (Sudhir and Kanpur, 2006).....	75
<b>Figure 5. 2</b> Impulsive mass ratios (Haroun, 1983).....	77
<b>Figure 5. 3</b> Coefficient $C_i$ (API650, 2013).....	79
<b>Figure 5. 4</b> Sloshing factor, $K_s$ (API-650) .....	80
<b>Figure 5. 5</b> Seismic diagram of tank (Kuan, 2009) .....	81
<b>Figure 5. 6</b> Classes of cylindrical steel tank.....	88
<b>Figure 5. 7</b> Dimensions of tanks.....	89
<b>Figure 5. 8</b> Meshed view of all tanks .....	89
<b>Figure 5. 9</b> Impulsive modal analysis results and frequencies.....	91
<b>Figure 5. 10</b> Simulation and application of mass model.....	91
<b>Figure 5. 11</b> Distribution point mass and sloshing effect.....	92
<b>Figure 5. 12</b> Convective modal analysis results and frequencies.....	93
<b>Figure 5. 13</b> Impulsive and convective tank shapes.....	95
<b>Figure 5. 14</b> Impulsive modal analysis results and frequencies of flat-closed tank.....	96
<b>Figure 5. 15</b> Impulsive modal analysis results and frequencies of conical-closed tank.....	98
<b>Figure 5. 16</b> Impulsive modal analysis results and frequencies of torispherical-closed tank.....	99
<b>Figure 5. 17</b> Convective modal analysis results and frequencies for flat-closed tank.....	101
<b>Figure 5. 18</b> Convective modal analysis results and frequencies for conical-closed tank.....	102
<b>Figure 5. 19</b> Convective modal analysis results and frequencies for torispherical-closed tank.....	104
<b>Figure 5. 20</b> Impulsive modal analysis results and frequencies.....	104
<b>Figure 5. 21</b> Convective modal analysis results and frequencies.....	105
<b>Figure 5. 22</b> Impulsive response spectrum analysis of el-Centro earthquake.....	106
<b>Figure 5. 23</b> Impulsive response spectrum analysis of Kobe earthquake .....	107
<b>Figure 5. 24</b> Convective response spectrum analysis of el-Centro earthquake.....	107
<b>Figure 5. 25</b> Convective response spectrum analysis of El-Centro earthquake.....	108
<b>Figure 5. 26</b> Impulsive directional deformation for $t=4$ mm .....	109
<b>Figure 5. 27</b> Impulsive directional deformation graph of all tanks $t=4$ mm .....	110
<b>Figure 5. 28</b> Impulsive directional deformation for $t=6$ mm .....	111
<b>Figure 5. 29</b> Impulsive directional deformation $t=6$ mm .....	111
<b>Figure 5. 30</b> Impulsive directional deformation for $t=8$ mm .....	112
<b>Figure 5. 31</b> Impulsive directional deformation graph of all tanks $t=8$ mm .....	113
<b>Figure 5. 32</b> Convective directional deformation graph of all tanks $t=4$ mm .....	113
<b>Figure 5. 33</b> Convective directional deformation graph of all tanks $t=6$ mm .....	114
<b>Figure 5. 34</b> Convective directional deformation graph of all tanks $t=8$ mm .....	115
<b>Figure 5. 35</b> Impulsive directional deformation for all parameters.....	116
<b>Figure 5. 36</b> Convective directional deformation for all parameters .....	116
<b>Figure 5. 37</b> Impulsive directional deformation graph of all tanks $t=6$ mm .....	117
<b>Figure 5. 38</b> Impulsive directional deformation graph $t=6$ mm .....	118
<b>Figure 5. 39</b> Impulsive directional deformation graph of all tanks $t=4$ mm .....	118
<b>Figure 5. 40</b> Impulsive directional deformation graph $t=8$ mm .....	119

<b>Figure 5. 41</b>	Convective directional deformation t=6 mm .....	120
<b>Figure 5. 42</b>	Impulsive directional deformation for all parameters.....	121
<b>Figure 5. 43</b>	Convective directional deformations for all parameters.....	121
<b>Figure 6. 1</b>	Equivalent (von –Misses) stress distribution on the tanks.....	125
<b>Figure 6. 2</b>	Comparison of equivalent stress for 6 mm thickness .....	126
<b>Figure 6. 3</b>	Comparison of equivalent stress under the el-Centro earthquake loads t=4 mm. ....	126
<b>Figure 6. 4</b>	Buckling of roof.....	127
<b>Figure 6. 5</b>	Comparison of equivalent stress under the el-Centro earthquake loads t=8 mm .....	127
<b>Figure 6. 6</b>	Stress distribution and buckling of flat-closed tank .....	128
<b>Figure 6. 7</b>	Convective stress distribution and buckling of all tanks .....	128
<b>Figure 6. 8</b>	Buckling of flat-closed tank t=4 and 8 mm .....	129
<b>Figure 6. 9</b>	Buckling of conical tank t=4 and 8 mm.....	130
<b>Figure 6. 10</b>	Buckling of torispherical tank t=4 and 8 mm .....	130
<b>Figure 6. 11</b>	Convective buckling of flat tank for t=4 and 8 mm.....	131
<b>Figure 6. 12</b>	Convective buckling of conical-closed tank t=4 and 8 mm .....	131
<b>Figure 6. 13</b>	Convective buckling of torispherical-closed tank t=4 and 8 mm .....	132
<b>Figure 6. 14</b>	Stress-strain graph of some composite materials (Daniel and Ishai, 1994) .....	133
<b>Figure 6. 15</b>	Composition of composites materials (Douglasb and Lysle, 2009) .....	133
<b>Figure 6. 16</b>	Application of epoxy carbon area (CNG, 2018).....	134
<b>Figure 6. 17</b>	Ductility tests on specimens reinforced with carbon fiber sheets (Wakui, 2009) .....	134
<b>Figure 6. 18</b>	Relationship ACP and transient structural.....	135
<b>Figure 6. 19</b>	Fabrics and tapes.....	136
<b>Figure 6. 20</b>	Application of epoxy carbon material (Gemite, 2013).....	137
<b>Figure 6. 21</b>	Strengthening technique with TPP (Prasad and Prasad, 2017).....	137
<b>Figure 6. 22</b>	Application of fibbers on the cylindrical tank .....	138
<b>Figure 6. 23</b>	Defining angle of epoxy carbon fibers in ACP.....	138
<b>Figure 6. 24</b>	Strengthening of open-top tank.....	139
<b>Figure 6. 25</b>	Comparison of equivalent stress .....	140
<b>Figure 6. 26</b>	Directional deformation graphs of open-top tank t=4mm .....	140
<b>Figure 6. 27</b>	Straitening of flat-closed tank.....	141
<b>Figure 6. 28</b>	Comparison of equivalent stress of flat-closed tank.....	141
<b>Figure 6. 29</b>	Directional deformation of flat-closed tank.....	142
<b>Figure 6. 30</b>	Strengthening of conical-closed tank.....	143
<b>Figure 6. 31</b>	Comparison of equivalent stress of conical-closed tank.....	143
<b>Figure 6. 32</b>	Directional deformation of conical-closed tank.....	144
<b>Figure 6. 33</b>	Strengthening of torispherical-closed tank .....	145
<b>Figure 6. 34</b>	Comparison of equivalent stress for torispherical-closed tank .....	145
<b>Figure 6. 35</b>	Comparison of directional deformation of torispherical-closed tank .....	146

<b>Figure 7. 1</b> Eulerian reference frame (SASIP, 2018) .....	150
<b>Figure 7. 2</b> Eulerian reference frame (SASIP, 2018) .....	151
<b>Figure 7. 3</b> Normal stress in the intersected Euler cell (SASIP, 2018) .....	151
<b>Figure 7. 4</b> Interaction of bodies .....	152
<b>Figure 7. 5</b> Established explicit dynamic analysis .....	152
<b>Figure 7. 6</b> Definition of material properties .....	153
<b>Figure 7. 7</b> Specify materials.....	154
<b>Figure 7. 8</b> Define Eulerian bodies only .....	155
<b>Figure 7. 9</b> Mesh models of tanks .....	155
<b>Figure 7. 10</b> Define eulerian bodies only .....	156
<b>Figure 7. 11</b> Directional deformation of open-top tank .....	157
<b>Figure 7. 12</b> Directional deformation of flat-closed tank.....	157
<b>Figure 7. 13</b> Directional deformation of conical-closed tank.....	158
<b>Figure 7. 14</b> Directional deformation of torispherical-closed tank.....	158
<b>Figure 7. 15</b> Directional deformation graphs t=6 mm.....	159
<b>Figure 7. 16</b> Buckling of shell tank.....	159
<b>Figure 7. 17</b> Cracks in the shell of tanks .....	160
<b>Figure 7. 18</b> Buckling of shell tanks .....	161
<b>Figure 7. 19</b> Directional deformation of different tanks t=8 mm.....	162
<b>Figure 7. 20</b> Directional deformation graphs t=8 mm.....	162
<b>Figure 7. 21</b> Occurred of elephant foot buckling .....	163
<b>Figure 7. 22</b> Directional deformation of different tanks t=4 mm.....	164

## LIST OF SYMBOLS

### Abbreviations

CST	Cylindrical Steel Tank
API	The American Petroleum Institute
FEM	Finite Element Method
DOF	Degree Of Freedom
NZSEE	New Zealand National Society for Earthquake Engineering
SUG	Seismic Use Group
I	Importance factor defined by Seismic Use Group
ASD	Allowable stress design

### Scalars

$C_i$	Seismic response coefficient for impulsive term
$C_c$	Seismic response coefficient for convective term
$d$	Vertical displacement of the liquid free surface(freboard)
$D$	Tank diameter in cylindrical containers
$E$	Elasticity Modulus
$f$	Natural frequency of vibration
$F_D$	Damping force vector
$F_{Dj}$	Damping forces in a typical MDOF system
$F_e$	Fluid pressure load vector at fluid-structure interface
$F_{sj}$	Stiffness forces in a typical MDOF system
$F_v$	Long-period site coefficient (at 1.0 second period)
$F_x$	Base horizontal reaction
$F_z$	Base vertical reaction
$g$	Acceleration due to gravity
$h_c$	Equivalent height of convective mass
$h_i$	Equivalent height of impulsive mass

$H_i$	Equivalent height of the equivalent single degree of freedom oscillator
$H_l$	Liquid height in tank model
$h_m$	Equivalent height of convective mass in simplified mechanical model
$h_r$	Pedestal wall thickness
$h_{\text{shaft}}$	Height of the supporting shaft
$h_{\text{top}}$	Freeboard (distance between the water free surface and the roof)
$H_w$	Height of the tank wall
$h_0$	Equivalent height of impulsive mass in simplified mechanical model
$h_3$	Height of water in the cylindrical portion of the elevated tank
$K$	Bulk modulus
$k_c E$	levated tank lateral stiffness
$p$	Hydrodynamic pressure
$P$	Impulsive force
$P_a$	Power index
$P_c$	Hydrodynamic convective force
$P_i$	Hydrodynamic impulsive force
$p_1$	Impulsive pressure
$p_2$	Convective pressure
$p_3$	Liquid pressure due to the wall deformation relative to the base
$R$	Tank radius in cylindrical containers
$R_c$	Response modification factor corresponding to convective term
$R_i$	Response modification factor corresponding to impulsive term
$t$	Time
$T$	Natural period of vibration
$T_c$	Natural period of convective mode
$T_i$	Natural period of impulsive mode
$t_w$	Thickness of the tank wall
$g$	Ground acceleration
$V_s$	Seismic base shear
$W_e$	Total effective weight of the system
$W_i$	Effective weight of the stored liquid corresponding to impulsive component
$W_r$	Weight of the tank roof
$W_w$	Weight of the tank wall

# CHAPTER I

## INTRODUCTION

### 1.1 Introduction

In this chapter, background of steel storage water tanks in industrial is identified and importance of numerical analysis of the cylindrical steel storage water tanks is observed under seismic ground motions. The main goal and organization of thesis are also outlined in this chapter.

### 1.2 Background of Steel Storage Water Tanks

Liquid storage steel tanks of engineering construction are used to store variety of liquids, industrial chemicals and firefighting water. They have been used for cooling purposes in nuclear power plants in recent years. There are different configurations of storage liquid tanks such as cylindrical steel vertical ground supported, cylindrical steel horizontal ground supported, rectangular steel, rectangular concrete, cylindrical above ground supported types. Cylindrical storage liquid steel tanks are used then other types because of their simplicity design and construction and also they are more resistant under the applied hydrostatics and hydrodynamic loads. Cylindrical storage liquid steel tanks can be constructed of different sizes to fulfill capacity requirements. CST (Cylindrical Steel Tank) has a vital role in cooling system. They have been also used in nuclear power plants in recent years.

Steel liquid tanks can be exposed during earthquakes and also they can cause great financial and environmental damage with their containing petroleum or other hazardous chemical liquid. Earthquake is a natural occurrence that is unpredictable and complex, so steel storage liquid tanks are expected to withstand durability against the earthquake loads. There are open-top, flat-closed, conical-closed and torispherical-closed top models. This thesis focuses on the design ground above cylindrical (vertical) steel storage liquid tanks. El-Centro and Kobe earthquake loads were used for analysis. Shell thickness effect

was investigated on the different roof type of cylindrical tanks, and they also were strengthened with epoxy-carbon composite materials.

Field investigations were carried out by various researchers to determine the type of damage caused by the earthquakes and the factor causing these damages. In the field surveys, it has been revealed that liquid tanks are performing poorly in earthquakes and it has become necessary to develop new methods for increasing earthquake resistance. Because of the simplicity design and low cost, very thin perimeter of walls are used in construction of steel storage water tanks (Bayraktar, et al., 2010). These thin-walled structures are exposed to internal pressures with axial compression resulting from stored liquids, roof loads, horizontal loads such as earthquakes, and friction dragging on the walls of stored materials (Sunitha and Jacob, 2015). There are two important factors impact on the steel tanks deformation after earthquake. These factors are the dynamic characteristics of earthquake force and structure. The steel structure is realized by soil components consisting of two lateral components, a vertical component and three dimensional components with coordinate axes around the structures. Steel storage tanks take several forms under the earthquake loads. The large axial pressure stresses caused by the beamlike bending of the tank wall can cause the "elephant foot" buckling of the wall. Their roof and the top can be damaged due to sloshing liquid (Mohsen and Ali, 2015).

Design of steel storage water tanks guidelines are only few presently available for earthquake resistance. Those guidelines are not accurate in terms of the seismic induced loads on the tank wall which can consequently affect the required section properties of the seismic performance steel structural system. The American Petroleum Institute (API) published standard for above steel storage tanks. API 650 standards have determined minimum requirements for design, fabrication, installation and testing of vertical cylindrical ground-supported open-top and closed-top, welded carbon or stainless steel storage tanks in various sizes and capacities for internal pressures approaching atmospheric pressure (Mark Baker, 2009). Most of the available codes and the API 650 code assume the rigid wall boundary condition when estimating the hydrodynamic forces acting on the tank wall. However, the tank wall elasticity can significantly increase the hydrodynamic pressure compared to the rigid wall assumption. As a result, further investigation is needed on the effect of wall flexibility on the seismic behavior of

cylindrical liquid filled tanks (Moslemi, 2005). In addition to the recommendation of the API-650 standards, ANSYS software has been developed and the influence of interaction fluid structure represents numerical models.

In addition to the recommendation of API-650 design steel storage liquid tanks standards, ANSYS numerical analysis software has been developed interaction fluid-structure effects on the numerical models.

Some scientist suggested like seismic isolation, floating roof to protect damages of earthquake, but these methods are not practical and economical. And also existing cylindrical steel tanks have not been sufficiently protected methods. This study is the most comprehensive study of the effects of four different roof shapes, three different shell thicknesses as well as the epoxy-carbon strengthening to against earthquake of cylindrical steel water tanks.

In this thesis, finite element model (FEM) is used to investigate response seismic ground supported storage water tank. It is preferred cylindrical vertical section such as open top and closed top models for analysis. ANSYS Explicit Dynamic analyses tool which include Euler body mesh provides a good interaction between water and shell. Impact analysis was performed under unexpected instantaneous an earthquake load to see the plastic deformation on the tank. And also tank shell wrap with composite material to decrease deformation. In this study is recommended design criteria for cylindrical steel storage water tanks under seismic ground movement.

The most parameters of this study are shape of the tank, the earthquake loads it is exposed and the properties of material to be used for strengthening. The pressure center can vary depending on the shape of the tank. Furthermore, the dynamic behavior of water tank under the seismic loads can be studied by the detailed seismic analysis using any finite element software package. Instantaneous stresses along the structure are calculated for a short period of time or a significant portion of the earthquake. The maximum stresses that occur during the entire analysis period are found by computer results. The choice of composite material for the reinforcement to the surface of the tank is easy to apply to existing tanks and to protect against damage from earthquakes.



### **1.3 Fem Seismic Analysis**

Finite element method (FEM) is a computational technique used to obtain approximate solutions of boundary value problems in engineering. Boundary value problems are also called field problems. Field variables are interest dependent variables governed by the differential equation. Boundary conditions are the values specified by field variables (or related variables such as derivatives) at field boundaries (Huddon, 2004).

Researchers have used different ways to handle the fluid-structure interaction problems. The fluid may be modeled by a solid structural or acoustic finite element or by using the added mass approach (Akkas et al., 1979 and Virella et al, 2006a). In the FEM, the liquid is modeled using the Eulerian, the Lagrangian or the Eulerian-Lagrangian approaches. On the other hand, in the added mass approach, a liquid mass that is obtained by different techniques is added to the mass of the structure at the liquid-structure interface (Bauer, 1964).

### **1.4 The Reason for Seismic Analysis of Cylindrical Storage Tanks**

Cylindrical steel tanks widely used around the world to storage water, chemical and petroleum liquid materials. They also consist of basic components in several industrial constructions especially in nuclear power plants. Many cylindrical steel liquid storage tanks suffered during the past earthquake due to lack of seismic design. As a results of these suffers, big economics and environmental damages came into being. Cylindrical steel storage tanks have very mixed problems due to the sloshing of the liquid inside under the earthquake loads. Some experimental and theoretical studies were conducted without these complex problems (Sunitha and Jacob, 2015). Many researchers have commonly used Finite Element Method (FEM) to solve numerical analysis. FEM has many advantages in solving complex mechanical problems. FEM displacement representation was used to established open top and closed top tank models by using ANSYS workbench 3D software. Open top tank model initially was used to perform numerical analysis and later the top of the open tank was closed and the same experiments were carried out for its.

The cylindrical steel storage tank and fluid body were modelled with ANSYS Workbench 16.2. The materials used to model the water storage tank are the structural steel and water element. The density of structural steel was  $7850 \text{ kg/m}^3$ , Young Module 210 GPa, and

Poisson Ratio 0.3. Water density of water  $1000 \text{ kg/m}^3$  and bulk module 2.2 GPa were determined. Modal analysis was carried out for all three (T1,T2,T3) tanks with different fluid fill levels. Modal analysis carried out for with different water levels of 10 m, 7.5 m and 5 m. Description of the 3D Finite Element Models, the problem of interaction between the shell and the liquid is modelled using Shell 281, Solid 186, Contact 174, and Target 170 elements.

This thesis focuses on the seismic design ground supported cylindrical (vertical) steel storage liquid tanks. Cylindrical steel water tanks are thin-walled structures. The wall thickness and the tank roof significantly effect on the deformation and buckling in the tanks. Depending on the earthquake ground motion, it is not possible to reduce the deformations and buckles in the tanks only by increasing the shell thickness. In addition, improper design of the tank roof can cause more buckling in increased shell thickness. In order to prevent buckling in the cylindrical steel liquid tanks, it is necessary to examine the relationship between shell thickness and roof shape. The seismic analyses were performed under the El-Centro and Kobe earthquake loads. First time history analysis using of the north-south component of the 1940 El Centro earthquake which had 6,9 magnitudes (magnitude 7.1 on the Richter scale) was performed. Second analysis was carried out under 1995 Kobe earthquake load which was measured 6,9 (7,3 on Reacher scale). While El-Centro has the highest acceleration in the range of 0-5 seconds, Kobe earthquake has acceleration in the range of 5-10 seconds. Directional deformation, Equivalent stress, and buckling results are presented for both impulsive and convective regions respectively.

In order to prevent the tanks from being deformed under destructive earthquake loads, some preventive works such as seismic isolation, floating roof have been made. However, these methods of protection are expensive and cannot be applied to existing tanks. The strengthening operation of cylindrical steel tanks with Epoxy-carbon composite material, which has 230 GB strength, has been carried out by the finite element method.

Explicit Dynamic tool in ANSYS Workbench reveals accurate results in dynamic analysis of structures under instantaneous and short forces. The Explicit Dynamic tool uses Eulerian Body with water to provide interaction between the water and the tank's structure. El-Centro earthquake 0.22 seconds data is used as displacement force for to see the deformation in the tank.

## 1.5 Organization of Thesis

In this study, linear and nonlinear behaviours of cylindrical steel tanks under El-Centro and Kobe earthquake loads are investigated by using finite element method (FEM) which can take into account linear and nonlinear behaviour sources of both liquid and tank. This thesis is most comprehensive with four different roof design and three shell thickness. However, previous studies are about the comparison of large tanks and long tanks, the effects of different thicknesses with only one tank model, protection with seismic isolation, or only buckling analysis. Within the scope of this thesis;

- The effects of liquid and ground interactions on the dynamic behaviour of steel water tanks to examine and how such interactions can be practically taken into account will be present.
- The actual behaviour of the tanks under seismic loads will be examined with computer programs which use the finite element method that can take into account all linear and nonlinear behaviour sources of liquid.
- The behaviour of tanks containing cylindrical steel tank under earthquake ground motions will be examined with using the finite element. In this context, natural vibrational frequencies of liquids of cylindrical tanks will be obtained API 650 standard formulation and compared with finite element results. According to the results obtained, a method for designing these structures will be developed.
- The accurate determination of the roof shape of cylindrical steel liquid tanks, which are becoming more and more popular every day, is of great importance especially for earthquake zones. In this study, it is the most extensive research on the market with four different tank models which are open-top, flat-closed, conical-closed and torispherical-closed.
- The standard shell thickness of the tank to be used in the analyses is 6 mm. This thickness will be reduced by 2 mm (will be determine 4mm) and thickness will be increased 2 mm (will be determine 8 mm) to select the three different thicknesses of 4,6 and 8 mm deformations, stresses, buckles of tank will be observed for each roof types.
- Steel water tanks which will be installed Turkey, its design in calculation principles will be determined that constructed in nuclear power plants to be and it will be aimed to prevent damages that may occur due to seismic ground motion.

This thesis organized in eight chapters.

The following chapter, Chapter 2, denotes the most related works on steel storage water tank. The related literature search describing previous investigations on the numerical simulation of tanks are also summarized in Chapter 2. It is noticed that there are serious gaps in seismic FEM analysis of steel tanks in the literature.

In Chapter 3, the general theory of FEM is presented. General knowledge and use areas of steel storage water tanks are also given in this chapter.

Chapter 4 deals with the finite element formulation of tanks containing three-dimensional liquids. A discussion has been made on how to consider the influence of fluid-structure tank on the finite element model of liquid-containing tanks. In addition, fluid equilibrium equations of motion corresponding to both impulsive and sloshing response components are discussed.

In Chapter 5, the FEM based ANSYS 3D software package was used to attain all numerical calculations and simulation models belong to seismic analysis of steel storage water tanks. Effect of parameters on cylindrical tank design is analysed in detail. Shell thickness effect on the roof types of cylindrical steel storage water tanks are investigated under the El-Centro and Kobe earthquake loading both impulsive and convective component separately.

In chapter 6, buckling analysis is performed of cylindrical steel water tanks which are under the El-Centro and Kobe earthquake seismic loading. There are many types of buckling in cylindrical steel tanks such as elephant foot buckling, diamond shape buckling and cracks on the top side of tanks due to sloshing effect of liquid. It was focused on the buckling in different shell thickness and different roof types of cylindrical steel tanks. On the other hand, strengthening of existing vulnerable cylindrical steel liquid tanks is recommended in this chapter. The tanks are covered with epoxy-carbon material using the Workbench ACP tool to reduce stress and deformation.

Impact analysis was carried out in chapter 7. The Explicit Dynamic tool in ANSYS workbench used Eulerian body with water to provide interaction between the water and the wall. El-Centro earthquake 0.22 seconds data was used as displacement force for to see the deformation on the tank.

Conclusions are given in Chapter 8. Recommendations for future works are also provided at the end of thesis.



## **CHAPTER 2**

### **LITERATURE REVIEW**

#### **2.1 Introduction**

This chapter is focus on the previous studies related with the steel storage tanks. All the literature presented herein is classified according to the working areas on steel storage water tank. Seismic behavior of cylindrical steel tanks and damaged during seismic events is discussed in section 2.2. literature of seismic response liquid storage tank is summarized in section 2.3. Researcher's significant contribution are also explained about the ground supported cylindrical liquid tanks. In section 2.4, design guidelines and existing standard codes of steel liquid storage tanks are reviewed along with a literature search on the application of seismic reinforcement to CST.

#### **2.2 Damage of CST**

There are many reports about the earthquake damage to steel storage tanks. Many researchers reported that those reports, steel liquid storage tanks can be informative as to the performance structure of during earthquakes. Many tanks were damaged during the past earthquake such as Long Beach (1933 ), Kern County(1952 ), Alaska (1964 ), Niigata (1964 ), Parkfield (1966), San Fernando (1971 ), Miyagi province (1978), Imperial County (1979), Coalinga (1983), Northridge(1994 ), Kocaeli(1999), Rinne (1967), Shibata (1974), Kono (1980), Manos and Clough (1985) end Sezen and Whittaker (2006) earthquakes (Moslemi, 2005).

Defect mechanism of steel liquid storage tanks depends on different parameters such as construction material, tank design, tank type, and supporting mechanism. Studies earthquake damage on steel storage tanks show that earthquake damage to tanks can be in various forms. These forms types are listed in the following categories:

1) Elephant-foot buckling in Figure 2.1 wall, because of exerted overturning moment, shell buckling caused by axial compression of the shell structure.



**Figure 2.1** Elephant foot buckling (Anumod, et al., 2014)

In Figure 2.2 Diamond shape buckles (Elastic buckling wall) caused by the compressive pressures made in the tank wall and in the middle part of the high altitude tanks.



**Figure 2.2** Diamond shape buckles (Mohsen and Ali, 2015)

2) Figure 2.3 is shown damage to the roof or the upper shell of the tank, due to sloshing of the upper portion of the contained liquid in tanks with in sufficient free board provided between the liquid free surface and the roof.



**Figure 2.3** Damage to the roof of tanks (Mohsen and Ali, 2015)

3) Spillover of the stored liquid.

4) Failure of piping and other accessories connected to the tank because of the relative movement of the flexible shell.

5) Damage to the anchor bolts and the foundation system are shown in Figure 2.4.



**Figure 2. 4** Damage to the anchor bolts and the foundation system (Mohsen and Ali, 2015)

6) Failure of supporting soil due to over-stressing

Because of excessive sloshing, some damage happened such as mode 3 and 4. In addition that mode 5,7 and 8 became due to liquefaction of the supporting soil, during niigata earthquake (1964). Mode 1 (elephant-foot) happened due to beamlike bending moment of tank wall in the 1964 Alaska and 1971 San Fernando earthquakes.



Many storage petroleum tanks lost after Niigate and Alaska earthquakes. Because of this important loss attracted many researchers to further investigate the seismic performance of liquid storage tanks particularly when the stored liquid is a hazardous material such as petroleum.

Main lifeline facility of Los Angeles area happened several damage during the Northridge Earthquake. Similarly, five steel tanks were damaged in the San Fernando area. All of tanks was suffered due to buckling form. Several other tanks damaged roof collapse because of the excessive sloshing of the stored tanks (Moslemi, 2005).

The base shear may come from above the friction causing the tank to slide. Floor elevation in bases or partially built-in tanks can damage the uninjured pipe connections of vertical displacements, may cause the plate shell connection to break due to excessive joint stresses, and may cause irregular placement of the foundation (Huddon, 2004). In Figure 2.5 tank sliding was shown. As shown in Figure 2.5, when a tank is subjected to a strong ground motion, the overturning moments occurred by hydrodynamic pressures and one side is upward when the weight of the tank can be balanced and prevents it from uplifting during the overturning moment (Mohsen and Ali, 2015).



**Figure 2. 5** Sliding and uplifting of tanks (Mohsen and Ali, 2015)

The importance of preventing such damages has led to a great deal of research to be carried out on dynamic behaviour of such cylindrical steel tank. These studies may be result in a better comprehension of the complicated behaviour of liquid containing structures under seismic movement.

Most of the above mentioned damage cases were simulated by Bakalis et al, in Figure 2.6. According to the Figure, the elephant foot buckling, the base plate failure, the anchor bolt failure are occurred because of the impulsive (rigid) pressure in the base of the tanks, and the buckling at the up side of the tank are caused by the convective (sloshing) effect.

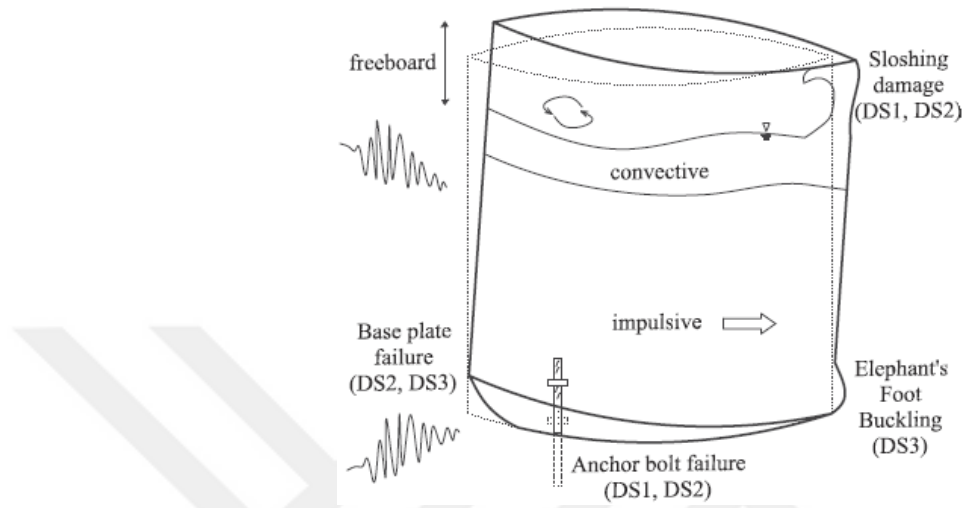


**Figure 2. 6** Simulation of all failure modes (Bakalis, et al., 2017)

### 2.3 Previous Study of Cylindrical Water Tanks

Cylindrical ground supported tanks are one of the most commonly used structure for cooling water and fuel storage. In particularly, dynamic behaviour of ground-supported cylindrical steel tanks crucial important because of application in industrial area and nuclear power plants.

There are comprehensive researches on the dynamic behaviour of steel liquid tanks. Theoretical and experimental studies have been carried out on the steel liquid tanks. Investigates on the dynamic behaviour of liquid containing tanks started in the late 1940's. Brooks T. Morris (1938) investigated consist largely of experiment on the gravity-wave formations in cylindrical tanks (Morris, 1938). The problem with a cylindrical tank containing liquid and a cylindrical scaffold surrounded by liquid is solved by Jacobsen (1949). Jacobsen also studied with Ayre (1951) the dynamic response of a cylindrical liquid tank exposed to horizontal ground motions, They estimated effective hydrodynamic and moments, in Ref (Jacobsen and Ayre, 1951).

Housner (1954,1957 and 1963) developed a simplified procedure for liquid response of rigid cylindrical water tanks anchored to the rigid structure and subjected ground motion. In previous studies, it was assumed that liquid was not to be incompressible and inviscid. With this assumption, attention should be drawn to the effect of wall flexibility. According the Housner, hydrodynamic loading assuming the hydrodynamic response to be divided into two degree of freedom (DOF) system for rigid tank. The first mode DOF accounting for the motion of the tank liquid system, with a part of the liquid being rigidly attached (impulsive mode). The second DOF for the motion of the sloshing liquid (convective mode). Impulsive water undergoes same acceleration as the ground under the seismic motions. This component to have a significant contribution on the overturning moment and base shear. This mechanical model was consisted base of API 650 standard condition for vertical cylindrical tanks (Housner, 1954, 1955 and 1963).

A mechanical model was developed by Housner in which is still widely used with certain modification in seismic design of steel storage tanks. Housner's model generalized by Vozaink and Mitchell for short and slender tanks (Michell R.S. and Wozniak, 1978). The approximate method of Housner is not capable of accounting for the effect of steel tank wall flexibility.

Veletos (1977) determined an approximate method which is based on assumptions that the tank-fluid system and that the fluid is incompressible. The magnitudes and distributions of the hydrodynamic forces, the base shear and overturning moment induced by these forces are evaluated for several different assumed modes of vibration (Veletos and Ahkok, 1977). The interaction between deformable sloshing fluid and tank shell was ignored because of the fact that the convective effects are characterized by oscillations of much longer periods than those characterized by the impulsive effects. Convective effects were evaluated for design applications (Veletos, 1977). Subsequently, Veletos and Yang presented could have important on dynamic loads induced by horizontal ground motion in cylindrical liquid filled tank. They obtained natural frequencies of the liquid tank system using Flugge's shell theory in combination with Rayleigh-Ritz type procedure using naturel frequencies of the liquid shell system. They performed shell and the simpler beam type analyses (Flugge, 1960).

Haroun and Housner (1981a) in Ref. (Moslemi, 2005) studied on a mechanical model that can include deformable wall effects. The three degree of freedom (DOF) is associated

with three equivalent mass models of the convective component which contributes to the slowing of fluid, impulsive and short-time component, which is the contribution of wall vibrations that can be deformed. They have also shown that the possibility of tank wall deformations can cause hydrodynamic pressures several times higher than those experienced in rigid wall tanks. Based on this work, it is derived to estimate the equivalent mass of the design model, the mechanical model. The liquid in the tank is assumed to be incompressible and not inviscid.

The severe damage to petroleum storage tanks during the Alaska earthquake (1964) led many practicing engineers and researchers to future investigate seismic behaviour of cylindrical steel liquid tanks and flexibility of container was significant factor in determining the response of coupled system.

Edwards (1969) for first time proposed the use of a finite element moment to estimate seismic response of deformable fluid cylindrical storage liquid tank. A vertical cylindrical storage tanks with height to diameter ratio smaller than one were analysed using finite element method to predict seismic stress and displacement. This FEM method was capable of accounting for the coupled interaction between elastic tank shell and storage liquid (Edwards, 1969). Shaaban and Nash(1975) performed a similar research of concerned with the seismic response by using finite element method (Shaaban and Nash, 1975).

Hunt and Priestley obtained derivation of mathematical equations regarding the contained fluid motion under dynamic stimulation. Fluid free surface displacement was experimentally measured for cylindrical water tank tested on a shake table and exposed to both sinusoidal and seismic excitations. They compared of predicted theoretical from results valuables with obtained through experimental results (Hunt and Priestley, 1978).

Some researchers coupled the analytic algorithms and the numerical methods in order to find the optimum solution for tank problem in the short time. Haroun and Housner (1981b-1983) developed a mechanical model for analysing the dynamic behaviour of deformable cylindrical steel tanks. They used boundary integral theory to model fluid region and shaped finite element method of tank shell. The study also showed the initial hoop stresses were investigated depending on the hydrostatic pressure of the roof effect of the vibration on the storage tank wall. To investigate the effect of the link between

fluid sloshing modes and shell vibration modes, the liquid free surface is presented by concentric ring rings in the hoop ring measured in direction rings. In order to consider influence of deformable cylindrical tank wall, coupling was constituted between fluid sloshing moods and shell vibration modes is negligible and a spring mass component added to simplified Housner's(1954) mathematical mode (Haroun and Housner, 1981a; Haroun and Housner, 1981b; Haroun, 1983) .

Veletsos and Kumar (1977) developed a simplified approach to estimate the effect of vertical ground motion in cylindrical liquid storage tanks (Hunt B. and Priestley, 1978). Haroun and Trayel (1985) studied influence of vertical ground component of ground excitation using both the finite element and analytical techniques. They calculated the axial and radial components of the wall displacement together with resulting stresses. The effect of liquid sloshing was ignored while the obtaining the dynamic response of tank (Haroun M. A. and Tayel, 1985). Machai (1979) performed a simplified study of vertical acceleration in the design tank. He reported that the vertical earthquake motions can be radial pulsation of tank wall liquid system and result in development of additional stress in the tank wall through direction of circumferential (Marchaj, 1979).

Veletsos and Tang (1987) generalized the mechanical model of the cylindrical tank. They also studied the dynamic behavior of fluid-filled tanks based on flexible bases through rigid foundation mats (Veletsos and Tang, 1990). The results of the study showed that the translational and rocking vibrations of the tank base caused the prolongation of the impulse period and also the effective damping was greater. At the same time, the vertical cylindrical tank also provides a dynamic response to a base motion swinging on arbitrary temporal variation (Veletsos and Tang, 1987; 1990).

Veletsos and Tang (1990) studied the coupling free vibration dynamic CST. The vibration mode of the container was performed using Flugge's exact equations of motion. The hydrodynamic pressure associated with the liquid in the tank was obtained using the velocity potential approach (Veletsos and Tang, 1990).

Virella et al, (2006) studied the mode shaped, natural periods and dynamic response of partly contained liquid tank. He performed computations using finite element method software (ABAQUES). He modelled fluid element using different two techniques. They also formulated to defining mass acoustic element based on linear wave theory. It was

verified that the tanks with height to diameter ratios greater than 0.63 have the similar to the first mode of the cantilever beam (Virella et al., 2006).

Xu et al. (2006 and 2007) studied on the performance of existing soil-structure interaction analysis methods through computer programs in the form of deep buried and / or buried nuclear power plants structure. Lysmer et al. (1999) investigated the seismic soil pressure calculations. They represent two broadly different SSI approaches used for the study. SASSI uses wave propagation theory and superposition principle to train the SSI phenomenon. The LS-DYNA adopts a direct approach to the SSI effect, which operates near field soil with an open FE model connected to a spring boundary for approximate wave propagation in the semi-area. Especially for normal soil pressure, SASSI and LS-DYNA give similar results in terms of shape and size Xu et al., (2006 and 2007) and Lysmer et al., (1999).

### **2.3.1 Vibration characteristic of cylindrical water tanks**

Vibration of Structures was studied by numerous investigators. Firstly (1564-1642), dependence of the natural frequency of a simple pendulum on the pendulum length was solved by Galileo Galilei. He developed experimental study observations on the vibration behavior of string and plates (Galilei, 1948). Sophie Germain (1821) published a simplified equation of the vibration of cylindrical shell. But it contained mistakes. Warburton (1976) indicated that problems of vibration concerning shell are very complicated. Shell extensional membranes and flexural deformation are coupled, and these effects must be simultaneously considered by any theory (Warburton, 1976).

Rayleigh in 1881, as cited in Ref. (Karim, 2008), suggested that the low frequency modes must be flexible and the extensional energy for a sufficiently thin shell to the total energy contribution may be insignificant. He also assumed that during the vibration, the displacement field is such that the two extension strains and the plane shear strain the middle surface would be zero. Rayleigh obtained the three displacement components which he called “inextensional displacements” resultant of three differential equations. He used the “inextensional displacements” to calculate approximate natural frequencies from identification of the strain and kinetic energies (Rayleigh principle). Rayleigh concluded that for “inextensional” modes the frequency is proportional with shell thickness because of the kinetic energy and flexural energy is proportional. He failed to emphasize the restrictions of this conclusion (Karim, 2008).

Foundations of the deformation of thin shells were laid by Love, as cited in Ref. (Karim, 2008), He criticized Rayleigh's hypothesis of the inextensible middle surface remarked that the in extensional displacements cannot satisfy the specified boundary conditions, therefore, Love considered that some stretching of the middle surface of a shell must occur. There was a sufficiently thin wall in the essence of Ali's argument, the flexural energy must become smaller than the extensional energy, because the former is proportional to a higher power of thickness, and therefore Rayleigh's hypothesis cannot be correct.

Arnold and Warburton (1949) developed the general question for vibration of thin cylinders. A theoretical and experimental investigation of the type of vibration associated with the bell-shaped crusts was performed. The cylinders are supported in such a way that the ends are circumferentially retained without any orientation constraint. The complexity of the vibration mode has been found to be very closely related to the natural frequency, for example cylinders having very small thickness-diameter cylinders having a length equal to or less than the diameter may have a majority of higher frequencies simple modes vibration. The frequency equation obtained by the energy method is based on the tension relations given by Timoshenko. In this approach, displacement equations comparable to Love and Flugge have developed. The results are given for cylinders of various lengths, each having the same thickness-to-diameter ratio, and at the same time for a very thin cylinder in which a lower frequency is obtained by a simpler vibration mode. It has been shown that there are three possible natural frequencies for a given nodal pattern, two of which normally occur beyond the aural range (Arnold and Warburton, 1949).

Watkins and Rebert (1965) investigated the vibrational characteristics of thin-walled, circular cylindrical and conical frustum shells with free-free and fixed-free boundary conditions. It was showed that the frequencies predicted by Rayleigh type vibration analyses are in good agreement with experimental results for cylindrical shells with either free-free or fixed-free boundary conditions and also for conical frustums with fixed-free ends. An adequate theory for prediction of the natural frequencies and mode shapes for free-free conical frustums has not yet been developed. It was determined experimentally that the mode shapes associated with the higher natural frequencies of free-free conical frustums exhibit a greater number of circumferential waves at the larger diameter than at

the smaller diameter. This difference in number of waves increased as the order of the mode or natural frequency increased for a given shell (Watkins and Robert, 1965).

Forsberg (1966) studied to determine the modal characteristics of thin-walled cylindrical shells having arbitrary homogeneous boundary conditions. The solutions obtained by various approximated techniques were examined by Forsberg using the exact solution of the differential equations of motion (as derived from Flugge, 2006) as a basis of comparison. He compared the results obtained by energy and finite difference techniques, as well as exact solutions for simplified differential equations (Donnell). The effect of omitting inplane inertia is also examined. The comparison; are made on the basis of frequency, mode shape and modal force distribution. The one dimensional finite difference solution was found to give good results but required a large number of points to accurately describe the lowest mode of long thin shells. The energy method was found to give excellent results for the frequency and reasonably accurate results for modal forces. The boundary behavior obtained from the two methods was found to be completely in error (Forsberg, 1966).

Joseph and Kostem (1982) conducted a study to determine vibrational characteristic and seismic analysis of cylindrical storage tanks expose to a horizontal component of seismic ground motion. It was scoped of the study includes empty, partially full, and completely full tanks. They expressed that in the form of cubic polynomials, were developed for empty tanks which accurately predict frequencies and radial mode shapes corresponding to base of the free vibration mode. These expressions form the basis of simplified procedures for determining shell stresses and displacements, base shears, and overturning moments excited in empty cylindrical tanks by seismic ground motion. The effects of a roof structure and support conditions upon the vibrational characteristics of cylindrical tanks were also examined. Analytical expressions, also in the form of cubic polynomials, were developed which accurately determine the free natural frequency of the shell and the" impulsive fluid mass. These expressions were applicable to tanks both half full and completely full with liquid (Joseph and Kostem, 1982).

Joseph and Kostem (1987) studied the cylindrical tank, built on grade and usually constructed in steel, aluminum or prestressed concrete, was one of the most common forms of liquid storage tanks. They summarized the all results, computer based, numerical analysis of lateral free vibration of cylindrical storage tanks. An analytical method which



accurately predicts the fundamental frequencies of a wide range of cylindrical storage tanks were developed. The procedure was applicable to tanks both completely full and partially full with liquid. Several numerical examples were presented which performed application of the procedure and verify its accuracy (Karim, 2008).

Medhat A. Haroun (2007) performed a theoretical and experimental analysis of the dynamic behavior of ground-supported, capable of deformed, cylindrical storage tanks were conducted. It was performed in three phases: (I) a detailed theoretical treatment of the coupled liquid-shell system for tanks rigidly anchored to their foundations; (II) an experimental method of the dynamic characteristics of full-scale tanks; and (III) a development of an improved seismic design procedure (Haroun, 2007).

Balendra et al, (2003) considered cylindrical liquid storage tanks anchored to rigid base slabs. By using finite elements for both liquid and tank wall, the natural frequencies of the coupled system were illustrated in graphical form for different tank dimensions, depths of liquid and shell thicknesses. From the mode shapes it was concluded that during coupled vibration a large core of liquid is practically unaffected (Balendra, et al., 1981).

### **2.3.2 Previous investigations on fluid-structure interaction**

Fluid structure interaction is one of most complex engineering analyses, in which the shell deforms or moves under the action of fluid pressure, and the shell in turn has an influence on the distribution and magnitude of the flow field. Numerous investigations have been made on fluid-structure investigation due to limitation of analytic methods for the realistic fluid effect on a deformable structure. The dynamic response of liquid storage tanks can be strongly influenced by the interaction between the flexible containing structure and the contained liquid. The dynamic response of flexible liquid storage tanks may have distinct characteristics at a significantly higher level than the respective solid storage tanks (Karim, 2008).

Hadi (1989) in Ref. (Karim, 2008) considered that the dynamic response of fluid containing cylindrical tank resting in elastic media under an arbitrary loading or base acceleration. A semi-analytical finite element procedure was used, and the combined effect of structure-soil-fluid interaction was focused on. The dynamic equilibrium equations were solved by the mode superposition and direct integration methods. The

modified Wilson scheme was used in the forced vibration problems. The seismic equilibrium equation was solved by Wilson step-by-step direct integration method.

Haroun and Al Zeiny (1995) in Ref (Karim, 2008) conducted the nonlinear uplift and contact mechanism between base plate and the underlying foundation of a thin-shelled liquid storage tank. Nonlinearities due to base plate contact with foundation, large deflection and plate hinge formation were investigated. The base plate was modelled as degenerated finite element, and the soil was modelled using Winkler type springs, which were assumed to work only in compression. It was found that neglecting the membrane stresses induced by large displacement resulted in conservative estimates of uplift displacement, while the simultaneous exclusion of the membrane stresses and the plastic hinges yielded reasonable values for the uplift displacement.

Hwang and Ting (1989) in Ref. (Özdemir, 2010) investigated the dynamic response of fluid storage tanks, including hydrodynamic interactions exposed to earthquake excitations using the combination of the boundary element method and the finite element method. Tank wall and inviscid fluid field were treated as two substructures of the total system-coupled through the hydrodynamic pressures. The boundary element method was used to determine the hydrodynamic pressures related with small amplitude excursions and negligible surface wave effects.

Tosaka et al. (1990) enabled a Lagrangian approach to handle the station of the free surface in a two-dimensional container with prescribed motion. The fluid was modeled as potential flow, and Boundary Elements were used to solve Laplace's equation. Examples of motion in rectangular and cylindrical containers were presented (Tosaka et al., 1990).

Nakayama and Tanaka (1990) developed a new computational method for the analysis of three-dimensional large- amplitude motion of liquids with free surfaces in moving containers. They considered the problem of a circular cylindrical container and nonlinear sloshing with large displacements. The domain was discretized using boundary elements. The solution procedure was particularized for horizontal motion of the containers only (Nakayama and Tanaka, 1991).

Malhotra (1997) carried out a study for seismic base isolation of vertical cylindrical liquid-storage tanks is recommended in which the base plate is supported on a soil bed,

and the tank wall is supported on a ring of vertically soft rubber bearings. The tank-liquid system was represented by a lumped-mass-static model and the rubber bearings were represented by a series of nonlinear hysteretic axial springs. The dynamic equilibrium equations were solved by the linear acceleration method. He also found that the isolation bearings is effective in reducing the overturning base moments and the axial compressive stresses in the tank wall, while maintaining the values of base uplift and plastic reactions in the base plate at reasonable levels (Malhotra, 1997).

Hosseini and Mehdi (2000) studied on the effect of the geometry of the tank foundation on the modal properties of the tank-liquid-soil system in which both fluid-structure and soil-structure interactions have been considered. For this aim, a set of cylindrical steel tanks with various height/radius and thickness/radius ratios were considered. The tank foundations were assumed to have two different geometries, namely square and circular in plan with different thicknesses, as well as various dimensions and diameters. Various conditions have been assumed for the subsoil varying from very soft to very stiff based on the value of shear wave velocity. They found that the natural periods of the system were quite sensitive to the foundation geometry. This sensitivity was much higher in the case of circular foundations, in particularly for lower height to radius ratios and lower wave values. It was concluded that by choosing appropriate values for foundation dimensions, it is possible to make the period values a few times longer. Consequently, using a specific foundation geometry may be a good tool for modifying the period of the whole tank-liquid-foundation system in seismic prone regions to make it far from the dominant frequency of the site (Hosseini and Mehdi, 2000).

Souli et al. (2000) and Souli and Zolesio (2001) in Ref. (Özdemir, 2010) established a procedure for fluid structure interaction problems based on Arbitrary Lagrangian Eulerian (ALE) algorithm of finite element method. A two-steps procedure based on operator split method was employed in a time step. First step solves the governing equations of structure and fluid in a Lagrangian manner. In the second step, advection of fluid material across element boundaries was carried out during fictitious time. The applicability of the procedure for sloshing tank problems was validated by analytical method. A similar study carried out by Tallec and Mourob (2001) in Ref. (Özdemir, 2010). They modeled viscous flows inside structures with large deformations as a unique continuous medium considering fluid-structure effects. Lagrangian algorithm was used for structure while

fluid domain was treated with arbitrary Lagrangian Eulerian (ALE) formulation. An implicit algorithm was employed, by solving successively the fluid and the structural part of the problem in each time step.

Aquelet and Souli (2003) presented the prediction of the local high pressure load on a wedge striking a free surface. The fluid-structure interaction was simulated by a fluid-structure coupling algorithm. In order to prevent fluid penetrations through the structure, spring elements were employed. Penalty forces were determined as proportional to penetration depth. High oscillation due to relative motion between fluid and structure was prevented by defining additional damping to the spring elements. In the sample modelling of the piston, the new penalty coupling model given good results by damping high oscillations. Then, the slamming was considered with this new program (Aquelet and Souli, 2003).

Cho et al. (2004) investigated the seismic response analysis of a base-isolated liquid storage tank on a half space using a coupling method that combined the finite elements and the boundary elements. The coupled dynamic system that considers the base isolation system and the soil-structure interaction effect was formulated in time domain. The finite element was used to model the structure, while the boundary element was used for the liquid, the two formulations were coupled using equilibrium and compatibility equations. The base isolation system was modelled using biaxial hysteric element. The homogeneous half space was idealized using the simple dashpot model with frequency dependent coefficient (Cho, et al., 2004).

Stefan Nicolici and Radu M Bilegan (2013) performed modelling problem of the fluid-structure interaction (FSI) in partially filled liquid containers. They focused on the sloshing phenomena and on the coupling computational fluid dynamics (CFD) analysis with the finite element stress analysis (FEM) used to estimate the sloshing vibration amplitude, convective mode frequency, pressure exerted on the shell and the effect of sloshing on the anchoring points forces. The interaction between fluids (water and air) and tank shell was modelled considering full and one-way coupling. Using the time history of an earthquake excitation, the results of the FSI model are compared with those obtained employing simplified mechanical models given in design codes. The coupling phenomenon was found to influence the sloshing effect, the impulsive pressure being amplified by the wall elasticity (Nicolici and Bilegan, 2013)

Djermane, M. and Chikhi, A. (2016) investigated the seismic behaviour of steel tanks. The cylindrical steel tanks are the most susceptible to damage because of dynamic buckling during earthquakes. Three criteria were used to estimate the critical peak ground acceleration which caused the tank uncertainty. The liquid was modelled using specific ANSYS finite elements and fluid-structure interaction. The calculation includes modal and time history analysis, including material and geometric non-linearity. The result values were compared with standard code provisions as well as the results of previous numerical research, and show the need to improve code provisions (Djermane and Chikhi, 2017).

### **2.3.3. Previous investigations on design code**

M.J.N. Priestley et. al (1986) A study group of the New Zealand National Society for Earthquake Engineering completed recommendations for the Seismic Design of Storage Tanks, in a form suitable to be used as a code by the design profession. The recommendations cover design criteria, loading, actions and details and were based on a consistent philosophy of serviceability under the design level earthquake. M.J.N. Priestley et. al. reviewed of the study group's recommendations. It was showed that design criteria and required performance were clearly stated in simple terms. Although most of the provisions were based on existing published information, it was necessary to extrapolate in some cases, particularly for tanks of unusual shape. It is the belief of the Study Group which drafted the Recommendations that the document was result in safe and economic tanks for regions of high seismicity (Davidson, et al., 1986).

There are some studies in the literature that criticizes the tank seismic design codes extensively. Hamdan (2000) in Ref. (Özdemir, 2010) reviewed the seismic design codes of cylindrical steel liquid storage tanks and correlated their provision with earthquake observations in terms of sloshing wave height. The other response parameters such as base shear, overturning moment,  $c$  and axial compressive stresses and buckling strength of tanks obtained from different codes were compared and weakness of the codes was addressed. He significantly purposed of this study was to determine the areas where current design guidelines need further development.

Jaiswal et al.(2007) reported that liquid storage tanks generally possess lower energy-dissipating capacity than conventional buildings. Tanks were subjected to hydrodynamic forces during lateral seismic excitation. These two aspects were recognized by most

seismic codes on liquid storage tanks and, accordingly, provisions specify higher seismic forces than buildings and require modelling of hydrodynamic forces in analysis. It was reviewed and compared provisions of ten seismic codes on tanks. This review revealed that there were significant differences among these codes on design seismic forces for various types of tanks. To achieve large differences in codes due to lack of unified approaches (Jaiswal, et al., 2007).

#### **2.3.4. Analytical and numerical approaches**

Many steel liquid storage tanks have suffered significant damage in past earthquakes. Such failures were caused by various causes. The most common is the dynamic buckling. Many theoretical and experimental research studies have been carried out without completely solving this complex problem.

Alemdar Bayraktar et. al. (2010) investigated the effect of finite element model updating on the earthquake behavior of steel liquid storage tanks considering fluid-structure interaction. They aim at, a cylindrical steel tank filled some liquid fuel oil located in Trabzon, Turkey was selected as an example. Firstly, finite element model of the storage tank was developed by ANSYS software and dynamic characteristics (natural frequencies, and mode shapes) were determined analytically. Experimental environmental vibration tests were carried out in the storage tank under natural excitations to obtain dynamic characteristics (natural frequencies, mode shapes and damping ratios). Peak Picking technique in the frequency domain was used to extract experimental dynamic characteristics. When the analytical and experimentally identified dynamic properties were compared, there were found some differences between the two results. To minimize these differences, initial finite element model of the storage tank was updated according to experimental results using some uncertainties modelling parameters such as elasticity modulus. To investigate the effect of finite element model updating on the earthquake behavior of the storage tank, earthquake analyses were performed before and after model updating. In the earthquake analyses, YPT330 component of 1999 Kocaeli earthquake was selected and applied to the models in the horizontal directions. It was seen from the analyses that the displacements and the stresses after model updating were more effective than the displacements and the stresses before model updating (Bayraktar, et al., 2010).

Sunitha K R and Bobby Jacob (2015) attempted to create a three dimensional finite element model of the steel tank to predict the performance under lateral loading. It was shown that the objective of the research was to study the dynamic properties of water tank during seismic loads. The dynamic properties were found out with model analysis results of water tank. Parametric study was done to find the influence of H/D ratio on the dynamic properties. The frequency of the structure changes with H/D ratio. Nonlinear time history analysis of the water tank under study was conducted and the response of the structure for two different earthquakes were found out (Sunitha and Jacob, 2015).

Anumod et. al. (2015) studied the effect of various components of earthquake on sloshing response of liquid storage tanks. Finite Element Modeling (FEM) strategy which was used to simulate dynamic response of the liquid tank system was described. Then, a parametric study for some vertical, cylindrical ground supported tanks with different aspect ratios excited by various time series of earthquake accelerations was performed. Fourth, the variations of maximum sloshing wave height during the above analysis were described. The tanks under this study were analyzed in a known earthquake in India and the effects on sloshing wave height were studied. Finally, the available simplified formulation for evaluating MSWH under unidirectional excitation was extended for bidirectional excitation and a simple procedure is developed with the help of software (Anumod, et al., 2014).

Taher Ghazvini et. al. (2013) investigated the seismic analysis of above ground storage steel tanks subjected to six correlated earthquake components. Using finite element method, linear properties of tank material including steel for cylindrical tanks were taken into with considering fluid-structure interaction. Effect of six correlated components of earthquake on linear dynamic responses of water storage tanks was investigated by finite element method. They considered that fluid-structure interaction based on Lagrangian-Lagrangian approach (Ghazvini, et al., 2013).

He Liu and Daniel H. Schubert (2001) developed a Finite Element Analysis (FEA) model of a ground level, cylindrical steel shell and roof tank structure with contained fluid under seismic load. They explored the effects large deformation and nonlinear material properties have on the seismic response of fluid/tank systems. The ANSYS program was selected for its ability to include shell and structural steel elements, contained fluid elements, fluid-structure interactions, material and geometric nonlinearities, and contact

type elements. They purposed of this study, analysis results from a linear elastic, small deformation fixed base model were compared with an elasto-plastic material property model with large deformation assumptions. Results showed that the significant difference in results based on the assumptions used and indicate that current design code based values may not be conservative in resultant loading calculations (Housner, 1955).

Cortés Salas Carlos and Sánchez Sánchez Héctor(2008) Carried out a revision, analysis and design criteria concerned with thin walls structures, it was proposed and applied in this study a procedure based on a numeric modelling where the mechanical characteristic of the materials was considered. Numeric analysis was obtained for two conditions: empty tanks vibration and full tanks where fluid-structure interaction is employed to take into account the flexible walls; real seismic record of Subduction originated in the Mexican Pacific Ocean was used by a time history analysis. Finally, they compered the numerical and theoretical results obtained of the real structures (Héctor and Carlos, 2008).

Mohsen Yazdanian et. al. (2016) conducted static, modal, response spectrum, and time history analyses were used in their study for the selected ground supported cylindrical storage tanks (CST)s using ANSYS finite element software. In the time history analysis method, the Tabas, Kobe and Cape Mendocino earthquake records were utilized on the first five CSTs to ascertain the effect of height to diameter ratio and the Tabas earthquake record was used for the rest of CSTs. Results showed that an increase in fluid height lead to a corresponding increase in the base shear. Based on observations, 100 % increase in the diameter showed 63 % increase in sloshing under the response spectrum and 70 % under time history analyses. Based on static and response spectrum analyses, the highest values of displacements were obtained at the lowest part of the tanks, while in time history analysis, the highest was obtained at the top of the tanks. All analyses showed that the maximum stress occurred at the height of 1 to 2 meter from the bottom of the tanks (Yazdanian, et al., 2016).

Naghdali Hosseinzadeh et. al. (2008) Compared the API650-2008 provisions with FEM analyses for seismic assessment of existing steel oil storage tanks. They classified 161 existing tanks in an oil refinery complex into 24 groups and investigated using both API650-2008 rules and numerical FEM models. Failure modes and dynamic characteristics of studied models were calculated by numerical FEM analysis and compared with code requirements. It was demonstrated that, in some cases, there are some



imperfections in the code requirements that require further investigation (Hosseinzadeh, et al., 2013).

Víctor Flores et. al (2009) Studied the mechanical behaviour of two geometries of the storage tanks under horizontal action at the base, by numerical procedure, based in the finite element method (FEM) through of the discretization dominion with triangular elements, satisfying the Laplace equation, also are reviewed others analytical and numerical solution that they were in Literature. They objectified to calculate and evaluate the distribution of the hydrodynamics pressures on the walls of containers under seismic acceleration, for which numerical models were made, that consider the properties of the material, the fluid characteristics and the real geometry of the steel storage tanks. It was observed that the impulsive hydrodynamic pressures obtained with this numerical procedure compared with the others were a good agree. Finally, the dynamic response of the tanks was analysed, involving the numerical modelling by FEM and simplified procedures of the two relevant codes (V́ctor, et al., 2009).

## **CHAPTER 3**

### **THEORY OF CYLINDRICAL WATER TANK**

#### **3.1 Introduction**

The aim of this chapter is to present general knowledge on fluid dynamic response for vertical cylindrical steel tank using analytical formulation. Hydrostatic pressure induces hoop forces and bending moments in wall. Net hydrostatic force is zero on container wall. Hence, causes no overturning moment on foundation or staging. At the same time, hydrostatic pressure affects container design only and not the staging or the foundation. Seismic design; hydrodynamic pressure is considered net hydrodynamic force on the container is not zero affects design of container, staging and foundation.

Two important analytical methods based on the lamina fluid theory and velocity potential theory are discussed. Firstly, the lamina fluid theory which is used as the basic for Housner's model (Housner, 1957 and 1963) is presented. Then the velocity potential theory capable of predicting the hydrodynamic pressure based on the velocity potential theory in which the flexibility of tank wall and maximum sloshing heights due to seismic motions are described. Since lamina-fluid theory is used in many literature and API 650 standards, Housner's lamina fluid is detailed in the following section.

#### **3.2 Theory of Hydrodynamic Fluid**

##### **3.2.1 Lamina fluid method (Housner's method)**

Housner (1957 and 1963) used the lamina fluid theory to calculate the impulsive and convective hydrodynamic pressures in both rectangular and cylindrical tanks. The liquid was assumed to be incompressible and undergo small displacements (Chen and Kianousha, 2010). Housner's method models the vibration of contained fluid in terms of an equivalent lumped mass mechanical system having two degrees of freedom. This

method is simple to use but neglects the effect of higher order sloshing modes and further cannot be readily used for coupled vibration analysis of elastic containers.

According to velocity potential theory, motion of fluid is represented by the continuity conditions that the interface between the fluid and the tank body and the boundary conditions of the free surface of the fluid contain. There are various evaluable methods for dynamic analysis of tanks using this theory. However, the most common method is based on the derivation of equation of motion for tank vibration, fluid, and their interaction use to velocity potential theory for stored liquid and shell theory for tank body. Then a variety of numerical analysis methods such as finite element method, boundary element method or boundary integral equation may be employed for solving the obtained equations.

### 3.2.2 Mechanical model of liquid storage tank

A lumped mass model of a cylindrical tank was developed by Housner (1957, 1963). He reported that the hydrodynamic behaviour of rigid tanks is consistent with continuous fluid mass impulsive and convective masses. Haroun, expanded Housner's model to take into account the flexibility of the tank. Haroun modelled convective, impulsive, rigid mass with continuous fluid mass model and prepared spinners to determine the dynamic properties of these masses. The rigid mass is in the tank bottom liquid mass which is rigid and moves with the tank; the impulsive mass is located on the rigid mass, liquid mass moving in the same direction; convective mass is the liquid at the top of the tank that causes sloshing mass. Figure 3.1 shows Haroun's mechanical mass model (Haroun, 1983).

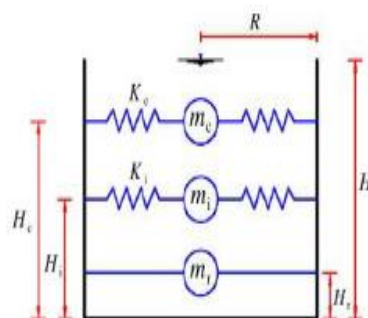


**Figure 3. 1** Haroun's spring mass model

Then the dynamic behaviour of only the impulse and convective mass 1. mod behaviours which can be sufficient accuracy estimated considering as a numerically was shown by

Malhotra (Malhotra, 1997). In this study, the simplified dynamics developed by Malhotra model is used. This model is shown in Figure 3. 2.

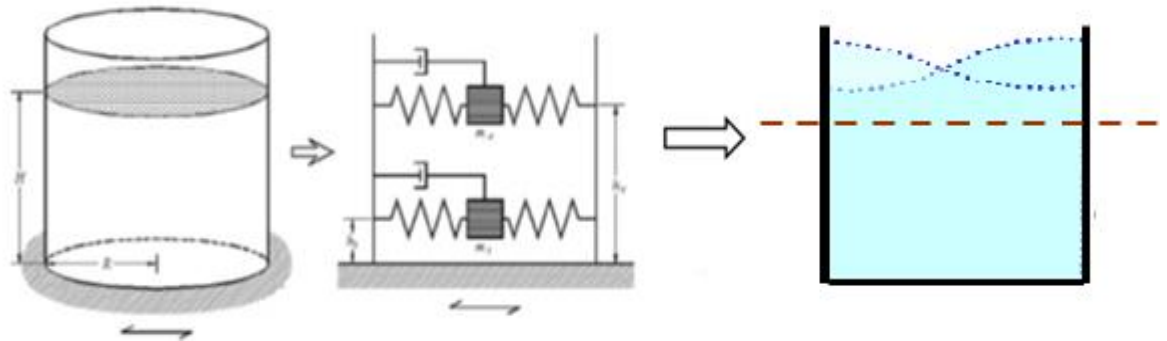


**Figure 3. 2** Mechanical analogue model for cylindrical liquid storage tanks (Malhotra, 1997)

Based on the Housner and Haroun model, seismic design criteria for liquid containing tanks were prepared such as API 650, Aurecode and New Zealand approaches. API 650, Eurocode, 8 approach use Housner Model and New Zealand code approach use the Haroun&Housner Model. In the next section, the seismic design of the cylindrical fluid tank will be analysed according to the American Petroleum Institute API 650 standard.

### 3.2.3 Hydrostatic and hydrodynamic pressure

Under static condition, liquid applies pressure on container. Fluid linearly varies with depth of liquid as shown in Figure 3.3. At depth  $h$  from liquid top, hydrostatic pressure  $P=\gamma*h$  (Sudhir and Kanpur, 2006).

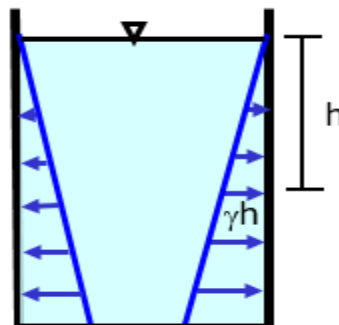


**Figure 3. 3** Hydrostatic pressure (Sudhir and Kanpur, 2006)

Hydrodynamic pressure has curvilinear variation along wall height its direction is opposite to base motion as shown in Figure 3.4.

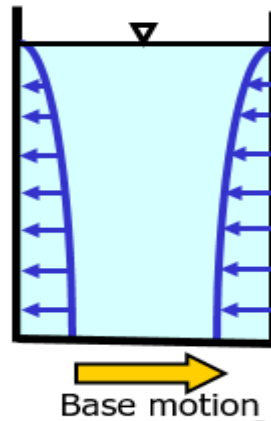


**Figure 3. 4** Hydrodynamic pressure (Sudhir and Kanpur, 2006)

This is hydrostatic pressure during base excitation; liquid exerts additional pressure on wall and base which is hydrodynamic pressure. This is in addition to the hydrostatic pressure. Hydrostatic pressure affects container design only and not the staging or the foundation. Seismic design; hydrodynamic pressure is considered net hydrodynamic force on the container is not zero. Affects design of container, staging and foundation (Sudhir and Kanpur, 2006).

The hydrostatic pressure is axisymmetric and hydrodynamic is asymmetric. The plane view of circular tank is presented in Figure 3.5.

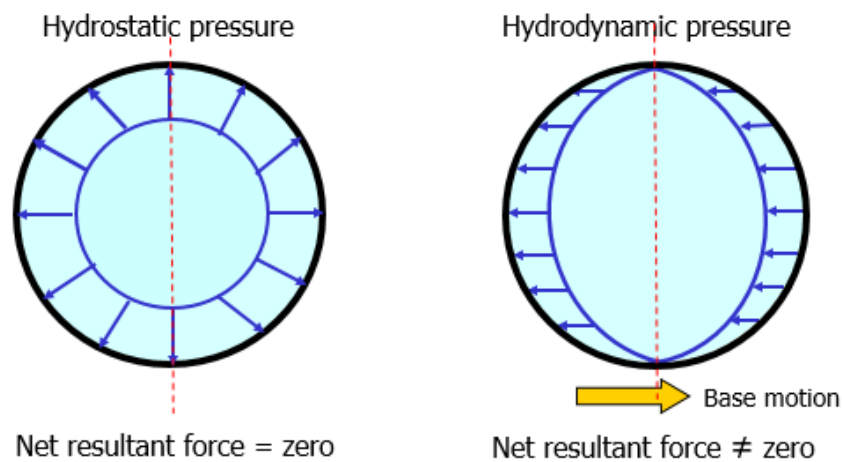


**Figure 3. 5** Circular tanks plan viewer (Sudhir and Kanpur, 2006)

Impulsive liquid is rigidly attached to wall, convective liquid moves relative to wall as if, attached to wall with springs, impulsive and convective liquid move are shown in Figure 3.6.

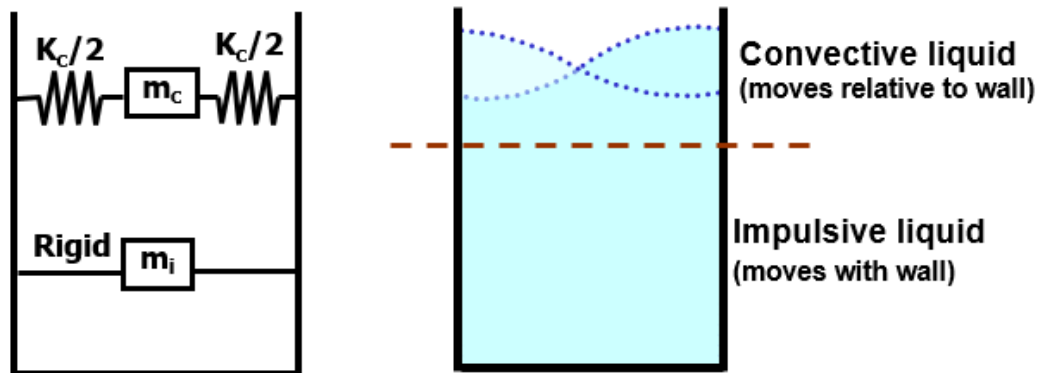


**Figure 3. 6** Represents impulsive and convective liquid

Impulsive as well as convective liquid causes nonuniform pressure on base. Nonuniform pressure on base causes overturning effect. This will be in addition to overturning effect of hydrodynamic pressure on wall. Hydrostatic and hydrodynamic pressure applied on the base are shown in Figure 3.7

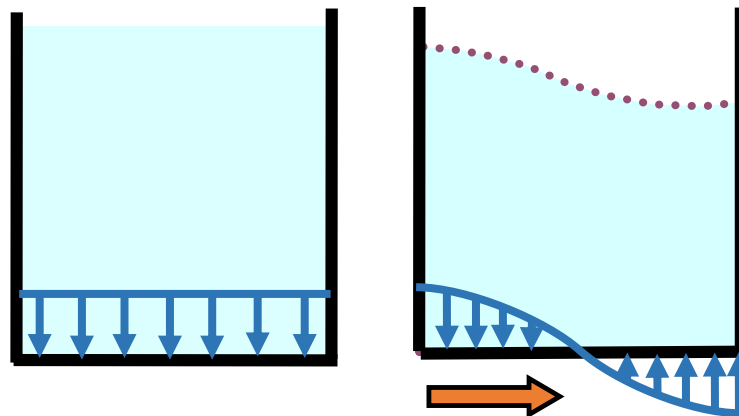


**Figure 3. 7** Hydrostatic and hydrodynamic pressure on base (Sudhir and Kanpur, 2006)

Impulsive liquid, moves with wall; rigidly attached and it has same acceleration as wall. Convective liquid also called sloshing liquid moves relative to wall it has different acceleration than wall Impulsive and convective liquid exert pressure on wall, nature of

pressure is different. Impulsive and convective fluid motions are represented in Figure 3.8.

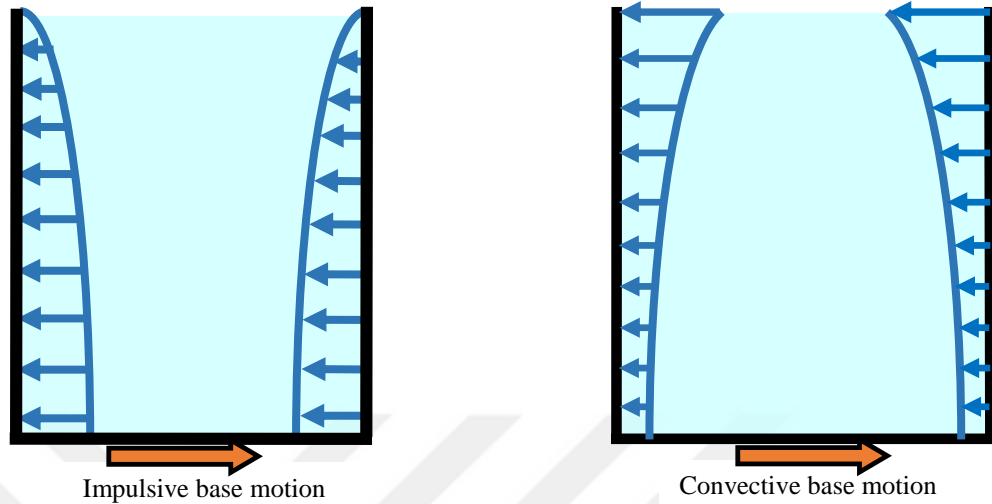


**Figure 3. 8** Impulsive base motion (Sudhir and Kanpur, 2006)

### 3.2.4 Impulsive pressure components

The natural vibration mode of fluid-filled shell, which can only be the base deformation, to evaluate  $m_f$  and  $m_r$  equivalent masses. The natural frequency impulsive  $\omega_f$ , is given by (Kim and Lee 1995).

$$[3.1] \quad \omega_f = \frac{P}{H} * \sqrt{\frac{E}{\rho_s}} \quad [65].$$

Figure 3.3,  $(H/R$  and  $h/R)$  displays  $P$  for different values.  $\omega_f$  is for tanks filled with water. Frequency  $\omega_f$  of a tank filled with density is  $\rho_l$  (Altun, 2013).

$$[3.2] \quad \omega_f = \omega_f * \sqrt{\left(\frac{\rho_w}{\rho_l}\right)}.$$

Frequency parameters can be found by Frequency curves of Haroun which is shown in Figure 3.9.

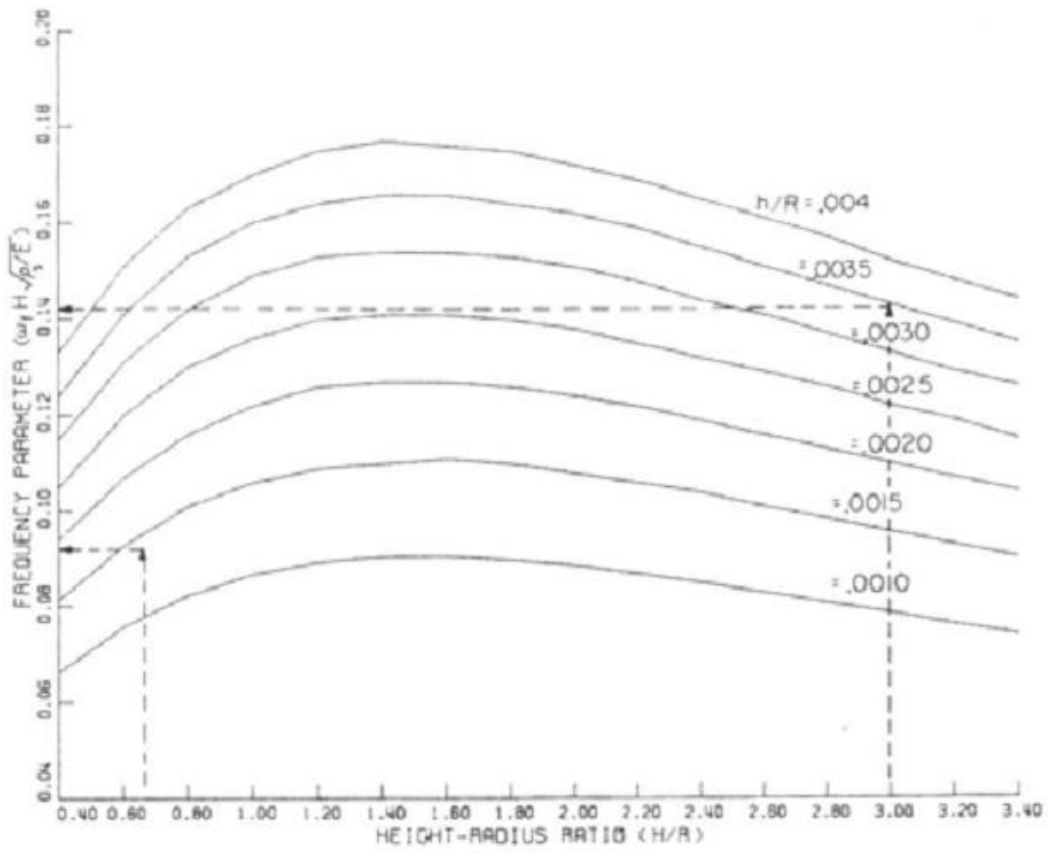


**Figure 3. 9** Frequency parameter (Haroun, 1983)

Impulsive Mass Ratios parameters developed by Haroun (1983) is showed in Figure 3.10

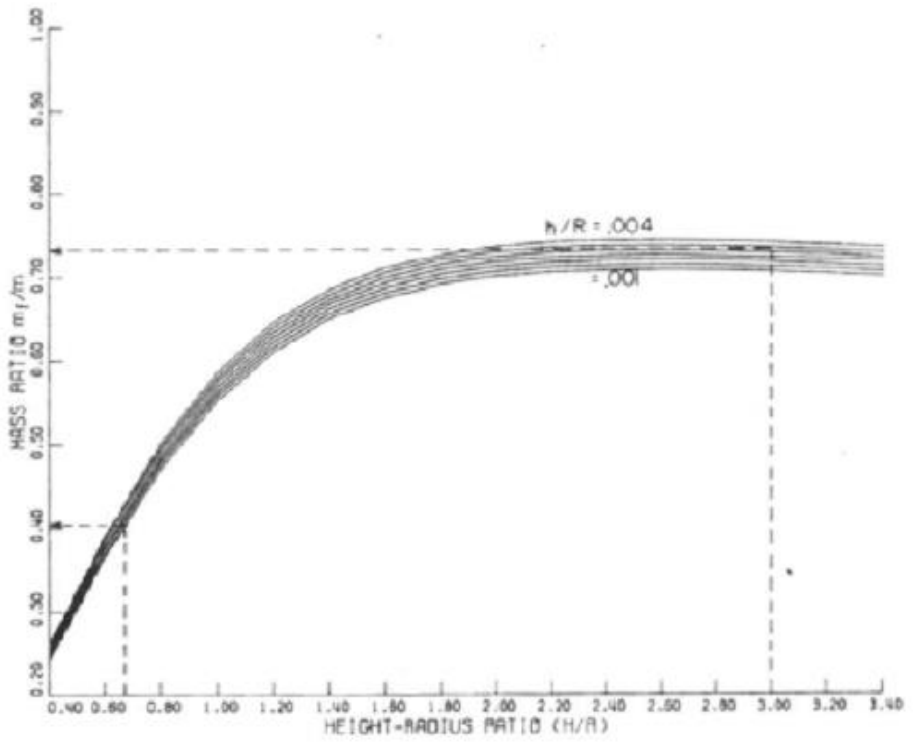


**Figure 3. 10** Impulsive mass ratios figure (Haroun, 1983)



Elevation of Impulsive mass ratio curve is also developed by Haroun which is in Figure 3.11.

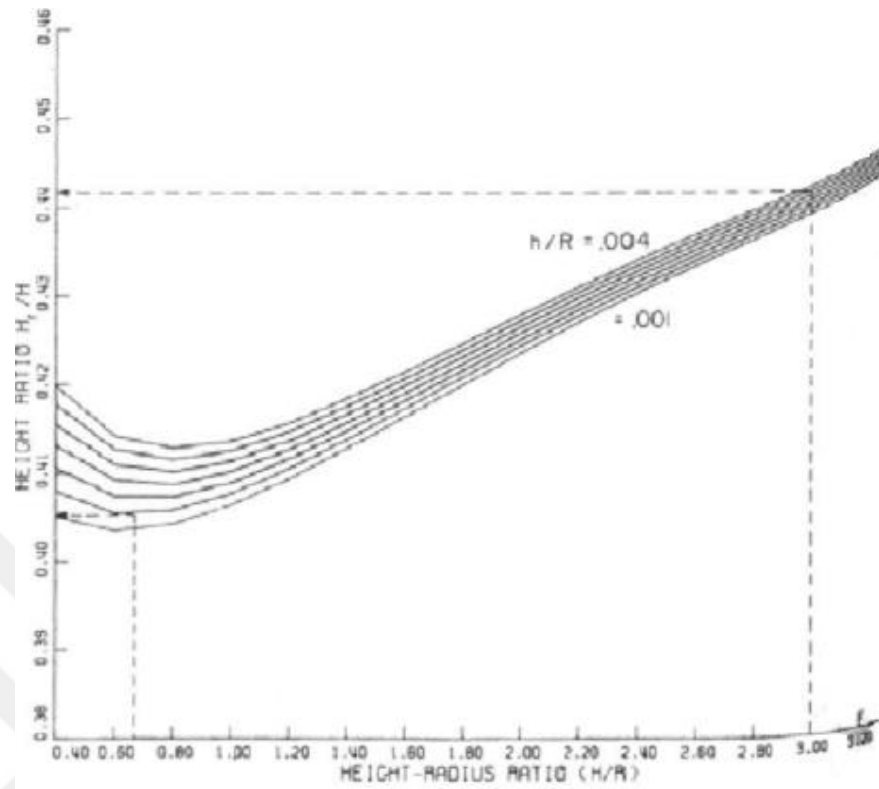


**Figure 3. 11** Elevation of impulsive mass ratios (Haroun, 1983)

Horoun's rigid mass ratios curve is shown in Figure 3.12. Impulsive rigid mass can be selected it.

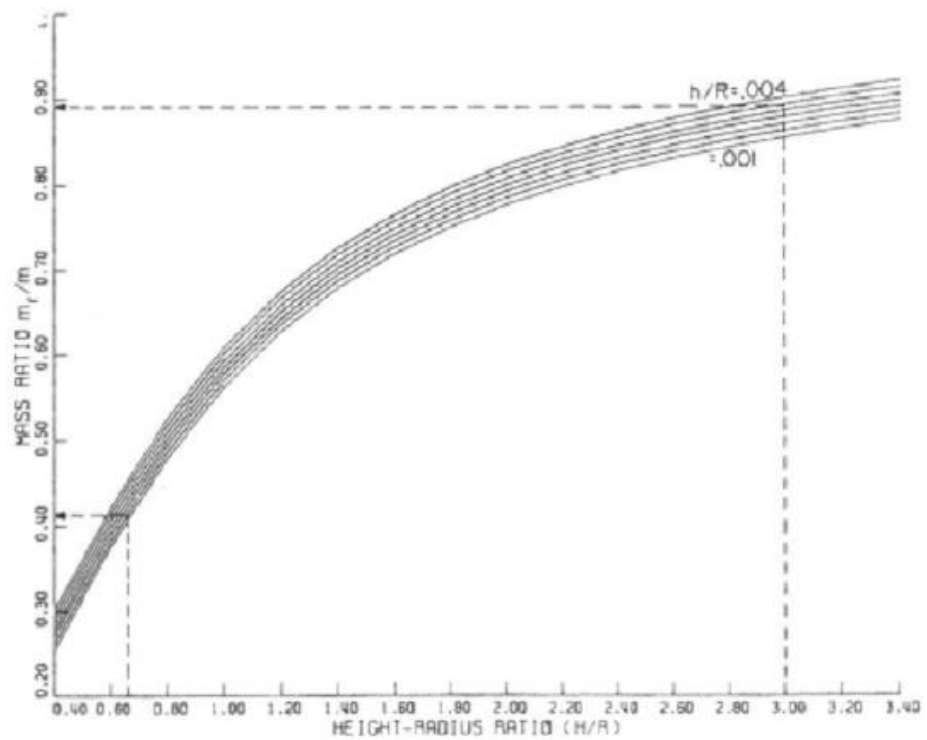


**Figure 3. 12** Rigid mass ratios (Haroun, 1983)

Other important curve is Ratio of the elevation of rigid mass which is shown Figure 3.13.

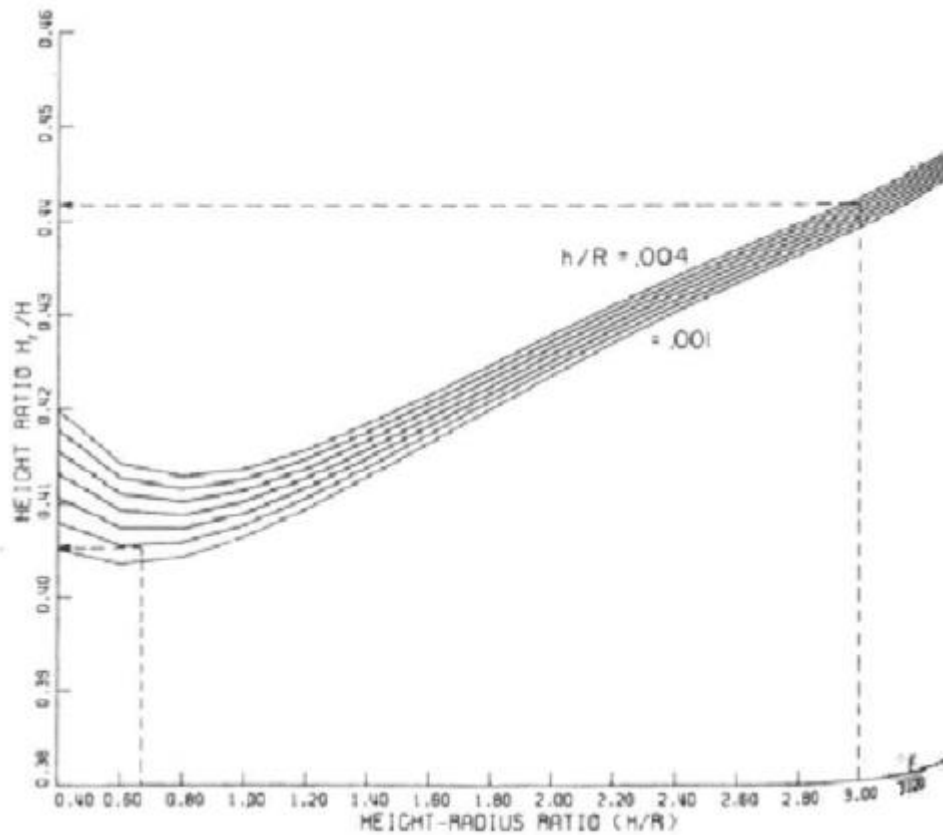


**Figure 3.13** Ratio of the elevation of rigid mass (Haroun, 1983)

The impulsive mode laterals to lateral mode of tank-liquid system and lateral seismic forces applied on a tank depend on period of this mode. Contrary to this assumption originally made by the Housner (1954) that tank is rigid so the impulsive mode period is zero, current design practice computes the period of impulsive mode depending on the value of impulsive mass and on the stiffness of the tank shell even though code uses Housner's method (such as, API 650). The mass density of tank wall is not included in any of impulsive period expressions given in codes; instead, mass density of fluid is used since mass of the wall is usually quite small as compared to fluid mass for steel tanks. The first impulsive mode period of a flexible anchored tank is around 0.5 seconds or less (Özdemir, 2010).

Özdemir (2010) detailed of the simplified methods developed for the seismic analysis of anchored cylindrical tanks subjected to uniaxial loading in Table 3.1

**Table 3. 1** Details of the simplified methods developed for the seismic analysis of anchored cylindrical tanks subjected to uniaxial loading

		Housner (1954)	Yang and Veletsos (1977)		Haroun and Housner (1981)	Malhotra et al. (2000)
Methodology	Fluid	Approximate method for fluid flow	Mathematical solution of Laplace Equation	Mathematical solution of Laplace Equation	Boundary solution technique	Mathematical solution of Laplace Equation
	Structure	-	-	SDOF System vibrate in a prescribed mode	Ring shaped finite elements	SDOF System vibrate in a prescribed mode
Tank wall flexibility		Not considered	Not considered	considered	considered	considered
Impulsive rigid component		considered	considered	considered	considered	-
Impulsive flexible component		-	-	considered	considered	considered
Higher tank-fluid system mode effects		-	-	-	Fundamental mode only	included into the 1st mode effects
Convective effect is evaluated from rigid tank assumption		yes	yes	yes	yes	yes
Convective effect		considered	considered	considered	considered	considered
Higher Sloshing Mode Effects		First mode only	First mode only	First mode only	First mode only	included into the 1st mode effects
Combination rules (impulsive and convective)		SRSS	SRSS	SRSS	SRSS	Numerical sum
and inertia effects		no	no	no	included	considered

According the Özdemir (2010), in the case of anchored tank, a reasonable estimate can be made of the effective shell stiffness, and thus of the impulsive period of vibration. For

unanchored tanks, the nonlinear uplift mechanism causes the stiffness to vary significantly with the amplitude of input motion and there is no true impulsive period of vibration. However, it is clear that any apparent period of vibration will be longer than the period of the anchored tank. Although impulsive period of anchored and unanchored tanks may be different, design codes do not give any expressions for unanchored tanks (Özdemir, 2010).

The evaluation of impulsive mode period, NZSEE (1986) guidelines have adopted the formula from Haroun and Housner (1981a) for fixed base circular tanks (NZSEE, 1986). Eurocode 8 (2006) has followed the expression given by Scharf (1990) (Eurocode 8 and Scharf, 1990). The expression suggested by Malhotra et al. (2000) is also given in Eurocode 8 (2006) document. API 650 (2005) gives an expression for the computation of impulsive period of a flexible tank taken from Malhotra et al. (2000), Malhotra (1997) and API650 (2013).

The impulsive mode periods are affected by the soil behaviour under the tank. In order to take into account, the soil effects on impulsive period of tank, ZSEE (1986) and Eurocode 8 (2006) define coefficients to modify the impulsive period of flexible tank resting on rigid foundation. These coefficients include the horizontal and sway stiffness ( $k_x$  and  $k_\theta$ , respectively), effective tank-liquid stiffness system ( $k_f$ ) and factors for converting static stiffness values to dynamic values ( $\alpha_x$  and  $\alpha_\theta$ ). Seismic codes of equations of impulsive period are compatibly presented in Table 3.2 (Özdemir, 2010).

**Table 3. 2** Equations for impulsive time period given in tank seismic design codes

Support Condition	Code	Resting on rigid foundation	Resting on soft soil including SSI effects
Anchored	API 650 Horizontal Vertical mode	$Ti = \left( \frac{Ci*H}{\sqrt{\frac{tu}{D}}} \right) * \frac{\sqrt{p}}{\sqrt{E}}$ (Malhotra et al., 2000)	No expressions are given mode No expressions are given
	Eurocode 8 Horizontal mode	$Ti = \frac{R(0,157(H/R)^2 + (\frac{H}{R}) + 1,49)}{\sqrt{\frac{Et(\frac{Z}{H}=1/3)}{\rho H}}}$ (Scharf,1990)	For rigid tank: $Ti^* = \pi R \sqrt{\frac{m_i + m_0}{k_x + k_a} + \frac{m_i + h_i'^2}{k_\theta + k_\theta}}$

	Vertical (breathing) mode	$Ti = \left( \frac{Ci * H}{\sqrt{\frac{tu}{D}}} \right) * \frac{\sqrt{p}}{\sqrt{E}}$ <p><math>Ci</math> is a coefficient given as function of H/D in graphical form</p> $Ti = 4R \sqrt{\frac{\pi \rho H (1 - \nu^2) I_0 \left( \frac{\pi R}{2H} \right)}{2EI_1 \left( \pi R / (2H) t \left( \frac{H}{Z} = \frac{1}{3} \right) \right)}}$ <p><math>I_0, I_1</math> are respectively modified Bessel's functions of order 0 and 1</p>	<p>For the flexible tank</p> $Ti^* = Tf^\theta \sqrt{\left( 1 + \frac{k_f}{k_x a_x} \left[ 1 + \frac{k_x a_x h_f^2}{k_\theta a_\theta} \right] \right)}$ $k_f = 4\pi^2 \frac{m_f^2}{T_f^2}$ <p>For rigid tank: <math>k_x, k_\theta, a_x, a_\theta</math> (Gazetetas, 1983)</p> $Tvr^* = 2\pi \sqrt{\frac{m_s}{k_v a_v}}$ <p>For flexible tank</p> $Tvd^* = Tvd^0 \sqrt{1 + \frac{k_l}{k_v a_v}}$ $k_l = 4\pi^2 \frac{m^2}{T_{vd}^2} \text{ (Gazetetas, 1983)}$
	NZSEE Horizontal mode	$Ti = \frac{1,61\pi H \sqrt{\frac{p}{E}}}{K_h}$ <p><math>K_h</math> is given in graphical form as a function of H/R and t/R.</p> $Tb = \frac{1,61\pi H \sqrt{\frac{p}{E}}}{K_v}$ <p><math>K_v</math> is given in graphical form as a function of H/R and t/R.</p>	<p>The same expression given in Eurocode 8 for deformable tank</p> <p>The same expression given in Eurocode 8.</p>

$\rho$ = mass density of fluid,  $E$  = modulus of elasticity of tank material,  $t$  =shell thickness,  $R$ = tank's radius,  $D$  = diameter of tank,  $tu$ = Equivalent uniform thickness of tank shell,  $H$ =Height of fluid,  $g$ =Acceleration due to gravity,  $hf$ = height of impulsive mass,  $h'i$ = height of impulsive mass for rigid tank,  $ms$ =total mass of the tank including base, support, and foundation,  $ml$ =total mass of the fluid,  $m0$ =mass of the foundation,  $kf$ = the stiffness of the deformable tank (Özdemir, 2010)

### 3.2.5 Convective pressure components

The period of the basic sloshing mode depends mainly on the diameter of the tank and a to lesser extent on the depth liquid. Convective mass and its elevation are shown in Figure 3.14.

$$[3.3] \omega_s = \frac{1,84 * g}{R} * \tanh\left(\frac{1,84 * H}{R}\right)$$

$$[3.4] m_s = 0,455 * \pi * \rho_l * R^3 * \tanh\left(\frac{1,84 * H}{R}\right)$$

$$[3.5] \frac{H_s}{H} = 1 - \frac{R}{1,84 * g} * \tanh\left(\frac{0,92 * H}{R}\right)$$

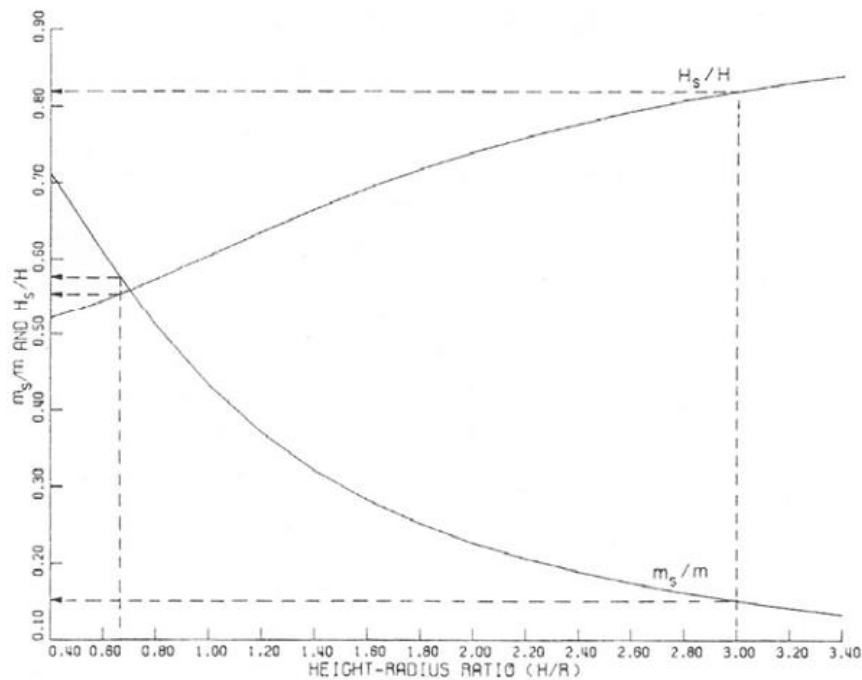


**Figure 3. 14** Convective mass (ms) and elevation (Hs)

### 3.3 API 650 Guidelines for Cylindrical Steel Tank

The API 650 guidelines specifies the minimum requirements for materials, design, manufacture, installation and inspection to storage tanks in perpendicular, cylindrical, open-top and closed-roof, steel tanks in various sizes and capacities for pressures approaching atmospheric pressure. This standard provides adequate safety and reasonable

saving tanks for industry to be used for storage of petroleum, petroleum products and other liquid products. This standard does not provide or maintain a fixed number of fixed allowable tank sizes; it is intended to allow the buyers to choose any size that best meets the requirements of the tank. This standard is intended to assist buyers and manufacturers in ordering, producing and assembling tanks (API650, 2013).

### 3.3.1 Chose seismic use group

There are three seismic use group which are SUG III, SUG II and SUG I.

SUG III in tanks are those providing necessary service to facilities that are essential for post-earthquake recovery and essential to the life and health of the public; or, tanks containing substantial quantities of hazardous substances that do not have adequate control to prevent public exposure (API650, 2013).

SUG II tanks are those storing material that may pose a substantial public hazard and lack secondary controls to prevent public exposure, or those tanks providing direct service to major facilities (API650, 2013).

SUG I tanks are those not assigned to SUGs III or II

### 3.3.2 Vibration structural period

The pseudo-dynamic modal analysis method used in this annex is based on the natural period of the structure and contents described in this chapter.

### 3.3.3 Impulsive period

The design methods in this section are independent of impulsive period of the tank. However, the impulsive period of the tank system can be estimated by Equation 3.6.

[3.6]The impulsive period equation 
$$T_i = \left( \frac{1}{\sqrt{2000}} * \left( \frac{C_i * H}{\sqrt{\frac{tu}{D}}} \right) * \left( \frac{\sqrt{p}}{\sqrt{E}} \right) \right)$$

Figure 3.15 displays coefficient  $C_i$ .

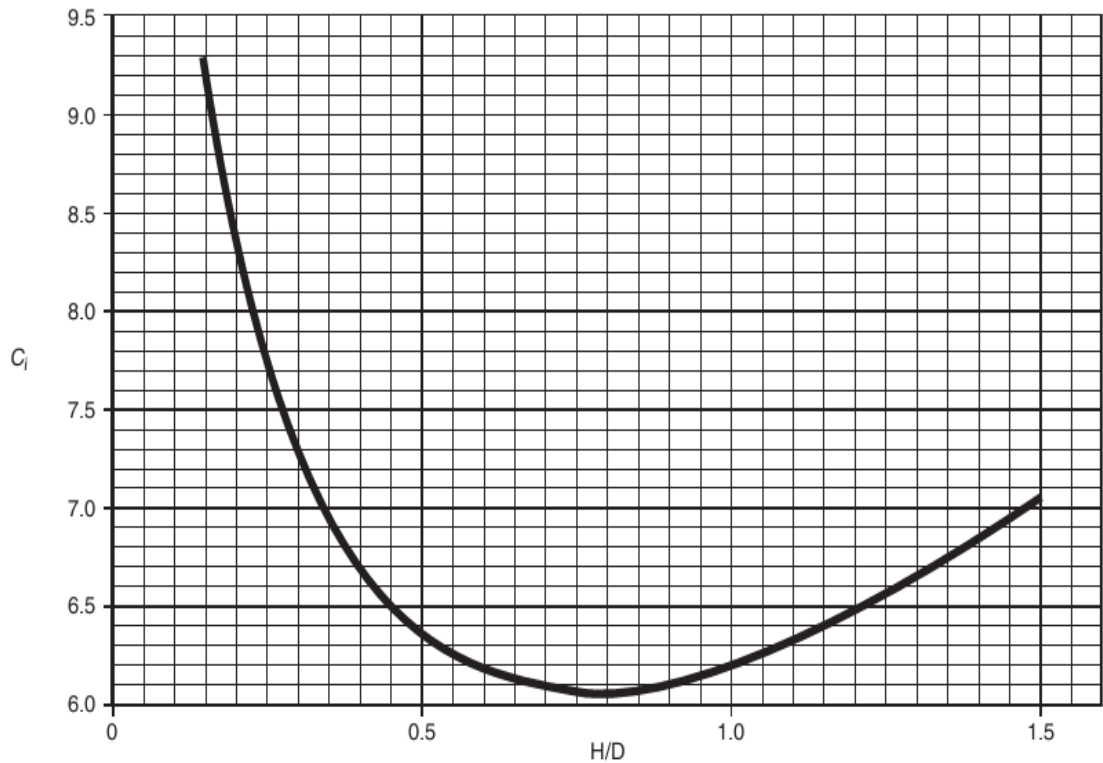


**Figure 3. 15** Coefficient (API 650, 2013)

### 3.3.4 Convective period

The first mode sloshing wave period, in seconds, can be estimated by equations 3.7. The convective period coefficient  $K_s$  can be calculated as Equation 3.8 or can be selected in Figure 3.16. (API650, 2013).

[3.7]The convective period equation  $T_c = 1,8 * K_s * \sqrt{D}$

$$[3.8]T_c = \frac{0,578}{\sqrt{\tanh\left(\frac{3,68 * H}{D}\right)}}$$

D = The factor obtained from Figure 3.16 for the nominal tank diameter ft,  $K_s = D / H$  ratio.



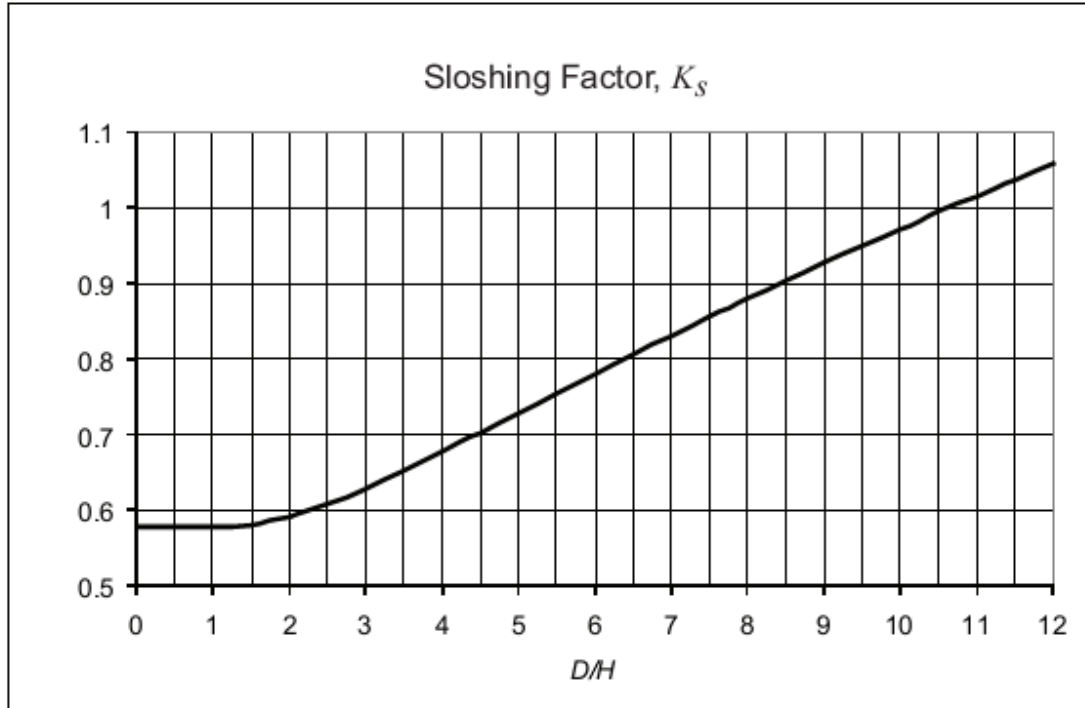


**Figure 3. 16** Convective factor,  $K_s$  (API650, 2013)

### 3.3.5 Design spectral response acceleration

The design response spectrum for ground supplied, flat-bottom tanks is defined by the following parameters:

The Impulsive spectral acceleration parameter ( $A_i$ ) can be calculated in 3.9 equation;

$$[3.9] \text{The impulsive spectral acceleration parameter } A_i = S_{DS}\left(\frac{I}{R_{wi}}\right) = 2,5 Q F_a S_a\left(\frac{I}{R_{wi}}\right)$$

However,

$$[3.10] \text{It should be } A_i \geq 0,07$$

$$A_i \geq 0,5 * S_1 * \left(\frac{I}{R_{wi}}\right) = 0,625 S_p\left(\frac{I}{R_{wi}}\right)$$

The Convective spectral acceleration parameter ( $A_c$ ) can be estimated equation 3.11.

When,  $T_C \leq T_L$

$$[3.11] A_c = K D_{D1} * \left(\frac{1}{T_c}\right) * \left(\frac{I}{R_{wc}}\right) = 2,5 * K * Q * A_0 * \left(\frac{T_S}{T_c}\right) * \left(\frac{I}{R_{wc}}\right) \leq A_i$$

When,  $T_C > T_L$

$$[3.12] A_c = K D_{D1} * \left(\frac{T_L}{T_c^2}\right) * \left(\frac{I}{R_{wc}}\right) = 2,5 * K * Q * A_0 * \left(\frac{T_S}{T_c}\right) * \left(\frac{I}{R_{wc}}\right) \leq A_i$$

Figure 3.17 shows ground-supported of response spectrum liquid storage tanks design.

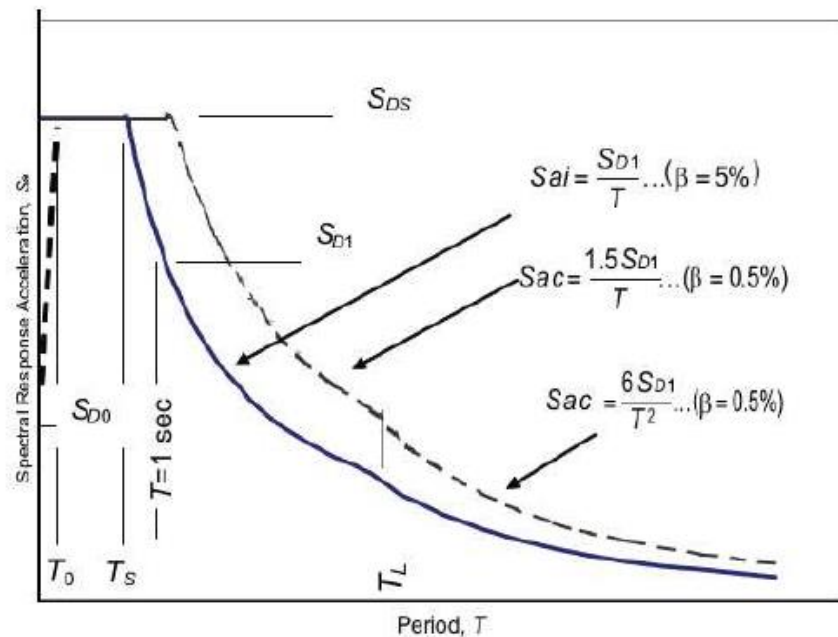


**Figure 3. 17** Design response spectra (API650, 2013)

### 3.3.6. Factors of seismic design

#### 3.3.6.1. Design forces

Seismic design force of equivalent lateral can be determined by the general relationship;

$$[3.13] F = A * W_{eff}$$

Where

A: coefficient of lateral acceleration, %g

$W_{eff}$  : weight effective.

#### 3.3.6.2 Modification factor of response

The grand-supported of response modification factor values shown in Table 3.3.

**Table 3. 3** Response modification factors (API650, 2013)

Anchorage System	$R_{wi}(impulsive)$	$R_{wc}(convective)$
Self-anchored	3,5	2
Mechanically-anchored	4	2

The force reduction factor R: (1) ductility  $R_\mu$ , (2) damping  $R_\beta$ , and (3) over-strength  $R_\Omega$ .

$$[3.14] R = R_\mu * R_\beta * R_\Omega$$

### 3.3.6.3 Importance factor

Table 3.4 shows I (importance factor) which is defined by the SUG (Seismic Use Group)

**Table 3. 4** Display importance factor (I) and SUG (seismic use group) (API650, 2013)

Seismic Use Group	I
I	1
II	1.25
III	1.5

### 3.4 Loads Design

Ground-supported flat-bottom storage tanks can be designed to withstand the seismic forces calculated by taking into account fluid mass, equivalent lateral forces and effective mass and fluid pressures to determine the lateral force distribution (API650, 2013).

$$[3.15] V = \sqrt{V_i^2 + V_c^2}$$

$$[3.16] V_i = A_i(w_s + w_r + w_f + w_i)$$

Where

$$[3.17] V_c = A_c W_c$$

#### 3.4.1 Product Weight Effective

$W_p$  (product weight) can determine the effective weights, the ratios equations are  $W_i/W_p$  and  $W_c/W_p$ . If  $D/H$  is equal to or greater than 1.333, the effective impulsive weight is given by Eq. 3.18;

$$[3.18] \text{Mass of impulsive equation } W_i = \frac{\tanh(0,866 \frac{D}{H})}{(0,866 \frac{D}{H})} W_p$$

If  $D/H$  is less than 1.333, the effective impulsive weight is defined in the 3.19 equation;

$$[3.19] W_i = \left[ 1,0 - 0,218 * \frac{D}{H} \right] * W_p$$

$$[3.20] \text{Mass of convective equation } W_c = 0,230 * \frac{D}{H} * \tanh \left( 1,84 \frac{D}{H} \right) * W_p$$

Figure 3.18 shows effective weight of liquid ratio.

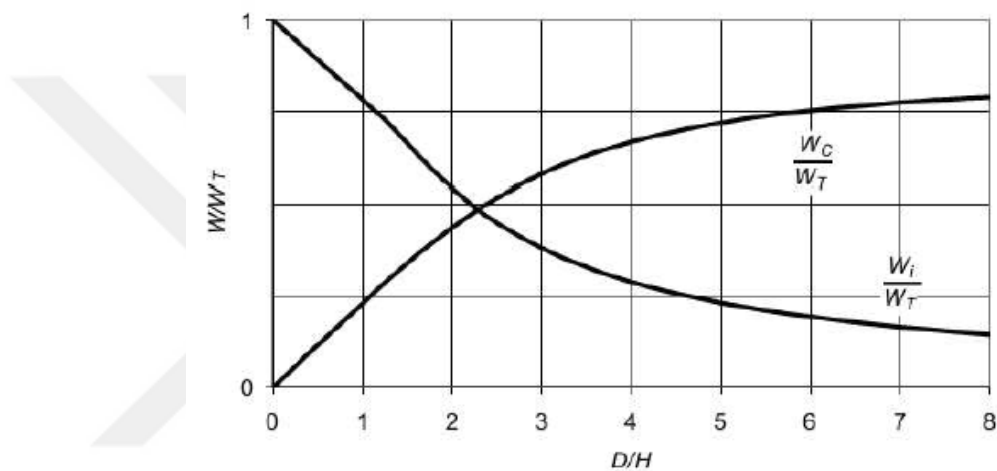


**Figure 3. 18** Effective weight of liquid ratio

### 3.5. Overturning Moment at the Base of Tank

The overturning moment at the base of the tank may be the SRSS sum of the impulsive and convective components multiplied by the corresponding moment arms. The reasons for the overturning moment are shown in Figure 3.19. Both the impulsive hydrodynamic pressure which is on the wall and the base and the convective hydrodynamic pressure in the base causes the overturning moment. The overturning moment is,  $M_{rw}$ :

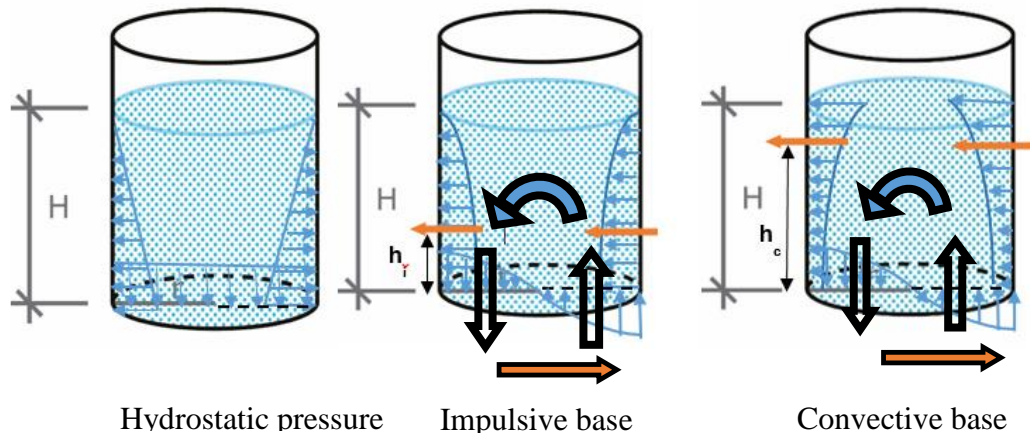


**Figure 3.19** Occurred of overturning moment

$$[3.21] M_{rw} = \sqrt{[A_i * (W_i * X_i + W_s * X_s + W_r * X_r)]^2 + [A_c * (W_c * X_{cs})]^2}$$

Slab Moment,  $M_s$ :

$$[3.22] M_s = \sqrt{[A_i * (W_i * X_{is} + W_s * X_s + W_r * X_r)]^2 + [A_c * (W_c * X_{cs})]^2}$$

### 3.6 Sloshing Effect in the Roof

When the earthquake motion is triggered on the tank by the fixed roof subjected to earthquake motion and the static liquid surface is close to the fixed roof, the liquid strikes the fixed roof as shown in Figure 3.20. The impulsive pressure  $P_i$  acts on the fixed roof at the moment that the sloshing liquid hits it, and the duration of acting of the impulsive pressure is very short. The hydrodynamic pressure  $P_h$  acts on the fixed roof after impulsive pressure diminishes as the sloshed contained liquid runs along the fixed roof (Nakashima, 2010).

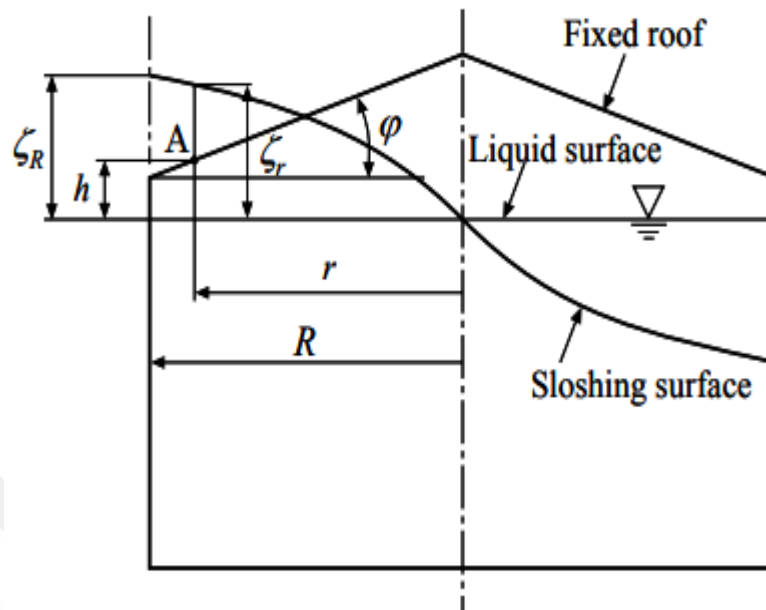


**Figure 3. 20** Sloshing configuration of fixed roof (Nakashima, 2010)

Figure 3.21 depicts the typical time evolution of the dynamic pressure at point A of the fixed roof.

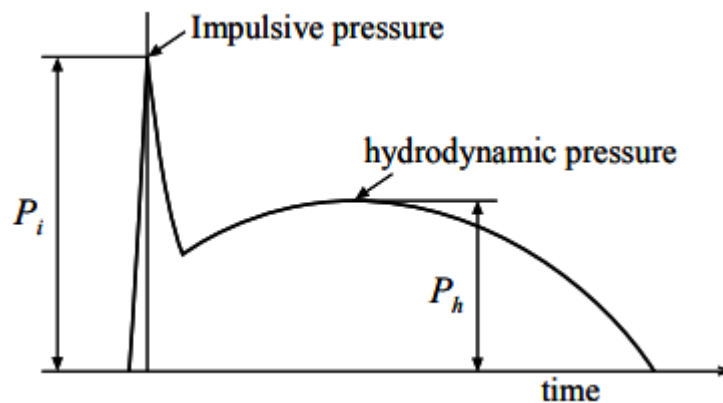


**Figure 3. 21** Impulsive and hydrodynamic pressure (Nakashima, 2010)

If the angle of roof is large, the restraint effect on the roof on sloshing is small as shown in Figure 3.22. Then, the sloshed liquid rises along the roof with a small resistance from the fixed roof, and the hydrodynamic pressure  $P_h$ . If the roof angle is small, the restraint effect on sloshing is great and the sloshing liquid hardly increases as shown in Figure 3.23. Then, the small hydrodynamic pressure  $P_h$  rises on the fixed roof where the angle is small.

$$[3.23] P_i = \frac{\pi}{2} \rho \cot \varphi \left( \dot{\zeta} \frac{A}{r} \right)^2 \text{ [N/m}^2\text{]},$$



**Figure 3.22** Sloshing at cone roof with 25 deg slope (Yoshio and Nobuyuki, 1977)

When the roof angle is small, the restraint effect on sloshing is great and the sloshing liquid hardly increases as shown in Figure 3.23.

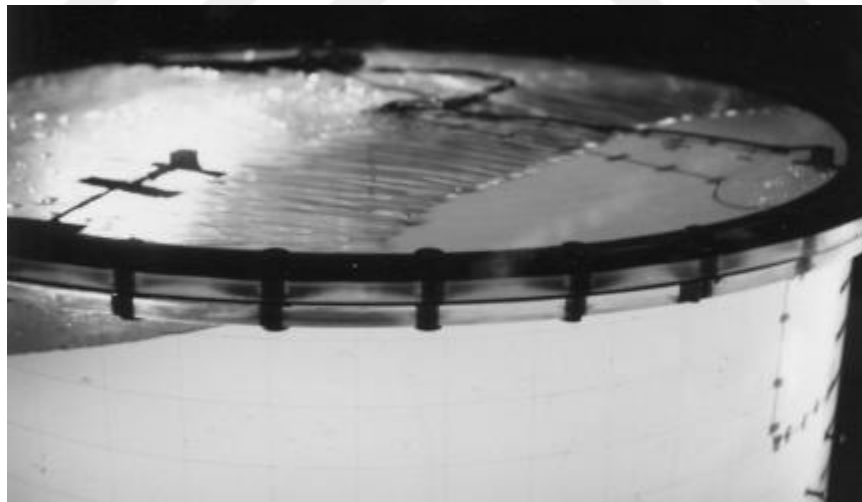


**Figure 3.23** Sloshing at flat roof (Yoshio and Nobuyuki, 1977)

Impulsive pressure  $P_i$  acting on the torispherical and conical roof tanks can be estimated by Equation (3.24). The following relationship is obtained to convert the impulse pressure shown in the literature, which is shown to the gravimetric unit to SI unit by the gravimetric unit;

$$[3.24] P_i = 34,97 \rho (\zeta_r^A)^{1.6} \text{ [N/m}^2\text{]},$$

Sloshing velocity  $\zeta_r^A$  at the point A is approximately given as Eq. (3.25) using the distance h from the static liquid surface to the fixed roof;

$$[3.25] \zeta_r^A = \zeta_r \omega_s \cos(\sin^{-1} \frac{h}{\zeta_r}) \text{ [m/s]},$$

where  $\omega_s$  is the circular natural frequency of the sloshing.

1. in the case of  $\phi \geq 5$  Impulsive pressure:

$$[3.26] P_i = \frac{\pi}{2} \rho \cot \varphi (\zeta_r^A \cos \theta)^2$$

hydrodynamic pressure:

$$[3.27] P_h = \rho g (\zeta_r - h) \cos \theta \text{ [N/m}^2\text{]}$$

2. in the case of  $\phi < 5$  Impulsive pressure:

$$[3.28] P_i = 34,97 \rho (\zeta_r^A \cos \theta)^{1.6} \text{ [N/m}^2\text{]},$$

Since the size of the impulsive pressure is high and the duration of motion is very short, the earthquake resistance test of the fixed roof must account for the dynamic response of the drainage pressure and the fixed roof. For example, if the fixed roof is assumed to be a single degree of freedom system and the impulse response is approached as the half-triangular pulse shown in Figure 3.24, the system's temporary response is obtained from the response given to the beam. In a very short time, the triangular impact load  $\Delta t$ . Thus, the impulse response of the fixed roof can be calculated using the load  $f_s$  obtained by integrating the impulsive pressure along the wetted surface of the roof. Motion equation of a single degree of freedom system is given as equation (3.29);

$$[3.29] m_r \ddot{x} + c_r \dot{x} + k_r x = f(t),$$

where  $m_r$ ,  $c_r$  and  $k_r$  are the equivalent mass, the equivalent damping coefficient and the equivalent stiffness of the fixed roof, the response  $x$  to the half-triangle pulse under the initial conditions  $x = 0$ ,  $\dot{x} = 0$  is obtained as following using the Duhamel integral;

$$[3.30] x(t) = \frac{4I}{k_r \omega_r \Delta t^2} \{2 \sin \omega_n \left(t - \frac{\Delta t}{2}\right) - 2 \sin \omega_n (t - \Delta t) - \sin \omega_n t\},$$



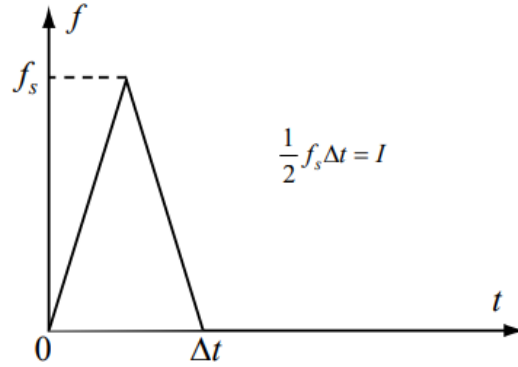


**Figure 3. 24** Pressure shape of half-triangle pulse (Yoshio and Nobuyuki, 1977)

Design shear force of the impulsive mass vibration should satisfy equation (3.31).

$$[3.31] fQ_y \geq Q_{dw}$$

Design shear force of the convective mass vibration should satisfy equation (3.32).

$$[3.32] sQ_y \geq Q_{ds}$$

Notations:

$fQ_y$  impulsive yield shear force (kN)

$sQ_y$  convective yield shear force (kN)

$Q_{dw}$  impulsive design shear force (kN)

$Q_{ds}$  convective design shear force (kN)

1 Design shear force

$Q_{dw}$  is given by the equation (3.33)

$$[3.33] Q_{dw} = D_s S_b = Z_s I D_s S_{al} m f$$

The design hoop stress at the bottom course of tank wall  $Q^\sigma h d$  is given by the equation (3.34)

$$[3.34] Q^\sigma h d = Q_{dw} / 2,5 H_1 t_0 + m 1 g / \pi r t_0$$

where,  $t_0$  is the wall thickness at the bottom. The design shear force of the convective mass vibration  $Q_{ds}$  is given by the equation (3.35)

$$[3.35] Q_{ds} = Z_s I D_s S_{al} m s$$

$sQ_y$ , is approximately given as shown in equation (3.36)

$$[3.36] sQ_y = 0,44fQ_y$$

## 2. Design yield shear force

The design yield shear force of the storage tank,  $Q_y$ , is determined in accordance with equation

$$[3.37] Q_y = 2\pi r^2 q_y / 0,44H_1$$

where,  $\epsilon\sigma_{cr}$  is the critical stress for the elephant foot bulge type buckling.

It can be further modified as shown in equation (3.38), when the yield of the anchor strap is evaluated (Nakashima, 2010),

$$[3.38] aQ_y = 2\pi r^2 a q_y / 0,44H_1$$

## 3.7 Summary

This chapter points that the dynamic responses of cylindrical liquid storage tanks. Two different theories are widely used to examine fluid dynamics in liquid containers. It also clarifies how to determine the velocity potential and consequently, hydrodynamic pressures for a cylindrical tank that it can be determined for deformable steel cylindrical tank under random seismic excitation. Using this theory, the analytical distribution of the hydrodynamic pressure on the walls of a cylindrical tank can be calculated under a real seismic record. The velocity potential method presented here is based on fluid dynamics response components because of the impulsive movement, convective free surface sloshing and flexible wall deformation. Impulsive and convective basic formulation showed with API 650, ZSEE (1986) and Eurocode 8. They showed on the same table as comparative to each other.

This chapter also brief of a general procedure for developing the equivalent mechanical models used in seismic analysis of tanks. Using these models, various dynamic responses such as natural frequencies, sloshing modes, base shear, sloshing displacement and overturning moment can be calculated much more simply. These equivalent models are the basis for most of the current codes and standards dealing with the seismic design of API 650. The provisions of API 650 provided in this chapter will then be used to verify the validity of the present applications in predicting the seismic response of cylindrical steel liquid tanks.

Formulation of roofs was presented in the end of this chapter. If the roof angle is large, the effect of the sloshing restraint on the roof is small. On the contrary, if the roof angle is small, the effect of holding on sloshing grows and the sloshing liquid does not increase its height.



## CHAPTER 4

### FINITE ELEMENT MODELLING

#### 4.1 INTRODUCTION

In this chapter, formulation of liquid structure interaction using finite element method (FEM) is represented. Equations of motion in fluid dynamics are formulated in chapter four. To solve these basic equations an appropriate method that can accurately simulate the actual behavior of liquid containers under dynamic loads. Firstly, the general equations of motion are derived for discrete MDOF (Multiple Degree of Freedom) structures as systems with a finite number of degrees of freedom. Then, an overview information on how the fluid-structure coupling effect is accounted for in the FEM method proposed together with the fluid effect equations is represented.

The finite element method (FEM) is the dominant discretization technique in structural mechanics. The basic concept in the physical explication of the FEM is the subdivision of the mathematical model into subdomains components of simple geometry called finite elements or elements for short. This process is called meshing. The response of each element is expressed in terms of a finite number of degrees of freedom characterized as the value of an unknown function, or functions, at a set of nodal points.

The response of the mathematical model is then considered to be approximated by that of the discrete model obtained by connecting or assembling the collection of all elements. The disconnection-assembly concept occurs naturally when examining many artificial and natural systems. For example, it is easy to visualize an engine, bridge, dam, building, liquid, airplane, or skeleton as fabricated from simpler components. Unlike finite difference models, finite elements do not overlap in space.

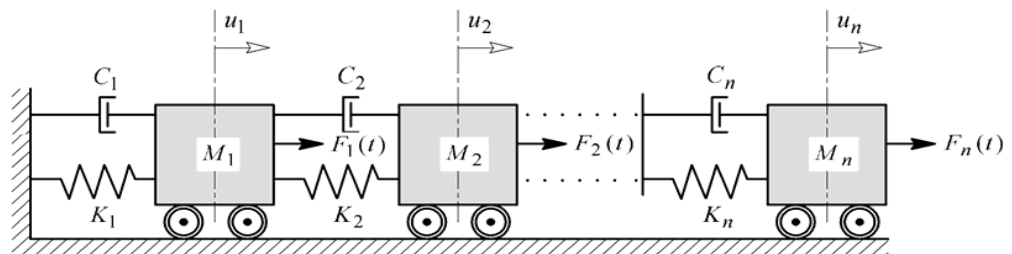
In order to obtain the history of the seismic response of liquid tanks, discrete structural equations and fluid domain equations should be considered simultaneously as coupled sets of simultaneous equations. This chapter is intended to address the issue using the

FEM. It also provides a brief discussion of the problems associated with fluid damping, and boundary conditions at the fluid-structure interface and the free surface of the fluid. Furthermore, the element types and meshing patterns used for FEM modelling are described. The general purpose FEM analysis software ANSYS is used for dynamic analysis of liquid tank models.

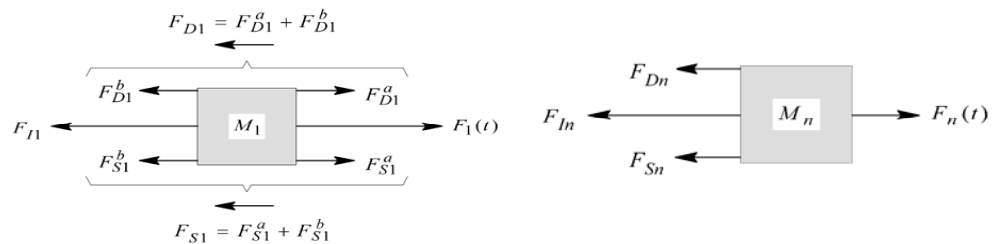
#### 4.2 MDOF Dynamic System

This section is presented, general formulation of typical MDOF system subjected to external forces  $F_j(t)$ ,  $j = 1$  to  $n$ . This classical idealization was developed for a typical MDOF system of equations. Figure 4.1 which is seen classic MDOF system with  $n$  degrees of freedom.

- The external force  $F_j(t)$ ,
- The stiffness force  $F_{Sj}$ ,
- The damping force  $F_{Dj}$ ,
- The inertia force  $F_{Ij}$  ( $j=1$  to  $n$ ).



a)



b)

**Figure 4. 1** (a) Classic MDOF system; (b) Free-body diagrams (Moslemi, 2005)

The stiffness and damping force act in the opposite direction of the external forces because they are the action-resistant internal forces applied. The inertial force is equal to the product of mass and the product of the acceleration acting on the opposite side of the acceleration. Based on the free body diagrams and the dynamic equilibrium state, it is obtained for each mass:

As shown in the figure, the stiffness and damping forces act in the opposite direction of the external forces because they are internal forces that resist the exerted motion. Inertial force is equal to the product of the mass times its acceleration which acts in the opposite direction of acceleration. From the free-body diagrams and based on the condition of dynamic equilibrium, as shown below.

$$[4.1] F_{Ij} + F_{Dj} + F_{Sj} = F_j(t)$$

The above equation contains n equations for j =1 to n

matrix form as:

$$[4.2] \{F_I\} + \{F_D\} + \{F_S\} = \{F^a\}$$

where,  $\{F^a\}$  denotes the applied load vector.

The inertia force vector  $\{F_I\}$  and the acceleration vector  $\{\ddot{u}\}$  are related through the mass

matrix  $\{M\}$  as:

$$[4.3] \begin{matrix} \{F_I\} \\ \left[ \begin{array}{cccccccc} F_{I1} \\ F_{I2} \\ \cdot \\ \cdot \\ \cdot \\ F_{In} \end{array} \right] \end{matrix} = \begin{matrix} [M] \\ \left[ \begin{array}{cccccccc} M_{11} & M_{12} & \cdot & \cdot & \cdot & M_{1j} & \cdot & \cdot & \cdot & M_{1n} \\ M_{21} & M_{22} & \cdot & \cdot & \cdot & M_{2j} & \cdot & \cdot & \cdot & M_{2n} \\ \cdot & \cdot & & & & \cdot & & & & \cdot \\ \cdot & \cdot & & & & \cdot & & & & \cdot \\ \cdot & \cdot & & & & \cdot & & & & \cdot \\ M_{n1} & M_{n2} & \cdot & \cdot & \cdot & M_{nj} & \cdot & \cdot & \cdot & M_{nn} \end{array} \right] \end{matrix} \begin{matrix} \{\ddot{u}\} \\ \left[ \begin{array}{c} \ddot{u}_1 \\ \ddot{u}_2 \\ \cdot \\ \cdot \\ \cdot \\ \ddot{u}_n \end{array} \right] \end{matrix}$$

In general, for a lumped mass idealization, the mass matrix is diagonal:

$$[4.4] \quad M_{ij} = 0 \quad \text{for} \quad i \neq j \quad \text{and} \quad M_{jj} = M_j \quad \text{or} \quad 0$$

The damping force vector  $\{F_D\}$  and the velocity vector  $\{\dot{u}\}$  are related through the damping matrix  $[C]$  as:

$$[4.5] \quad \begin{aligned} \{F_D\} &= [C]\{\dot{u}\} && \text{or} \\ \begin{Bmatrix} F_{D1} \\ F_{D2} \\ \cdot \\ \cdot \\ F_{Dn} \end{Bmatrix} &= \begin{bmatrix} C_{11} & C_{12} & \cdot & \cdot & \cdot & C_{1j} & \cdot & \cdot & \cdot & C_{1n} \\ C_{21} & C_{22} & \cdot & \cdot & \cdot & C_{2j} & \cdot & \cdot & \cdot & C_{2n} \\ \cdot & \cdot & & & & \cdot & & & & \cdot \\ \cdot & \cdot & & & & \cdot & & & & \cdot \\ C_{n1} & C_{n2} & \cdot & \cdot & \cdot & C_{nj} & \cdot & \cdot & \cdot & C_{nn} \end{bmatrix} \begin{Bmatrix} \dot{u}_1 \\ \dot{u}_2 \\ \cdot \\ \cdot \\ \dot{u}_n \end{Bmatrix} \end{aligned}$$

The stiffness force vector  $\{F_S\}$  and the displacement vector  $\{u\}$  are related through the stiffness matrix  $[K]$  as:

$$[4.6] \quad \begin{aligned} \{F_S\} &= [K]\{u\} && \text{or} \\ \begin{Bmatrix} F_{S1} \\ F_{S2} \\ \cdot \\ \cdot \\ F_{Sn} \end{Bmatrix} &= \begin{bmatrix} K_{11} & K_{12} & \cdot & \cdot & \cdot & K_{1j} & \cdot & \cdot & \cdot & K_{1n} \\ K_{21} & K_{22} & \cdot & \cdot & \cdot & K_{2j} & \cdot & \cdot & \cdot & K_{2n} \\ \cdot & \cdot & & & & \cdot & & & & \cdot \\ \cdot & \cdot & & & & \cdot & & & & \cdot \\ K_{n1} & K_{n2} & \cdot & \cdot & \cdot & K_{nj} & \cdot & \cdot & \cdot & K_{nn} \end{bmatrix} \begin{Bmatrix} u_1 \\ u_2 \\ \cdot \\ \cdot \\ u_n \end{Bmatrix} \end{aligned}$$

It can be written now the equations of motion for a MDOF system subjected to external dynamic forces ( $F_j(t)$ ,  $j=1$  to  $n$ ) by substituting Eqs. (4.3) to (4.6) into Eq. (4.2):

$$[4.7] [M] \{\ddot{u}\} + [C] \{\dot{u}\} + [K] \{u\} = \{F_a\}$$

This matrix equation represents  $n$  differential equations governing the motion of a MDOF system subjected to external dynamic forces. The equations are coupled and must be solved simultaneously.

### 4.3 Coupling of Fluid-Structure

This chapter is presented various physical aspects of fluid-structure interaction and reviews the basic equations that govern fluid dynamics. The fluid and the structure interactions at an interface cause the hydrodynamic pressure to apply a force exerted on the structure and the structural motions produce an effective fluid load.

In order to completely describe the fluid-structure interaction problem,  $\{F_a\}$  in Eq. (4.7) is separated into the fluid pressure load acting at the interface  $\{F_e^{pr}\}$  and resultant of all other forces  $\{F_e\}$ . So, the structural equation is rewritten as:

$$[4.8] [M_e] \{\ddot{u}_e\} + [C_e] \{\dot{u}_e\} + [K_e] \{u_e\} = \{F_e\} + \{F_e^{pr}\}$$

The fluid pressure load vector  $\{F_e^{pr}\}$  at the interface  $S$  is obtained by integrating the pressure over the area of the surface:

$$[4.9] \{F_e^{pr}\} = \int_S \{N'\} p \{n\} d(S)$$

in which,

$\{N'\}$  = shape functions employed to discretize the displacement component  $u, v$ , and  $w$  (obtained from the structural element)

$p$  = The fluid pressure element

$\{n\}$  = The normal at the fluid boundary.

Using the finite element approximating shape functions for the spatial variation of the fluid



pressure, one can write:

$$[4.10] p = \{N\}^T \{P_e\}$$

Where,

$\{N\}$  = element shape function for pressure

$\{P_e\}$  = nodal pressure vector

Substituting the finite element approximating function for pressure given by Eq. (4.10) into Eq. (4.9):

$$[4.11] \{F_e^{pr}\} = \int_S \{N'\} \{N\}^T \{n\} d(S) \{P_e\}$$

It can be written in matrix notation to get the discretized wave equation:

$$[4.12] [M_e^p] \{\ddot{P}_e\} + [K_e^p] \{P_e\} + \rho_0 \{R_e\}^T \{\ddot{u}_e\} = \{0\}$$

By comparing the integral in Eq. (4.11) with the matrix definition of  $\rho_0 [R_e]^T$  in Eq. (4.12), it becomes clear that:

$$[4.13] \{F_e^{pr}\} = [R_e] \{P_e\}$$

It can be found coupling matrix with comparing Eq. (4.12) and Eq. (4.13),

$$[4.14] \{R_e\}^T = \int_S \{N'\} \{N\}^T \{n\} d(S)$$

The substitution of Eq. (4.13) into Eq. (4.8) as: results in the dynamic elemental equation of the structure:

$$[4.15] [M_e] \{\ddot{u}_e\} + [C_e] \{\dot{u}_e\} + [K_e] \{u_e\} - [R_e] \{P_e\} = \{F_e\}$$

#### 4.4 Derivation of Hydrodynamic Fluid Matrices

In hydrodynamic fluid-structure interaction problems, the structural dynamics equation needs to be considered along with the Navier-Stokes equations of fluid momentum and the flow continuity equation. The fluid momentum and continuity equations are simplified to get the wave equation using the following assumptions;

1. The fluid is compressible (density changes due to pressure variations).
2. The fluid is inviscid (no viscous dissipation).
3. There is no mean flow of the fluid.
4. The mean density and pressure are uniform throughout the fluid.

Hence, the wave equation of the fluid system can be written in general three dimensional

space  $(x, y, z)$  as:

$$[4.16] \quad \nabla^2 p(x, y, z, t) = 0$$

in which,  $p = p(x, y, z, t)$  is the hydrodynamic pressure. Since the fluid viscosity is neglected, the above equation is referred to as the lossless wave equation. In order to accurately simulate the fluid-structure interaction problem, the discretized structural equation, Eq. (4-7) and the wave equation, Eq. (4.16) have to be considered simultaneously in fluid-structure interaction problems. To discretize the wave equation within fluid domain, first the following coupling stiffness matrix operators (gradient and divergence) are introduced:

$$[4.17] \quad \nabla() = \{L\}^T = \left[ \frac{\partial}{\partial x} \quad \frac{\partial}{\partial y} \quad \frac{\partial}{\partial z} \right]$$

$$[4.18] \quad \nabla() = \{L\}$$

Therefore, Eq. (4.16) is rewritten as follows:

$$[4.19] \quad \nabla \cdot \nabla p = 0$$

or in matrix notation as:

$$[4.20] \quad \{L\}^T (\{L\}p) = 0$$

The hydrodynamic pressure  $p$  in this equation could be due to horizontal and vertical dynamic excitations of the tank walls and floor. Dynamic motions at these boundaries are

related to the hydrodynamic pressure in fluid domain by defining appropriate boundary conditions along fluid-structure interfaces as follows:

$$[4.21] \quad \frac{\partial p(x,y,z,t)}{\partial n} = p(x,y,z,t)$$

The normal structure acceleration at the fluid-structure interface as:

$$[4.22] \quad \{n\} \cdot \{\nabla p\} = -\rho_l \{n\} \frac{\partial^2(u)}{\partial t^2}$$

$$[4.23] \quad \{n\}^T \cdot \{Lp\} = -\rho_l \{n\}^T \left[ \frac{\partial^2(u)}{\partial t^2} \right]$$

$\rho_o$  = mean fluid density

$a_n$  = acceleration component on the boundary along the direction outward normal.

$\{u\}$  = displacement vector of the structure at the interface

$\{n\}$  = unit normal to the interface S

t = time

In deformable containers  $a_n$  is the sum of the ground acceleration and the wall acceleration relative to the ground. While, in rigid containers it is obviously equal to the ground acceleration.

Based on the small-amplitude wave assumption on the fluid free surface, one can write the

following boundary condition accounting for the sloshing effects:

$$[4.24] \quad \frac{1}{g} \frac{\partial^2 p}{\partial t^2} + \frac{\partial p}{\partial z} = 0$$

where, g is the acceleration due to gravity and z represents the vertical direction. This equation is the same as Eq. (3.8) but it is written in terms of fluid pressure rather than velocity potential function. By applying this boundary condition, one can obtain the convective pressure distribution within the fluid domain.

If only the impulsive component of the fluid response is to be considered, the abovementioned boundary condition at fluid free surface should be replaced with the following boundary condition which imposes zero impulsive pressure at the free surface:

$$[4.25] \text{ at } z = Hl, p(x, y, z, t) = 0$$

in which, Hl is the height of the stored liquid. Employing the finite element shape functions for the spatial variation of the fluid pressure p and displacement components u, the following equations can be found to be;

$$P = \{N\}^T \{P_e\} = 0 \text{ and}$$

$$[4.26] \ u = \{N'\}^T \{u_e\}$$

where,

$\{u_e\}$  = nodal displacement component vectors.

$\{N\}, \{P_e\}$ , and  $\{N'\}$  are as defined previously in section 4.3.

Here for simplicity in deriving the equations, the following notation is introduced:

$$[4.27] \ \{B\} = \{L\}\{N'\}^T$$

Finally, using finite element discretization and imposing the previously mentioned boundary

conditions, the discretized wave equation in matrix notation can be found to be:

$$[4.28] \ [M_e^p] \{\ddot{P}_e\} + [K_e^p] \{P_e\} + \rho_0 [R_e]^T \{\ddot{u}_e\} = \{0\}$$

$$[M_e^p] = \frac{1}{g} \int_S \{N\}\{N\}^T dA = \text{fluid mass matrix (fluid)}$$

$$[K_e^p] = \int_{vol} \{B\}^T \{B\} d(vol) = \text{fluid stiffness matrix (fluid)}$$

$$\rho_0 [R_e] = \rho_0 \int_S \{N\}\{n\}^T \{N'\}^T d(S) = \text{coupling mass matrix (fluid-structure interface)}$$

$$\rho_0 [R_e] = \int_{vol} \rho_0 \{N\}\{n\}^T \{N'\}^T d(S) = \text{coupling matrix (fluid-structure interface)}$$

In these equations,  $A_e$  and  $Vol$  represent free surface and volume of the fluid element, respectively. As mentioned before,  $S$  denotes fluid-structure interface.

Dissipation of energy due to fluid damping can be accounted for by adding a dissipation term to the above equation to get:

$$[4.29] \quad [M_e^p] \{\ddot{P}_e\} + [C_e^p] \{\dot{P}_e\} + [K_e^p] \{P_e\} + \rho_o [R_e]^T \{\ddot{u}_e\} = \{0\}$$

where,  $[C_e^p]$  is the matrix representing the damping in fluid which depends on several factors such as fluid viscosity, and pressure wave absorption in fluid domain as well as at the boundaries. This will be further discussed later in this chapter.

Eq. (4.29) together with Eq. (4.15) describe the complete finite element discretized equations for the fluid-structure interaction problem. These equations can be rewritten in assembled form as:

$$\begin{bmatrix} [M_e] & [0] \\ [M^{fs}] & [M_e^p] \end{bmatrix} \begin{Bmatrix} \{\ddot{u}_e\} \\ \{\ddot{P}_e\} \end{Bmatrix} + \begin{bmatrix} [C_e] & [0] \\ [0] & [C_e^p] \end{bmatrix} \begin{Bmatrix} \{u_e\} \\ \{P_e\} \end{Bmatrix}$$

$$[4.30] \quad \begin{bmatrix} [K_e] & [K^{fs}] \\ [0] & [K_e^p] \end{bmatrix} \begin{Bmatrix} \{u_e\} \\ \{P_e\} \end{Bmatrix} = \begin{Bmatrix} \{F_e\} \\ \{0\} \end{Bmatrix}$$

In which,

$$[M^{fs}] = \rho_o [R_e]^T$$

$$[K^{fs}] = - [R_e]$$

It can be observed from Eq. (4.30) that the coupling matrix  $[R_e]$  transfers the structural acceleration to the fluid domain as well as the fluid pressure to the structure.

In a fluid-structure interaction problem all the submatrices with superscript  $p$  in addition to the coupling submatrices ( $[M^{fs}]$  and  $[K^{fs}]$ ) are generated by the fluid elements. While all other submatrices without a superscript are generated by the compatible structural elements used in the finite element model.

The direct integration as well as the modal superposition methods are used to determine the time history response of the fluid-tank system. Using the direct integration scheme, the displacement and hydrodynamic pressure values at time increment  $i + 1$  can be calculated given the displacement and hydrodynamic pressure at time increment  $i$ . In this technique, the step by step integration is used directly to obtain the solution for the original equations of motion of the system. During each time step, the structural characteristics are assumed to be constant. However, these structural properties could differ from one step to another in nonlinear systems or remain the same during all steps in systems having linear behaviour. The modal superposition method uses the natural frequencies and mode shapes of a linear structure to determine the response to transient forcing functions (Moslemi, 2005).

The accuracy of the time history dynamic solution depends on the integration time step defined for the solution algorithm. It should be noted that a time step that is too large may cause errors in the overall system's response. On the other hand, a time step that is too small results in time and computer resource wastes. In this study, an integration time step of 0.005 second is used to be small enough to characterize the fluid-structure response in systems with linear elastic behaviour. This was also suggested in various research studies conducted on liquid containers (Barton and Parker, 1987, Mirzabozorg, et al., 2003; Kianoush et. al., 2006). It is worth pointing out that 0.005 seconds is the time step considered for time history dynamic analyses is smaller than those of recorded ground accelerations used in this study. Moreover, the results of dynamic analysis using a smaller time step shows that using 0.005 sec as an integration time step is adequate to provide accurate results.

#### **4.5 Fluid Damping**

Damping is present in most systems, including liquid containers, and therefore should be accurately calculated in a dynamic analysis. In fact, damping in liquid tanks is dependent on a variety of factors, and as a result, evaluating the damping properties of a liquid-filled tank is a difficult task to be considered further. In engineering, an ideal fluid is usually assumed in the field of dynamic analysis of liquid storage tanks. In doing this, the potential equation of the liquid may be divided into two decoupled components: (1) the impulsive component which describes the interaction of the liquid and the shell and (2)

the sloshing motion of the free liquid surface which may be accounted for by the convective component.

The assumption of damping effect is made that the mechanical energy decreases in time with  $E_{mech} = \text{const } e^{-2\gamma t}$ . The damping factor  $\gamma$  can be calculated by the following equation using the time-based mean value of the mechanical energy dissipation  $\dot{E}_{mech}$ : (Basler and Hofmann, 2015).

$$[4.31] \quad \gamma = \frac{|\bar{\dot{E}}_{mech}|}{2E_{mech}}$$

It is possible to transform the volume integral in an integral over the fluid surface by using the velocity potential  $\Phi$ :

$$[4.32] \quad E_{kin} = -\frac{\rho L}{2} \int_A \Phi \frac{\partial \Phi}{\partial n} dA$$

The expression  $\partial \Phi / \partial n$  indicates the velocity normal to the surface of the liquid (positive inside). The impulsive pressure on the surface is denoted by  $\rho L \Phi$ .

Due to the assumed rigid tank walls on the free liquid surface, only fluid velocities normal to the boundary can occur. The kinetic energy is calculated using the following Eq. (33):

$$[4.33] \quad E_{kin} = \frac{\rho L}{2} R^2 \int_0^1 \int_0^{2\pi} \Phi \frac{\partial \Phi}{\partial \xi} \zeta d\zeta d\varphi.$$

The components of the fluid velocities can be calculated using the following relations:

$$[4.34] \quad v_\xi = \frac{1}{H} \frac{\partial \Phi_{1,n}}{\partial \xi} \Big|_{\zeta=1} = q e^{i\Omega t} \frac{1}{H} J_1(\lambda_n) \sinh(\lambda_n \alpha_L \xi) \lambda_n \alpha_L \cos \varphi.$$

Velocity in axial direction on the tank wall: Velocity in circumferential direction on the tank wall:

$$[4.35] \quad v_{\varphi} = \frac{1}{r} \frac{\partial \Phi_{1,n}}{\partial \varphi} \Big|_{\zeta=1} = -qe^{i\Omega t} \frac{1}{R} J_1(\lambda_n) \cosh(\lambda_n \alpha_L \xi) \sin \varphi.$$

- Velocity in circumferential direction on the tank bottom:

$$[4.36] \quad v_{\varphi} = \frac{1}{r} \frac{\partial \Phi_{1,n}}{\partial \varphi} \Big|_{\xi=0} = -qe^{i\Omega t} J_1(\lambda_n \zeta) \frac{1}{\zeta R} \sin \varphi.$$

- Velocity in radial direction on the tank bottom:

$$[4.37] \quad v_{\zeta} = \frac{1}{R} \frac{\partial \Phi_{1,n}}{\partial \zeta} \Big|_{\xi=0} = qe^{i\Omega t} \frac{\lambda_n}{R} \left[ J_0(\lambda_n \zeta) - \frac{1}{\lambda_n \zeta} J_1(\lambda_n \zeta) \right] \cos \varphi$$

#### 4.6 Finite Element Modelling

The purpose of this section, the 'open top' and 'closed top' ground supported steel storage water tanks types is to modelled with finite element method. The tanks are assumed to be rigidly connected to the rigid ground. It may be occurred sliding and uplifting. The diameter of tanks and contain amount of water such that are adjusted to the same extent. The dimension of tanks and other characteristics will be detailed in next chapter.



All tanks are modelled using shell 181 elements, water is modelled with solid187 elements. In general, as the mesh size is reduced, that is, as the number of elements is increased, the accuracy of the solution increases. This model can be mesh refined to achieve the required accuracy by using only as many degrees of freedom as necessary. The mesh refinement is continued until the difference between the results obtained from one mesh and the previously refined mesh becomes negligible. Open-top tank mesh model is shown in Figure 4.2.

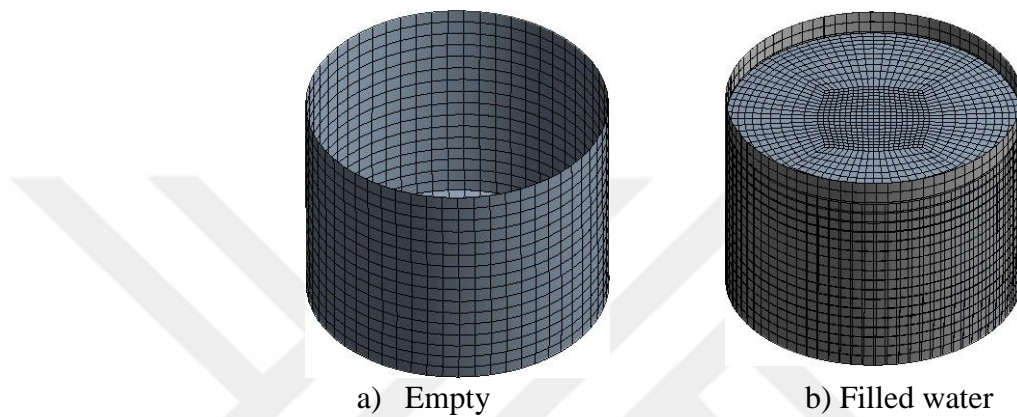


**Figure 4. 2** Open top tank model a) Empty model b) Filled water model

Cylindrical steel tanks can be closed in different shapes. An example with a torispherical-dome shape closed is shown in Figure 4.3.

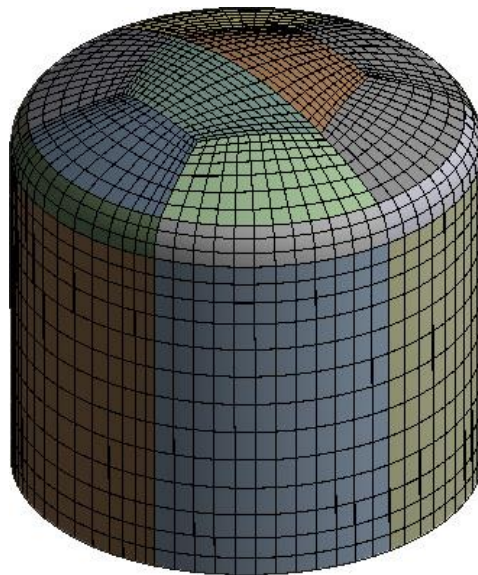


**Figure 4. 3** Torispherical-closed tank model

In Figure 4.4, half geometry section is shown as mesh model.

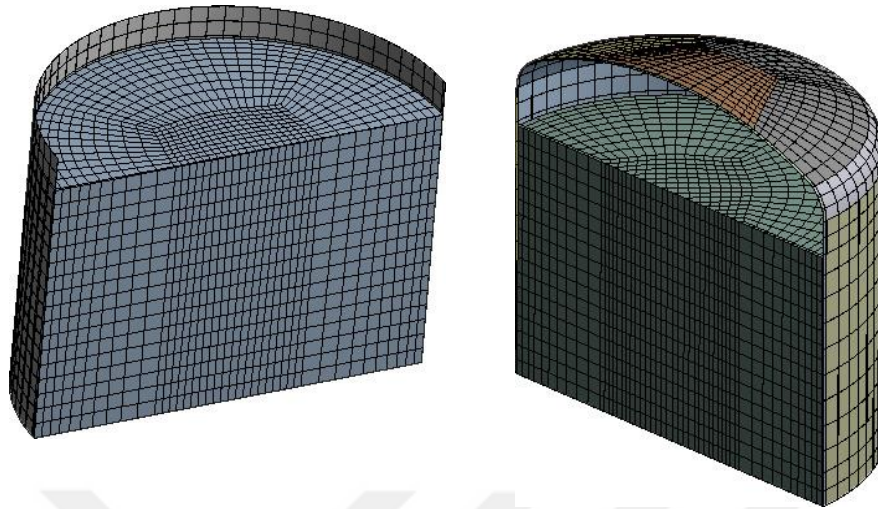


**Figure 4. 4** Half cross section geometry of tank

#### **4.6.1 Finite element geometries**

The degrees of freedom of the element determine the importance for which the element is applicable: structural and fluid or coupled-field. Select an element type with the necessary degrees of freedom characterize the model's response. Including unnecessary degrees of freedom increases the solution memory requirements and running time. Similarly, selecting element types with unnecessary features for example, using an element type with plastic capability in an elastic solution and also increases the analysis run time.

In the finite element model, the tank walls and all other structural parts in the elevated tanks are modelled using four-node quadrilateral shell elements. It is a four-node element with six degrees of freedom at each node: translations in the x, y, and z directions, and rotations about the x, y, and z-axes. If the membrane option is used, the element has translational degrees of freedom only. The degenerate triangular option should only be used as filler elements in mesh generation. Shell element should be well-suited for linear, large rotation, and/or large strain nonlinear applications. Change in shell thickness may be accounted for in nonlinear analyses. In the element domain, both full and reduced integration schemes are supported. It accounts for follower (load stiffness) effects of distributed pressures. The following Figure shows the geometry, node locations, and the

element coordinate system for this element. The element is defined by shell section information and by four nodes I, J, K, and L.

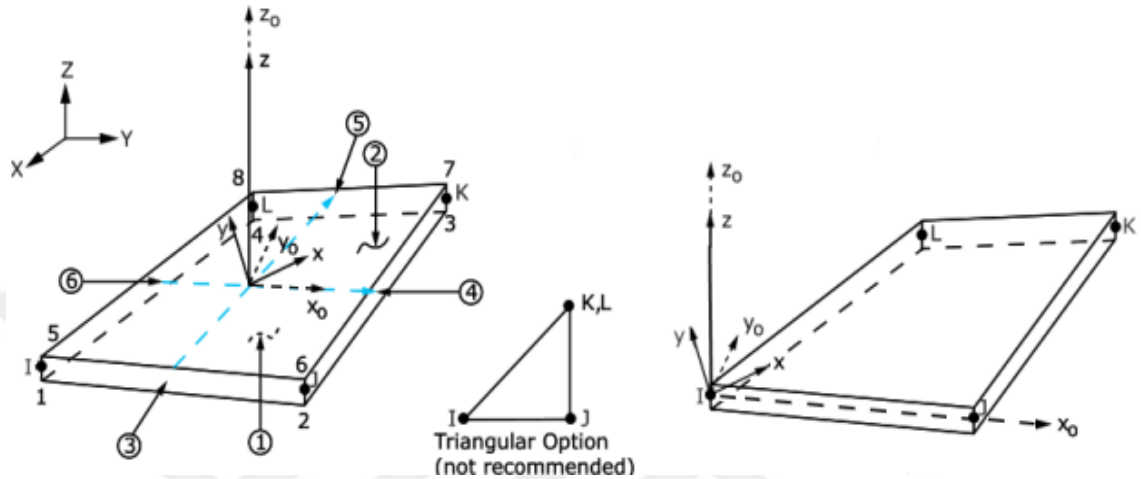


**Figure 4. 5** Geometry of shell element

The 3-D 20-node solid element (it exhibits quadratic pressure behaviour) can be used for fluid element. Generally, it uses for modelling the fluid medium and the interface in fluid-structure interaction problems. 3D 20-node solid element is illustrated in Figure 4.6.

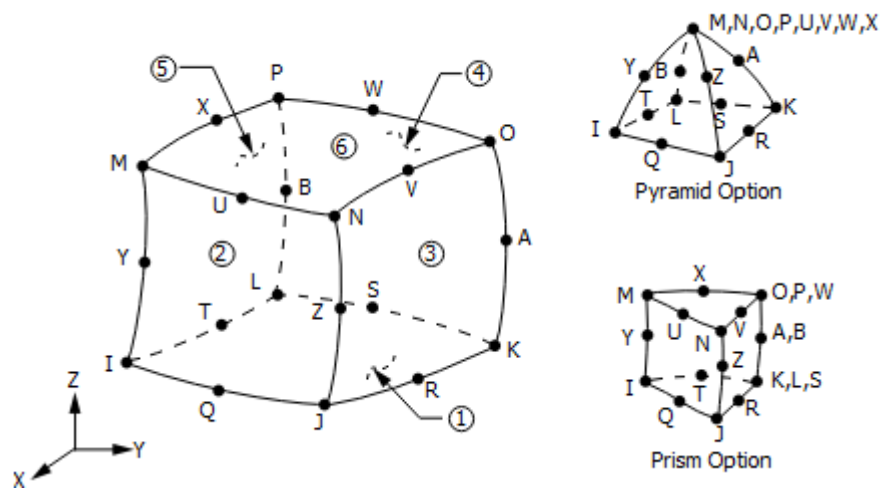


**Figure 4. 6** 3D 20-node solid element

In the fluid medium and the interface in fluid/structure interaction problems can be used 3D 20 node element. Typical applications include sound wave propagation and submerged structure dynamics. The governing equation for acoustics, namely the 3D wave equation, has been discretized taking into account the coupling of acoustic pressure and structural motion at the interface. The element node has four degrees of freedom per node: translations in the nodal x, y and z directions, and pressure. The translations are applicable only at nodes on the interface. Acceleration effects like those in sloshing problems can be included. The mean flow effect or incompressible fluid can be simulated. These elements have the capability to include damping of sound-absorbing material at the interface as well as damping within the fluid.

#### 4.6.2 Fluid hydrodynamic bearing

The form of the Reynold's equation used to describe hydrodynamic lubrication is deduced from the Navier-Stokes equations considering the following assumptions (Bonneau, et al., 2018).

- The flow is laminar and continuous.
- The flow is viscous (see note below).
- The flow is incompressible (see note below).
- The fluid inertia effects are negligible.
- The thickness of the fluid is very small when compared to other dimensions of the fluid domain.
- There is no slipping between the fluid film and the shaft and bearing journal walls.

It can be written in Cartesian coordinates as:

$$[4.38] \quad \frac{\partial}{\partial x} \left( \frac{h^3}{12\mu} \frac{\partial p}{\partial z} \right) + \frac{\partial}{\partial z} \left( \frac{h^3}{12\mu} \frac{\partial p}{\partial x} \right) = \frac{U}{2} \frac{\partial h}{\partial x} + \frac{\partial h}{\partial t}$$

It can be written in matrix notation to create the following discretized wave equation:

$$[4.39] \quad [M_F]\{\ddot{p}_e\} + [C_F]\{\dot{p}_e\} + [K_F]\{p_e\} + \bar{\rho}_0[R]^T\{\ddot{u}_{e,F}\} = \{f_F\}$$

For the pressure-only element, the pressure shape functions are used to determine the fluid stiffness matrix from the left-hand side of Eq. (4.38), giving similar to Eq. (4.39). The film thickness  $h$  is approximated with the same shape functions to obtain the element internal fluid forces from the right hand side of Eq. (4.38).

$$[4.40] \quad [M_s]\ddot{\bar{u}} + [C_s]\dot{\bar{u}} + [K_s]\bar{u} = \{f_s\} + \{f^{pr}\}$$

For the coupled-field element (PRES and U degrees of freedom), the fluid-structure interaction matrix Eq. (4.40) is introduced. The assembled stiffness matrix is then unsymmetrical and expressed as:

$$[4.41] \quad [K] = \begin{bmatrix} [K_s] & -[R] \\ 0 & [K_F] \end{bmatrix}$$

Where;

$[K_s]$  = structural stiffness matrix

$[R]$  = interaction matrix

$[K_F]$  = fluid stiffness matrix

## 4.7 Summary

In this chapter, the equation of motion for a typical structural MDOF system exposed to external dynamic forces was obtained. The method for coupling the fluid and structural property in finite element modelling of the liquid tanks was discussed. The coupling matrix transferring the structural motion and the hydrodynamic pressure between the structure and the fluid was improved.

The formulation of finite element for the coupled system of liquid tanks in the time domain was represented. In providing these formulations, convenient boundary conditions available in typical liquid tanks were applied. In addition, problems related to the damping properties of the fluid domain were discussed. Using the proposed finite element technique, the effects of both impulsive and convective parts and their damping effects can be taken into account. The proposed technique is general and can be used for any tank configurations, or any direction of seismic excitation. This method can account for all appearances of structural and fluid components in the time domain. Some significant properties of the elements employed in this study for finite element modelling.



## CHAPTER 5

# SEISMIC ANALYSIS OF CYLINDRICAL STEEL STORAGE WATER TANKS

### 5.1 Introduction

Cylindrical steel tanks are widely used to store water. They have been becoming widespread for cooling in nuclear power plants. Water is essential for people's basic life, and nuclear power plants have great pre-requisites for the development of the industry. Because of this importance tanks should not be damaged during earthquakes. Contrary to other constructions, these structures are in contact with the liquid and the response under seismic load is quite different. Due to the fluid-structure interaction, the earthquake behaviour of liquid storage tanks is extremely complicated, which leads to a tedious design process (Bayraktar, et al., 2010). When a tank containing liquid is subjected to earthquake movement on tank walls, the liquid is subjected to horizontal acceleration. The tank walls will be exposed due to hydrodynamic pressure. The liquid at the bottom of the tank behaves like a mass rigidly attached to the tank wall. This fluid mass is called as the impulsive mass moving with the wall. Impulsive hydrodynamic pressure behaves on tank walls due to impulsive liquid mass. The liquid mass in the upper part of the tank experience sloshing motion. This mass is called convective fluid. Thus the hydrodynamic response is divided into impulsive and convective components to accurately investigate dynamic behaviour of tanks. Housner (1963) proposed two mass model for cylindrical tank. This model has been commonly used by many international codes such as API650, IITK-GSDMA Guidelines For Seismic Design of Liquid Storage Tanks (Scharf, 1990). In this study, seismic behaviour of liquid storage tanks are accepted that the fundamental impulsive (rigid) and convective (sloshing) frequency modes are separated like it is in many studies (Hamdan, 2000). Separated impulsive and convective Spring Mass Model and description of hydrodynamic pressure distribution on tank wall are presented Figure 5.1.

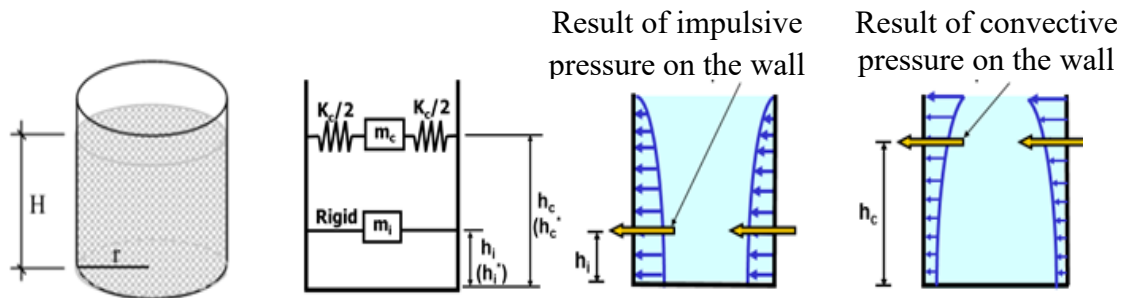


**Figure 5. 1** Spring mass model of tank & hydrodynamic pressure distribution (Sudhir and Kanpur, 2006)

$m_i$  = Impulsive liquid mass

$m_c$  = Convective liquid mass

$K_c$  = Convective spring stiffness

$h_i$  = Location of impulsive mass (without considering overturning caused by base pressure)

$h_c$  = Location of convective mass (without considering overturning caused by base pressure)

$h_i^*$  = Location of impulsive mass (including base pressure effect on overturning)

$h_c^*$  = Location of convective mass (including base pressure effect on overturning)

The finite element method has advantages during solving general problems with a complex structure shape. In this chapter, some basic seismic values were calculated by the API 650 standard, followed by the El-Centro and Kobe earthquakes data being used for the non-linear analysis. Unlike previous studies, the top of the tank in this study was flat-closed, conical-closed and torispherical-closed, for the directional-deformation analysis. The most important goal of this work is to protect the existing tanks from seismic damage by closing them in the shape of a torispherical.

## 5.2 Seismic Analysis with API 650

Seismic behaviour of cylindrical steel storage tanks under seismic loading include several critical failures to the structure that are not exhibited during normal operating levels.



Those risks could include elephant-foot buckling or diamond-shape buckling, hydrodynamic-hoop stresses, sloshing forces and uplift. In the United States, these failure criteria are often accounted for by using the design standard developed by the American Petroleum Institute (API650) (Sudhir K. J. and Kanpur, 2006). This standard has been used worldwide for a seismic-friendly design of steel storage tanks. API 650 establishes minimum requirements for material, design, fabrication, erection and testing for vertical, cylindrical, aboveground, open-top and closed-top tanks as well as steel storage tanks in various sizes and capacities (internal pressures not exceeding the weight of the roof plates), but a higher internal pressure is permitted when additional requirements are met (API650, 2013). Impulsive and convective components of the seismic load have been calculated via the API-650 as well as the finite element method. The values of the model tanks were specified in Table 5.1.

**Table 5. 1** Dimensions and properties of tanks

<b>Parameter and unit</b>	<b>Open-top tank</b>	<b>Flat-closed tank</b>	<b>Conical-closed tank</b>	<b>Torispherical-closed tank</b>
	<b>parameter value</b>	<b>parameter value</b>	<b>parameter value</b>	<b>parameter value</b>
Inner diameter of tank m.	15.08	15.08	15.08	15.08
Tank height without roof m.	11.31	11.31	11.31	11.31
Tank height with roof m.	11.31	11.31	14.27	14.27
Water height m.	10	10	10	10
Shell thickness mm.	4,6 and 8	4,6 and 8	4,6 and 8	4,6 and 8
Density of tank steel kg/m <sup>3</sup>	7850	7850	7850	7850
Density of water kg/m <sup>3</sup>	1000	1000	1000	1000
Young's modulus of tank wall Gp.	200	200	200	200
Poisson's ratio of tank wall $\nu$ .	0.3	0.3	0.3	0.3
Bulk modulus of elasticity of water Gp.	2.2	2.2	2.2	2.2

The model of steel tank of radius 7.54 meters and a total height of 11.31 meters. The tank is filled with water up to a height of 10 meters. The thickness of the tank walls 0.006 m.

[5.1] The total volume of water =  $\pi R^2 h = \pi \times 7.54^2 \times 10 = 1780.4 \text{ m}^3$

Mass Density of Water =  $1000 \text{ kg/m}^3$

[5.2] Thus, the total mass of water in the tank =  $m_w = 1000 \times 1780.4 = 1780400 \text{ Kg}$

$$[5.3] R/h = 7.54/10 = 0.754$$

$$[5.4] h/R = 10/7.54 = 1.32$$

$$[5.5] \text{Mass of impulsive equation } m_i = m_w \frac{\tanh(1.74 \frac{R}{h})}{(1.74 \frac{R}{h})}$$

$$m_i = 1780400 \frac{\tanh(1.74 * 0.754)}{(1.74 * 0.754)}$$

$$m_i = 1173539.90 \text{ Kg}$$

The Figure 5.2 shows the ratio of impulsive ratio (Haroun, 1983)

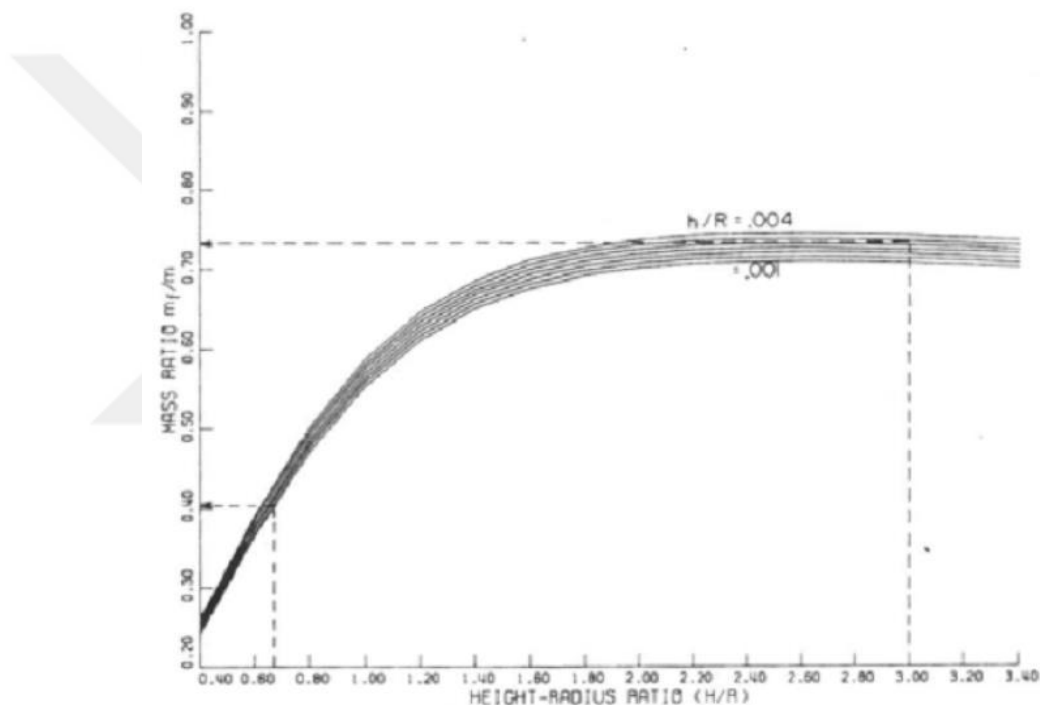


**Figure 5. 2** Impulsive mass ratios (Haroun, 1983)

Convective mass was calculated by Haroun (1983)

$$[5.6] \text{Mass of convective equation } m_c = 0.455 * \pi * \rho_l * R^3 * \tanh\left(1.84 \frac{h}{R}\right)$$

$$m_c = 0.455 * \pi * 1000 * 7.54^3 * \tanh(1.84 * 1.32)$$

$$m_c = 603291.22 \text{ Kg}$$

Impulsive and convective masses should be total water mass.

$$[5.7] \text{Convective spring stiffness equation } k_c = m_c \frac{g}{R} 1.84 \tanh \frac{1.84h}{R}$$

$$k_c = 421535.68 \frac{9.81}{7.54} 1.84 \tanh \frac{1.84 * 10}{7.54}$$

$$k_c = 993928.66 \text{ N/m}$$

$$[5.8] \text{ Location of convective mass equation } h_c = \left[ 1 - \frac{\cosh\left(1.84 \frac{h}{R}\right)}{1.84 \frac{h}{R} \sinh\left(1.84 \frac{h}{R}\right)} \right] h$$

$$h_c = \left[ 1 - \frac{\cosh(1.84 * 1.32)}{1.84 * 1,32 \sinh(1.84 * 1.32)} \right] 10$$

$$h_c = 7,60 \text{ m}$$

$$[5.9] \text{ Location of impulsive mass equation } h_i = 3/8h$$

$$h_i = 3.75 \text{ m}$$

The natural frequency of impulsive mass can be calculated with follow equation.

$$[5.10] \omega_i = \frac{2\pi}{C_i * h_i} * \sqrt{\frac{E * t}{p * r}}$$

$$\omega_i = \frac{2\pi}{6.32 * 10} * \sqrt{\frac{210.10^9 * 0.006}{7850 * 7.54}}$$

$$\omega_i = 20.51 \text{ rad/sn} = 3.24 \text{ Hz}$$

The natural frequency of convective(sloshing) can be found with follow equation.

$$[5.11] \omega_c = \frac{2\pi}{C_c * \sqrt{r}}$$

$$\omega_c = \frac{2\pi}{1.48 * \sqrt{7.54}}$$

$$\omega_c = 1.54 \text{ rad/sn} = 0.246 \text{ Hz}$$

### 5.2.1 Impulsive naturel period

The impulse mode refers to the lateral mode of the tank-liquid system, and the lateral seismic forces applied to a tank depend on the period of this mode. Contrary to the assumption initially made by Housner (1954), the tank is solid so the impulsive mode period is zero, the current design practice calculates of the impulse mode depending on the value of impulsive mass and the rigidity of the tank shell, but uses the code Housner's

method (API650, 2013). The mass density of the tank wall is not included in the impulse period expressions given in the codes; instead, the mass density of liquid is used because the mass of the wall is usually quite small compared to the liquid mass for steel tanks. The first impulsive mode period of a flexible anchored tank is around 0.5 seconds or less (Özdemir, 2010) . The impulsive period can be calculated with 5.12 equation. Coefficient  $C_i$  can be determined in Figure 5.3 curve.

$$[5.12] \text{ The impulsive period equation } T_i = \left( \frac{1}{\sqrt{2000}} * \left( \frac{C_i * H}{\sqrt{tu}} \right) \right) * \left( \frac{\sqrt{p}}{\sqrt{E}} \right)$$

$$T_i = \left( \frac{1}{\sqrt{2000}} * \left( \frac{6,2 * 10}{\sqrt{\frac{0,012}{15,08}}} \right) \right) * \left( \frac{\sqrt{7850}}{\sqrt{220000000}} \right) \Rightarrow T_i = 0.29 \text{ sec}$$

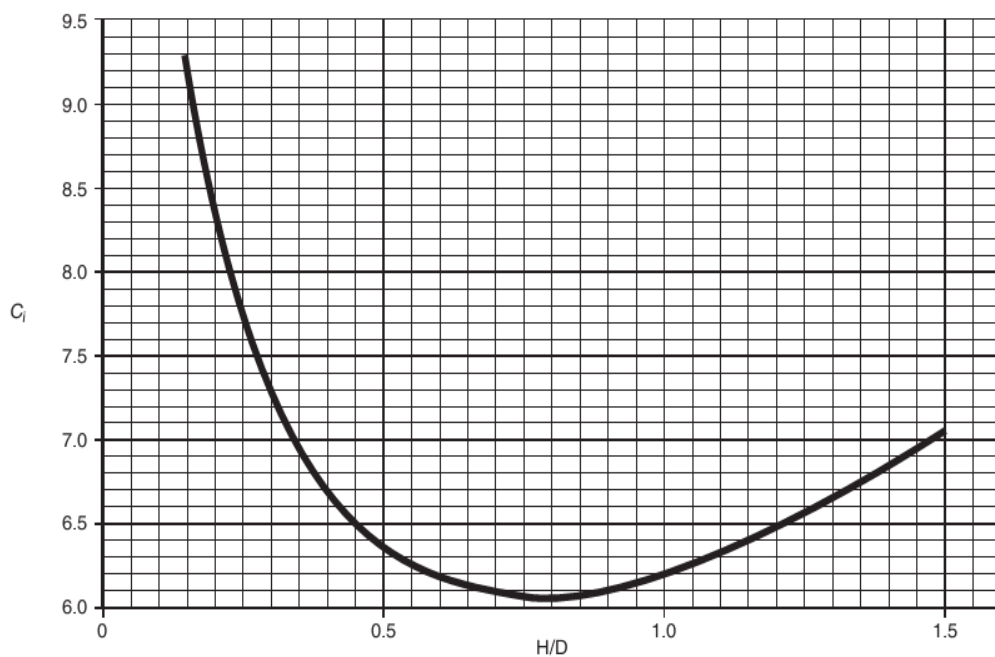


**Figure 5. 3** Coefficient  $C_i$  (API650, 2013)

Recommended design value for the first impulsive and convective modes of vibration as function of liquid-height to tank radius  $H/r$  for vertical circular tanks are listed in Table 5.2

**Table 5. 2** Recommended design value for the first impulsive and convective modes of vibration as function of liquid-height to tank radius H/r for vertical circular tanks

H/r	$m_i/m_w$	$m_c$	$c_i$	$c_c$	$h_i/H$	$h_c/H$	$h_i'/H$	$h_c'/H$
0.3	0.176	0.824	9.28	2.09	0.4	0.521	2.54	3.414
0.5	0.3	0.7	7.74	1.74	0.4	0.543	1.46	1.517
0.7	0.414	0.586	6.97	1.6	0.401	0.571	1.009	1.011
1	0.548	0.542	6.36	1.52	0.419	0.616	0.721	0.785
1.5	0.86	0.314	6.06	1.48	0.439	0.69	0.555	0.734
2	0.763	0.237	6.21	1.48	0.448	0.751	0.5	0.764
2.5	0.81	0.19	6.56	1.48	0.452	0.794	0.48	0.796

### 5.2.2 Convective (sloshing) period

The period of convective (sloshing) mode depends on the diameter of the tank and to a lesser extent on the depth of liquid. The periods of convective mode are very long (up to 6-10 seconds for large tanks) and are more influenced by the level of seismic ground displacements rather than ground accelerations. API 650 recommends the expression derived by Housner (1954). Sloshing factor can be selected with curve in Figure 5.4.

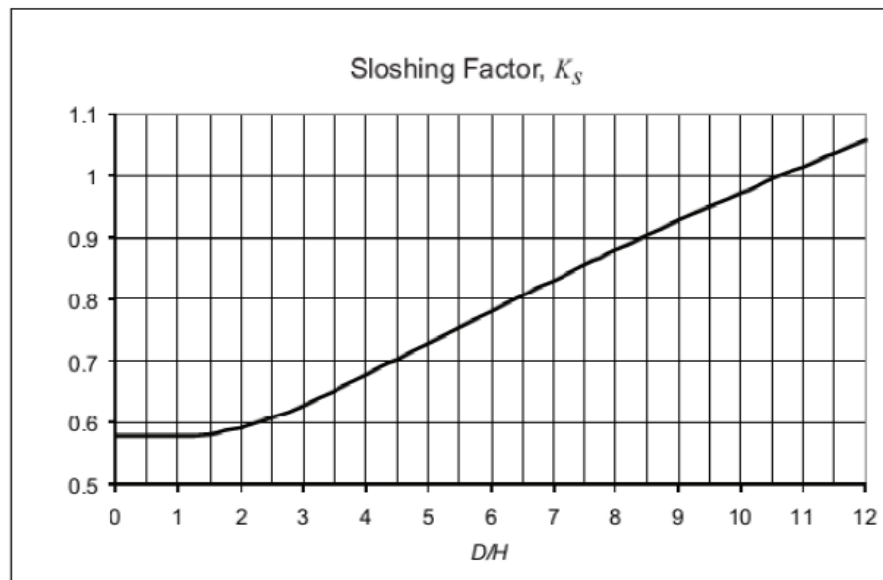


**Figure 5. 4** Sloshing factor,  $K_s$  (API-650)

[5.13] The convective period equation  $T_c = 1.8 * K_s * \sqrt{D}$

$$T_c = 1.8 * 0.578 * \sqrt{10}$$

$$T_c = 3.29$$

### 5.2.3 Spectral acceleration and design loads

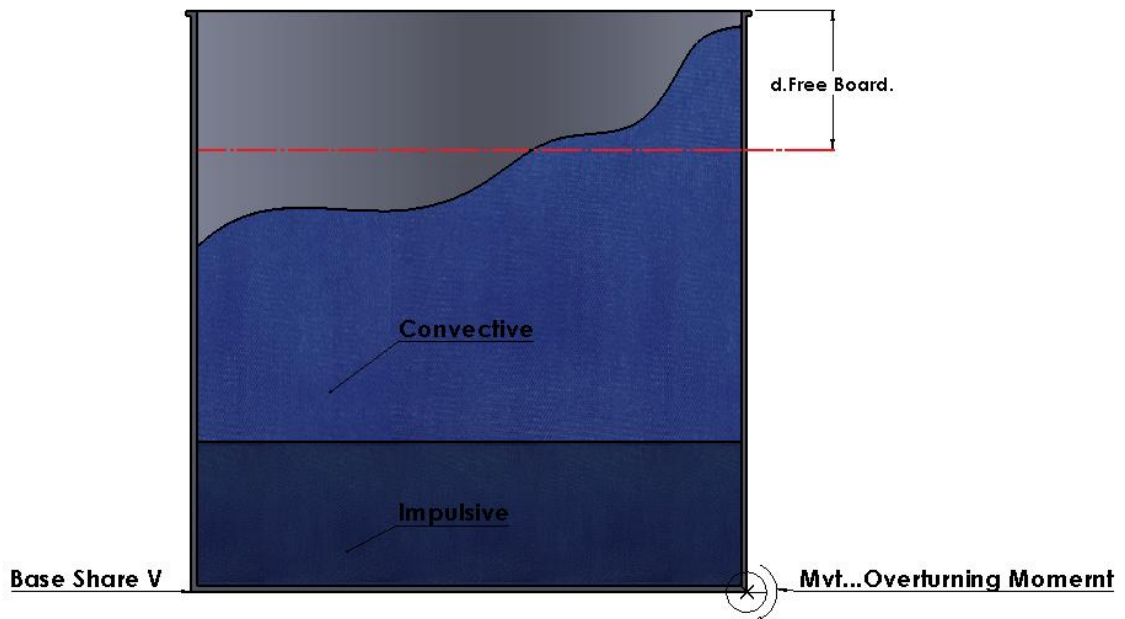


Figure 5. 5 Seismic diagram of tank (Kuan, 2009)

#### Variables of Mass

$M_s$  = Mass of Shell = 58263 N

$M_r$  = Fixed Roof Weight (Framing, 10% of design live load Included) = 11248 N

$M_i$  = Mass of impulsive = 1173539.90 N

$M_c$  = Mass of Convective = 603291.22 N

$h_s$ =5.08 m(this value was assumed to be  $0.45 \times H_{tank}$ )

$h_i$ =3.75 m.

$h_c$ =7.60 m.

#### Seismic Variables

SUG = Seismic Use Group (Importance factor depends on SUG) = 3

Site Class = E

$S_{a0}$  = 5% damped design spectral response acceleration parameter according to the specific procedures in zero period = 0.4 Decimal% g

$S_{ai}$  = 5% damped, site specific MCE response spectra at the calculated impulsive period including site soil effects = 1.32 Decimal %g

$S_{ac}$  = 5% damped, site specific MCE response spectra at the calculated convective period including site soil effects = 0.24 Decimal %g

$A_v$  = Vertical Earthquake Acceleration Coefficient = 0.55 Decimal %g

$R_{wi}$  = Force reduction factor for the impulsive mode using permissible stress design methods =4

$R_{wc}$  = Force reduction factor for the convective mode using permissible stress design methods = 2

$C_i$  = Impulsive tank system coefficient (Figure 4.1) = 7.05

$t_u$  = Equivalent uniform thickness of tank system = 6 mm.

$E$  = Elastic Modulus of Tank Material = 193928.770 Mpa.

$H$  = Tank's Design Liquid Level = 10 m.

$D$  = Tank's Diameter = 15.08 m.

$D/H$  = Ratio of Tank Diameter to Design Liquid Level= 1.5

$T_L$  = 12 seconds (from ASCE 7 maps-API 650)

$S_s$ =103g selecting (ASCE 7 values are based on the USGS 1996 values-API 650)

Assuming Site Class D, and interpolating

$F_a$  = 1.09

$Q$  = 0.67 for ASCE methods, (ASCE 7 values are based on the USGS 1996 values-API 650)

Therefore

$$S_{DS} = QF_a S_s = 75\% g$$

$R_{wi}$  = Force reduction factor for the impulsive mode using permissible stress design methods

= 3.5 tank is self-anchored (see Table 5.3)

$R_{wc}$  = Force reduction factor for the convective mode using permissible stress design methods

= 2 tank is self-anchored (see Table 5.3)

I = Importance factor defined by Seismic Use Group (SUG) = 1.5 (see table 5.4)

The sloshing height of water can be calculated equation below.

$$[5.14] \text{ Sloshing height equation } d = 0.84 R \frac{S_c(T_{con})}{g}$$

$$d = 0.84 * 7.54 \frac{1.5}{9.81} = 0.96 \text{ m}$$

$$[5.15] \text{ The impulsive spectral acceleration parameter } A_i = S_{DS} \left( \frac{I}{R_{wi}} \right) = 2.5 Q F_a S_o \frac{I}{R_{wi}}$$

$$[5.16] A_i = 0.75 * \left( \frac{1}{3.5} \right) = 0.21$$

$$[5.17] A_i \geq 0.07$$

[5.18] The convective spectral acceleration parameter

$$T_c = 3.29 \text{ second} < T_L$$

$$[5.19] A_c = K S_{D1} \left( \frac{1}{T_c} \right) \left( \frac{I}{R_{wc}} \right) = 1.5 (0.44) \left( \frac{1}{6.09} \right) \left( \frac{1}{2} \right) = 0.054 < 0.21$$

Figure 5.3 shows display response factors for ASD methods.

**Table 5. 3** Display response modification factors for ASD methods (API650, 2013)

<b>Anchorage System</b>	<b><math>R_{wi}</math> (impulsive)</b>	<b><math>R_{wc}</math> (convective)</b>
Self-anchored	3.5	2
Mechanically-anchored	4	2



Seismic use group can be determined in Figure 5.4.

**Table 5. 4** Display importance factor (I) and seismic use group (API650, 2013)

Seismic Use Group	I
I	1
II	1.25
III	1.5

The approximate formula for the recommended design curve (I=1.0) is:

$$[5.20] S_a = 0.4 + 4 * T(g) < T < 0.24 s$$

$$S_a = 1.33(g) \text{ for } 0.24 \leq T \leq 0.65 s$$

$$S_a = 2.167 - 128 * T(g) \text{ for } 0.65 < T < 1.25 s$$

$$S_a = 1.02 * \left(\frac{0.6}{T}\right)^{0.8} - 128 * T(g) \text{ for } 1.25 s < T$$

$$T_0 = 0.00 \text{ sn, } S_0 = 0.40 \text{ g}$$

$$T_i = 0.23 \text{ sn, } S_{ai} = 1.32 \text{ g}$$

$$T_A = 0.24 \text{ sn, } S_a = 1.33 \text{ g}$$

$$T_B = 0.65 \text{ sn, } S_b = 1.33 \text{ g}$$

$$T_1 = 1.00 \text{ sn, } S_1 = 0.89 \text{ g}$$

$$T_c = 3.63 \text{ sn, } S_{ac} = 0.24 \text{ g}$$

$$[5.21] \text{The impulsive spectral acceleration parameter } A_i = S_{DS}\left(\frac{I}{R_{wi}}\right) = 2.5 Q F_a S_a\left(\frac{I}{R_{wi}}\right)$$

$$[5.22] A_i = 0.75 * \left(\frac{1}{3.5}\right) * 1.32 = 0.285$$

$$[5.23] A_i \geq 0.07$$

[5.24] The convective spectral acceleration parameter

$$T_c = 3.29 \text{ second} < T_L$$

$$[5.25] V_i = A_i(m_s + m_r + m_f + m_i)$$

$$V_i = 0.285(571560.03 + 27327.71 + 28929.69 + 11546050.70)$$

$$V_i = 3469552.42 \text{ N}$$

Coefficient to adjust spectral acceleration from 5%-0.5% damping (K)  $K = 1.5$

Convective spectral acceleration parameter ( $A_c$ )

$$[5.26] A_c = KQ\left(\frac{I}{R_{wc}}\right)S_a=1.5(1)\left(\frac{1}{2}\right)0.24=0.18<0.285$$

$$[5.27] V_c = A_c W_c$$

$$V_c = 0.18 * 5918286,87$$

$$V_c = 1065291.64 \text{ N}$$

Calculating the base shear

$$[5.28] V = \sqrt{V_i^2 + V_c^2}$$

$$V = \sqrt{263469552.42^2 + 1065291.64^2}$$

$$V = 3613896.79 \text{ N}$$

Determining the Seismic Overturning Moment

$$[5.29] M_{rw} = \sqrt{[A_i(m_s * h_s + m_i * h_i)]^2 + A_c(m_c * h_c)]^2}$$

$$M_{rw} = \sqrt{[0,285(571560.03 * 5.18 + 11512426.40 * 3.75)]^2 + 0,18(5918286.87 * 7.60)]^2}$$

$$M_{rw} = 21875380.59 \text{ N}$$

The maximum allowable product design stress  $S_d$  and the maximum allowable hydrostatic test stress,  $S_t$  shall be as shown in Tables 5.5.

**Table 5. 5** Permissible plate materials and allowable stresses (API650, 2013)

Tank material	Min. Yield Strength	Min. Tensile Strength	Design Stress ( $S_d$ )	Hydrostatic Stress( $S_t$ )
SA 537 CLASS-	345 Mpa	485 Mpa	194 Mpa	208 Mpa

Initially in this chapter, four steel cylindrical tanks (open-top, flat-closed, conical-closed and torispherical-closed models) having different aspect ratios are modelled in 3-D space and their free vibration (modal analysis) results are compared with those obtained through API 650 approaches.

The aim of this thesis is to carry out the seismic analysis of cylindrical steel tanks with four different roof types by the method of ten decades. In the following table, some seismic conditions calculated for the over-open tank model by the API 650 standardization formula to validate the model are presented in Table 5.6.

**Table 5. 6** Results calculated of cylindrical model tank according the API 650 formulation

<b>Title</b>	<b>Value</b>
The total volume of water	1780,4 m <sup>3</sup>
Total mass of water in the tank	1780400 Kg
Ratio of radius to water height (R/h)	0.754 m
Ratio of height to radius (h/ R )	1.32 m
Mass of impulsive	1173539,90 Kg
Mass of convective	603291,22 Kg
Location of impulsive mass( $h_i$ )	3.75 m
Location of convective mass ( $h_c$ )	7.60 m
The natural frequency of impulsive mass( $\omega_i$ )	3.26 Hz
The natural frequency of convective(sloshing) ( $\omega_c$ )	0.246 Hz
The impulsive period <b><math>T_i</math></b>	0.29 sec
The convective period <b><math>T_c</math></b>	3.29 sec
Mass of Shell	5939.14 Kg
Weight of Fixed Roof	1146.58 Kg
Location of System <b><math>h_s</math></b>	5.08 m
Sloshing height of Water <b><math>d</math></b>	0.96 m
Calculating the base shear <b><math>V</math></b>	3613896.79 N
The Seismic Overturning Moment	21875380.59 N

Minimum yield Strength	345 Mpa
Min. Tensile Strength	485 Mpa
Design Stress ( $S_d$ )	194 Mpa
Hydrostatic Stress( $S_t$ )	208 Mpa

### 5.3 Seismic Analysis with Finite Element Method

This section deals with seismic analysis of cylindrical steel storage water tanks. In this study, the dynamic results of finite element method are compared with those recommended by current practice and current code provisions.

#### 5.3.1 Modal analysis

The modal analysis determines the vibration characteristics (natural frequencies and mode shapes) of a structure or a machine component. At the same time, it can serve as a starting point for another, more detailed, dynamic analysis, such as a transient dynamic analysis, a harmonic analysis, or a spectrum analysis. Natural frequencies and mode shapes are important parameters in the design of a structure for dynamic loading conditions. A modal analysis can also be made on a pre-stressed structure. The dynamics loading of a structure are physically decomposed by frequency and position. Natural vibration modes are specific to a dynamic system and are defined by their physical properties (mass, stiffness, damping) and their spatial distribution. Each mode is defined in terms of its modal parameters: natural frequency, modal damping factor, and characteristic displacement pattern, namely mode shape. Each natural mode is determined by both the stimulus source (s) properties as well as the mode shape of the system. These properties can be given as partial differential equations. The solution of the equation provides the natural frequencies, damping factors and mode shapes.

Any nonlinearity of material behaviour, which is nature to modal analysis, is ignored. Depending on demand, orthotropic and temperature dependent material properties can be used. The critical requirement is to define the hardness and mass in a certain way. The hardness can be determined, for example, using hyperelastic material models (linearized to an equivalent combination of initial mass and shear modulus) or isotropic and orthotropic elastic material models (Young's modulus and Poisson's ratio, e.g.) using, for

example, spring constants. The mass can be derived from material density or from distant masses. (ANSYS, 2018).

Four cylindrical steel tank models with different aspect ratios, representative of four classes of tanks namely "open-top", "flat-closed", "conical-closed" and "torispherical-closed" are considered for 3-D FEM analysis throughout this chapter. In this study, the effect of soil-structure interaction is not included. Since only ground supported tanks are considered, the tank floor is not included in the FEM model. The tank walls and base are considered to be of constant thickness. Sample tank models are shown in Figure 5.6.



a) Open-top

b) Flat-closed

c) Conical-closed

d) Torispherical-closed

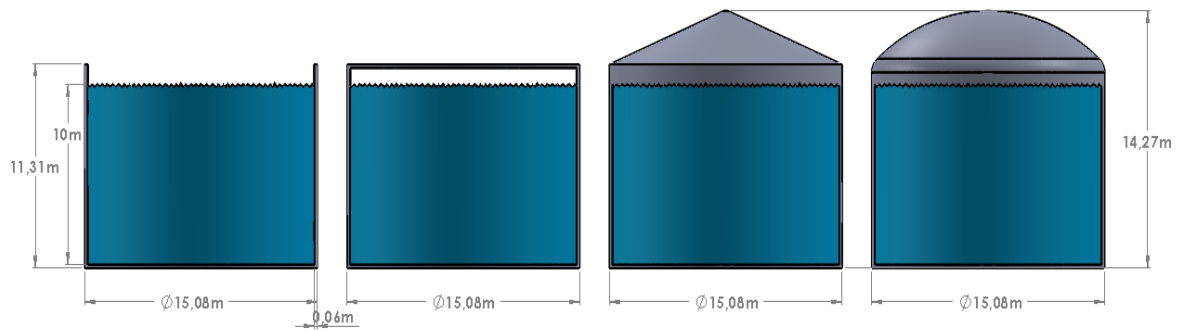
**Figure 5. 6** Classes of cylindrical steel tank

Table 5.7 shows the minimum shell thickness of cylindrical steel tanks according the API 650 standard. Since the tank used in this study had a diameter of 15.08 m, the minimum tank shell thickness was determined to be 6 mm. Then, the analyses were carried out at 4 mm and 8 mm shell thickness with a 2 mm reduction and a 2 mm increase.

**Table 5. 7** Shell thickness according the API 650 standard (API650, 2013)

Diameters	Minimum Thickness
$\leq 15 \text{ m (50')}$	5 mm (3/16 in)
$15\text{m} < D \leq 36 \text{ m}$ or $50' < D \leq 120'$	6 mm (1/4 in)
$36\text{m} < D \leq 60 \text{ m}$ or $120' < D \leq 200'$	8 mm (5/16 in)
$>60 \text{ m (200')}$	10 mm (3/8 in)

Representative view and measurements of the analysed tanks are presented in Figure 5.7 respectively for open-top, flat-closed, conical-closed and torispherical-coated tanks.



**Figure 5. 7** Dimensions of tanks

### 5.3.1.1 Verification of model

Numerical verification is necessary to show that numerical models can predict responses with reasonable accuracy and precision. For this reason, a seismic and dynamic modal analysis of the sample tank model was carried out. Modal analysis is used to understand the behaviour of a structure. The cylindrical steel storage tank and fluid body were modelled with ANSYS Workbench 16.2. The materials used to model the water storage tank are the structural steel and water element. The density of structural steel was  $7850 \text{ kg/m}^3$ , Young Module  $210 \text{ GPa}$ , and Poisson Ratio  $0.3$ . Water density of water  $1000 \text{ kg/m}^3$  and bulk module  $2.2 \text{ GPa}$  were determined.

Modal analysis was carried out for all three (T1,T2,T3) tanks with different fluid fill levels. Modal analysis carried out for with different water levels of  $10 \text{ m}$ ,  $7.5 \text{ m}$  and  $5 \text{ m}$ . Description of the 3D Finite Element Models The problem of interaction between the shell and the liquid is modelled using Shell 281, Solid 186, Contact 174, and Target 170 elements. The mesh model of tanks is shown in Figure 5.8.

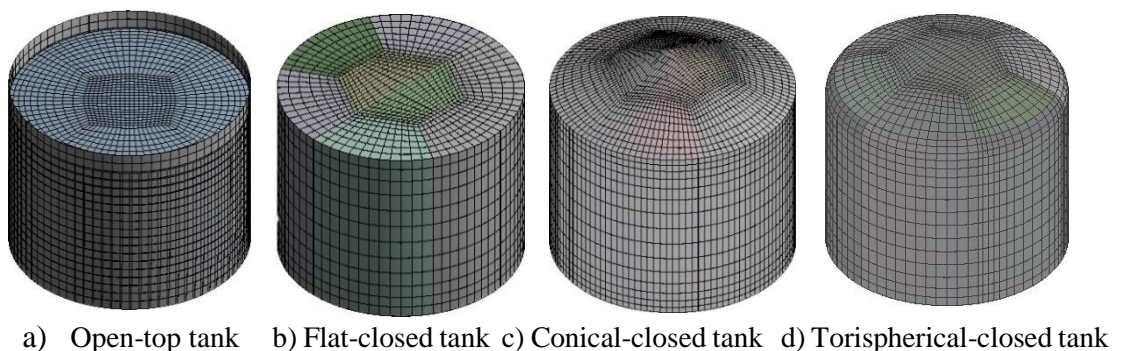
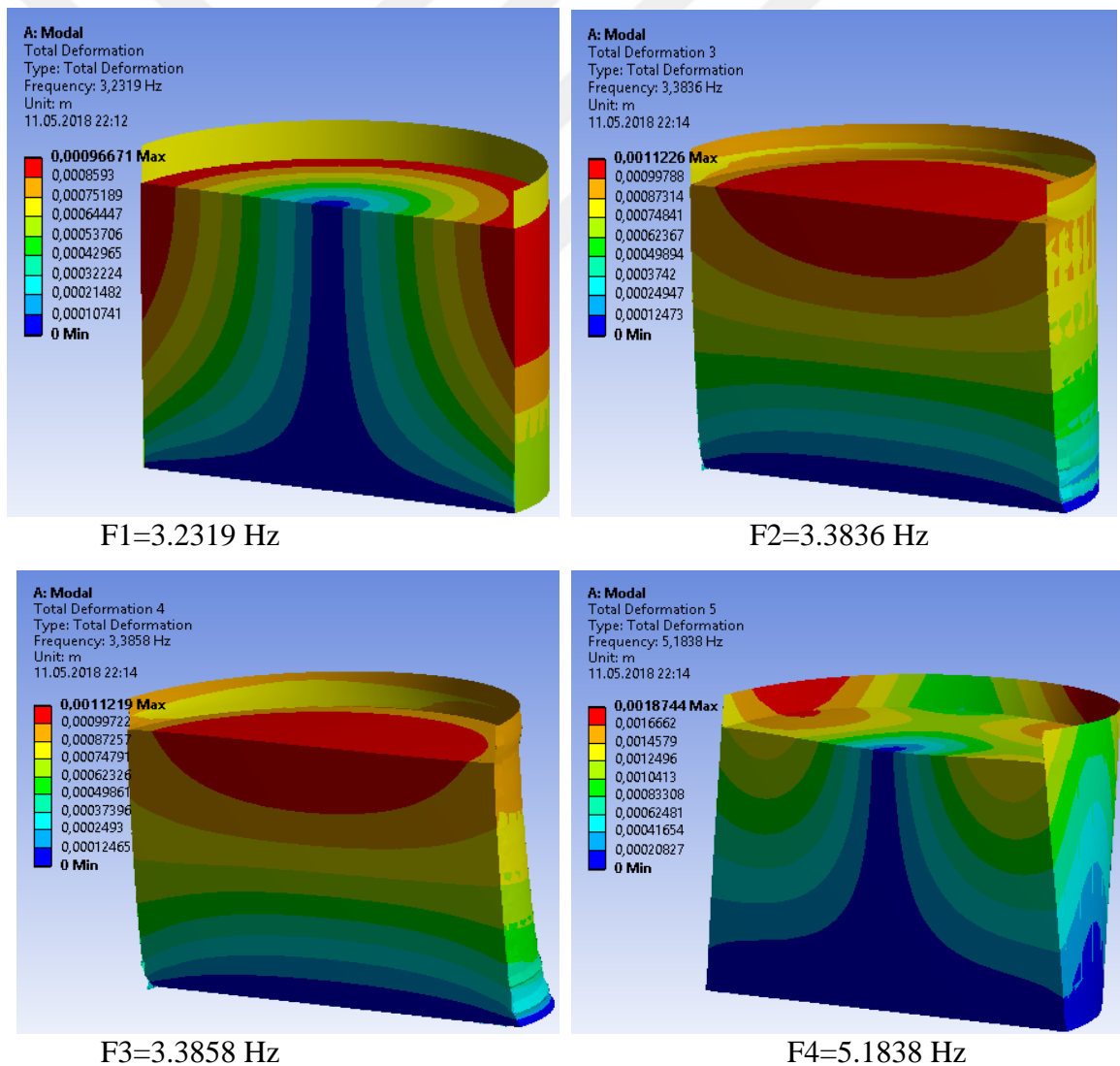


**Figure 5. 8** Meshed view of all tanks

### 5.3.1.2 Modal analysis of open tank model

A modal analysis determines the vibration characteristics of a structure or a machine component. In designing structure that is exposed to a dynamic load, the natural frequencies and mode shapes of a structure are very important. It can be considered as a starting point for a transient dynamic analysis. At the same time, the response of a structure may be evaluated when these modes are excited. Modal analysis was performed in ANSYS Workbench software. If the model parameters are defined true, it can be obtained results close to accurate values.

Generation and Meshing of the finite elements for the shell of the tanks are based on the width of the plates used to form them. It is assumed that the damping factor is 2% for both tanks. The first 6 modes and frequencies values of the open tank model are shown in Figure 5.9.



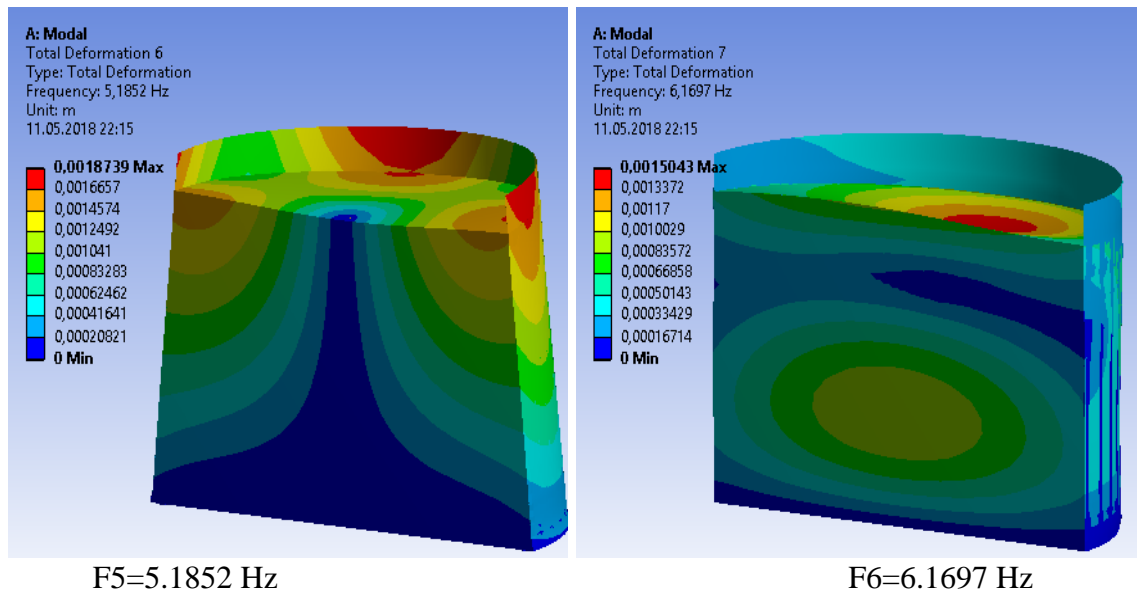
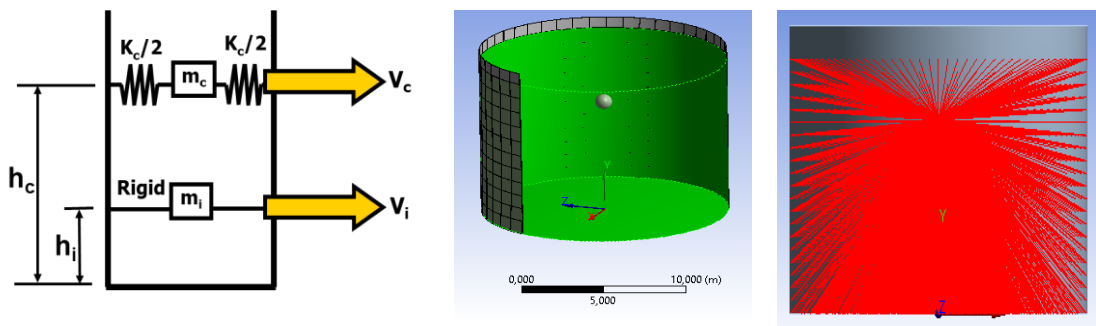


**Figure 5. 9** Impulsive modal analysis results and frequencies

The motion of contained fluid in vertical cylindrical tanks on-ground, fixed to the under the base of tank, may be expressed as the sum of two separate contributions, called “impulsive” and “convective,” respectively. When the water tank is accelerated under seismic conditions a part of the liquid mass moves in unison with the tank. This part of the liquid mass is known as the impulsive mass. The vibration modes set up by this mass are called the impulsive modes. Other part of the liquid mass be exposed vibration due to it’s inertia properties and cause sloshing. This part of the liquid mass is called the convective mass and the vibration modes set up by this mass are called the convective modes. Housner’s spring mass model and application of convective mass in FEM model is shown in below.

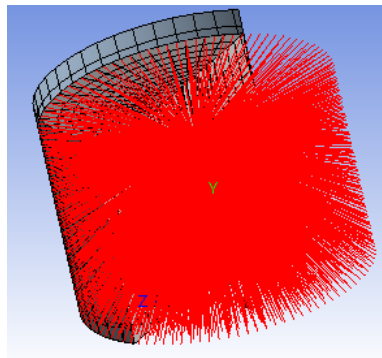


a) Housner’s spring mass model      b) Added convective mass      c) Simulation of convective mass

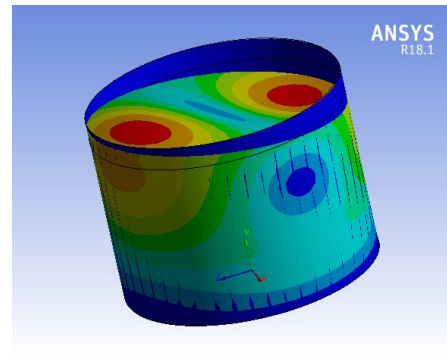
**Figure 5. 10** Simulation and application of mass model



The convective mass is located at the position indicated by  $h_c$  in the upper part of tank and represents the liquid mass causing the liquid face sloshing. Point mass was moved with liquid mass and it exposed the sloshing the face of water. Distribution of convective mass and sloshing of water are shown in Figure 5.11.



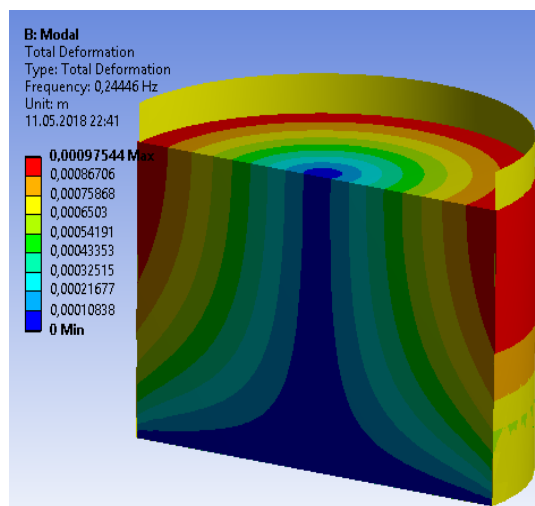
a) Distribution of convective mass



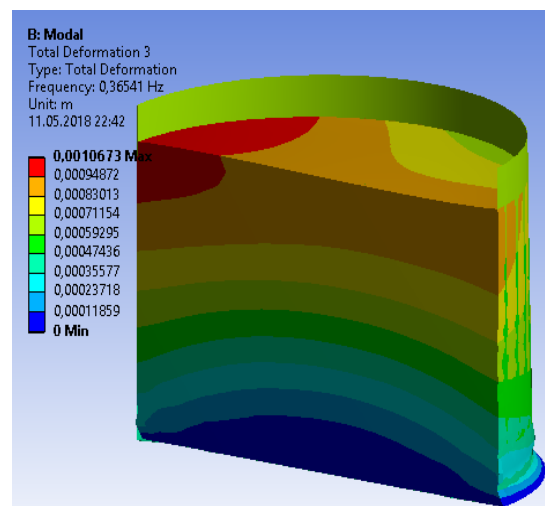
b) Convective (Sloshing) effect of water

**Figure 5. 11** Distribution point mass and sloshing effect

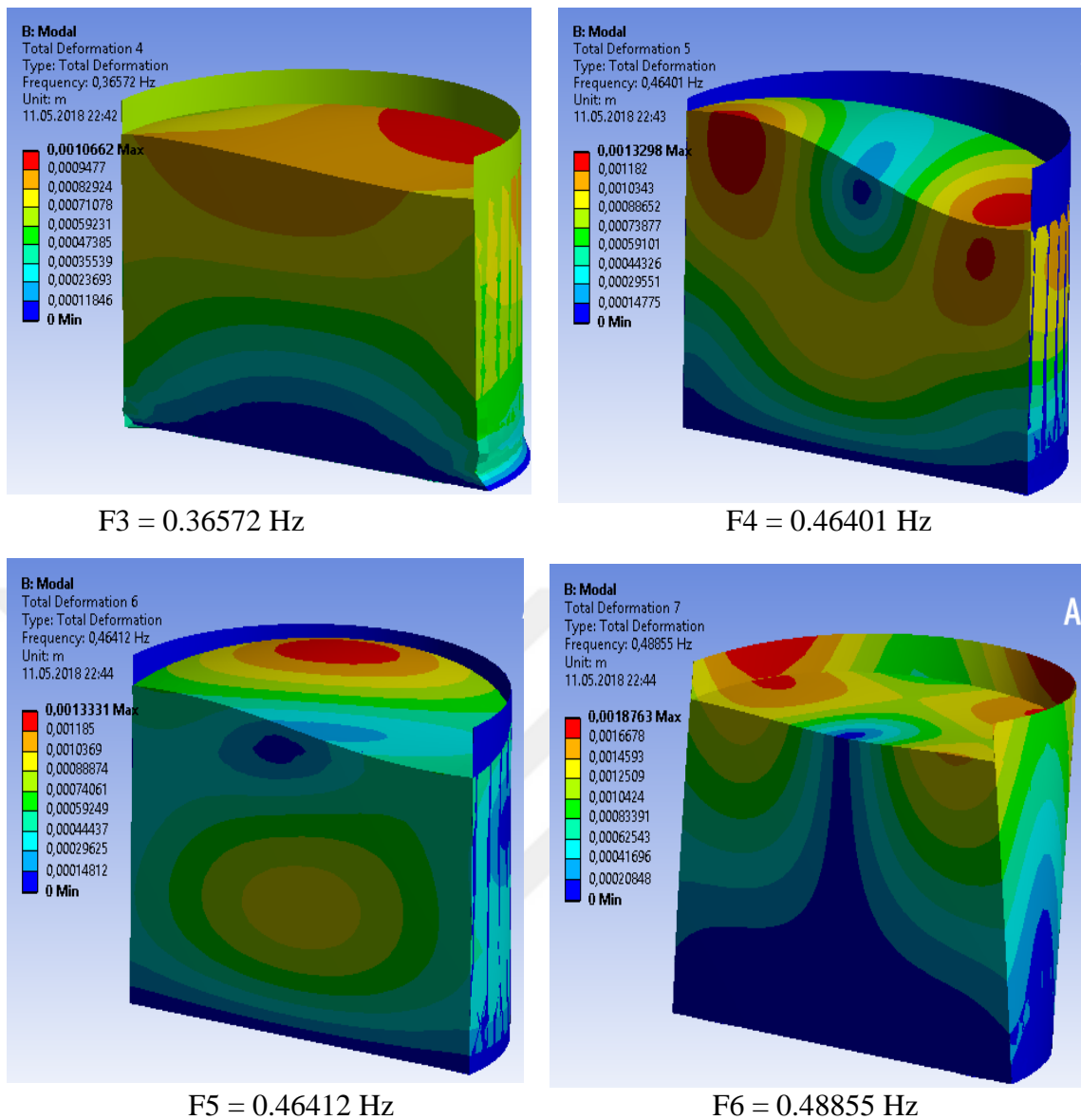
Interaction between structure and liquid has vital importance. Great effort was made to accurate the interaction between the shell and the liquid. The results of the modal analysis performed in the ANSYS workbench software using the finite element model were compared the API 650 formulation calculated method. The first convective modes are shown in Figure 5.12



F1 = 0.24446 Hz



F2 = 0.36541 Hz



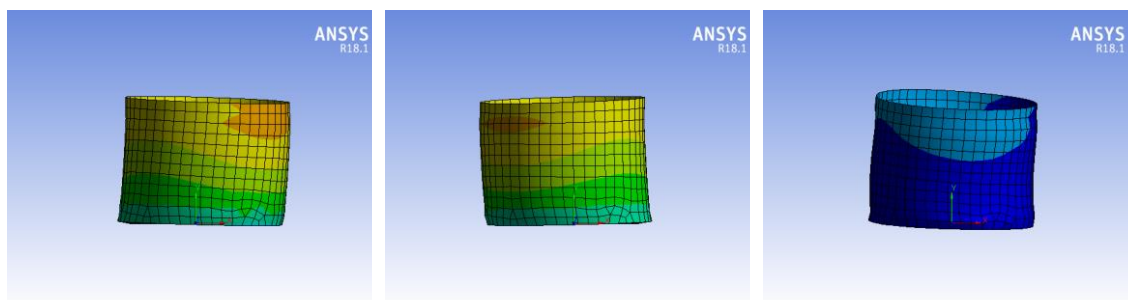
**Figure 5. 12** Convective modal analysis results and frequencies

Table 5.8 compares the results between FEM analysis frequencies and API 650 formulation calculated frequencies values respectively. In fact, in this study, there is no analysis about the different level of water in the tank, but in the literal data in the literature, the frequency values should increase as the water level is decreased. In the case of model verification, frequency values for different water levels are shown in the table below.

**Table 5. 8** Modal analysis results of circular steel water tank

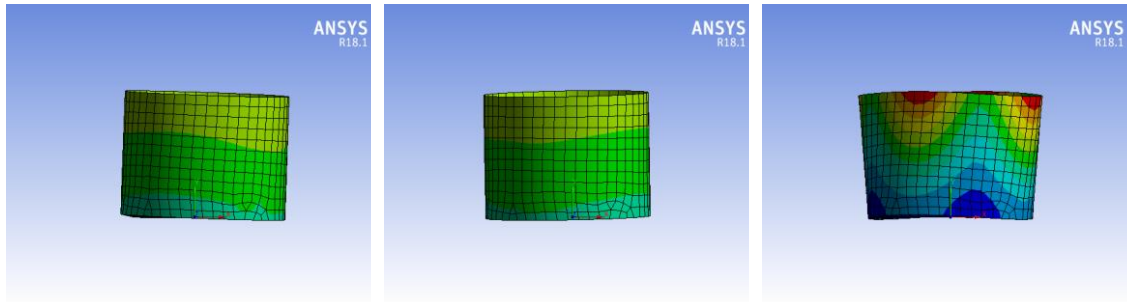
Depth of Liquid		Impulsive Frequency (Hz)		Convective Frequency (Hz)	
		Fem Model	API 650	Fem Model	API 650
10 m.	Mod1	3,2319 Hz	3,24 Hz	0.24446 Hz	0,246 Hz
	Mod2	3,3836 Hz	NA	0.36541 Hz	NA
	Mod3	3,3858 Hz	NA	0,36572 Hz	NA
	Mod4	5,1838 Hz	NA	0,46401 Hz	NA
	Mod5	5,1852 Hz	NA	0,46412 Hz	NA
	Mod6	6,1697 Hz	NA	0,48855 Hz	NA
7.5 m.	Mod1	4,2803 Hz	4,29 Hz	0,28136 Hz	0,279 Hz
	Mod2	4,4083 Hz	NA	0,4301 Hz	NA
	Mod3	4,412 Hz	NA	0,43064 Hz	NA
	Mod4	5,5081 Hz	NA	0,53004 Hz	NA
	Mod5	5,54 Hz	NA	0,53011 Hz	NA
	Mod6	6,4914 Hz	NA	0,60361 Hz	NA
5 m.	Mod1	5,7826 Hz	5,80 Hz	0,34523 Hz	0,339 Hz
	Mod2	5,879 Hz	NA	0,56491 Hz	NA
	Mod3	5,9026 Hz	NA	0,56559 Hz	NA
	Mod4	6,2702 Hz	NA	0,63665 Hz	NA
	Mod5	6,2723 Hz	NA	0,63683 Hz	NA
	Mod6	6,3601 Hz	NA	0,70427 Hz	NA

Some basic impulsive mode shapes are shown below.



a) Impulsive tank shapes

Some convective mode shapes are shown below.

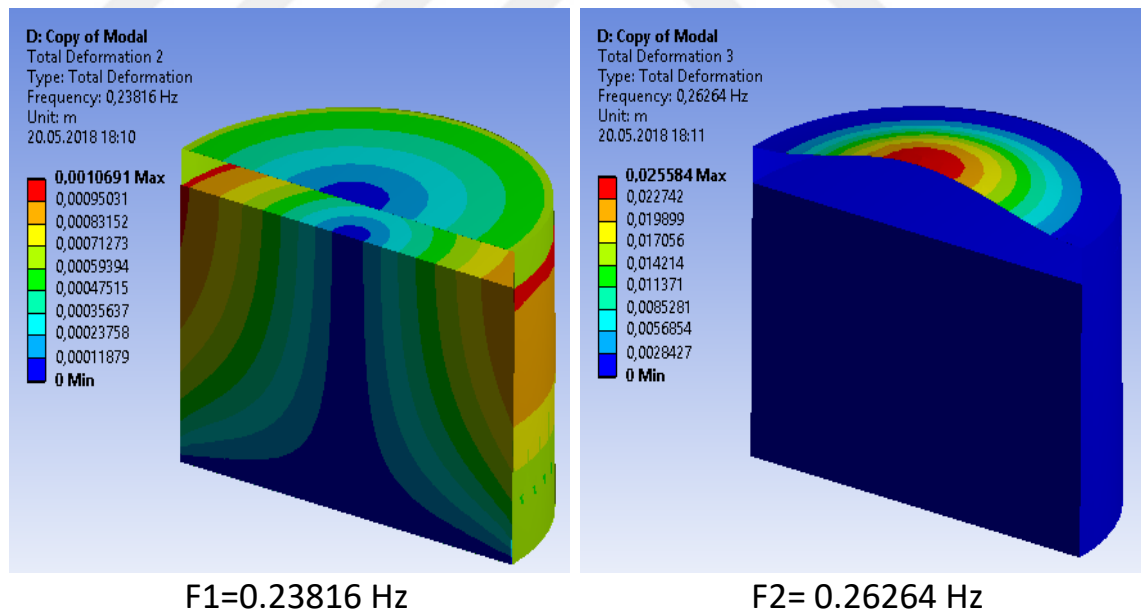


b) Convective tank shapes

**Figure 5. 13** Impulsive and convective tank shapes

### 5.3.1.3 Modal analysis of flat, conical and torispherical closed top tanks model

The impulsive modal analysis results of roof flat-closed tank are shown in Figure 15.14. In this model, the frequencies values differed from open-top tank model. This requires focusing on the seismic analysis of flat-closed top tanks.



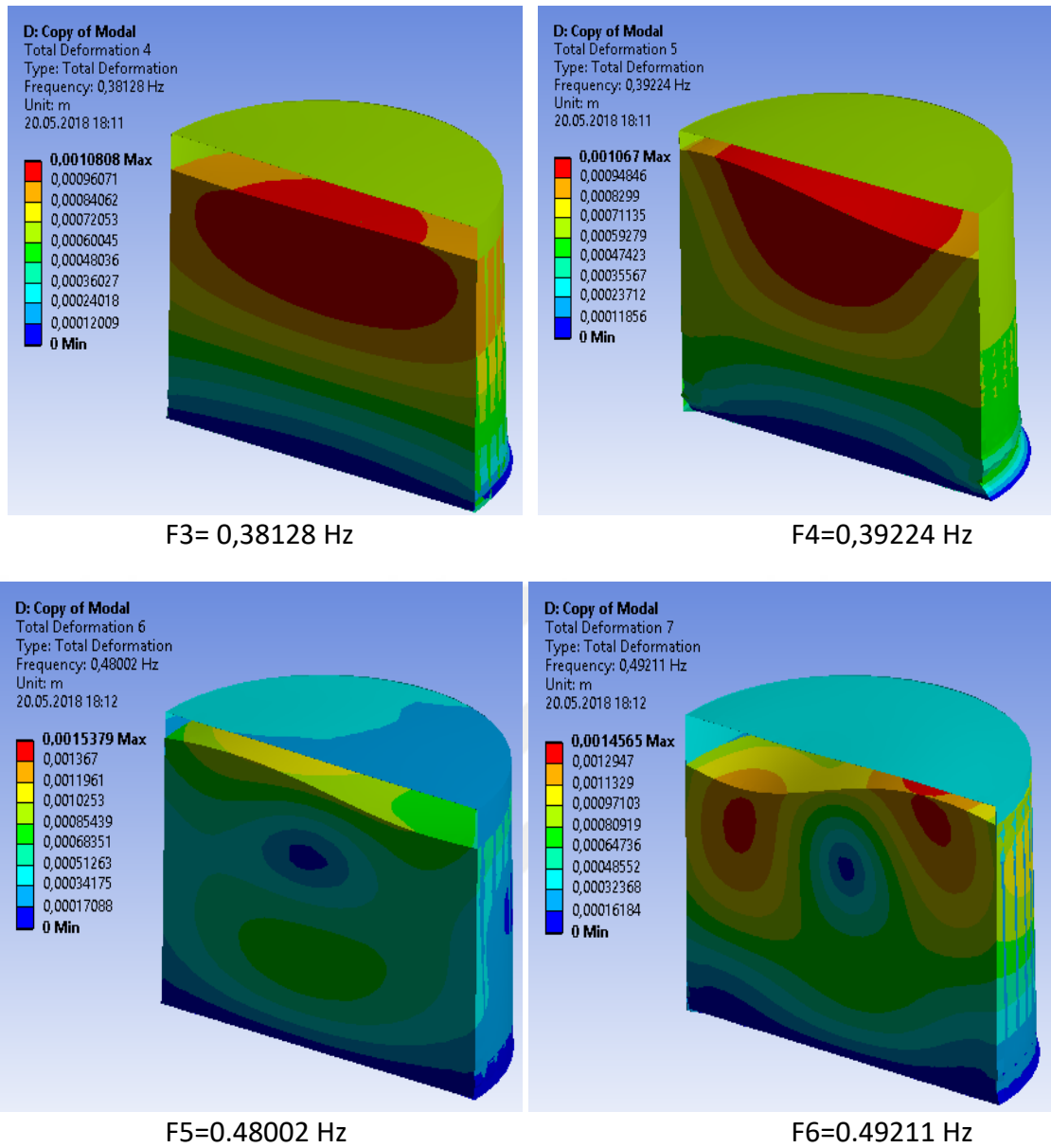
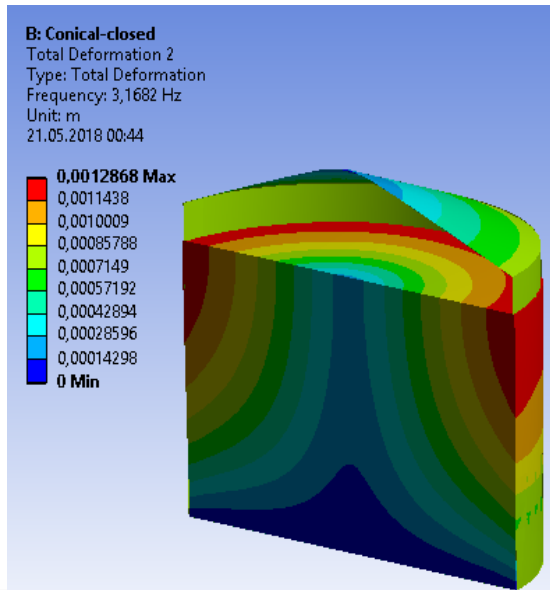
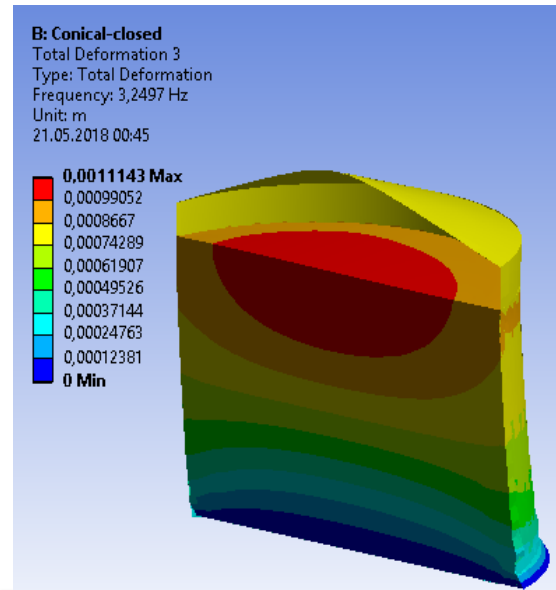


**Figure 5. 14** Impulsive modal analysis results and frequencies of flat-closed tank

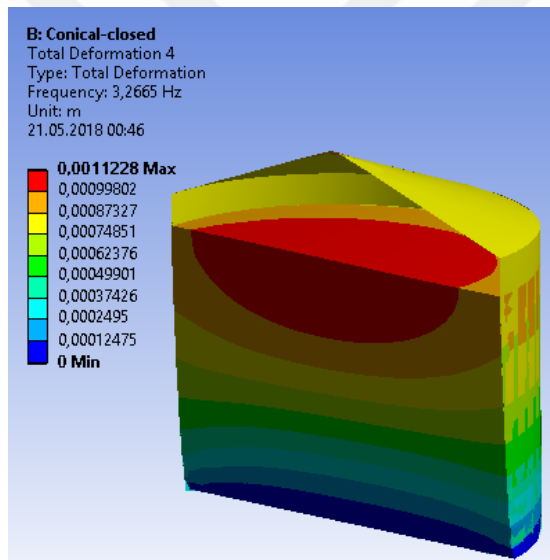
Figure 5.15 shows impulsive modal analysis results of conical-closed tank. Conical modal results values similar the open-top tank modal results.



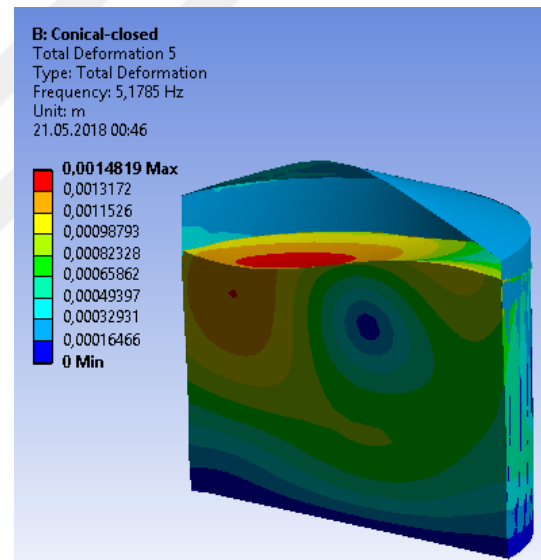
F1=3.1682Hz



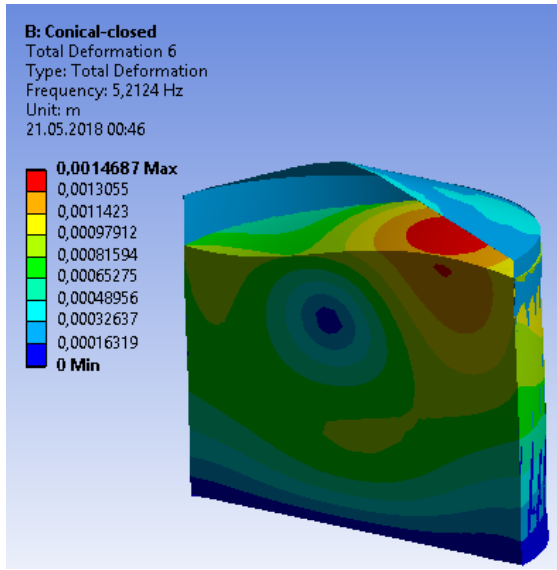
F2=3.2497Hz



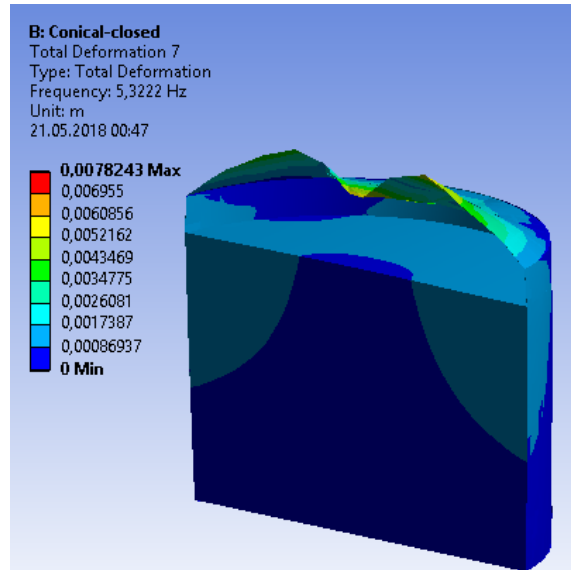
F3=3.2665 Hz



F4=5.1785Hz



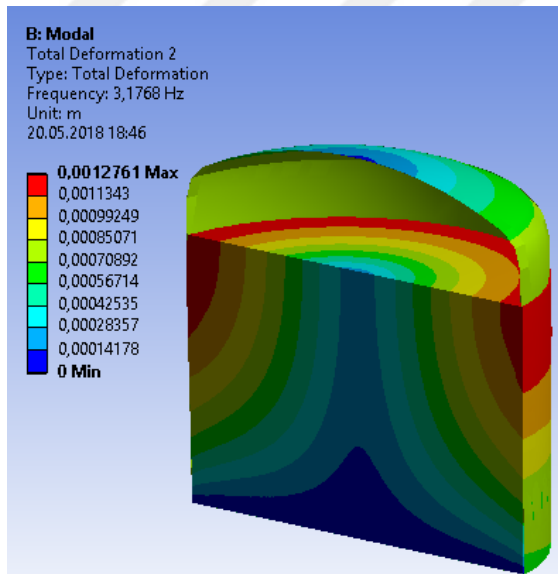
F5=5.2124Hz



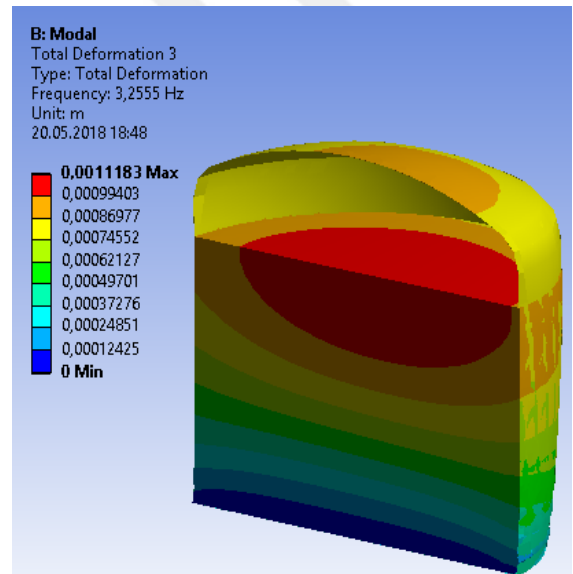
F6=5.3222 Hz

**Figure 5. 15** Impulsive modal analysis results and frequencies of conical-closed tank

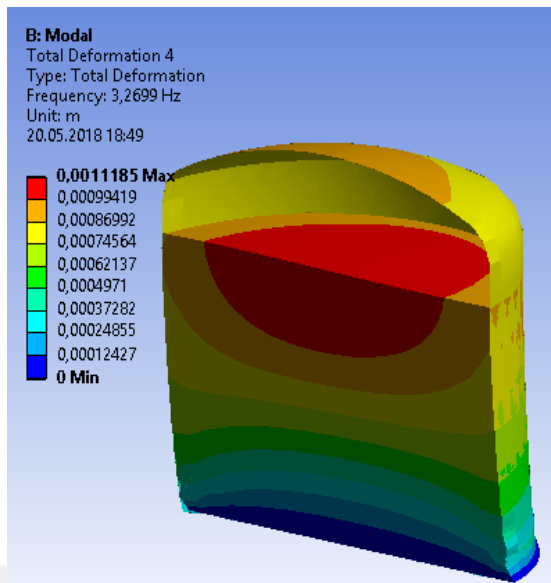
Torispherical-closed tank's impulsive natural vibration results values are shown in Figure 5.16. Results similar the open-top and conical-closed top tank model results.



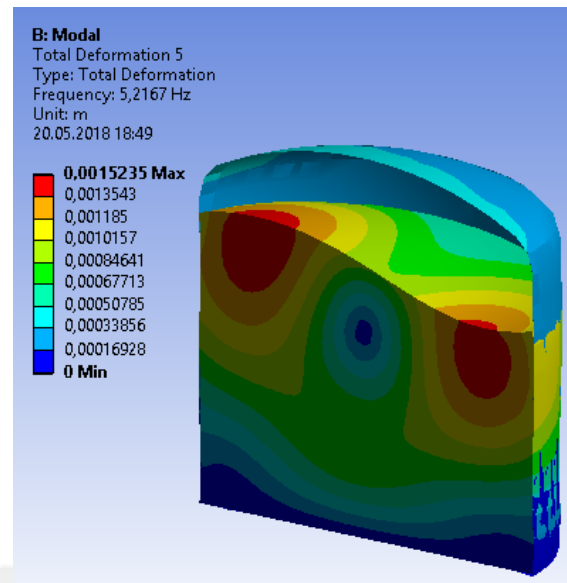
F1=3.1768 Hz



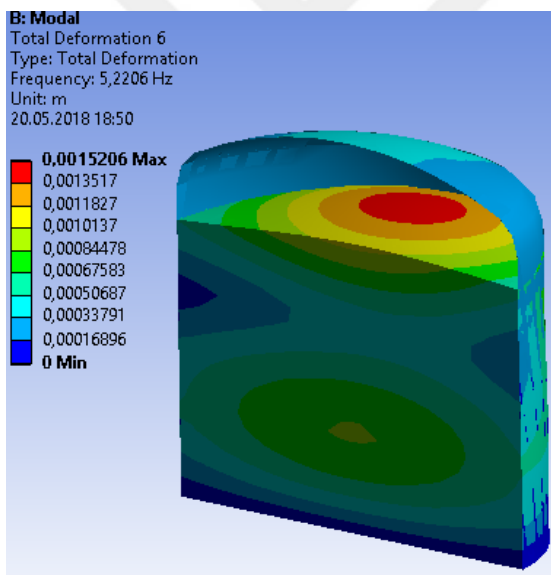
F2= 3.2555 Hz



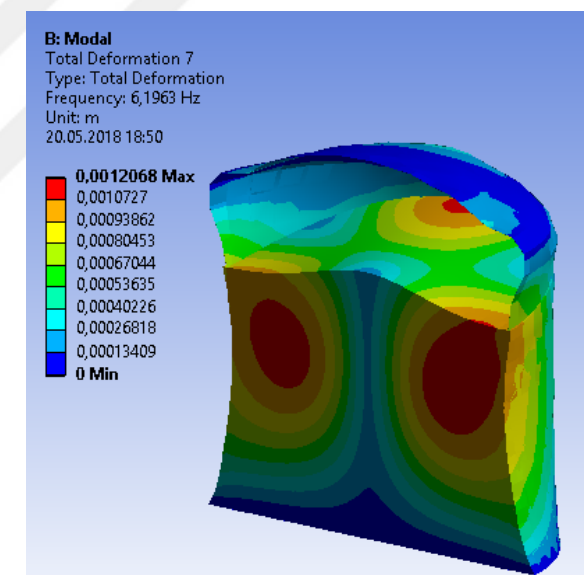
F3= 3.2699 Hz



F4= 5.2167 Hz



F5= 5.2206 Hz

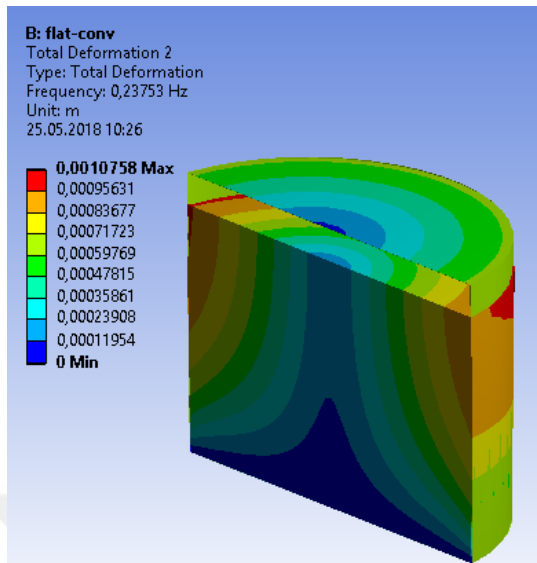


F6=6.1963 Hz

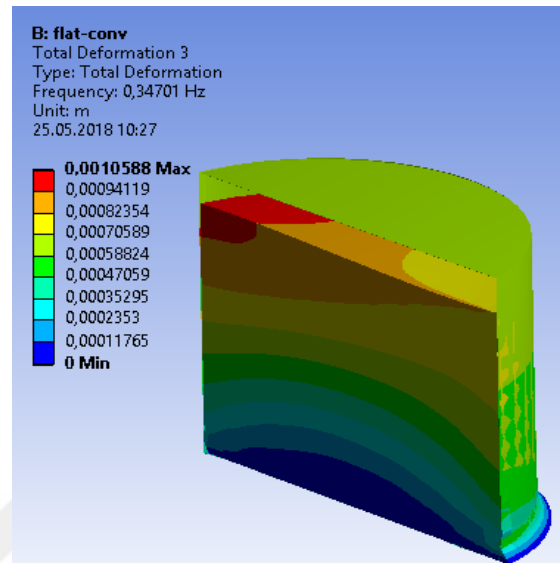
**Figure 5. 16** Impulsive modal analysis results and frequencies of torispherical-closed tank



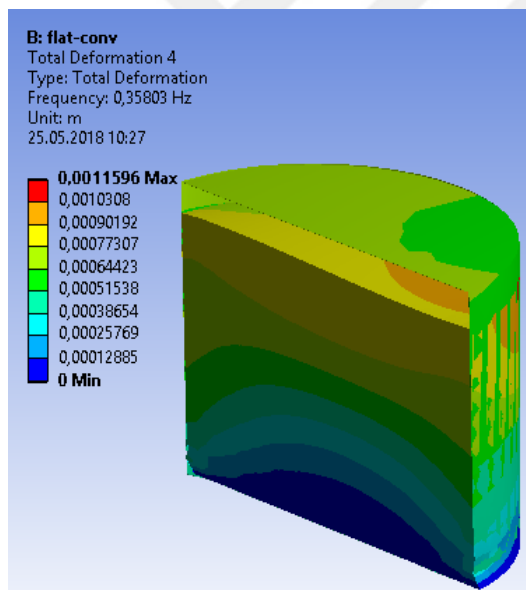
Convective free vibration results are shown in Figure 5.17, Figure 5.18 and Figure 5.19 for flat-closed, conical-closed and torispherical-closed top respectively.



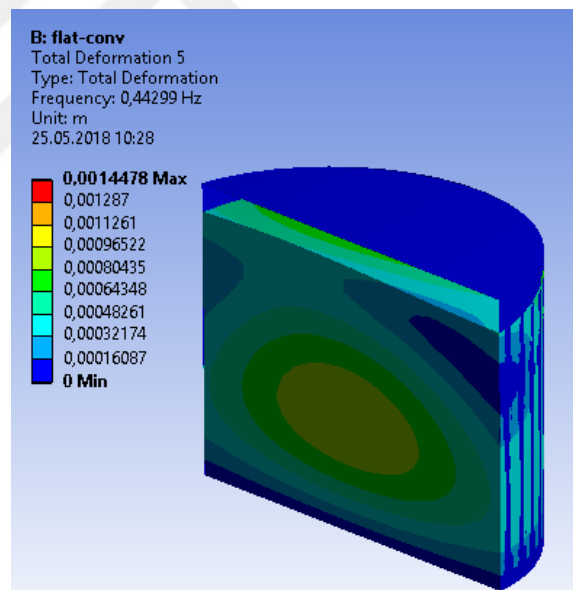
F1= 0.23753 Hz



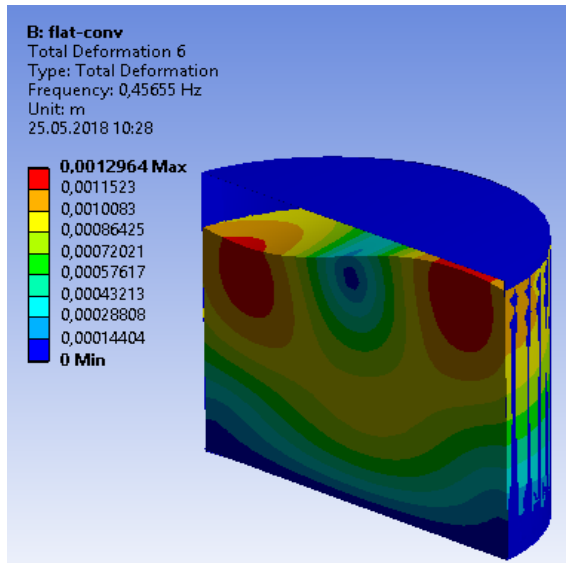
F2= 0.34701 Hz



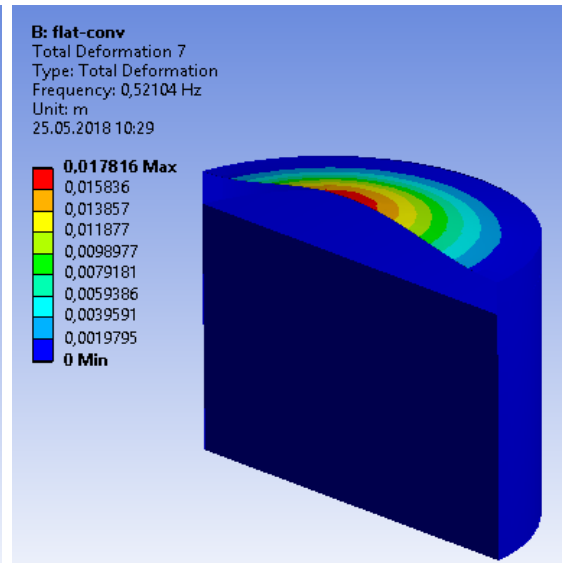
F3=0.35803 Hz



F4= 0.44299 Hz



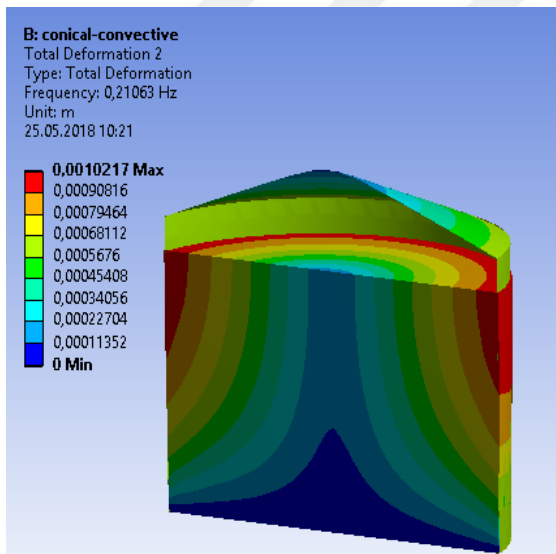
F5= 0.4641 Hz



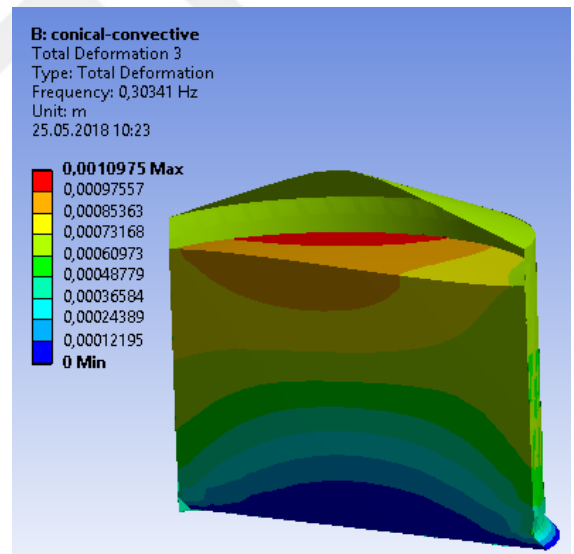
F6= 0.51963 Hz

**Figure 5. 17** Convective modal analysis results and frequencies for flat-closed tank.

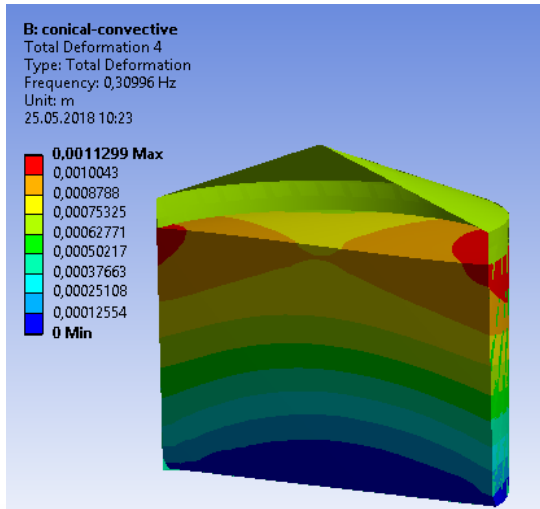
Figure 5.18 shows convective modal analysis results of conical-closed tank.



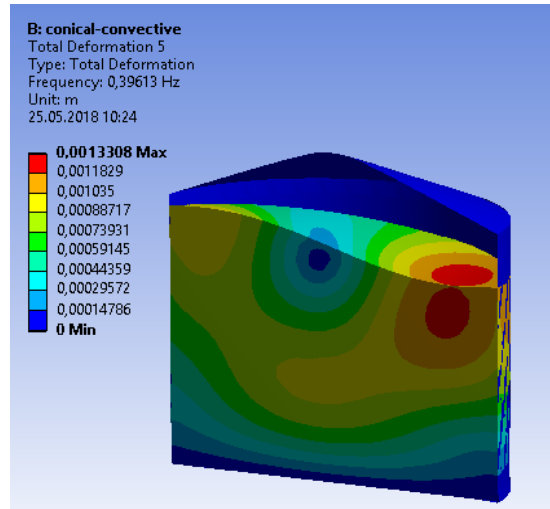
F1= 0.21063 Hz



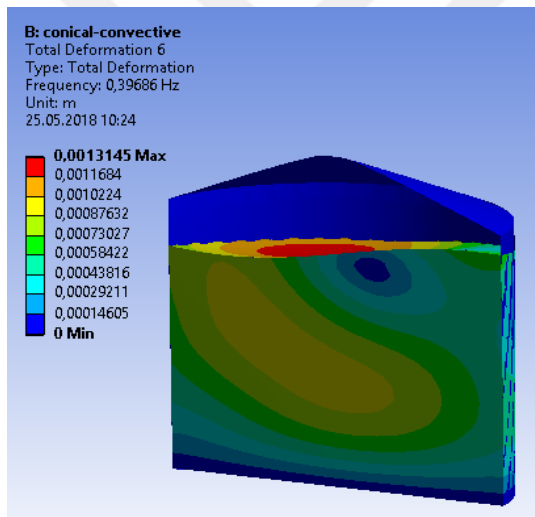
F2= 0.30341 Hz



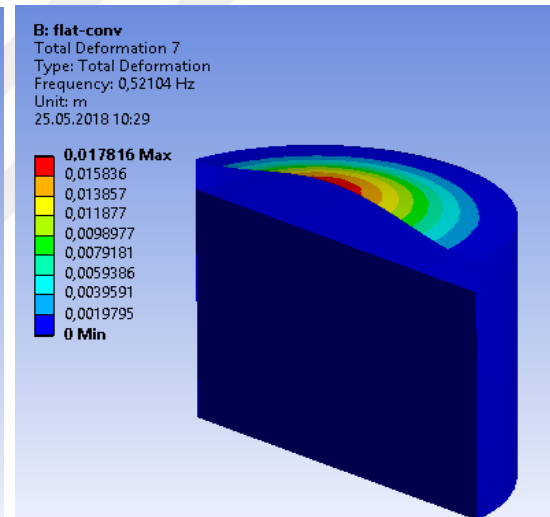
F3= 0.30996 Hz



F4= 0.39613 Hz



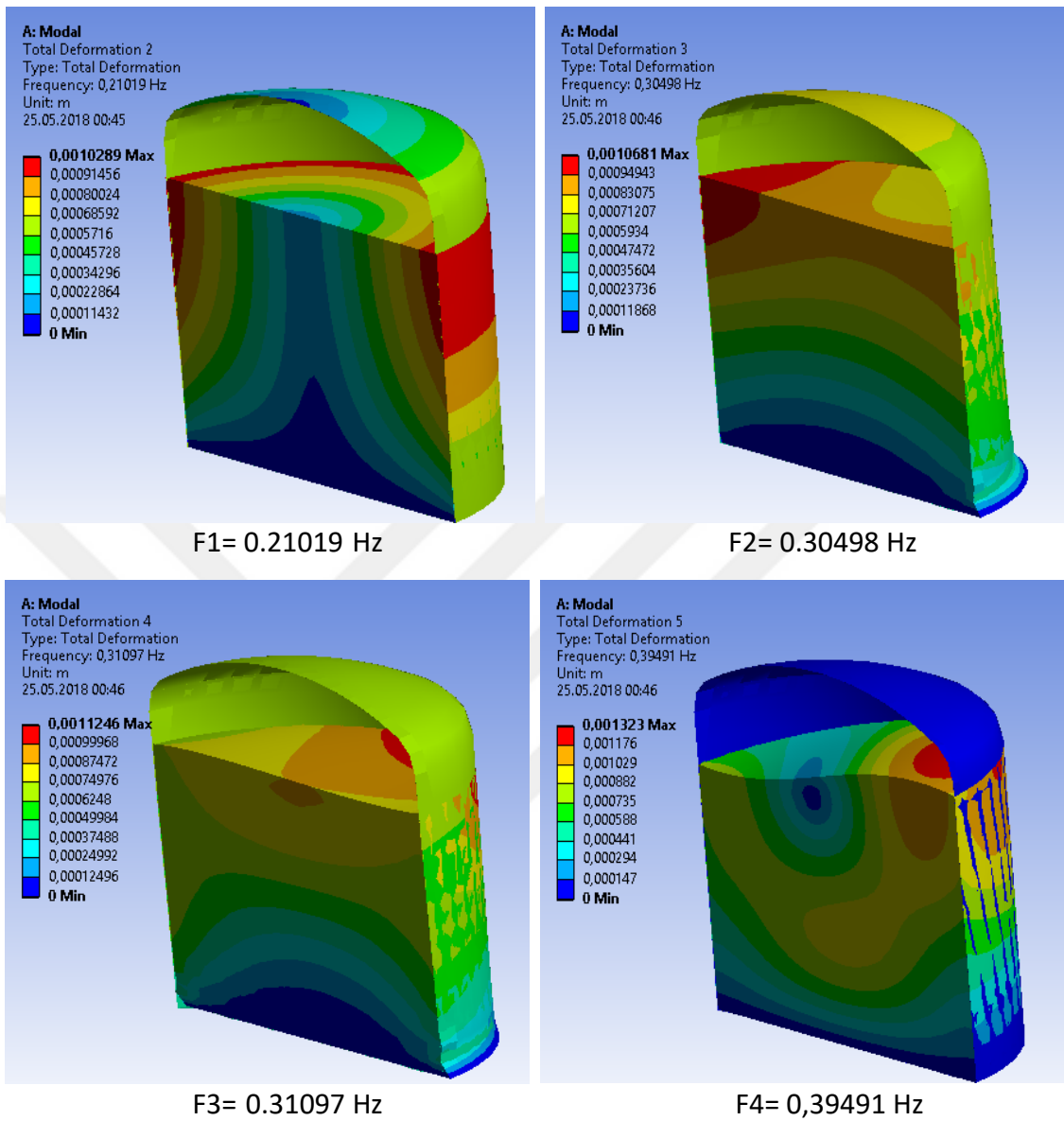
F5= 0.39686 Hz



F6= 0.53104 Hz

**Figure 5. 18** Convective modal analysis results and frequencies for conical-closed tank.

Figure 5.19 shows convective modal analysis results of torispherical-closed tank.



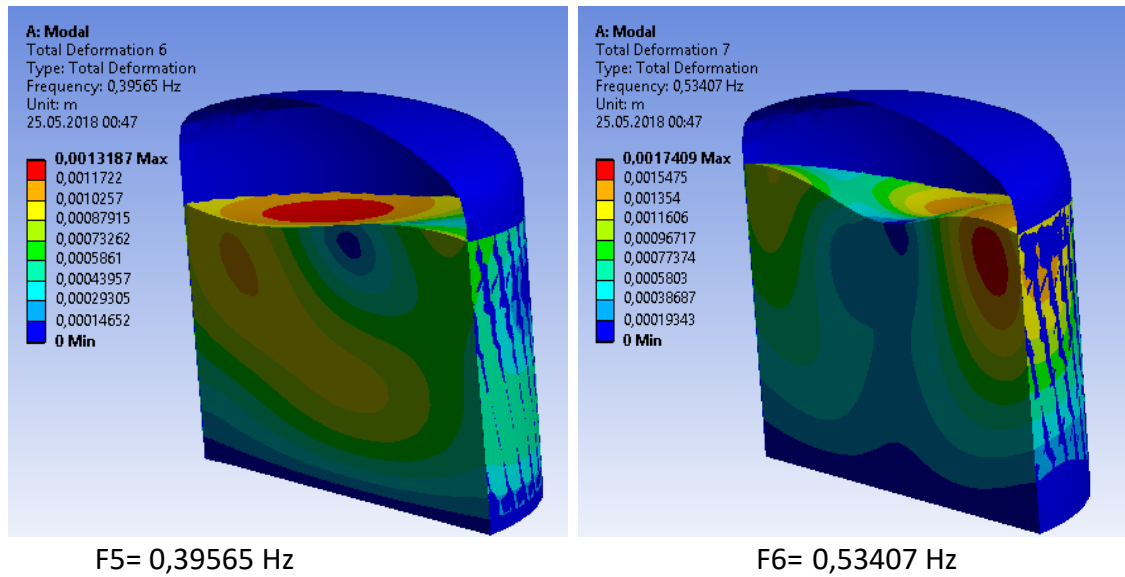


**Figure 5. 19** Convective modal analysis results and frequencies for torispherical-closed tank

Modal analysis was performed for four different roof-type tanks, which are the open-top, flat-closed, conical-closed and torispherical-closed tanks. Furthermore, frequency modes have also been compared to determine presence of a roof on the impulsive and convective periods. These comparisons are shown with graphs in the Figure 5.20 and Figure 5.21. In Figure 5.8, the flat-closed-top tank model in the impulsive period attracts attention with its low frequency values. Torispherical-closed-top tank has maximum frequencies and deformation values.

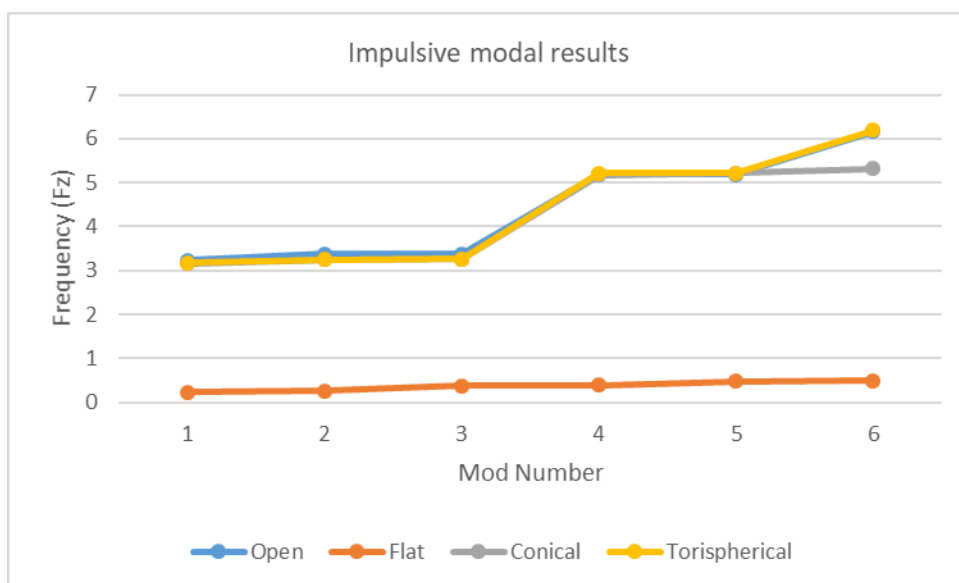


**Figure 5. 20** Impulsive modal analysis results and frequencies

Figure 5.21 shows very different results in convective period, with the open-top tank and the values in the flat-closed tank overlapping at the same time, the flat tank has highest frequencies while torispherical tank has the lowest frequency and deformation

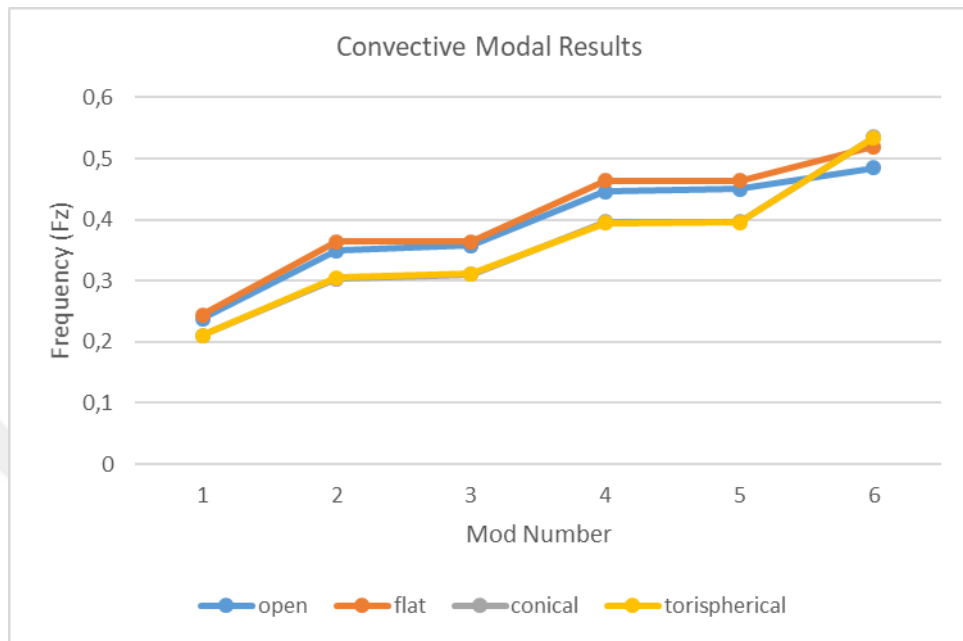


**Figure 5. 21** Convective modal analysis results and frequencies

#### 5.4 Analysis of Response Spectrum

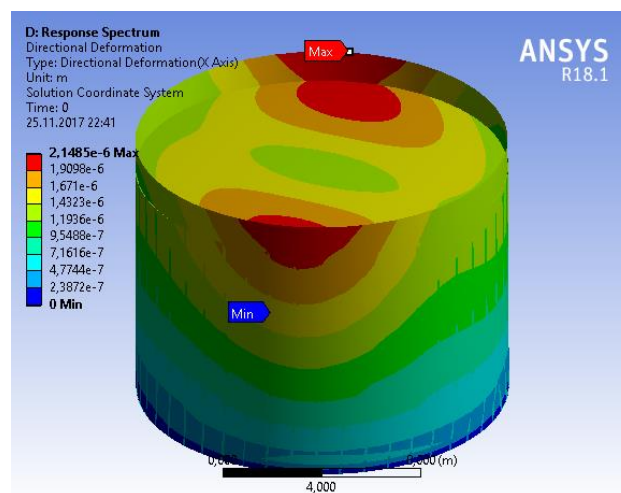
Response spectrum analysis is a linear-dynamic statistical analysis method that measures the contribution of each natural vibration mode to show the possible maximum seismic response of an elastic structure. Response-spectrum analysis provides information about dynamic behaviours by measuring pseudo-spectral acceleration, velocity, or displacement as a function of the structural period for a given time history and damping level. For envelope response spectra, the smooth curve is practical to represent the peak response for each realization of the structural period.

Response-spectrum analyses are useful in decision making because structure type selection is related to dynamic performance. While shorter-term structures gain greater momentum, longer-term experiences tend to be more intense. Structural performance targets must be considered during preliminary design and response spectrum analysis. (Ondrej, 2014).

Response spectrum analyses are widely used in civilian structure designs, for example in high buildings under wind loads. Another priority application is for nuclear power plant designs under seismic loads. A Response Spectrum analysis is similar to a Random Vibration Analysis. However, unlike a Random Vibration analysis, responses from an Interference Spectrum analysis are the deterministic maximum. For a given stimulus, the maximum response is calculated according to the method used to combine the input Response Spectrum and modal responses.

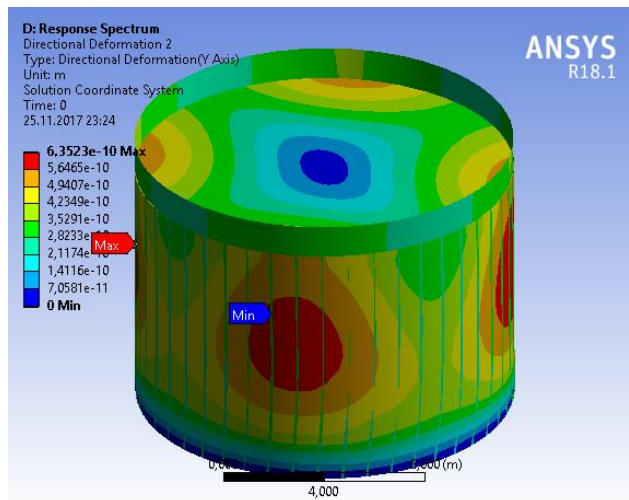
The results of modal analysis and design response spectra were used for spectral analysis. In addition to earthquake performance, two earthquakes, EL Centro earthquake and Kobe earthquake, ground motions were obtained from response spectrum analysis. The results obtained from the response spectrum analysis on the circular steel water tank subjected to earthquake ground motion data are shown below. Impulse and convective outcomes are presented respectively.

Figure 5.22 shows response spectrum analysis under the El-Centro earthquake load. The red zones on the upper side of tank presents the maximum directional deformation and is  $2.1485 \times 10^{-6}$  m. the blue region in bottom has minimum directional deformation and is about 0 m.



**Figure 5. 22** Impulsive response spectrum analysis of el-Centro earthquake

In addition to that, response spectrum analysis is showed under the Kobe earthquake load in Figure 5.23. The red zones on the middle side of tank has the maximum directional deformation and is  $6.3523 \times 10^{-10}$  m it is spread on all four side of the cylindrical tank. the blue region in bottom has minimum directional deformation and is about 0 m.



**Figure 5. 23** Impulsive response spectrum analysis of Kobe earthquake

Figure 5.24 shows response spectrum analysis under the El-Centro earthquake load for impulsive region. Maximum directional deformation is  $2.9904 \times 10^{-5}$  m and the minimum deformation occurred 0 m in the bottom of tank.

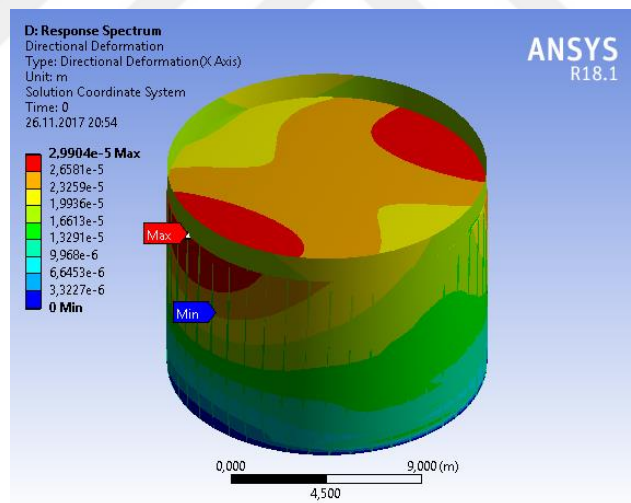


**Figure 5. 24** Convective response spectrum analysis of el-Centro earthquake

Figure 5.25 shows response spectrum analysis under the Kobe earthquake load for convective region. Maximum directional deformation is  $6.4452 \times 10^{-8}$  m it is occurred upper side of tank and the minimum deformation occurred 0 m in the bottom of tank.



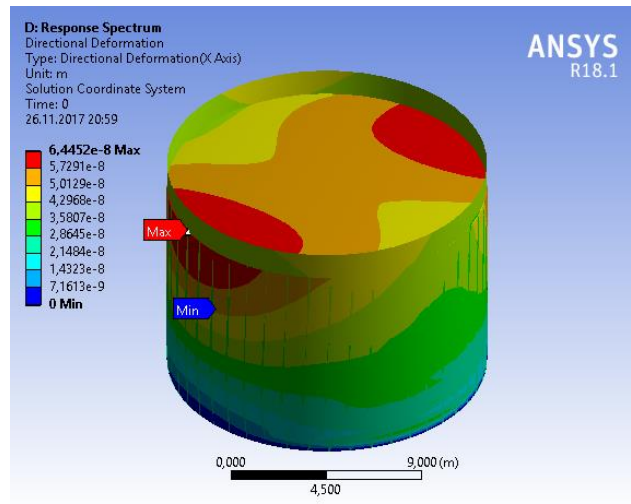


**Figure 5. 25** Convective response spectrum analysis of El-Centro earthquake

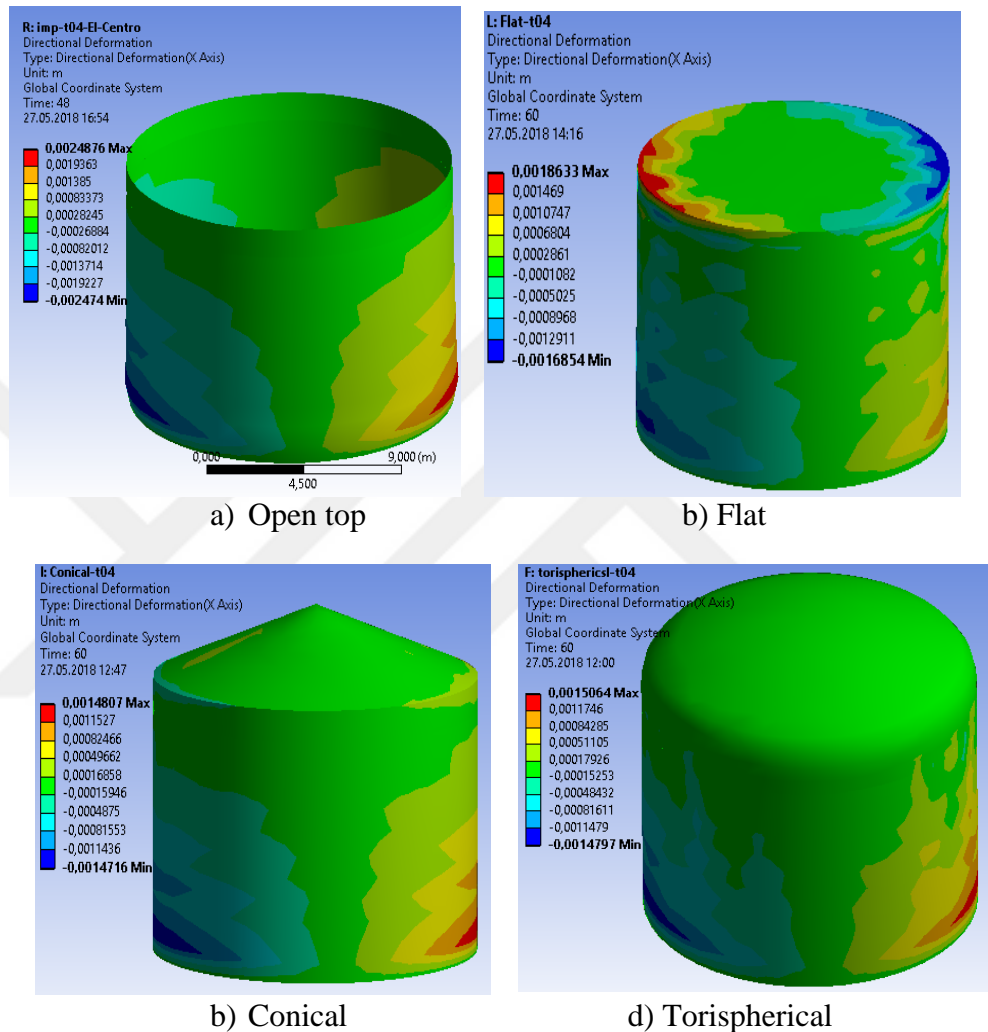
## 5.5 Time History Analysis

Time-history analysis is a step-by-step analysis of a dynamic response to a given load, which can vary with time. The analysis may be linear or nonlinear. Time-history analysis is used to determine the dynamic response of a structure to arbitrary loading. If the load includes ground acceleration, displacements, speeds and acceleration will depend on ground motion. Any number of time-history analysis cases can be defined. The time history may always differ according to the load applied and the type of analysis to be performed. Time-history analysis using the north–south component of the 1940 El-Centro (Magnitude: 6.9) earthquake was performed. The time history of the tanks is separated into impulsive and convective components in order to perform the time-varying response characteristics of the tank models.

### 5.5.1 Directional deformation under El-Centro earthquake

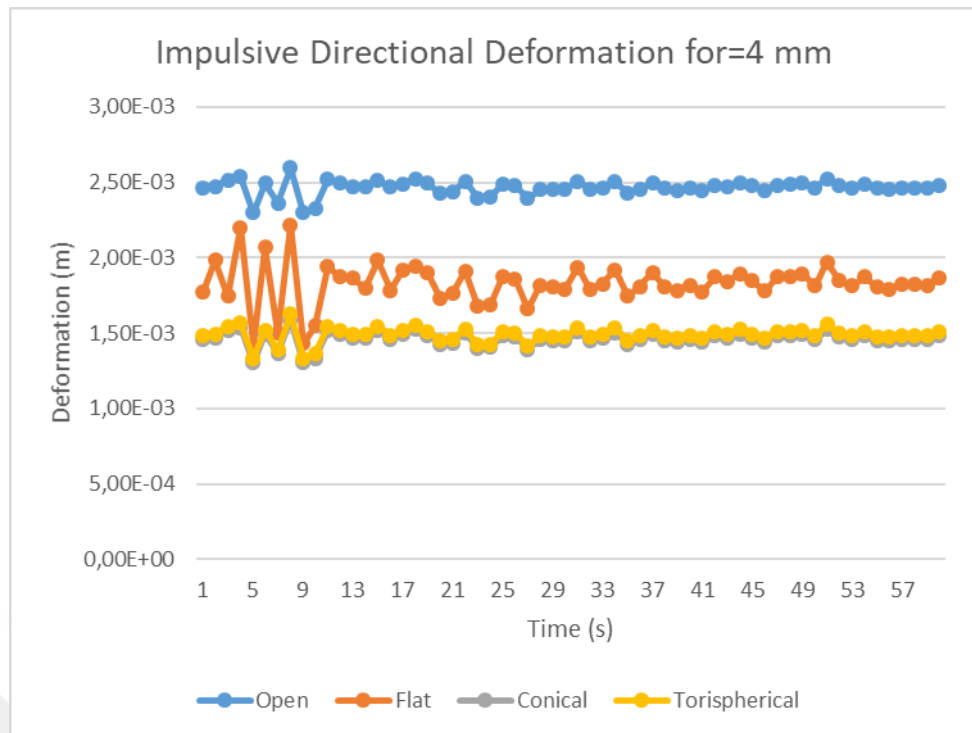
Transient behaviour of the water for El-Centro earthquake is shown in Figure 5.26 and the results are compared with that of impulsive directional deformation. These analyses were conducted using ANSYS transient structural tools for 4 mm tanks shell. Figure 5.26 shows impulsive directional deformation for open, flat, conical and torispherical tank models. Red colours show maximum deformation in the bottom of tanks and blue colour layers show the minimum deformation on the tanks. Directional deformation of the open-top, conical-closed and torispherical-shaped tanks occurs at the bottom of the tank. However, in the case of a flat-closed roof of tank in Figure 5.26(b), directional

deformation is seen not only on the base, but also on the roof. Maximum deformation value is seen 0.002487 m on the open-closed tank, it occurred 0.001863 m on the flat closed tanks. Conical and torispherical closed tanks have 0.00150 m maximum deformation.



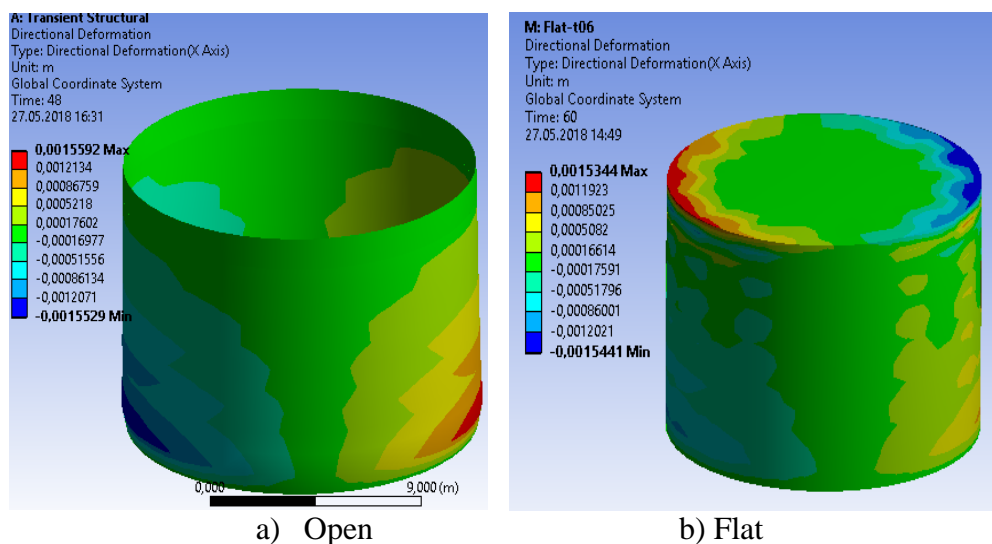
**Figure 5. 26** Impulsive directional deformation for t=4 mm

The Figure 5.27 shows the comparison of impulsive directional deformation for all tanks. Maximum directional deformation was occurred on the open-top tank model and conical and torispherical closed tanks have lowest deformation, and also their curves was overlapped.



**Figure 5.27** Impulsive directional deformation graph of all tanks t=4 mm

The Figure 5.28 shows the directional deformation of 4-mm tanks. The open tank model 0.00155 m and flat model is 0.00153 m. Conical and torispherical models have 0.0009196 m and 0.0009577 m respectively.



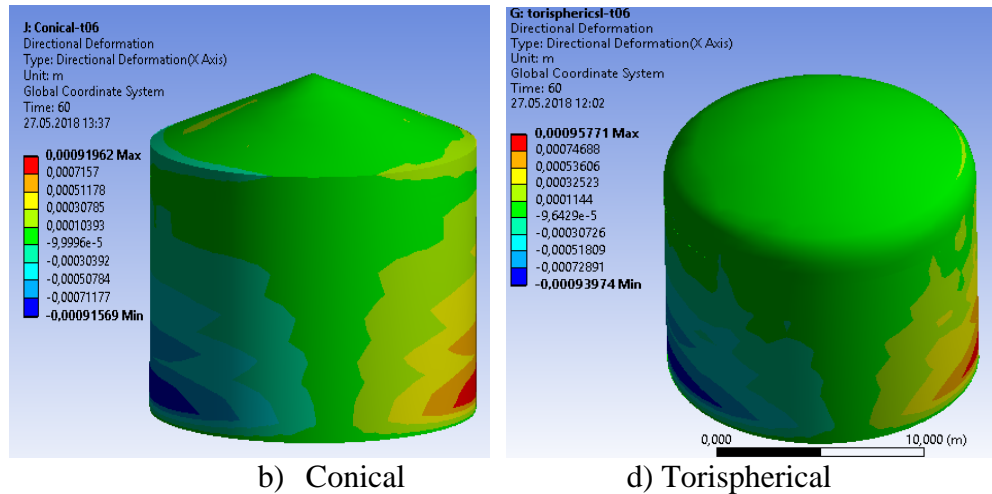


**Figure 5. 28** Impulsive directional deformation for t=6 mm

According to the API 650 standard, the tank shell thickness required is 6 mm. In Figure 5.29, directional deformation is compared for all tanks. Open-top and flat-closed tanks have the highest maximum deformation, but when the open-top tank behaves to close linearly, the flat model shows more nonlinear behavior. There is another important difference in the flat-closed tank model compared to the others. The conical and torispherical models have the lowest maximum directional deformation with overlap curves.

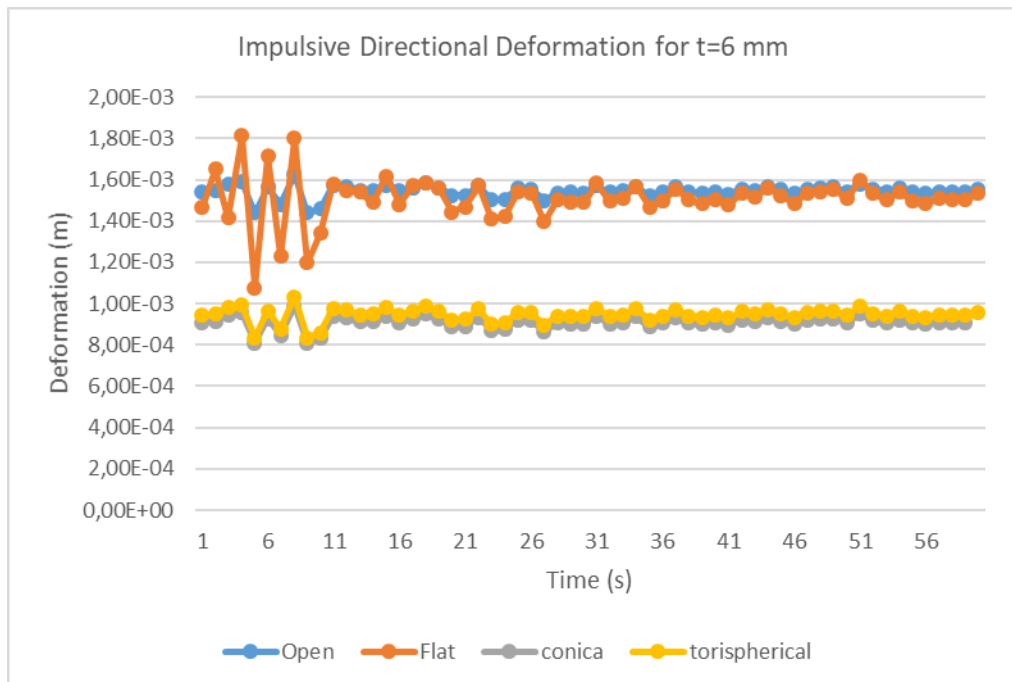


**Figure 5. 29** Impulsive directional deformation t=6 mm

Figure 5.30 shows impulsive directional deformation for shell 8 mm. maximum deformation is occurred only bottom in the open-top, conical-closed and torispherical-closed tanks. There is a significant difference in the flat-closed tank, the maximum deformation is more common in the roof, and also it has higher maximum deformation than the other three models.

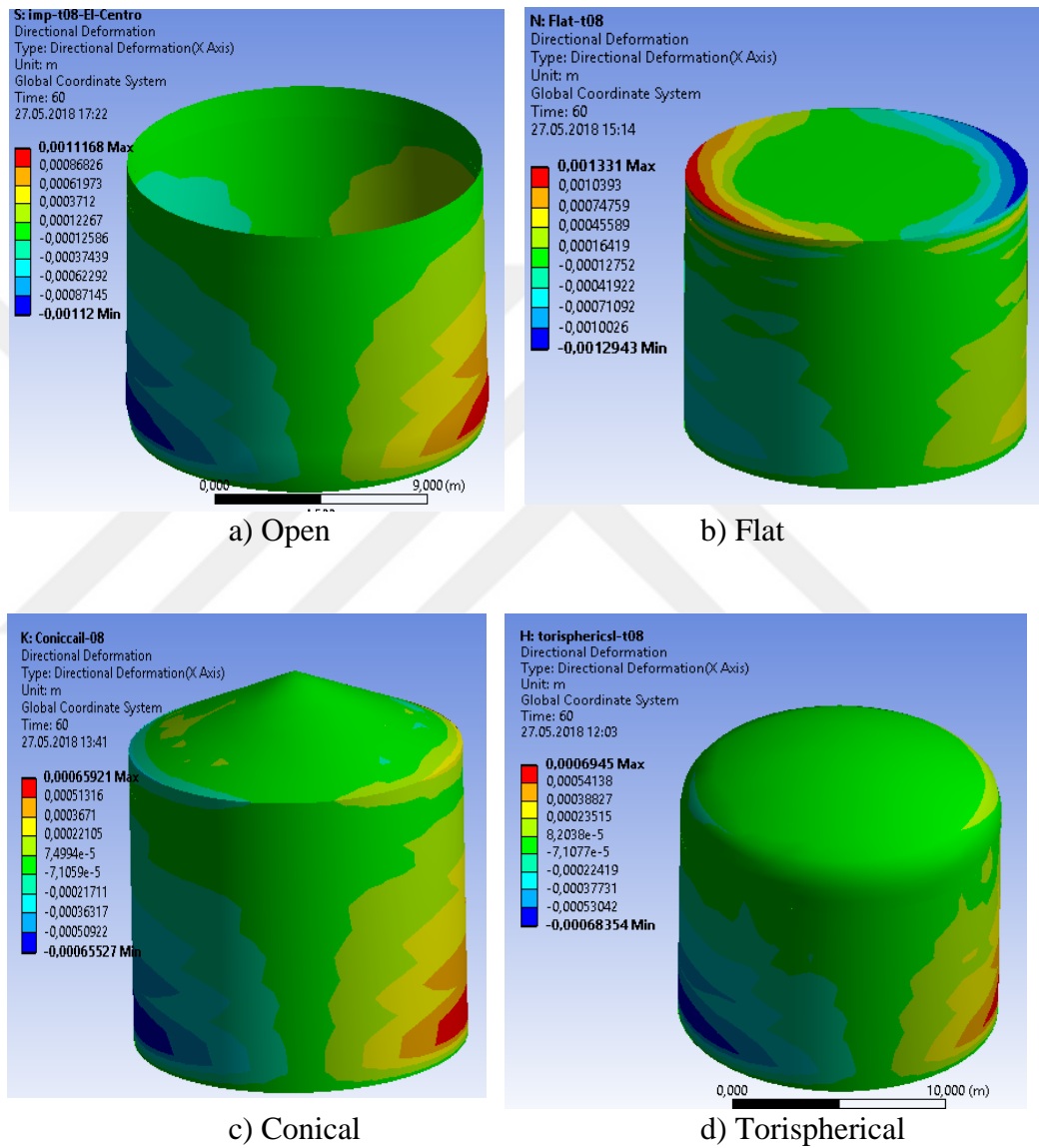


**Figure 5. 30** Impulsive directional deformation for t=8 mm

Figure 5.31 shows the directional deformation of tanks with a thickness of 8 mm. Directional deformation decreased due to increase of wall thickness in all models, but it increased in flat closed tank. This interesting situation because of the change the center of pressure on in the flat-closed tank. Normally, when shell thickness is increased,

reduction of deformation is expected, but flat-closed of the tank roof reverses this situation. Therefore, the flatness of the roof does not provide any advantage the shell thickness selected above the standard.

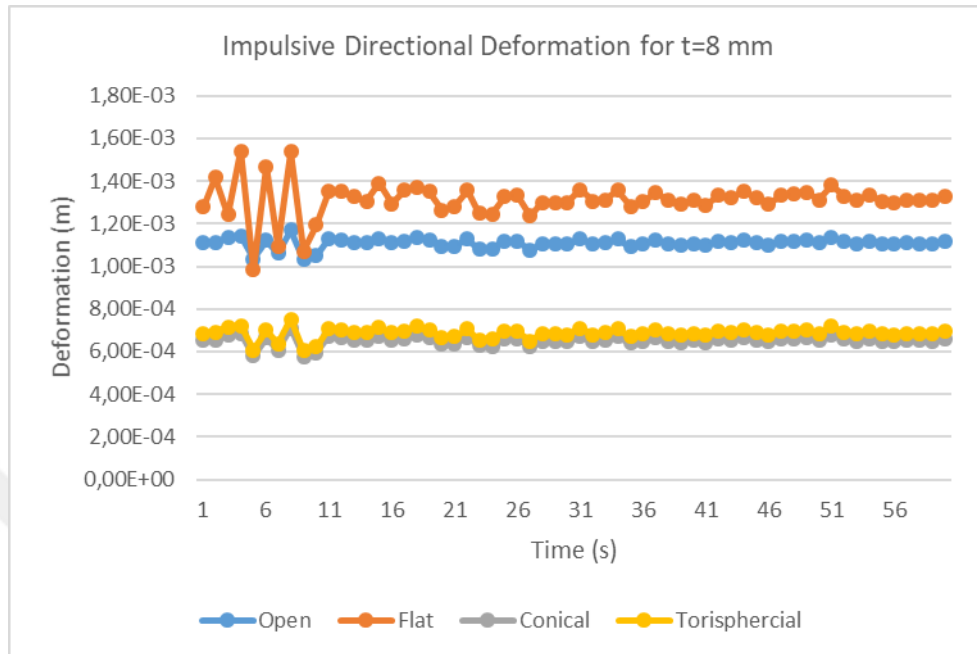


**Figure 5. 31** Impulsive directional deformation graph of all tanks t=8 mm

Convective directional deformation results are shown in Figure 5.32, 5.33 and 5.34. Time history analysis was carried out for 4 mm, 6 mm and 8 mm shell thickness under the El-Centro earthquake loads as convective. When looking at Figure 5.32, it is observed that

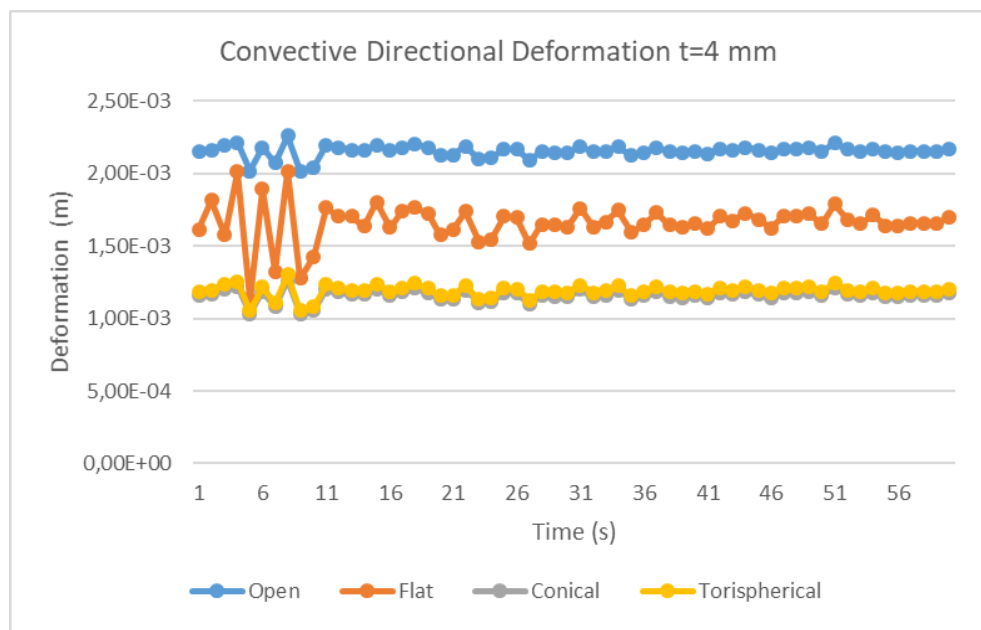


**Figure 5. 32** Convective directional deformation graph of all tanks t=4mm

the deformation in the flat-closed tank decreases, but the best result is again taken in the conical and torispherical models.

As mentioned earlier, according to the API 650 standard, the tank shell thickness should be 6 mm. Looking carefully at Figure 5.33, it is observed that the deformation in the flat-closed tank model is greater. As mentioned earlier, according to the API 650 standard, the tank shell thickness should be 6 mm. Looking carefully at Figure 5.33, it is observed that the deformation in the flat-closed tank model is greater. However, the impulsive 6-millimeter flat-closed tank has fallen below the slightly open tank model. Excessive deformation of the convective shows that the sloshing effect continues at the top of the tank.

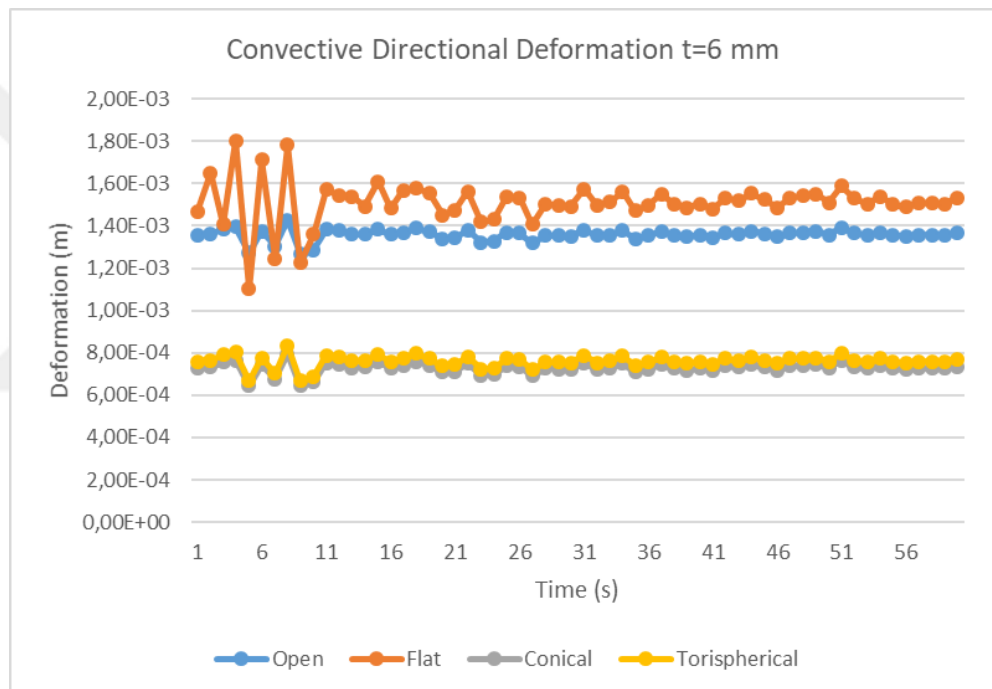
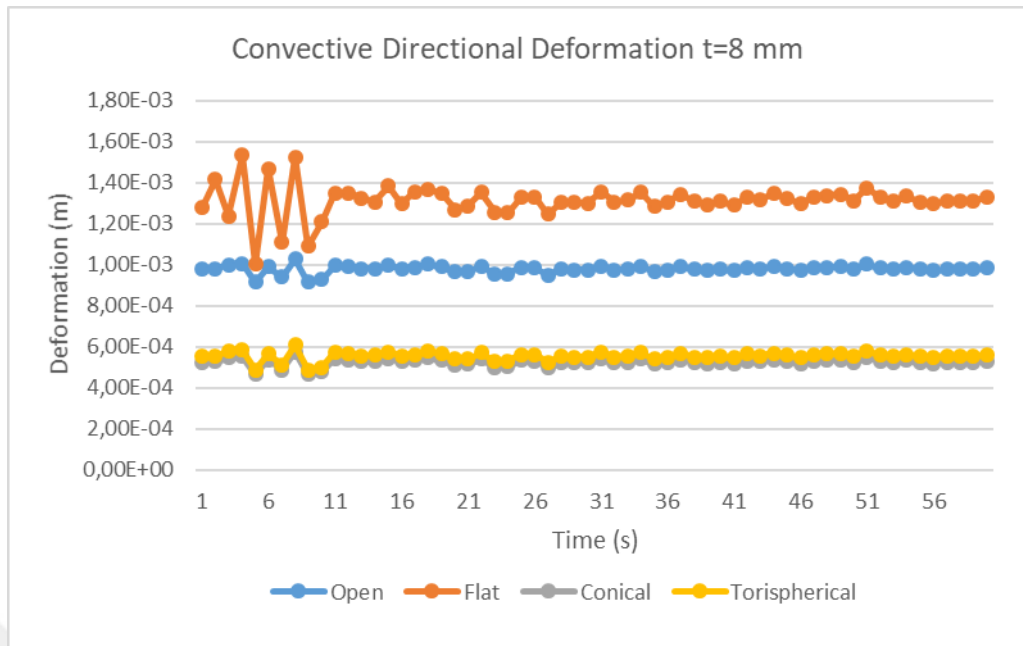


Figure 5. 33 Convective directional deformation graph of all tanks t=6mm

In Figure 5.34, it is expected that the deformation is expected to decrease in tanks with a thickness of 8 millimeters, but on the contrary, it is observed that the deformation increases significantly in the flat-closed tank. There are no any advantages in flat-closed tank increase of thickness of shell.



**Figure 5. 34** Convective directional deformation graph of all tanks t=8mm

Figures 5.35 summarize the impulsive directional deformation of all tanks with three different thickness parameters under the El-Centro earthquake loading. Maximum directional deformation is occurred around the 2.50E-03 m with t= 4 mm shell thickness in open-top tank model. Secondly, Flat t04 follow with 2.00E-03 m maximum values. Conical and torispherical models perform very well with 4 mm shell thickness. They perform a linearly behaviour with under the 1.00E-03 m deformation value.

In 6 millimeters tanks, the highest maximum deformation occurred on a flat-closed tank about 1.0075E-03 m. The shell thickness of 6 mm is also in accordance with API 650 standard. In this case, the API 650 standard is required to be checked, since maximum directional deformation occurs in the flat-closed tank with the 6 mm shell thickness.

Figures 5.36 summarize the convective directional deformation of all tanks with three different thickness parameters under the El-Centro earthquake loading. The yellow, red and black colours show directional deformation of flat-closed tanks with shell thickness of 4, 6, 8 mm, respectively. The flat-closed tank also has the maximum deformation in the 6 mm and 8 mm categories. Conical-closed and torispherical-closed tanks are also observed with very good performance with low deformation. However, with the effect of convective (sloshing) it seems that some more deformation continues to the end.



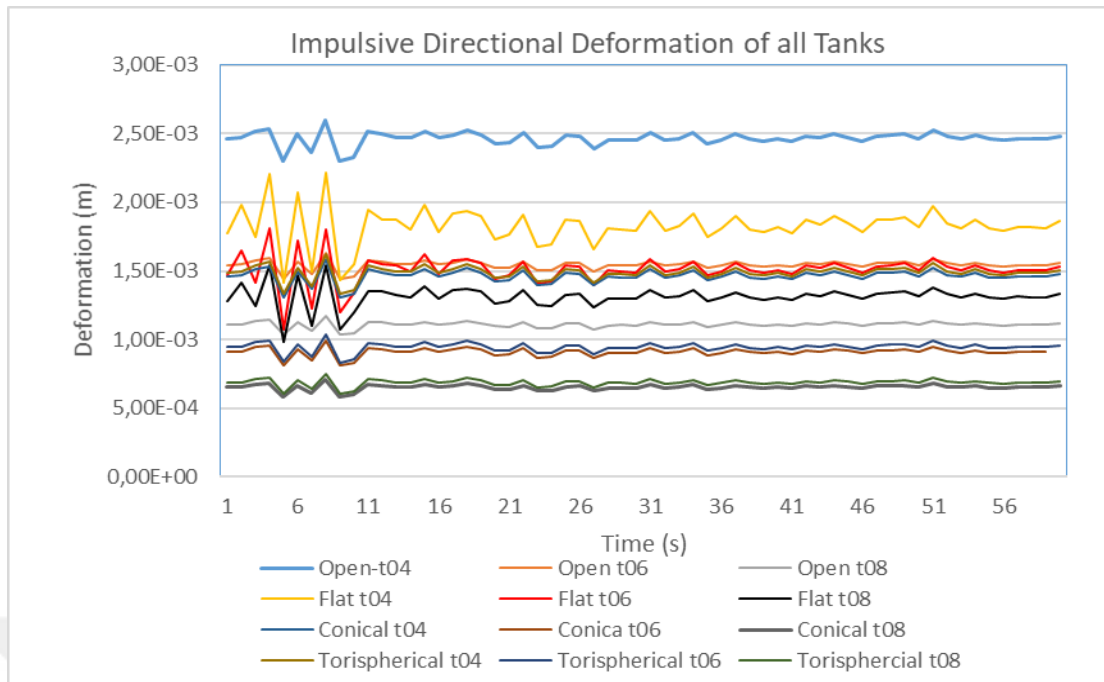


**Figure 5. 35** Impulsive directional deformation for all parameters

Carefully looking at both graphs, plastic deformation in the flat-closed tank starts at the first few seconds. Convective directional deformation is shown in Figure 5.36 for all parameters.

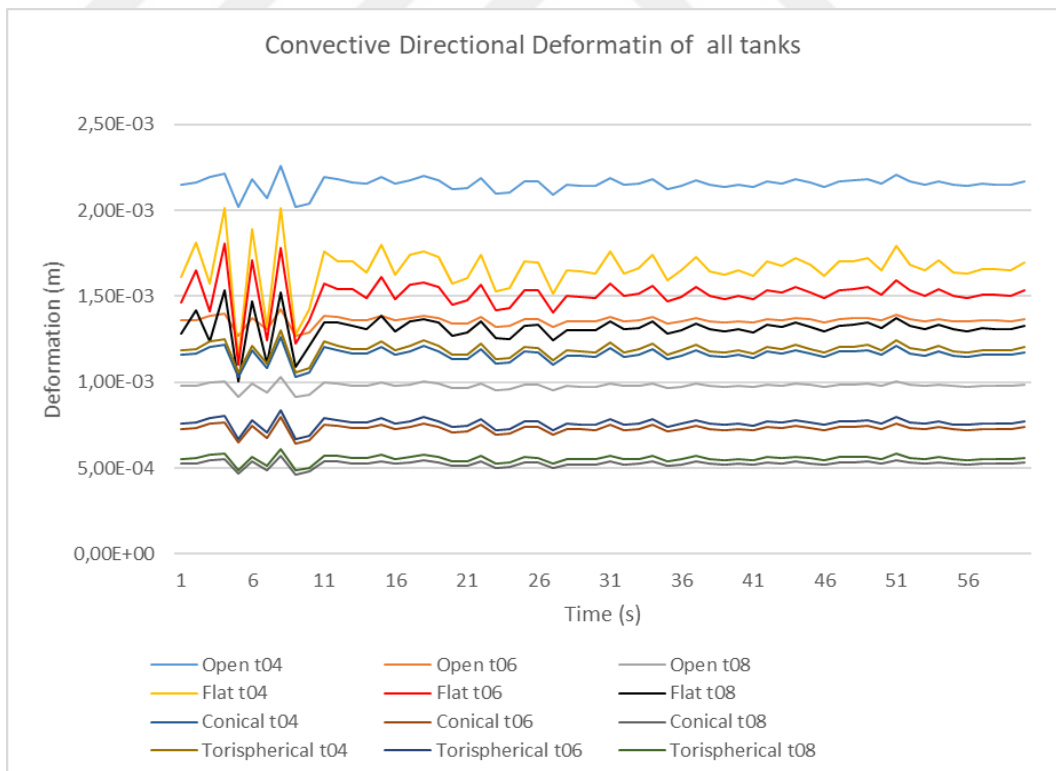


**Figure 5. 36** Convective directional deformation for all parameters

### 5.5.2 Impulsive directional deformation under Kobe earthquake

The transient behaviour of the contained water for Kobe earthquake is shown in Figure 5.37 and the results are compared with that of impulsive directional deformation. Figure 5.37 shows impulsive directional deformation for open, flat, conical and torispherical at 6 mm shell thickness tank models. Directional deformations of the open-top, conical-closed and torispherical-shaped tanks occur at the bottom of the tank, whereas the top is seen to slide upward in the flat-closed model. Red colours show maximum deformation. While the maximum deformation was 0.0015473 m in open-top tank, conical-closed model has 0.0009122 m maximum deformation. The highest deformation was 0.0016901 m in flat-closed model and the lowest deformation is found in the 0.0094816 m torispherical-closed model.

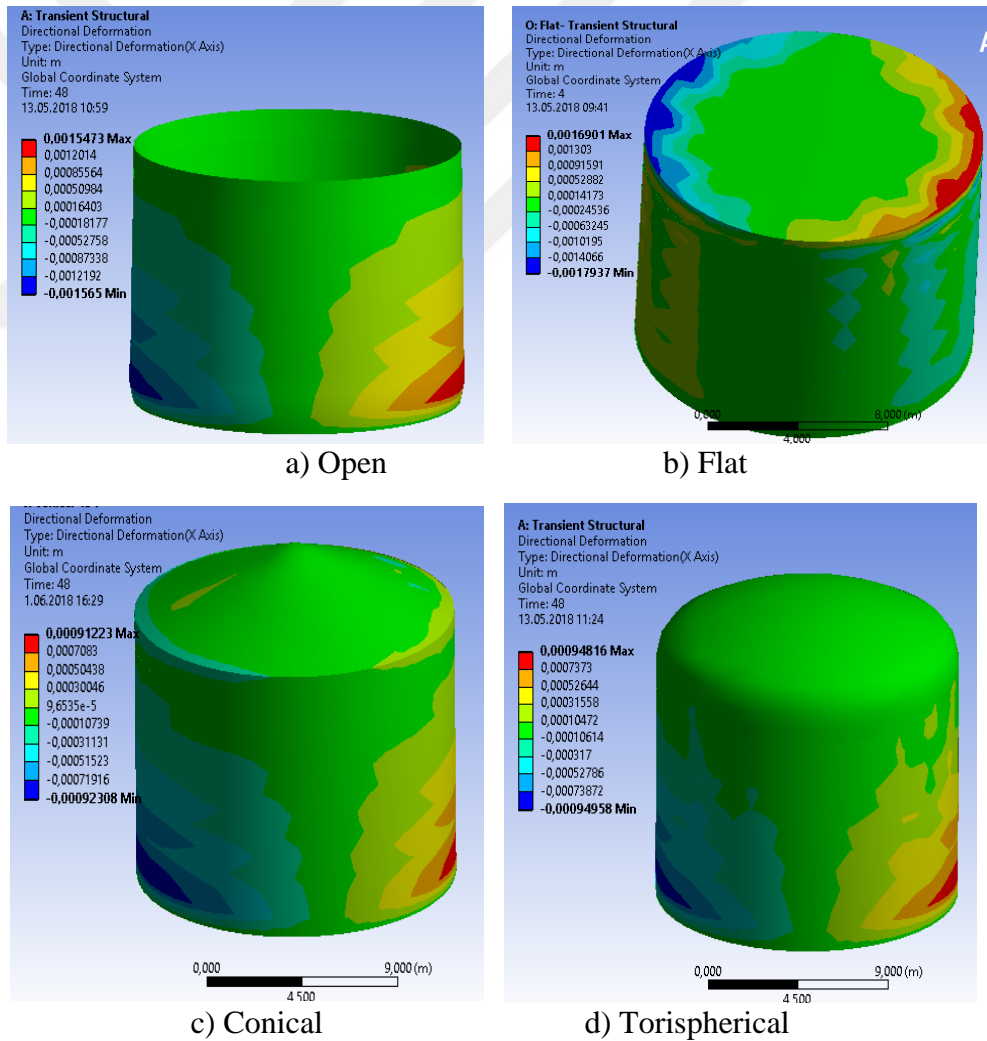
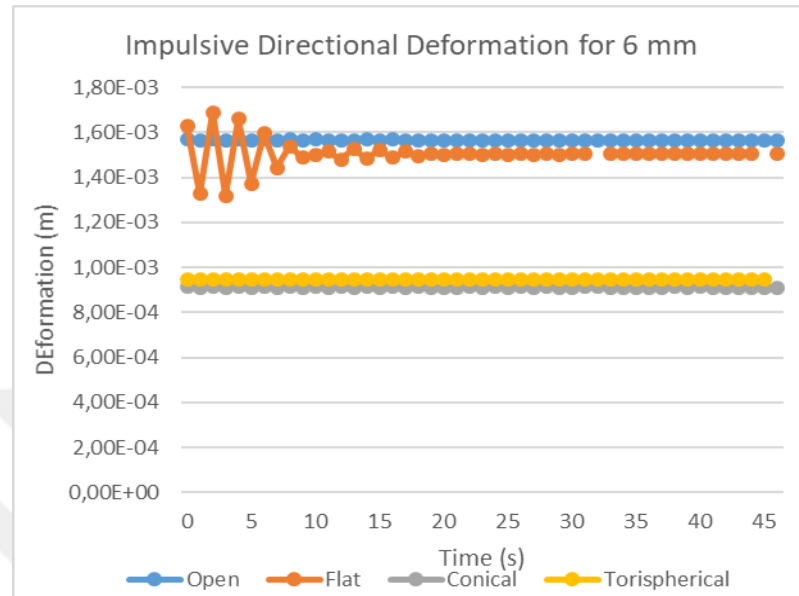


Figure 5. 37 Impulsive directional deformation graph of all tanks t=6mm

In Figure 5.38 maximum directional deformation is occurred in flat-closed model. It has between  $1.40E-03$  m and  $1.70E-03$  m variable deformation. Open-top tank model has around the  $1.60E-03$  m deformation. Conical and torispherical have below  $1.00E-03$  m directional deformation.



**Figure 5. 38** Impulsive directional deformation graph t=6 mm

After this stage comparison graphs of tanks which are shell thickness at 4 mm and 8 mm will be displayed. In Figure 5.39 shows graph of impulsive directional deformation at 4 mm shell thickness tanks. Maximum directional deformation is occurred in open-top tank model. It performs a linearly behavior. However, in flat closed tank is performed the nonlinear behavior between the  $1.50 E-03$  m and  $2.50E-03$  m values. Conical and torispherical-closed tanks overlapped have  $1.50e-03$  linearly directional deformation.

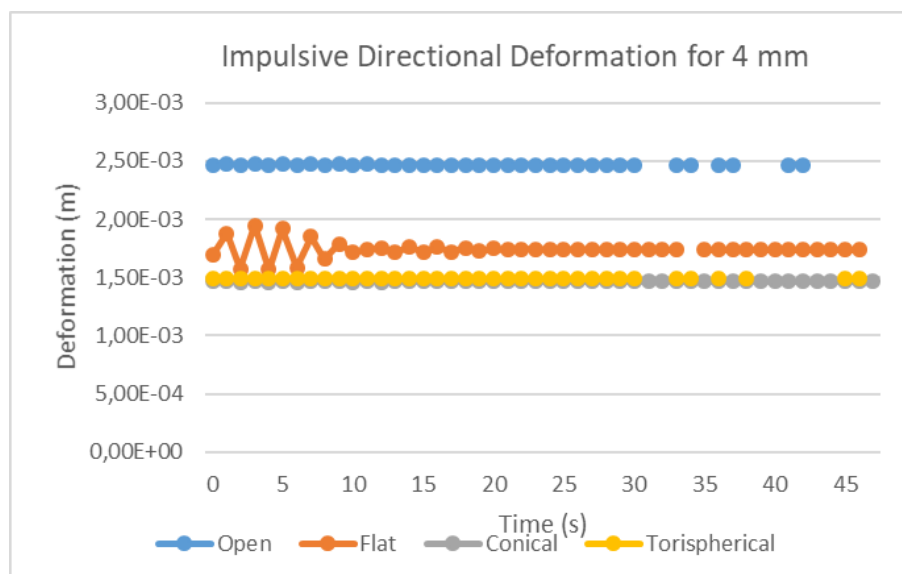


**Figure 5. 39** Impulsive directional deformation graph of all tanks t=4mm

In Figure 5.40 flat-closed tank has highest maximum directional deformation with  $1.40 \times 10^{-3}$  m values. Open-top tank has around the  $1.1 \times 10^{-3}$  m directional deformation. Maximum deformation is around the  $7.00 \times 10^{-4}$  m in conical and torispherical closed tanks.

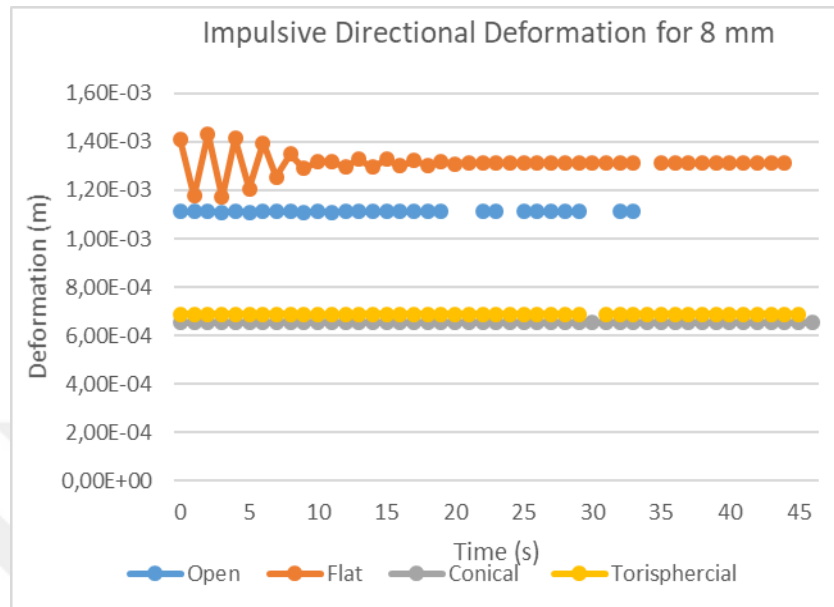


**Figure 5. 40** Impulsive directional deformation graph t=8 mm

### 5.5.3 Convective directional deformation under Kobe earthquake

In this section, the seismic analysis was performed for all tanks in the convective period. In Figure 5.41 the convective maximum directional deformation is 0.0016887 m for the flat tank model whereas convective maximum directional deformation is 0.00013602 m for the open-top model. Conical-closed and torispherical-closed tanks models are lowest directional deformation, conical model is 0.00073023 m and torispherical model remains 0.00076298 m directional deformation.

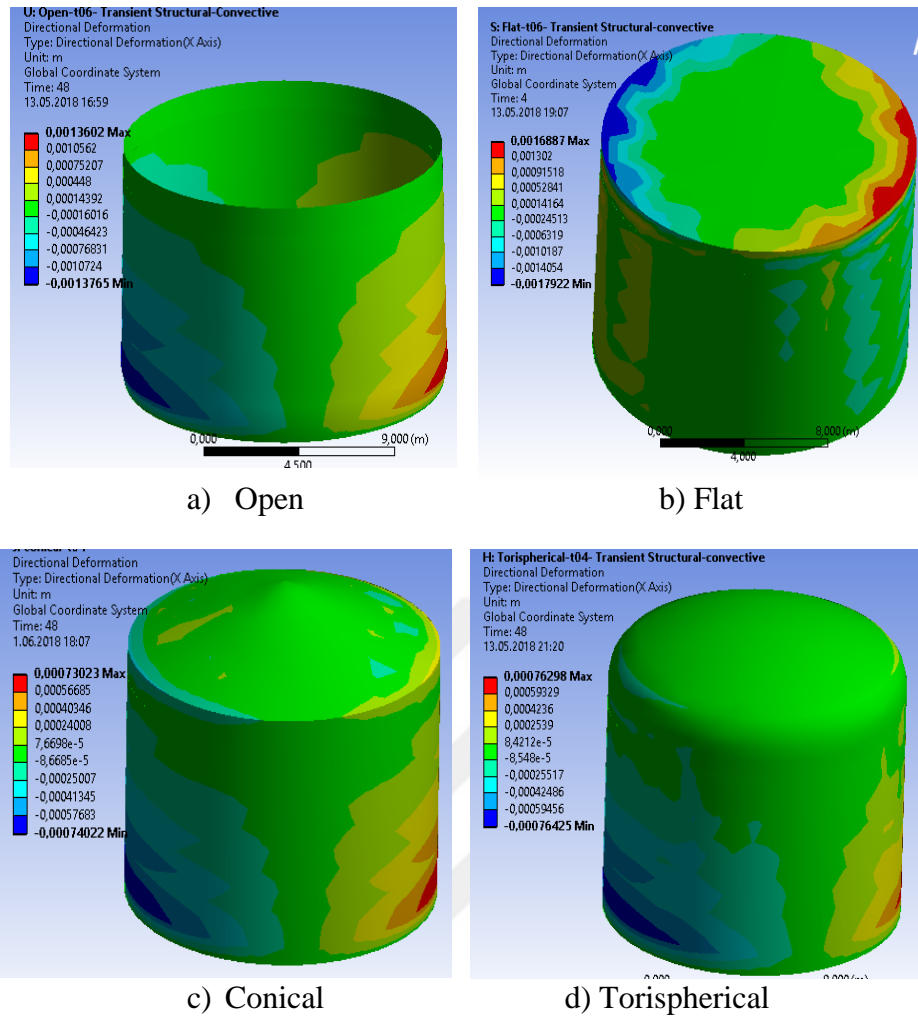


**Figure 5. 41** Convective directional deformation  $t=6$  mm

Figures 5.42 summarize the impulsive directional deformation of all tanks with three different thickness parameters under the Kobe earthquake loading. Maximum directional deformation is occurred around the  $2,50E-03$  m with t04 shell thickness in open-top tank model. Under the Kobe earthquake loading, the open-closed, conical-closed and dome-closed tanks exhibit linear behaviour, while the flat-closed tank model draws attention with its nonlinear behaviour.

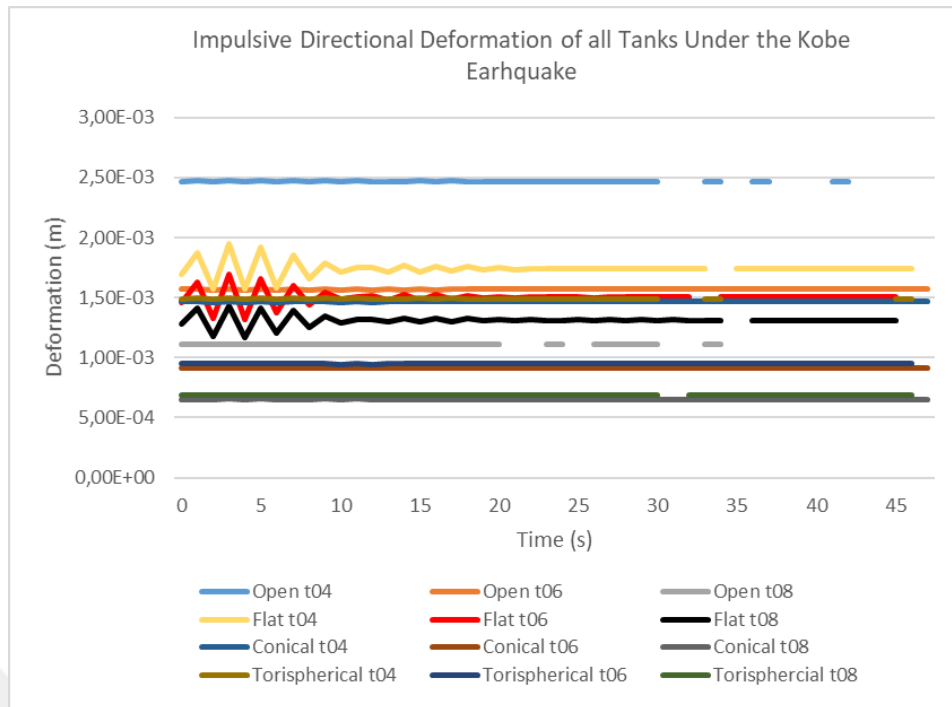


**Figure 5. 42** Impulsive directional deformation for all parameters

Figures 5.43 summarize the convective directional deformation of all tanks with three different thickness parameters under the Kobe earthquake loading. Open-top tank performs a linearly behaviour with all thickness.

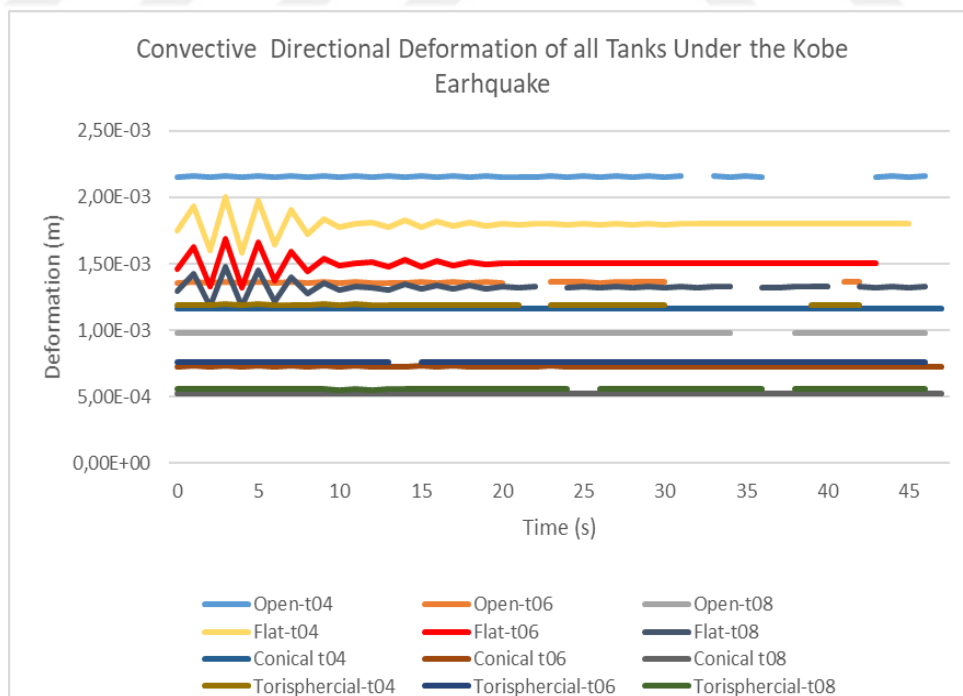


**Figure 5. 43** Convective directional deformations for all parameters

As its thickness increases, directional deformation decreases. The yellow, red and black colours show directional deformation of flat-closed tanks with shell thickness of 4, 6, 8

mm, respectively. The flat-closed tank also has the maximum deformation in the 6 mm and 8 mm categories. Conical-closed and torispherical-closed tanks are also observed with very good performance with low deformation.

## 5.6 Summary

Modal analysis was performed beginning of this chapter. Impulsive and convective modal analysis results were optioned separately. The frequency values calculated with API 650 were verified with the FEM model results. Transient seismic analysis was carried out based on modal analysis under the both El-Centro and Kobe earthquake loads.

Then, transient seismic analysis was performed with the FEM model to examine the time-dependent on movements of the cylindrical steel water tank. Model were also carried out for flat-closed, conical-closed and torispherical-closed tanks respectively. Three different thickness were determined to see the effect of shell thickness on the tank roof. According to API 650 standardization, shell thickness should be 6 mm. The shell thickness is reduced to 2 mm and increased to 2 mm; 4 mm, 6 mm and 8 mm are determined respectively for all tanks. Analyses were made separately with impulsive and convective records with El-Centro and Kobe earthquake records.

Maximum directional deformation occurred in the flat-closed tank. The most buckling was occurred in flat-closed tank. One of the biggest reasons for this is that the pressure centre changes due to the flatness of roof tank. The deformation calculation was performed via transient structural analysis which was not exceeding the limit of the tank, so that the tank can be safe under the analysis condition.

The significant finding in this chapter is that if the top of the tank is in the shape of a conical and torispherical dome, the deformation is majorly reduced. The flat-closed tank has a maximum directional deformation in both impulsive and convective periods. As a result, the flat-closed roof tank does not provide any advantage in directional deformation, if the tank is flat-closed, the deformations and buckling will be more likely to occur even if the shell thickness is increased. However, the existing tanks can be prevented from being damaged by being closed in the shape of a conical and torispherical dome so that they are not damaged by directional deformation during the earthquake.

Djermane A. and Chikhi performed dynamic buckling of steel tank for broad and tall tank, neglecting convective mass. They compared the numerical results with some

standard code guidelines. According to their results, it turns out that broad tanks confirm with EC8 code results, but need to be developed tall tanks (Djermane A. and Chikhi, 2017) . The tall tank measures used by the Djermane A. and Chikhi, in the study are similar to the tank sizes in this case. Therefore, the results obtained in this study will contribute to the development of current design standards.

According the N. Buratti and M. Tavano, elephant foot buckling is greatly influenced by the formation of plasticity in other parts of the structure (Buratti N. and Tavano, 2014). This idea is to some degree correct, but the greatest cause of elephant foot buckling is insufficient shell thickness.

Nakasima, M. and Naito have experimentally proved that the pressure and stresses increase occurring in the tank roof decrease as the angle between the liquid surface and the tank roof increases, while the angle decreases, the hydrodynamic pressures and stresses increase (Nakashima, 2010). In this thesis, according to the results obtained with respect to the different tank roof, it was proven that more deformation occurs in the roof of the flat-closed tank. The biggest reason for this is change of the pressure centre because of the angle between the surface of the tank and the surface of the tank is zero. Deformation and buckling are reduced with the growth of the angle in conical-closed and torispherical-closed tanks. One of the most important results in this section is the effect of shell thickness on the lid shape. Generally, directional deformation is decreased depending on the thickness of the shell, whereas deformation is not decreased in the flat-closed model.



## **CHAPTER 6**

# **BUCKLING ANALYSIS AND STRENGTHENING OF CYLINDRICAL STEEL TANK**

### **6.1 Introduction**

In this chapter, buckling analysis is performed of cylindrical steel water tanks which are under the El-Centro and Kobe earthquake seismic loading. As mentioned earlier, the most common types of buckling in cylindrical steel tanks are elephant foot buckling, diamond shape buckling and cracks on the top side of tanks due to sloshing effect of liquid. It will be focused on the buckling in different shell thickness and different roof types of cylindrical steel tanks.

On the other hand, strengthening of existing vulnerable cylindrical steel liquid tanks are performed in this chapter. One of the considerable aims of this thesis is to strengthen the tank exposed to deformation under the loads of the earthquake. It is possible to replace the steel tank with the new undeformable a tank made of thicker shell, but this will increase the cost considerably. Strengthening of existing tank at low cost is great importance. Composite materials are widely used to fabricate cylindrical shells which can be the structural elements in storage tanks, cisterns for transportation pressure vessels, rocket components.

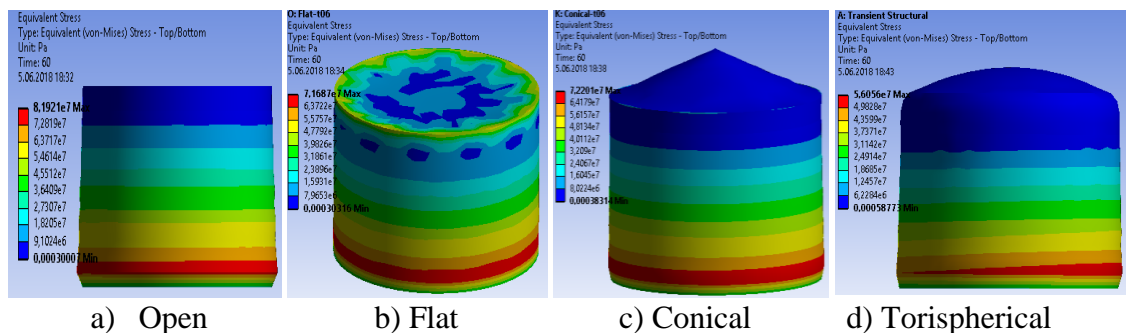
### **6.2 Buckling Analysis of Cylindrical Steel Tanks**

As a thin walled structure, cylindrical steel tank may be buckled due to subjected earthquake loads. There are some buckling such as elephant's foot buckling, diamond shape buckling and shell buckling. Elastic plastic buckling is often referred to as elephant foot buckling which is an outward bulge located just above the tank base. It is a result of both internal hydrodynamic and hydrostatic pressures, and vertical stresses in the shell. More specifically, results from the combined action of vertical compressive stresses,

exceeding the critical stress, and hoop tension close to the yield limit. The elephant foot buckling is generally completely in the bottom of the tanks because of the reversed in the direction of seismic excitation. (Niwa 1982, Quizlet 2018, Hamdan 2000, Douglas and Lysle, 2009, CNG United USA, 2018, Virella, 2006, Godoy, 2016 and Architectural, 2010). According to the fragility report by the American Lifelines Alliance; among these drawbacks, the dynamic collapse of tank walls is the most common and most dangerous (ASCE, 2001).

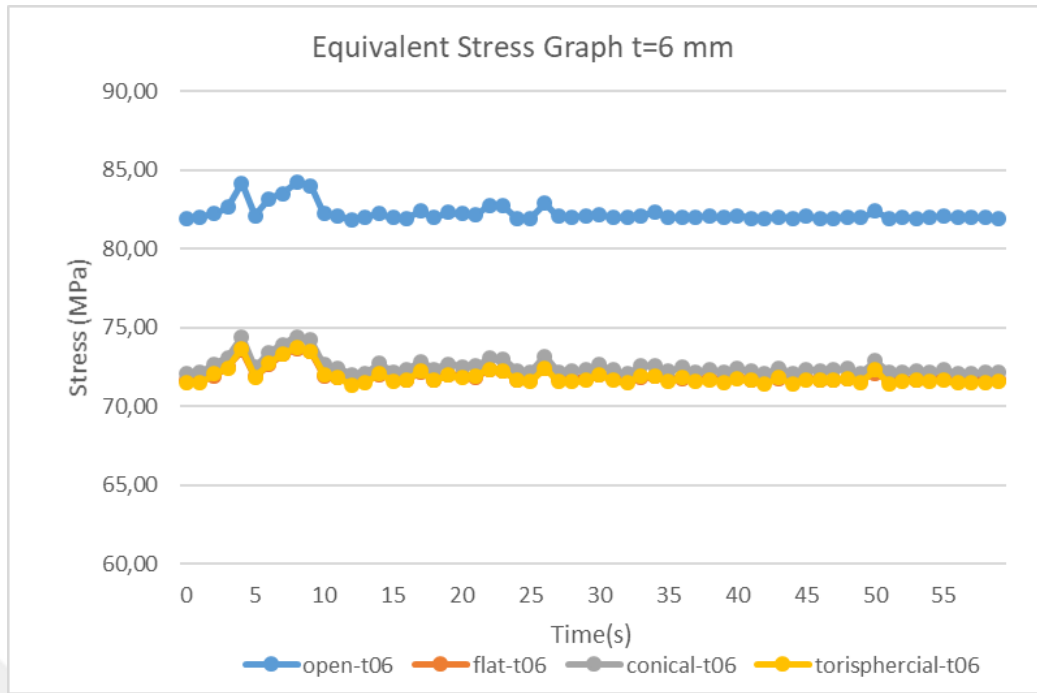
### 6.2.1 Equivalent stress and buckling analysis under the El-Centro earthquake

In this section, relationships between equivalent stress (von-Mises stress) and buckling are investigated of cylindrical steel tanks which are 6 mm shell thickness for open-top, flat-closed, conical-closed and torispherical-closed tanks. Equivalent stress usually occurred in the bottom of tanks. Figure 6.1 (a,b,c,d) show the stress distribution its maximum values are shown in red. The maximally elephant foot buckling was occurred bottom of open-top tank model. Secondly elephant foot buckling became in the torispherical tank model. It is observed that the lowest elephant foot buckling occurred in the conical model and a few buckles show in the roof. On the other side, the elephant foot buckling did not occur flat-closed tank model, but the roof of the tank collapsed because of the changed of the pressure center.



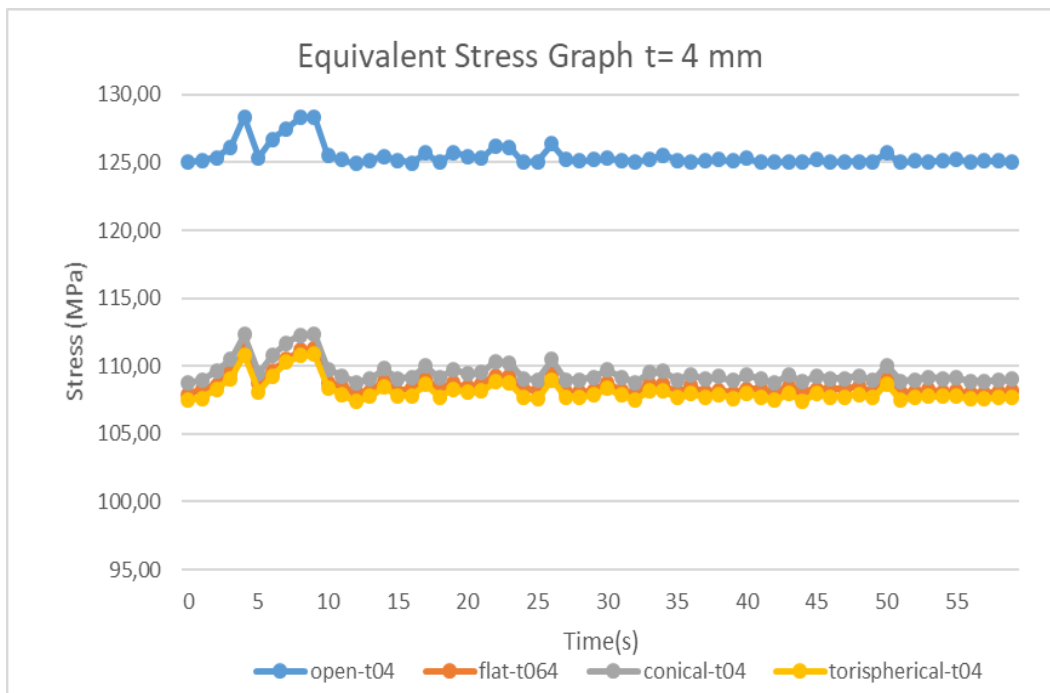
**Figure 6. 1** Equivalent (von –Mises) stress distribution on the tanks

Figure 6.2 shows the comparison of equivalent stress (von-Mises stress) under the El-Centro earthquake loading. Maximum stress is between 80 MPa and 85 MPa in the open-top tank. Stress is reduced 70 MPa in the flat-closed, conical-closed and torispherical models.



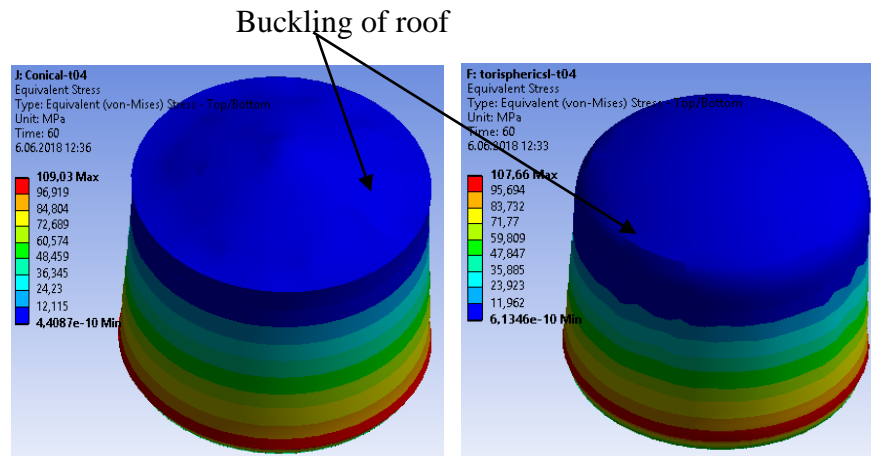
**Figure 6. 2** Comparison of equivalent stress for 6 mm thickness

Figure 6.3 shows the stress comparison of 4 mm tanks. Open-top tank has maximum equivalent stress and is around the 125 MPa. All of the closed roof tanks seem to have decreased stress and is about 110 MPa.



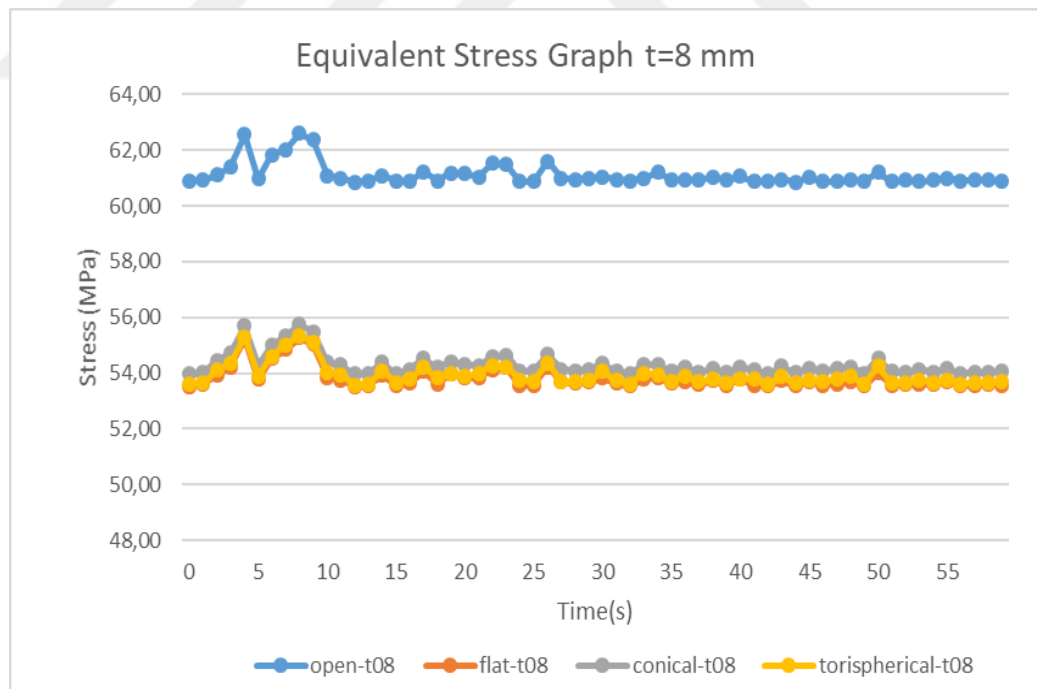
**Figure 6. 3** Comparison of equivalent stress under the el-Centro earthquake loads t=4 mm.

In Figure 6.4 shows the buckles of roof because of thin walled shell.



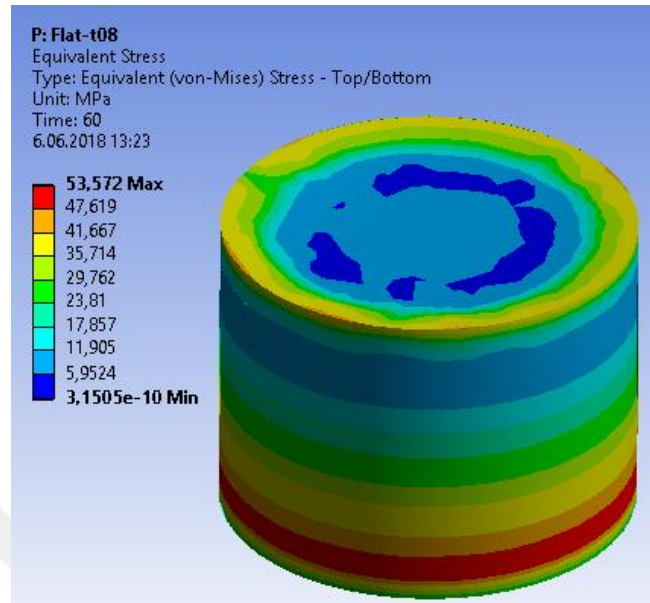
**Figure 6. 4** Buckling of roof

Figure 6.5 shows the comparison of equivalent stress. The equivalent stress of the open-top tank model was between 60 Mpa and 62 Mpa with the increase of the tank thickness to 8 mm, it seems to be around 54 Mpa in the closed roof models.



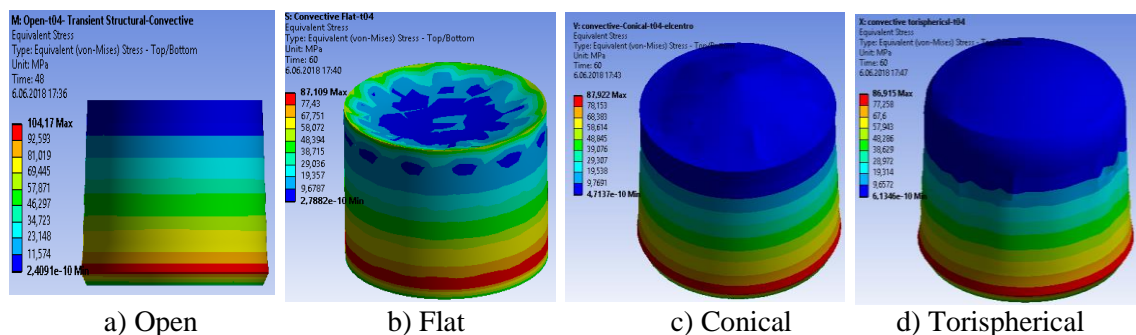
**Figure 6. 5** Comparison of equivalent stress under the el-Centro earthquake loads t=8 mm

Figure 6.6 also points out that there is a slight increase in stress at the edges of the flat-closed tank lid while buckling decreased its shell.



**Figure 6. 6** Stress distribution and buckling of flat-closed tank

Figure 6.7 summarizes of the convective equivalent stress under the El-Centro earthquake loading. Sloshing effect particularly is seen on the closed tanks model. In flat-closed tank stress and buckling are increased due to increasing hydrodynamic sloshing effect upper side of tank. Again depending on the effect of sloshing, cracks appear on the roof of the conical model and on the upper side of the torispherical model.



**Figure 6. 7** Convective stress distribution and buckling of all tanks

## 6.2.2 Buckling analysis under the Kobe earthquake

Model tank shell thickness should be 6 mm according to API 650 standard. In order to be able to see the buckling in the shell, simulations were repeated for 4 mm and for 8 mm shell thickness. These thickness measurements are 2 mm lower and 2 mm higher than in the standard. In Figure 6.8 (a), the reduction of the shell thickness to 4 mm caused the buckling of the roof to increase. In Figure 6.8 (b), it is observed that buckling was decreased with shell thickness was 8 mm, but the centre of the pressure was changing and more deformation occurs because the roof is flat.

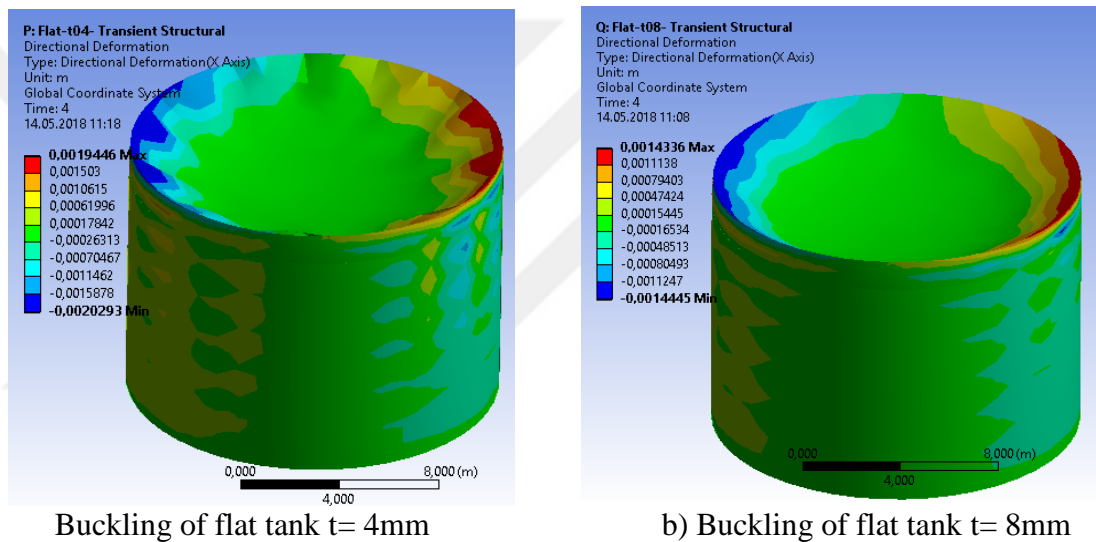
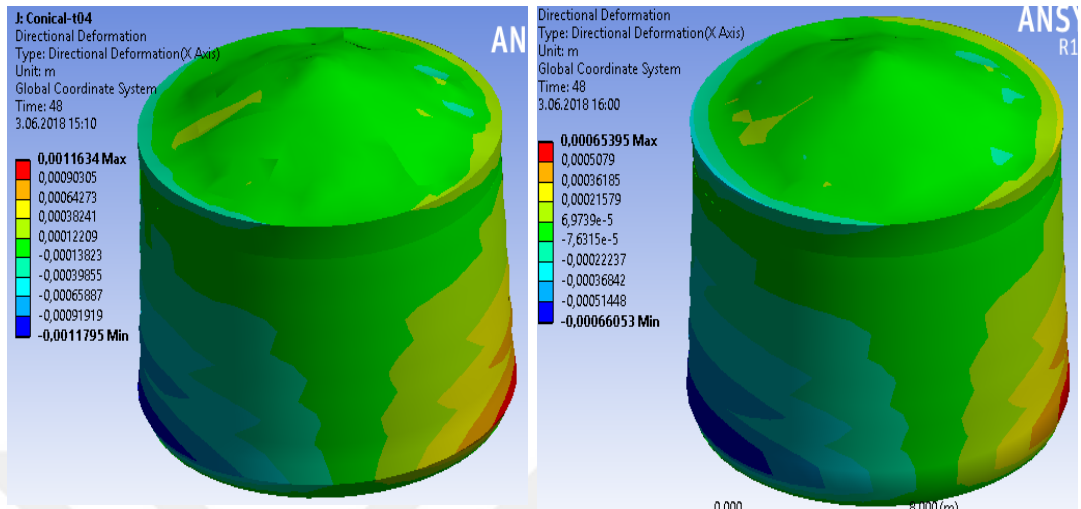


**Figure 6. 8** Buckling of flat-closed tank  $t=4$  and  $8\text{ mm}$

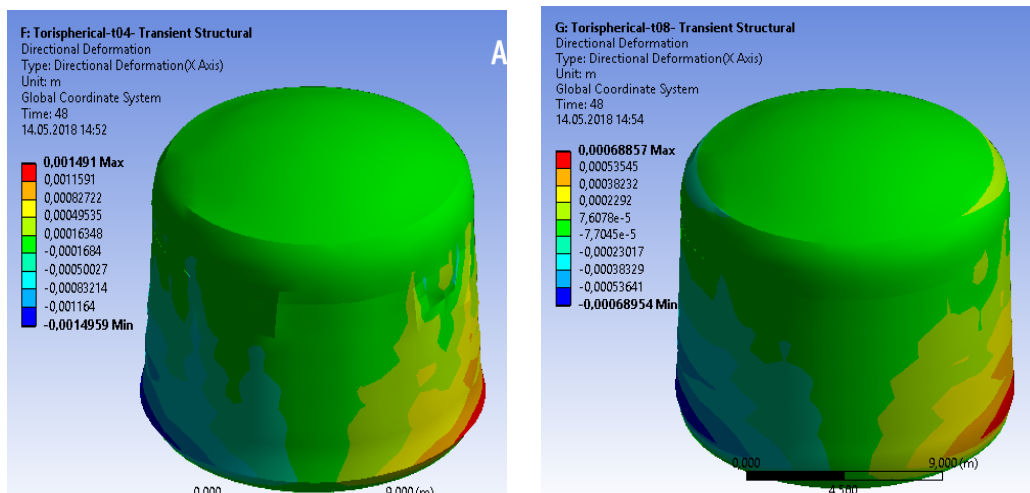
Figure 6.9, a similar situation exists in the conical model. When the shell thickness is reduced by 2 mm, the cracks on the roof increase, while the shell thickness increases by 2 mm and the absence of cracks in the tank is observed.



a) Buckling of conical tank  $t=4\text{mm}$       b) Buckling of conical tank  $t=8\text{ mm}$

**Figure 6. 9** Buckling of conical tank  $t=4$  and  $8\text{ mm}$

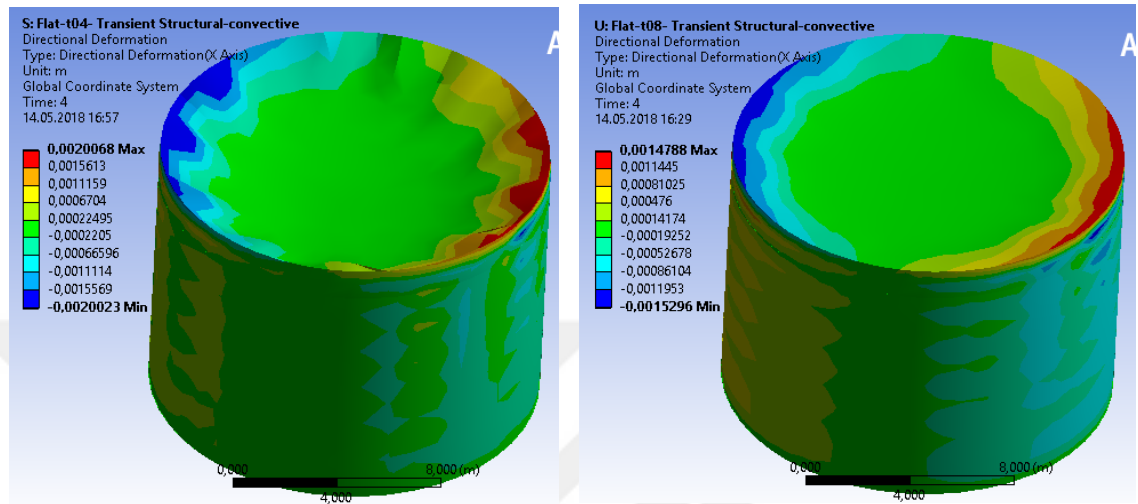
In Figure 6.10 (a) and (b) shows convective directional deformation and buckling for 4 mm and 8 mm in torispherical-closed tank. It seems that these two models have less buckling. Particularly when the crustal thickness is 8 mm, buckling was reduced.



a) Buckling of flat tank for 4 mm      b) Buckling of flat tank for 8 mm

**Figure 6. 10** Buckling of torispherical tank  $t=4$  and  $8\text{ mm}$

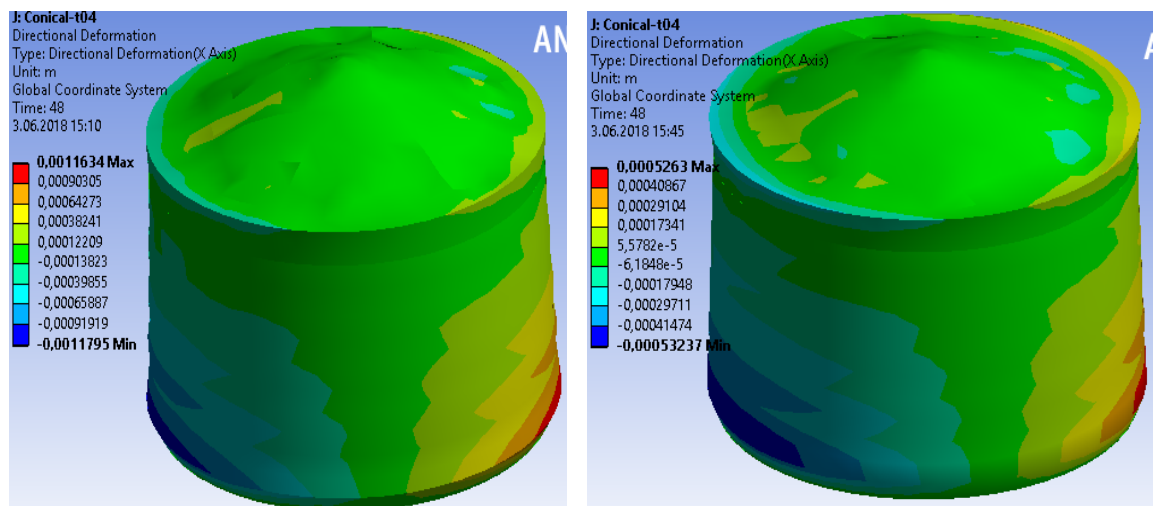
Simulations and analyses were carried out within the convective region. Results appear that the flat-closed of the cylindrical steel tank roof, especially with increased shell thickness, does not provide an advantage. When focus on the roof of the flat-closed tank in Figure 6.11(a), the buckling seems to be excessive, while in Figure 6.11 (b) the buckling is reduced by a shell thickness of 8 mm.



a) Buckling of flat tank for 4 mm                      b) Buckling of flat tank for 8 mm

**Figure 6. 11** Convective buckling of flat tank for  $t=4$  and 8 mm

In Figure 6.12, it is seen that the buckling occurred in the roof of the tank of 4 mm with the sloshing effect in the conical-closed tank model disappears at the 8 mm tank.

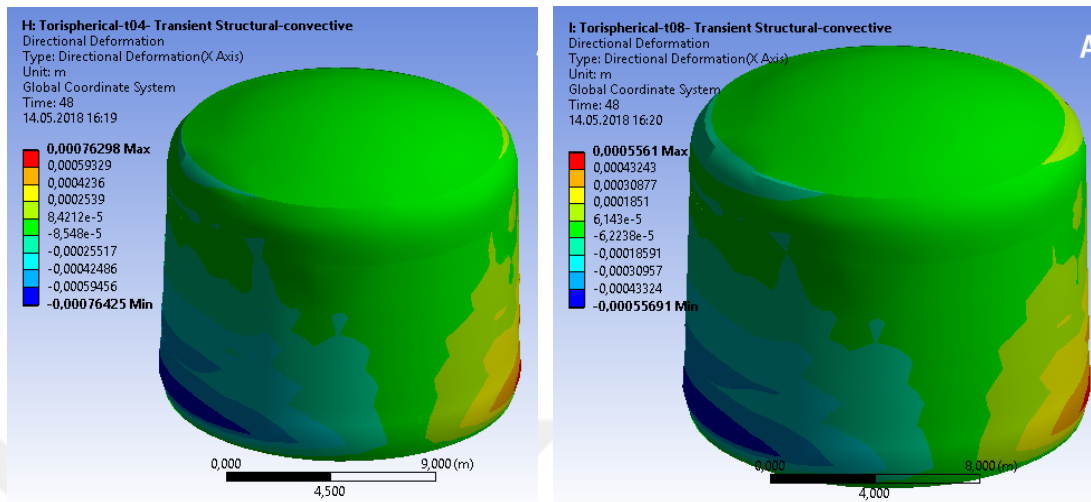


a) Buckling of flat tank for 4mm                      b) Buckling of flat tank for 8m

**Figure 6. 12** Convective buckling of conical-closed tank  $t=4$  and 8 mm



In Figure 6.13 (a) and (b) shows convective directional deformation and buckling for 4 mm and 8 mm. It seems that these two models have less buckling. Particularly when the crustal thickness is 8 mm, buckling was reduced.



a) Buckling of flat tank for 4 mm

b) Buckling of flat tank for 8 mm

**Figure 6. 13** Convective buckling of torispherical-closed tank  $t=4$  and 8 mm

### 6.3 Strengthening of Cylindrical Steel Tanks

In order to preserve of cylindrical steel liquid tanks damaging from earthquake loads, seismic isolation, multistage increasing thickness and floating roof like studies have been carried out by researchers so far. Application of some of this methods expensive or complicate. In this section, the epoxy-carbon coating method is suggested to improve of seismic performance of cylindrical steel tanks.

#### 6.3.1 Strengthening of cylindrical steel tank

One of the considerable aims of this thesis is to strengthen the tank exposed to deformation under the loads of the earthquake. It is possible to replace the steel tank with the new undeformable a tank made of thicker shell, but this will increase the cost considerably. Strengthening of existing tank at low cost is great importance.

Composite materials are widely used to fabricate cylindrical shells which can be the structural elements in storage tanks, cisterns for transportation pressure vessels, rocket components. The theory of cylindrical shells and its application to the analysis of cylindrical structures is described in numerous publications (Vasiliev and Morozov, 2018). Stress-Strain graphics of composite materials is given in Figure 6.14.

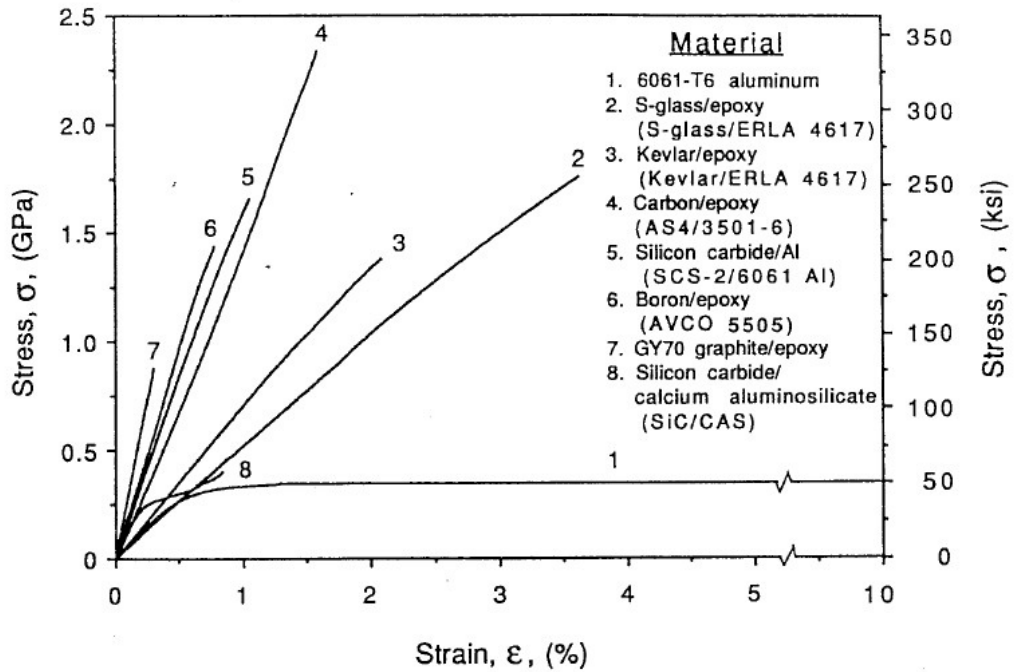


**Figure 6. 14** Stress-strain graph of some composite materials (Daniel and Ishai, 1994)

The composite material represents the combination or combination of two different and insoluble materials. These materials are distinguishable on the microscopic scale. Although each phase has its own characteristics, the properties of the composite material and the structural stability are due to the fact that each acts on its own (CNG). The materials consist of a fiber reinforcement combined with a matrix material. Allow the stiffness and strength of the material to change with loading direction. Composition of composite materials is shown in Figure 6.15.

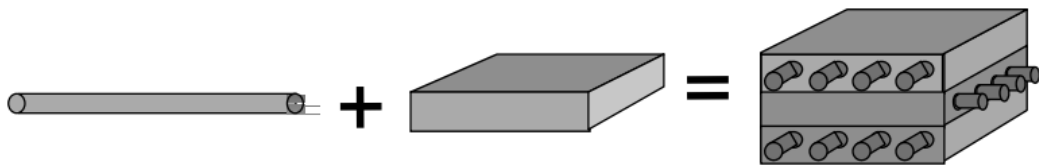


**Figure 6. 15** Composition of composites materials (Douglasb and Lysle, 2009)

**Fiber/Filament Reinforcement**

- High strength
- High stiffness
- Low density

**Matrix**

- Good shear properties
- Low density
- Good shear properties

**Composite**

- High strength
- High stiffness
- Low density

Composite materials are widely used in aerospace structures and pressure vessel tanks, especially to protect against high air pressure. Some examples are shown in Figure 6.16.

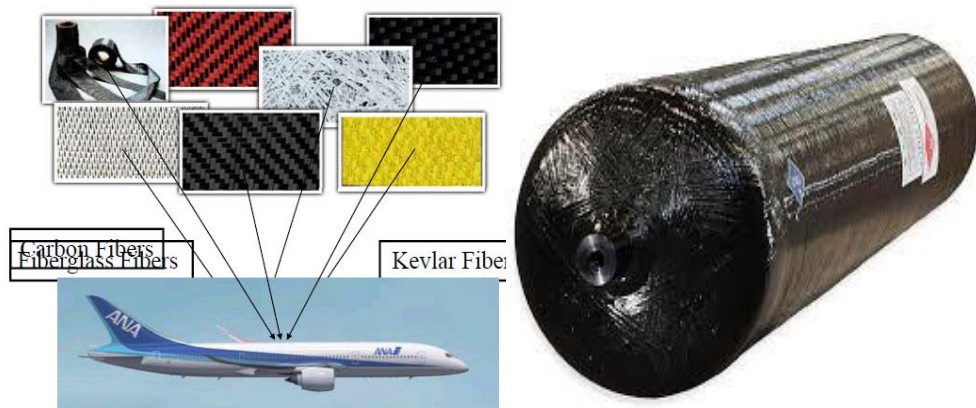


**Figure 6. 16** Application of epoxy carbon area (CNG, 2018)

Carbon fibres are widely used in strengthening reinforced concrete structures. Figure 6.17 shows the ductility test of the carbon-fibres reinforced column. Epoxy-carbon applied to the concrete surface using epoxy resin to increase the earthquake resistance is  $2.35 \times 10^5$  Mpa with Young's modulus and Strength is between 2,500-4,500 MPa. (Wakui, 1997).

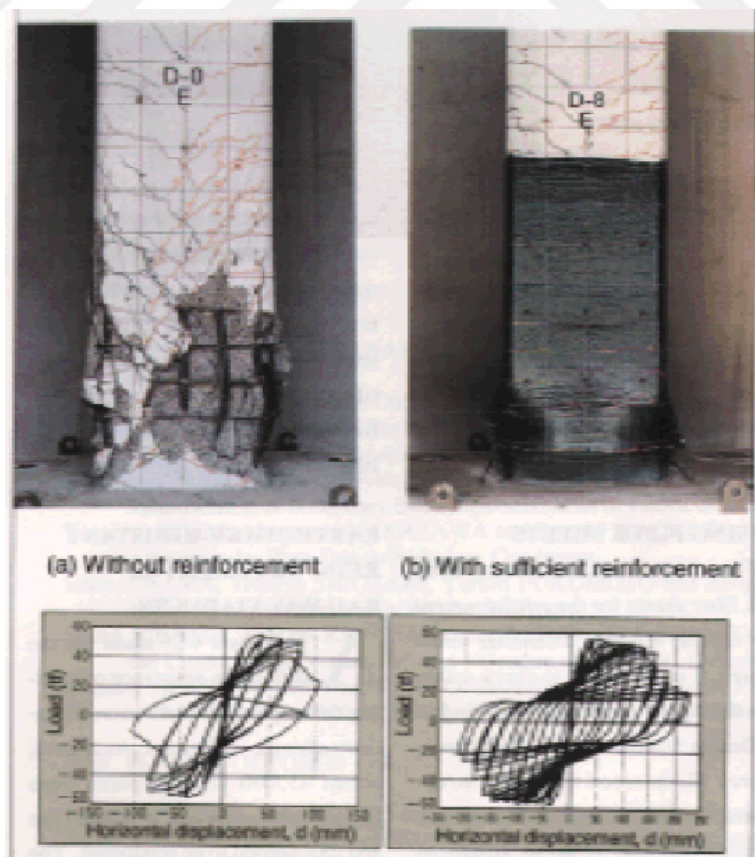


**Figure 6. 17** Ductility tests on specimens reinforced with carbon fiber sheets (Wakui, 2009)

The ANSYS Composite Prepost (ACP) module was used to perform the structural analysis of the composite wrap around the cylindrical water tank and the analyses were carried out. ANSYS is able to model and examine composite structures in more detail in this module. Relationship between transient analysis and ACP (pre) is shown in Figure 6.18.

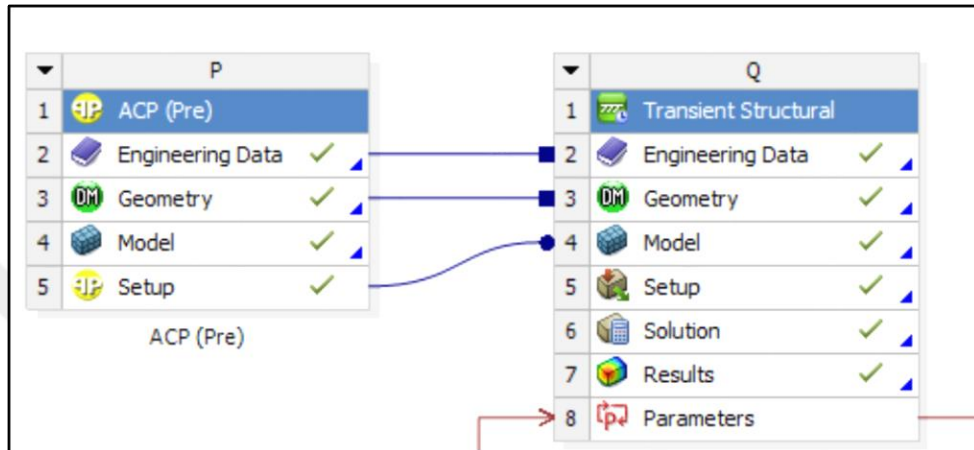


**Figure 6. 18** Relationship ACP and transient structural

Figure 6.19 shows materials properties. Composite modelling in Workbench provides the ability to account for variability in the mechanical properties of composite materials due to any scalar user-defined quantity. Temperature, Shear Angle (defined through ACP-Pre draping), and Degradation Factor are predefined variables in Workbench Engineering Data to be used for refining a composite material's behaviour.

The screenshot displays three windows from the Engineering Data Sources software:

- Engineering Data Sources:** A table with columns A (Data Source), B (Location), and C (Description). Row 9 shows 'Fluid Materials' and row 10 shows 'Composite Materials'.
- Outline of Composite Materials:** A table with columns A (Material), B (Add), C (source), and D (Description). Row 3 is selected, showing 'Epoxy Carbon UD (230 GPa) Prepreg'.
- Properties of Outline Row 3: Epoxy Carbon UD (230 GPa) Prepreg:** A table with columns A (Property), B (Value), and C (Unit). It lists various material properties such as Density, Orthotropic Secant Coefficient of Thermal Expansion, Orthotropic Elasticity, Young's Modulus in X, Y, and Z directions, Poisson's Ratio in XY, YZ, and XZ directions, and Shear Modulus in XY and YZ directions.

Engineering Data Sources		
A	B	C
1	Data Source	Location
9	Fluid Materials	Material samples specific for use in a fluid analysis.
10	Composite Materials	Material samples specific for composite structures.

Outline of Composite Materials			
A	B	C	D
1	Contents of Composite Materials	Add	source
2	Material		
3	Epoxy Carbon UD (230 GPa) Prepreg		

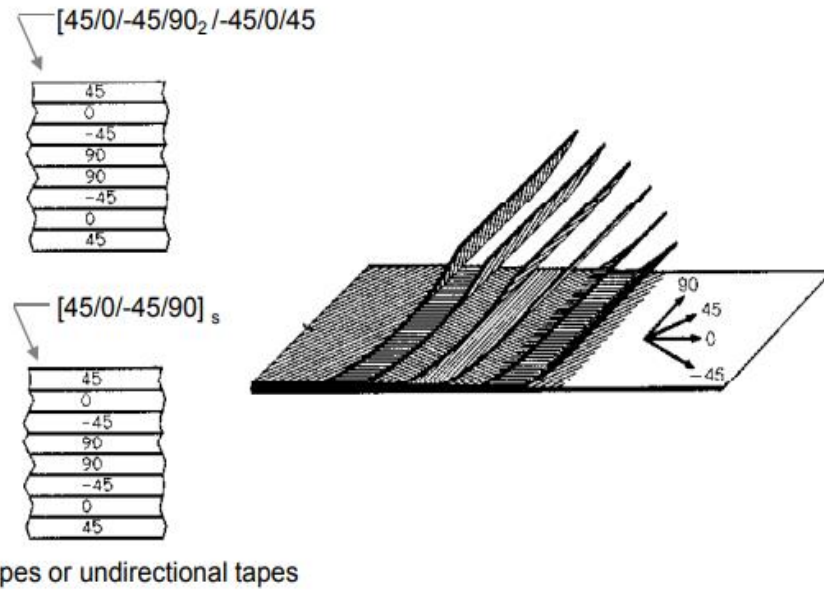
  

Properties of Outline Row 3: Epoxy Carbon UD (230 GPa) Prepreg		
A	B	C
1	Property	Value
2	Density	1490
3	Orthotropic Secant Coefficient of Thermal Expansion	
8	Orthotropic Elasticity	
9	Young's Modulus X direction	1,21E+11
10	Young's Modulus Y direction	8,6E+09
11	Young's Modulus Z direction	8,6E+09
12	Poisson's Ratio XY	0,27
13	Poisson's Ratio YZ	0,4
14	Poisson's Ratio XZ	0,27
15	Shear Modulus XY	4,7E+09
16	Shear Modulus YZ	3,1E+09

**Figure 6. 19** Fabrics and tapes

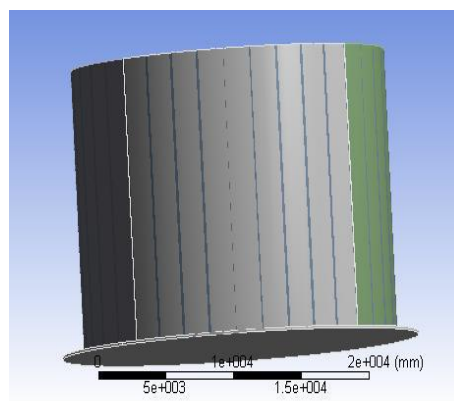
- When the fabric layers are used in a laminate. The fabric warp angle is used as the floor direction angle. The fabric angle is enclosed in parentheses to define the layer as a fabric layer.
- The laminate is made from both fabric and tape layers (hybrid laminate). The parentheses around the fabric layers separate the fabric layers from the belt layers.
- When the laminate is symmetrical and odd numbered, the center line is drawn to indicate that the middle layer is the middle plane.

Figure 6.20 presents the application of epoxy-carbon material.



**Figure 6. 20** Application of epoxy carbon material (Gemite, 2013)

Prasad, K. J., and Prasad C. S. tried a strengthening technique of cylindrical steel tank with GFRP composite material using design method of CATIA and ANSYS finite element analysis software. They also provided that thermo plastic polyethylene was coated around the tank with a thickness of 2mm as shown in Figure 6.21 (Prasad and Prasad, 2017).



**Figure 6. 21** Strengthening technique with TPP (Prasad and Prasad, 2017).

In Figure 6.22 is shown application of epoxy-carbon fibres on the cylindrical liquid tank. Some companies are using epoxy carbon to protect the technique of wrapping cylindrical steel tanks from corrosion. However, there is no coating technique in order to increase resistance against deformation.





**Figure 6. 22** Application of fibers on the cylindrical tank

These specified angles are the helical of the fibres that it is spirally wrapped. In the program, fibre angles can be changed parametrically. The adjustment of the ideal angle of the layers is effective in strengthening. Determining of angles and tan tank are shown in below.

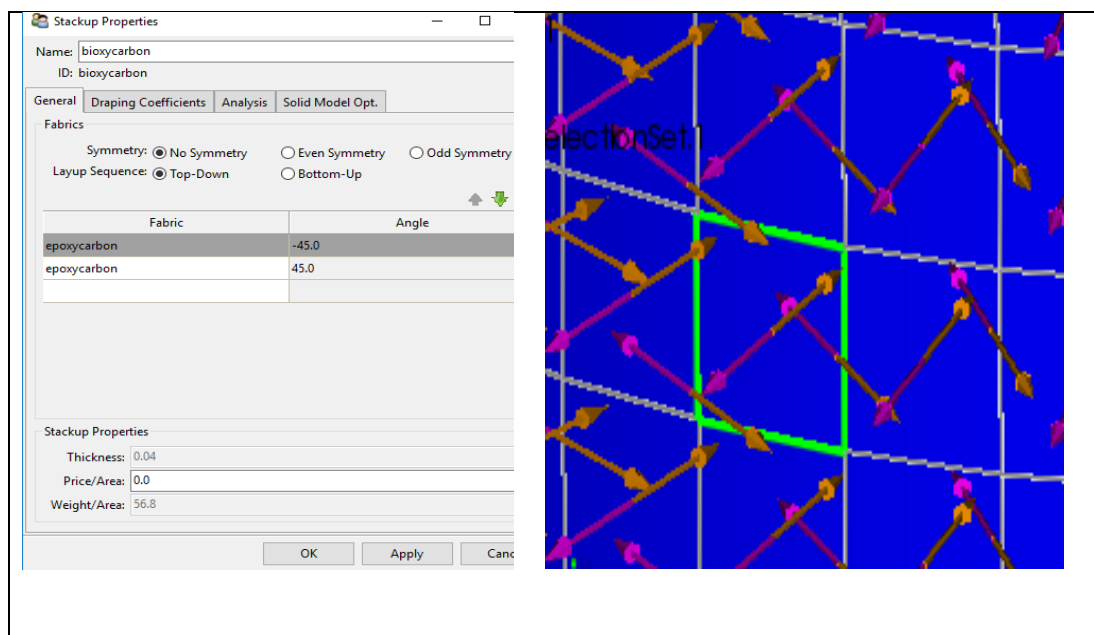


**Figure 6. 23** Defining angle of epoxy carbon fibers in ACP.

### 6.3.2 Result of strengthening tanks

After had coated of tank with epoxy –carbon composite material, in directional deformation and Equivalent (von-Misses) stress seriously was decreased. In Figure 6.24 shows distribution of the equivalent stress before and after strengthening open-top tank. Analysis was performed as impulsive under the E-Centro earthquake loads. The red colors show the maximum hoop stress and, blue color shows the minimum stress. It is observed that after strengthening with epoxy-carbon in the cylindrical steel tank (in Figure 6.24 (b)), there is a serious decrease in the hoop stress. In addition, that due to the stress reduction, it appears that the elephant foot buckling in the bottom of the tank disappears. The maximum hoop stress in the unprotected tank is 81.92 MPa, while the maximum equivalent stress is reduced to 63.40 MPa after it was coated with the epoxy-carbon.

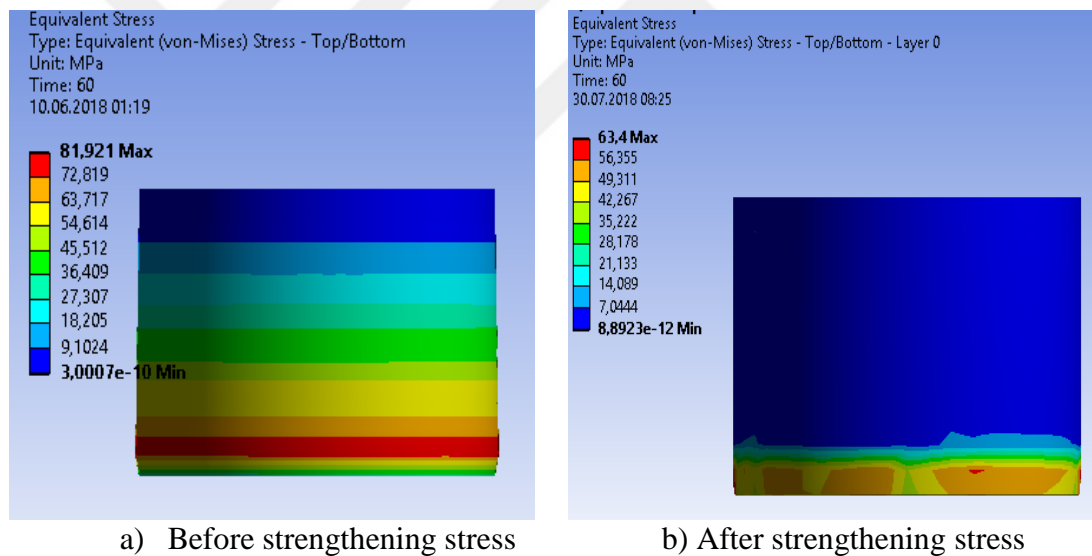
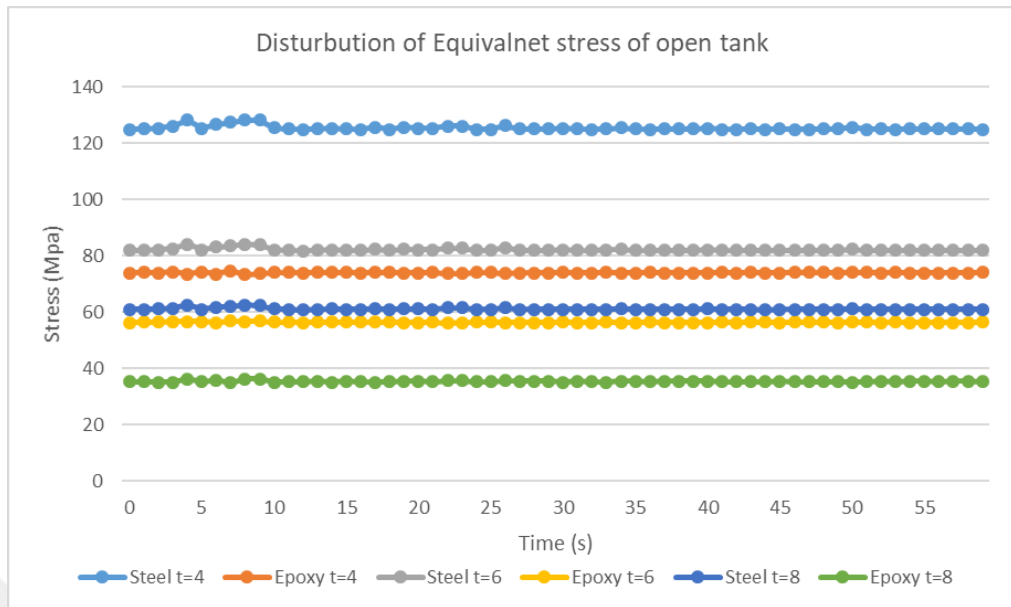


Figure 6. 24 Strengthening of open-top tank

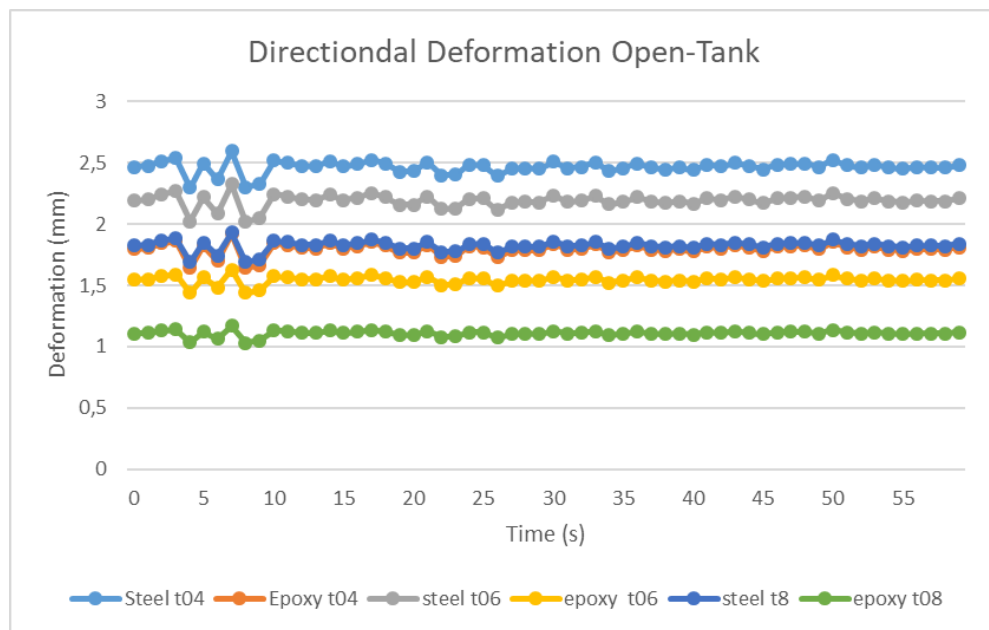
In Figure 6.25 shows distribution Equivalent stress as determined different shell thickness of open-top tanks. It is shown that, it is protected the cylindrical steel tank with epoxy-carbon composite material, it provides better protection than increasing its thickness. As seen in the graph, maximum stress value of tank which is at 4 mm shell thickness is between 6 mm and 8mm unprotected tanks stress value.





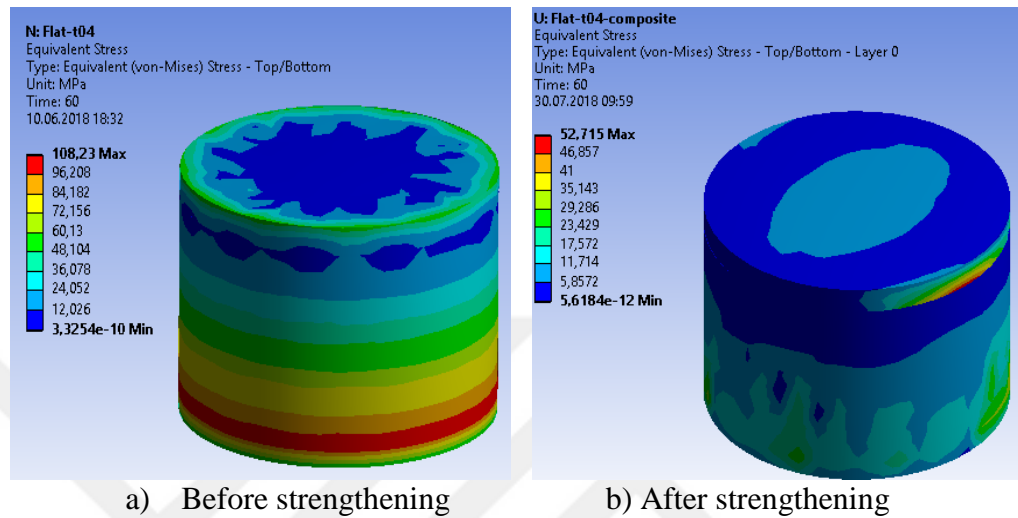
**Figure 6. 25** Comparison of equivalent stress

Figure 6.26 shows directional deformation for all shell thickness of open-top tank. Maximum directional deformation is about the 2.5 mm in unprotected tank, while it is occurred below the 2 mm in coated tank with epoxy carbon at 4 mm shell thickness. In 6 mm shell thickness directional deformation decreased from 2.2 mm to 1.5 mm. At the same time, directional deformation decreased from 1.8 mm to 1.2 mm at the 8 mm shell thickness.



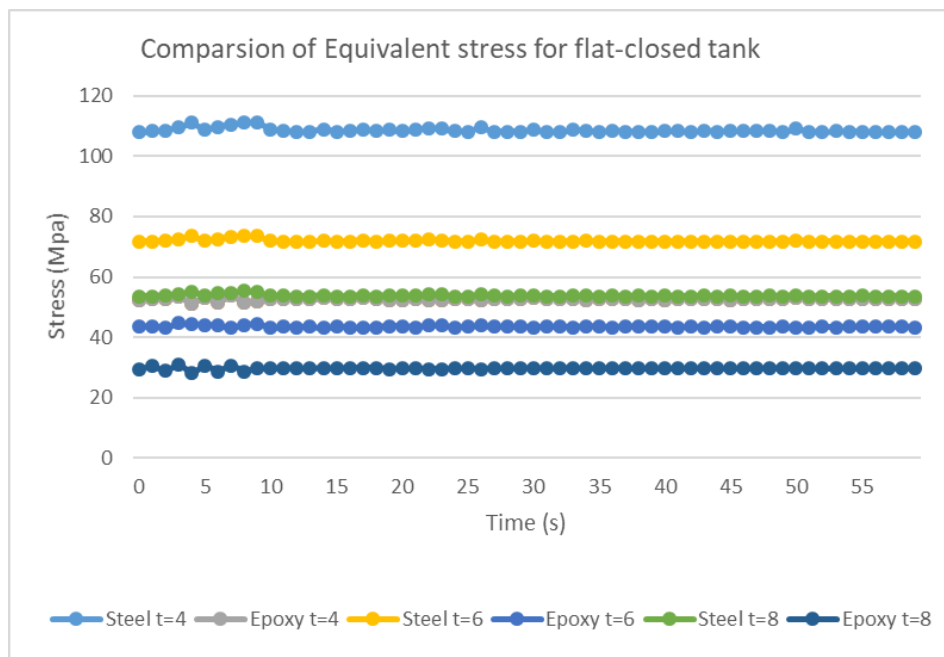
**Figure 6. 26** Directional deformation graphs of open-top tank t=4mm

In Figure 6.27 is shown difference between unprotected and covered flat-closed tank. The red-colored maximum stress in Figure 6.27(a) is almost disappear in the reinforced tank in Figure 6.27 (b). While maximum von-misses stress is occurred 108.23 Mpa in cylindrical steel tank, it is decreased to 52.71 Mpa in strengthening of tank with epoxy-carbon.



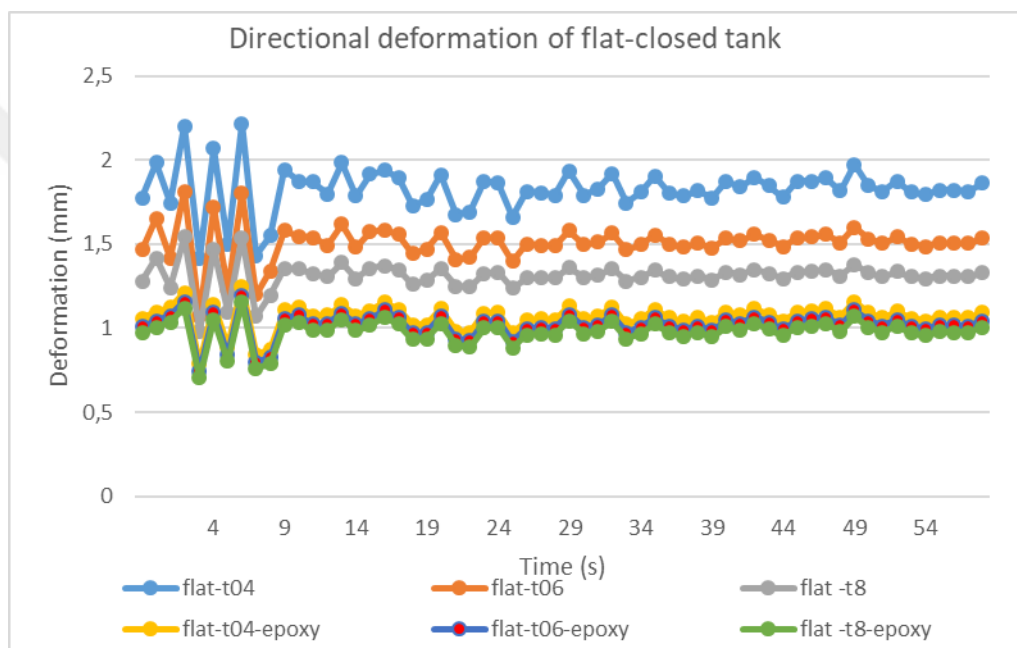
**Figure 6. 27** Straightening of flat-closed tank

Stress curves are shown at different shell thickness of flat-closed tanks in Figure 6.28. Seismic performance of Epoxy carbon reinforced tanks is very good. Stress curves are shown at different shell thickness of flat-closed tanks in Figure 6.28. Von-Mises stress is lower in the all strengthened tanks than the unprotected all cylindrical steel tanks.



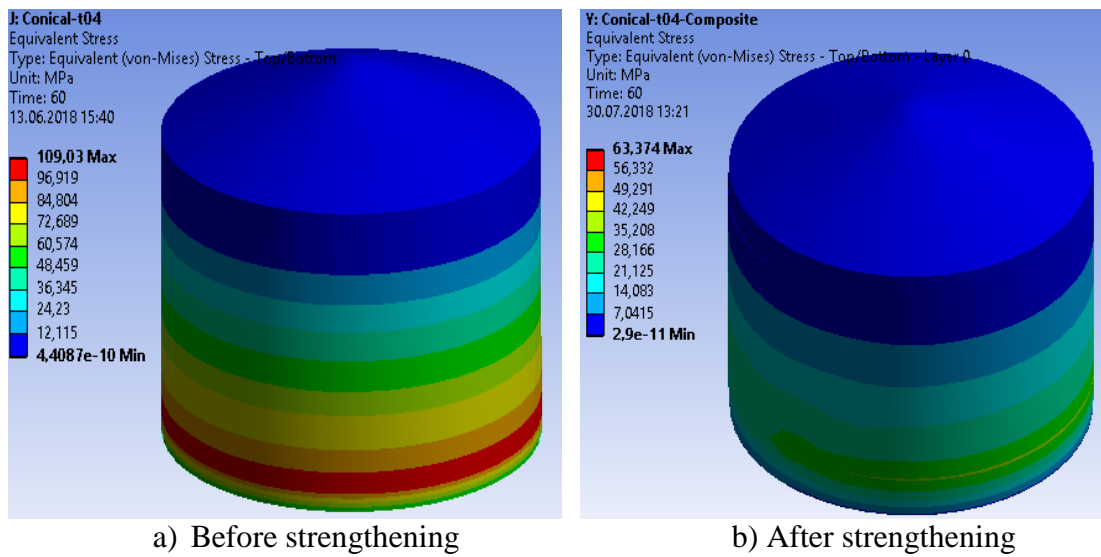
**Figure 6. 28** Comparison of equivalent stress of flat-closed tank

A directional deformation curve is drawn for each of the tanks under the study in terms of different thickness a flat-closed tank versus strengthening of flat-closed tanks. Figure 6.29 show the directional deformation curves for flat-closed tanks with different shell thickness. Normally shell thickness is 6 mm, but directional deformation is around the 1 mm at 4 mm shell thickness in tank, while directional deformation is about 2 mm in tank with 6 mm shell thickness. It can also be deduced that the seismic performance of the 4 mm flat-closed cylindrical steel tank can be improved by covering the tank with epoxy-carbon material, better than a 6 mm unprotected tank.



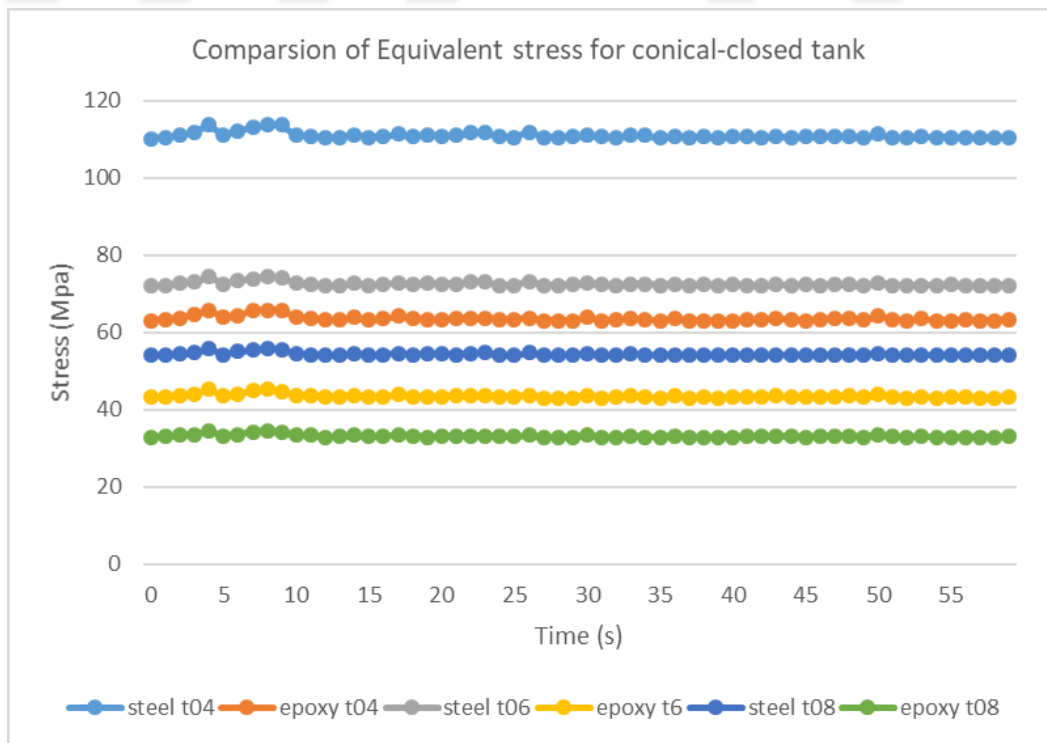
**Figure 6. 29** Directional deformation of flat-closed

Figure 6.30 shows the von-Mises stress of conical-closed cylindrical steel tank under the el-Centro earthquake loading. Red lines which are show the maximum stress in the unprotected steel tank, they are disappear after the strengthening of conical tank. While maximum stress is 108.03 Mpa in the unprotected tank, it is 63.37 Mpa in the protected tank with epoxy-carbon material.



**Figure 6.30** Strengthening of conical-closed tank

Stress curves are shown at different shell thickness of conical-closed tanks in Figure 6.31. Seismic performance of Epoxy carbon reinforced tanks is very good. Stress curves are shown at different shell thickness of conical-closed tanks in Figure 6.31. Von-Mises stress is lower in the all strengthened tanks than the unprotected all cylindrical steel tanks.



**Figure 6.31** Comparison of equivalent stress of conical-closed tank

A directional deformation curve is drawn for each of the tanks under the study in terms of different thickness a conical-closed tank versus strengthening of conical-closed tanks. Figure 6.32 show the directional deformation curves for conical-closed tanks with different shell thickness. Normally shell thickness is 6 mm, but directional deformation is below the 1 mm at 4 mm shell thickness in tank, while directional deformation is about 1.6 mm in tank with 6 mm shell thickness. It can also be deducted that the seismic performance of the 4 mm conical-closed cylindrical steel tank can be improved by covering the tank with epoxy-carbon material, better than a 6 mm unprotected tank. As a result, directional deformation is more linearly in protected tank than unprotected conical tank.

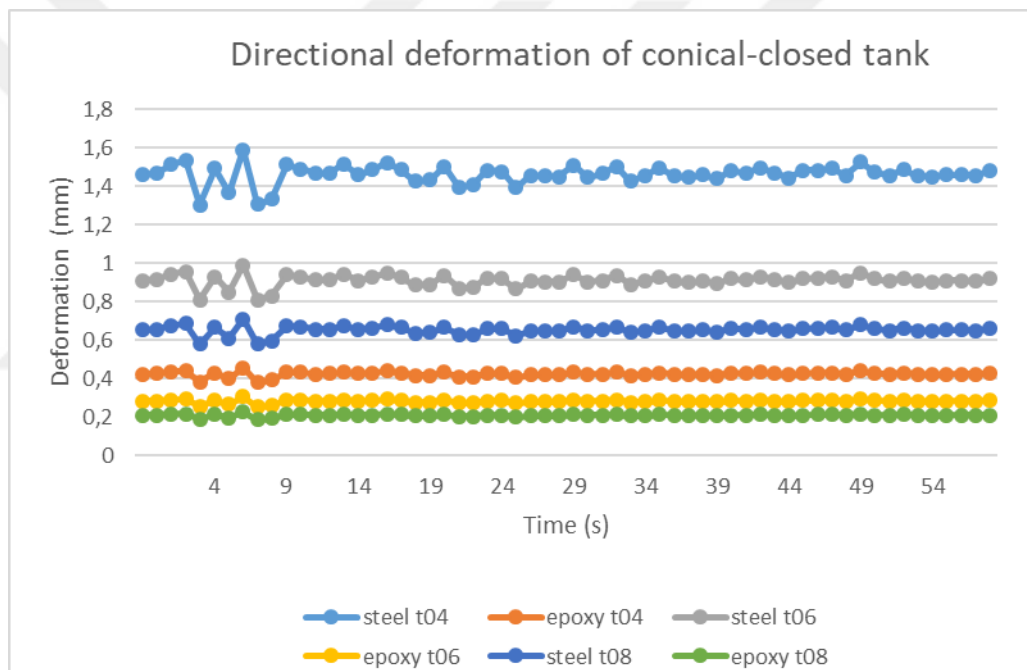
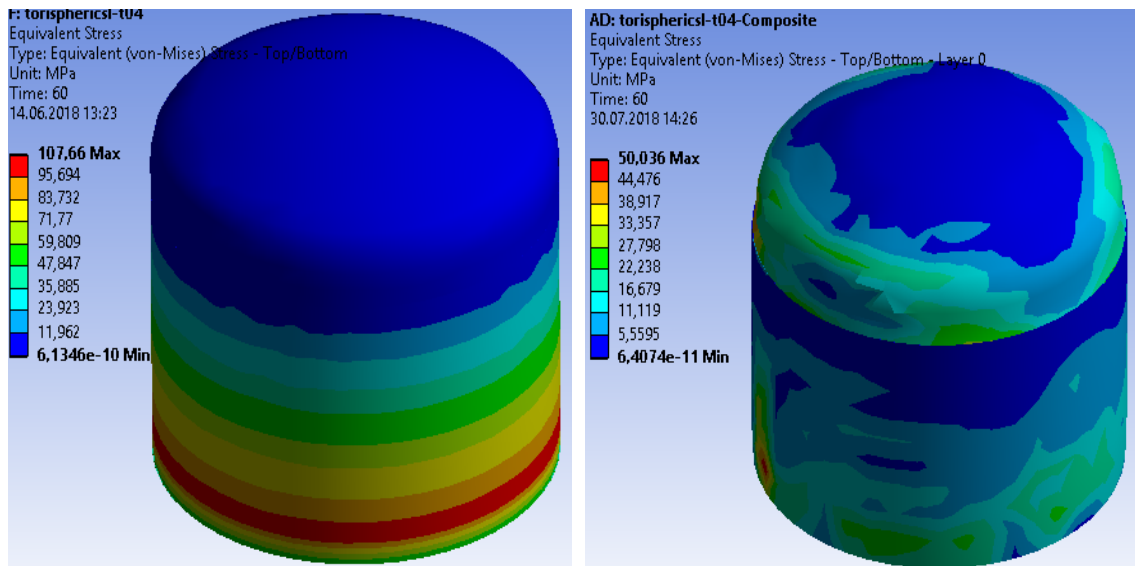


**Figure 6. 32** Directional deformation of conical-closed tank

Figure 6.33 shows the von-Misses stress of torispherical-closed cylindrical steel tank under the el-Centro earthquake loading. Red lines which are show the maximum stress in the unprotected steel tank (Figure 6.33(a)), they are disappear after the strengthening of conical tank. Although there is a little bit stress increase on the roof of tank, it is observed that the stress on the bottom of tank is seriously reduced due to strengthening in general. While maximum stress is 107.66 Mpa in the unprotected tank, it is 50.036 Mpa in the protected tank with epoxy-carbon material.



a) Before strengthening torispherical tank    b) After strengthening torispherical tank

**Figure 6. 33** Strengthening of torispherical-closed tank

Stress curves are shown at different shell thickness of torispherical-closed tanks in Figure 6.34. Von-Mises stress is lower in the all strengthened tanks than the unprotected all torispherical-closed cylindrical steel tanks.

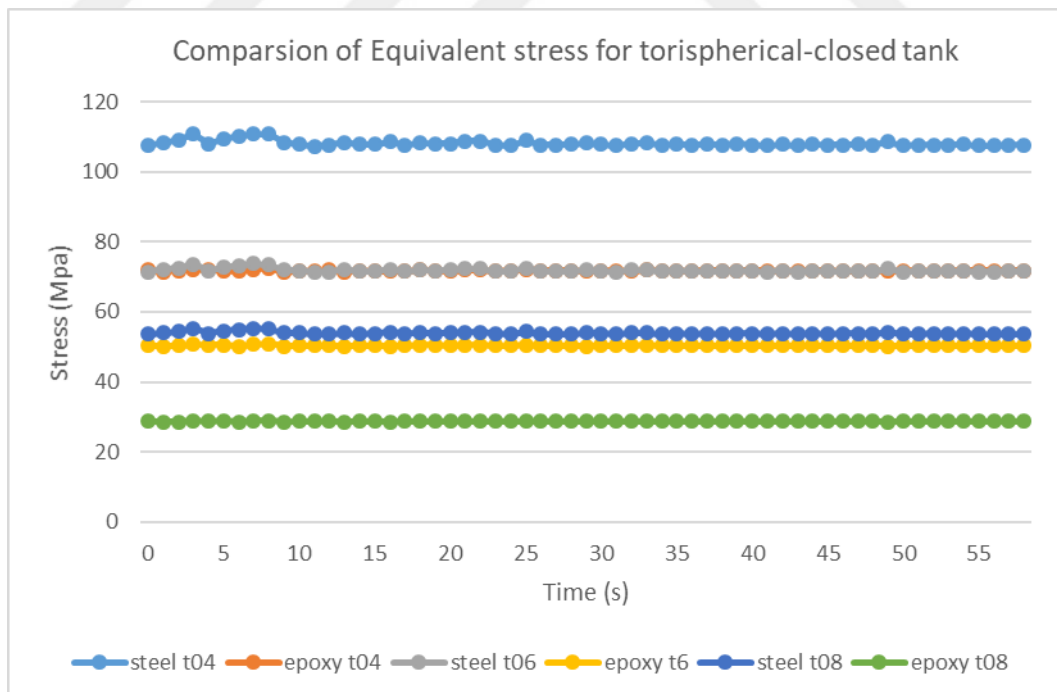


**Figure 6. 34** Comparison of equivalent stress for torispherical-closed tank

A directional deformation curve is drawn for each of the tanks under the study in terms of different thickness a torispherical-closed tanks versus strengthening of torispherical-closed tanks. Figure 6.35 show the directional deformation curves for torispherical-closed tanks with different shell thickness. Normally shell thickness is 6 mm, but directional deformation is between the 1.4 and 1.6 mm at 4 mm shell thickness in tank, while directional deformation is below the 1 mm in tank with 6 mm shell thickness. It can also be deduced that the seismic performance of the 4 mm conical-closed cylindrical steel tank can be improved by covering the tank with epoxy-carbon material, better than a 6 mm unprotected tank. As a result, directional deformation is more linearly in protected tank than unprotected conical tank.

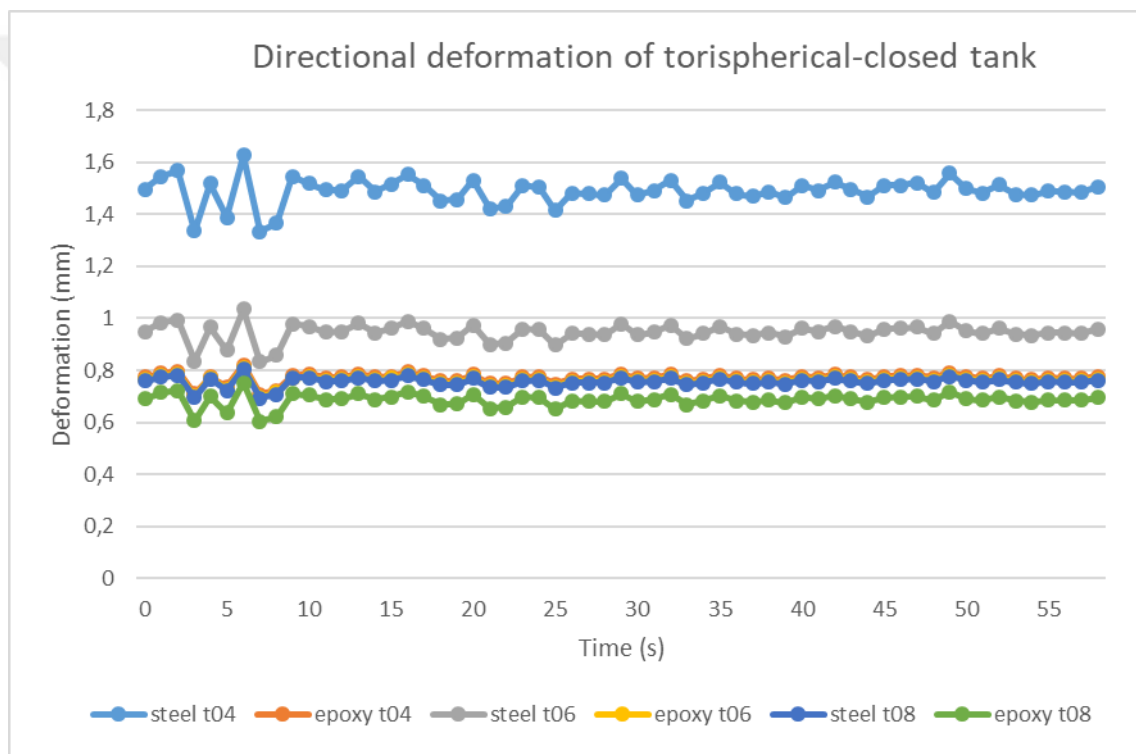


**Figure 6. 35** Comparison of directional deformation of torispherical-closed tank

#### 6.4 Summary

Cylindrical steel tanks are exposed such as shell buckling, elephant foot buckling, roof buckling. These buckles usually are occurred because of the stress subjected the earthquake loading. In the previous chapter, seismic performance of cylindrical steel

tanks with different roof were examined under the both El-Centro and Kobe earthquake loads. The best roof type determined to increase seismic performance.

In this chapter, strengthening of cylindrical steel tanks were performed with epoxy-carbon composite material. In addition to the previous chapter, the work to reduce buckles was made by reducing the stresses and deformations in the tanks. To sum up, the maximum von-Misses stress in the unprotected tank is 81.92 MPa, while the maximum environmental stress is reduced to 60.40 MPa after it was coated with the epoxy-carbon in open-top tank. While maximum von-misses stress is occurred 108.23 Mpa in cylindrical steel tank, it is decreased to 52.71 Mpa in strengthening of tank with epoxy-carbon in flat-closed tank. While maximum stress is 108.03 Mpa in the unprotected tank, it is 63.37 Mpa in the protected tank with epoxy-carbon material in conical-closed tank. While maximum stress is 107.66 Mpa in the unprotected tank, it is 50.036 Mpa in the protected tank with epoxy-carbon material in torispherical-closed tank. Depending on the decrease in stress, there have been serious reductions in directional deformation and buckles of the open-top, flat-closed, conical-closed and torispherical-closed tanks respectively.

Some companies have coated of cylindrical steel tanks to protect them against corrosion. This technique can be used particularly to improve the seismic performance of tanks in earthquake zones.

Prasad, K. J., and Prasad C. S. performed seismic analysis and design of a cylindrical tank strengthened by GFRP and thermo plastic polyethylene composites. This study has the first studies on this subject, but it has limited results and suggestions

In this section, it is observed that after the strengthening, the tension is reduced by about 50% according to the results obtained for different thicknesses and different roof types. It has been found that even a 4 mm tank exhibits seismic performance at tank level of 6 mm after retrofitting.

Recommendation-1 Tanks with weak walls can be reinforced with epoxy carbon to make seismic performances compatible with the standards.

Recommendation-2 In particular, strengthening tanks built in earthquake zones with epoxy-carbon can be made compulsory.



## **CHAPTER 7**

### **IMPACT ANALYSIS OF CYLINDRICAL STEEL WATER TANK**

#### **7.1 Introduction**

In this chapter, explicit dynamic analysis will be performed at three different thickness and four roof type of cylindrical steel tanks. If the product needs to withstand impact or short-term high pressure loads, the design can be improved with ANSYS explicit dynamics. Specialized problems require sophisticated analytical tools to accurately predict the effect of design on product or process behaviour. Gaining insight into such complex reality is especially important when it is too costly or impossible to do physical testing. The ANSYS explicit dynamic package allows to capture the physics of short-term events for products exposed to highly nonlinear, transient dynamic forces. Custom, accurate and easy-to-use tools are designed to maximize user productivity. With ANSYS, you can learn how a build reacts to heavy loads. Algorithms based on the first principles correctly predict complex reactions such as large material deformations and failures, interactions between objects, and fluids with rapidly changing surfaces.

Defaults are safe and reasonable values for most options; this means less time spent tuning and running problems, optimizing products for performance, durability, and cost, and spending more time waiting for design flaws.

#### **7.2 Explicit Dynamics Analysis**

Variety of engineering simulations can be performed with the Workbench Explicit Dynamic method. ANSYS explicit dynamics is a transient explicit dynamic, which includes of nonlinear dynamic behaviour of solid, fluid, gases and their interaction. A typical simulation consists of setting up the model, interactions and the applied loads, solving the model's nonlinear dynamic response over time for the loads and interactions, then examining the details of the response with a variety of available tools.

The Explicit Dynamics application has objects arranged in a tree structure that guides at different stages of a simulation. By expanding objects, it can be exposed details about the object and use related tools and specifications to accomplish this part of the simulation. Objects are used to identify environmental conditions, such as contact surfaces and loads, and to describe the results that they want to be available for examination.

The Explicit dynamic analysis is used to determine the dynamic response of a structure due to stress wave propagation, impact, or time-dependent loads due to rapidly varying time. The momentum changes between moving objects and inertial effects are often an important aspect of the type of analysis performed. This type of analysis can also be used to model highly nonlinear mechanical events. Nonlinear materials can be caused by material (hyperelasticity, plastic flows, failure, eg.), contact (high-speed collisions and impact, eg.), and geometric deformation (buckling and sagging, eg). Events with timescales of less than 1 second (typically 1 millisecond) are effectively simulated by such analyses.

### **7.2.1 References of Eulerian (virtual) body**

In a Eulerian reference frame, the grid remains stationary throughout the simulation. Material flows through the mesh. The mesh does not therefore suffer from distortion problems and large deformations of the material can be represented. Because of large deformations of steel tank material, using a Eulerian reference frame is preferable.

Solid, liquid and gaseous materials can be used with Euler (Virtual) reference frame in Explicit Dynamic analysis. The Euler reference frame should only be used when very large deformation or material flow is expected, since the cost of calculation and the approximation of the material interfaces are approx.

A volume of liquid (VOF) method is used to monitor the amount of material in each cell. Each material has a volume fraction and the sum of the volume fraction of each material plus the sum of the void volume is equal to one.

$$[6.1] \quad \sum_{i=1}^{i=nmat} F_i + F_{void} = 1$$

Almost all isotropic material properties can be used in an Euler reference frame to represent solids, liquids or gases. Special processing is required to calculate the tensile

ratios of each material in a cell, the pressure and stresses, and also the resulting tensile tensor, which is then used to calculate cell facets, momentum and mass transport (ANSYS, 2018).

### 7.2.2 Explicit fluid-structure interaction

In the Explicit Dynamics system, rigid bodies can be either Lagrangian reference frame or Eulerian reference frame. The reference frames can be combined simulatively to allow the best solution technique to be applied to each material being modeled. During the simulation, the organs represented in the two reference frames will automatically interact with each other. For example, if a body is filled with steel using a Lagrangian reference frame and another body filled with water using the Euler reference frame, the two bodies will automatically interact with each other if they are in contact. The interaction between Eulerian and Lagrangian bodies provides an ability to interact tightly in a bidirectional fluid structure in the Explicit Dynamics system.

In the following simple example, a body with a Lagrangian reference frame (gray) moves from left to right on a body with Euler reference frame. As the body moves, Euler cells act as a moving border in the Euler region, progressively covering their volumes and faces. This leads to a material flow in the Euler Domain. At the same time, a stress field will develop in the Euler region resulting in external forces applied to the moving Lagrangian body. These forces will return to the movement and deformation (and stress) of the Lagrangian body as shown in Figure 7.1.

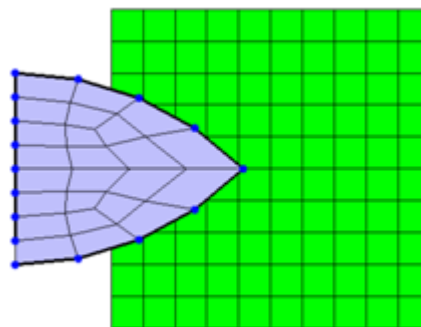


**Figure 7. 1** Eulerian reference frame (SASIP, 2018)

In more detail, the Lagrangian body covers areas of the Euler area. The intersection between Lagrange and Euler bodies leads to an updated control volume in which the

conservation equation of mass, momentum and energy is solved. Update control volume is illustrated in Figure 7.2.

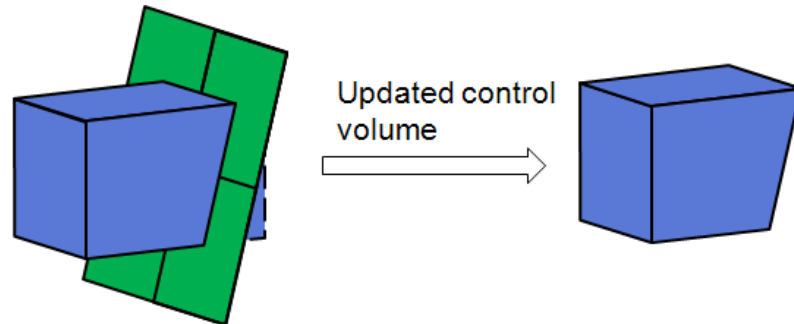


**Figure 7. 2** Eulerian reference frame (SASIP, 2018)

At the same time, normal stress on the intersecting Euler cell will move over the intersecting area of the Lagrangian surface. Figure 7.3 shows normal stress in interaction Eulerian cells.

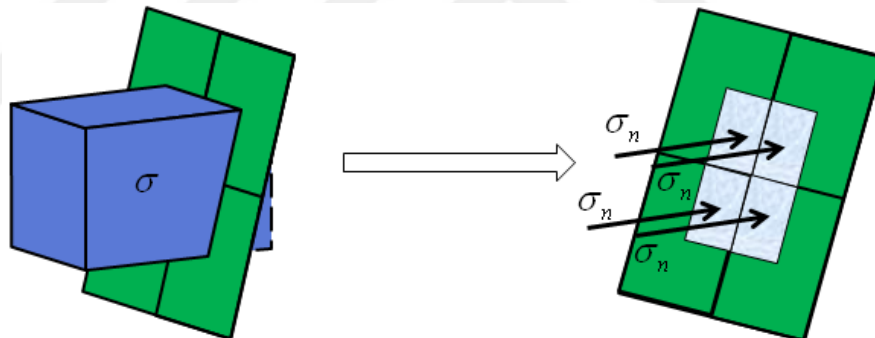


**Figure 7. 3** Normal stress in the intersected Euler cell (SASIP, 2018)

This provides a bidirectional interconnected fluid structure interaction. During a simulation, the Lagrangian structure can move and deform. Large deformations can cause erosion of elements from the Lagrangian body. In such cases, the connection interfaces are automatically updated.

To achieve precise results when combining Lagrangian and Euler objects in Explicit Dynamics, it is necessary to ensure that the size of the cells of the Euler dominant is smaller than the minimum distance along the thickness of the Lagrangian objects. If this is not the case, material leakage can be seen in the Euler region with the Lagrange structure. (SASIP, 2018)

Body interaction between tank's shell and water was performed automatically as frictionless as shown in Figure 7.4.

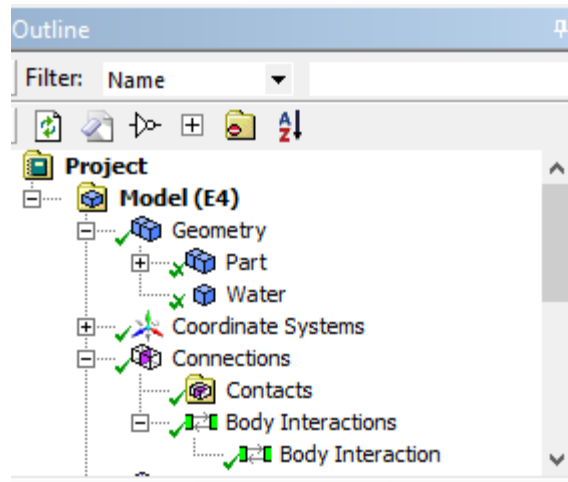


**Figure 7. 4** Interaction of bodies

### 7.3 Setting up Procedure 3d Explicit Dynamic Analysis

Setting-up process is composed of three consecutive steps named as pre-processor, execution and results. First step begins with create an Explicit Dynamics Analysis system by double-clicking on the system as shown in Figure 7.5.

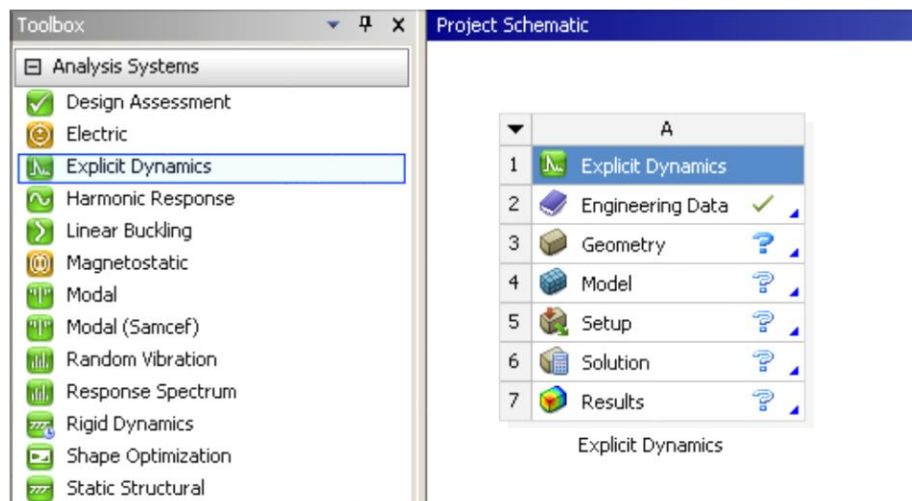


**Figure 7. 5** Established explicit dynamic analysis

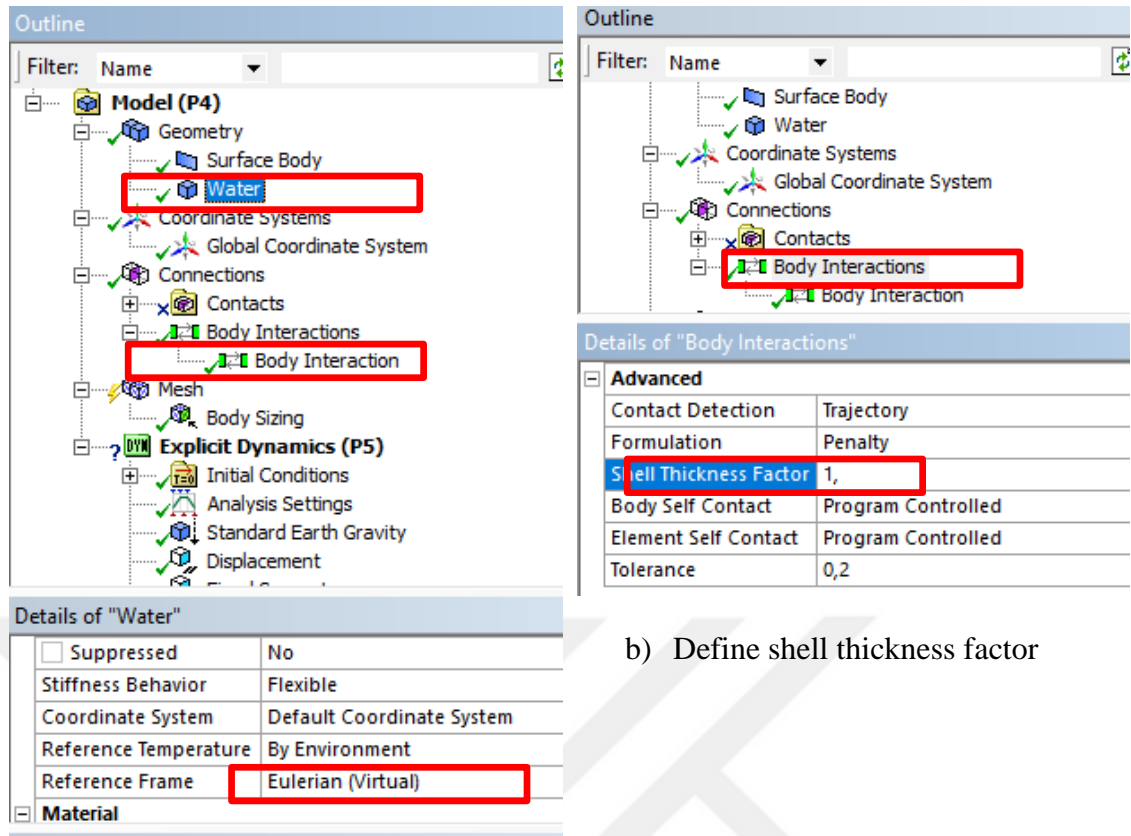
Properties of water material can be defined the under “Engineering Data” option. Density and Isotropic are added the following and physical properties can be defined by dropping

and drop them to the specified material. While defining Poisson ratio of water should be defined as in the Figure 7.6.

Property	Value	Unit
Material Field Variables	Table	
Density	1000	kg m <sup>-3</sup>
Isotropic Elasticity		
Derive from	Bulk Mo...	
Young's Modulus	1,32	Pa
Poisson's Ratio	0,5	
Bulk Modulus	2,2E+09	Pa
Shear Modulus	0,44	Pa

**Figure 7. 6** Definition of material properties

In the following Figure 7.7 (a and b) defines are significantly vital. Reference frame define “Eularian (Virtual)” for water and shell thickness factor should be 1.



a) Define Eulerian (virtual)

b) Define shell thickness factor

**Figure 7.7** Specify materials

In Figure 7.8 shows of the Scope. The scope should be changed to “Eulerian Bodies only” (there is no need to extend the Euler mesh to cover the tank shell). Total cells should be reduced the from 250000 to 25000 (this is a simple model, so a very fine Euler mesh is not needed).

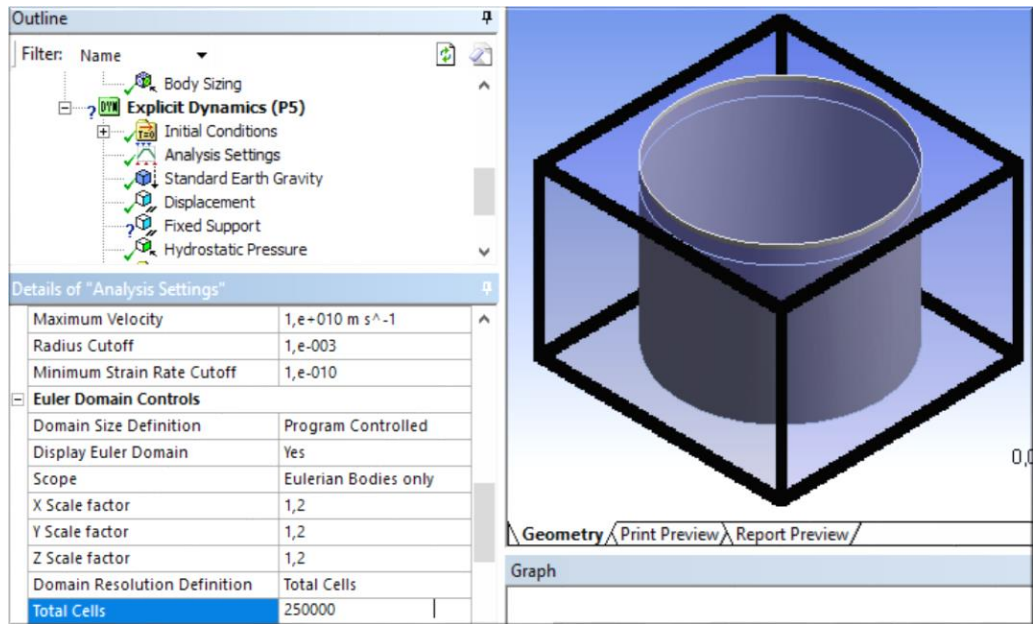


Figure 7. 8 Define Eulerian bodies only

After setting accurately explicit dynamic of water tank, it can be meshed. The mesh body size defined 1m. Mesh model of tank is shown in Figure 7.9.

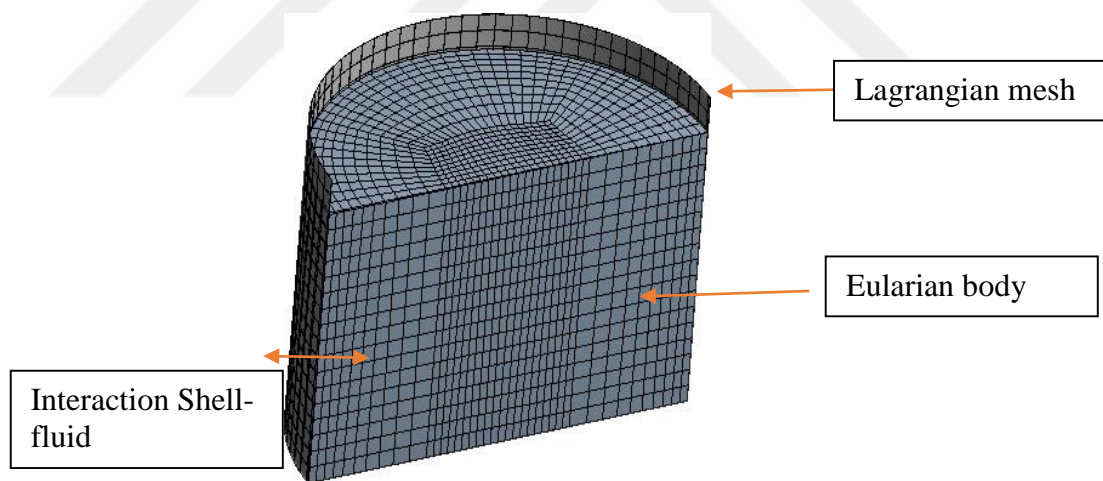
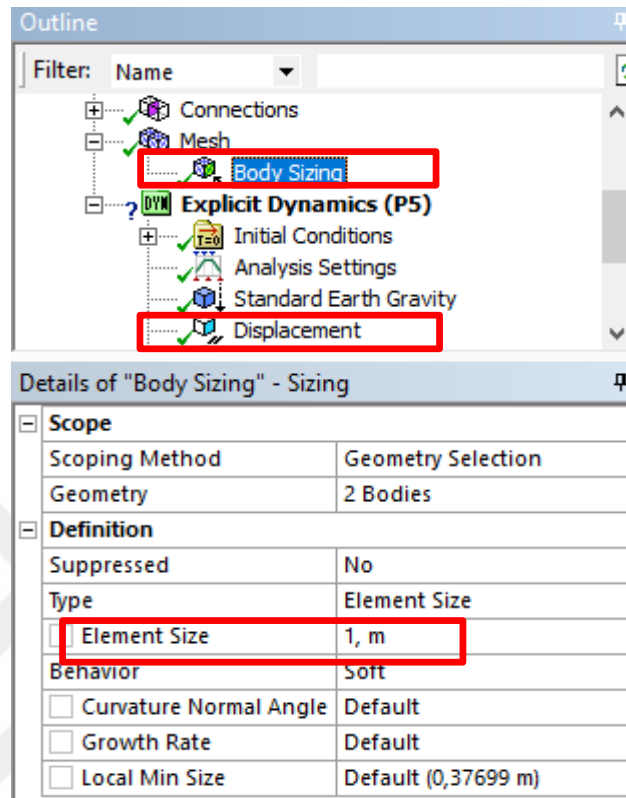


Figure 7. 9 Mesh models of tanks

The explicit dynamic analysis is used to determine the dynamic response of a structure due to stress wave propagation, impact, or time-dependent loads due to rapidly varying time. The momentum changes between moving objects and inertial effects is often an important aspect of the type of analysis performed. This type of analysis can also be used to model highly nonlinear mechanical events. Nonlinear materials can be caused by material contact and geometric deformation. Events with less than 1 second time scales are simulated with this type of analysis effectively (SASIP, 2018). In the analysis, explicit



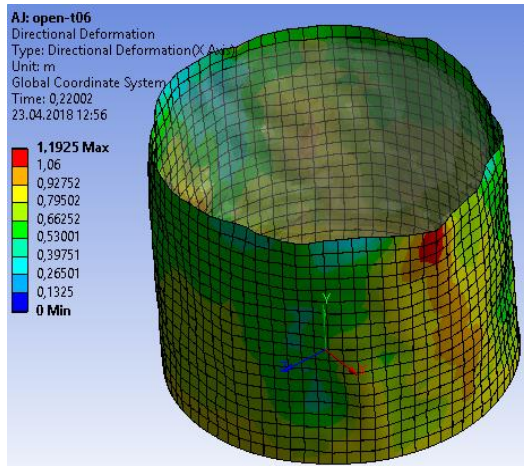
dynamic, 0.22 second earthquake values were defined as displacement force. Figure 7.10 is shown defining body size and displacement.



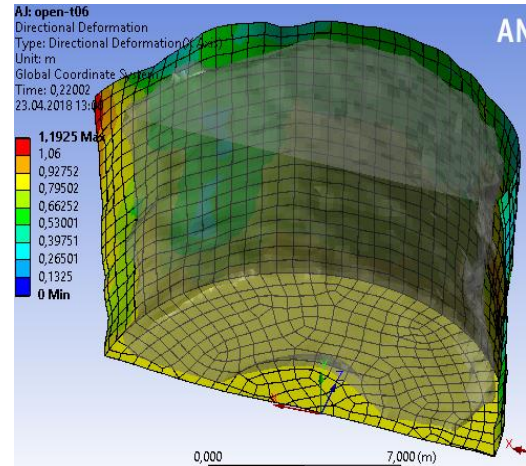
**Figure 7. 10** Define eulerian bodies only

#### **7.4 Performed Explicit Dynamic Analysis and Evaluation of Directional Deformation**

After making all the adjustments for the analysis, the results of "Directional Deformation" relative to the X axis of the tank used as the model are shown in Figures 7.11, 7.12, 7.13 and 7.14. It was observed that the effect of directional deformation due to the hydrodynamic convective pressure on the upper side of the steel tank was observed in images given as full and half geometry to see the impact of water on the walls. In the open-top tank model, the maximum directional deformation reached around 1.192 m. When the tank wall was examined, it was observed that the deformation was more common in the lower regions, but the maximum deformation occurred on the upper side of the tank walls with sloshing effect.



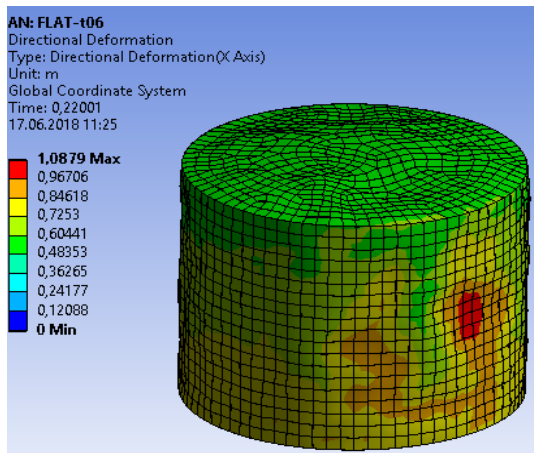
a) Directional deformation



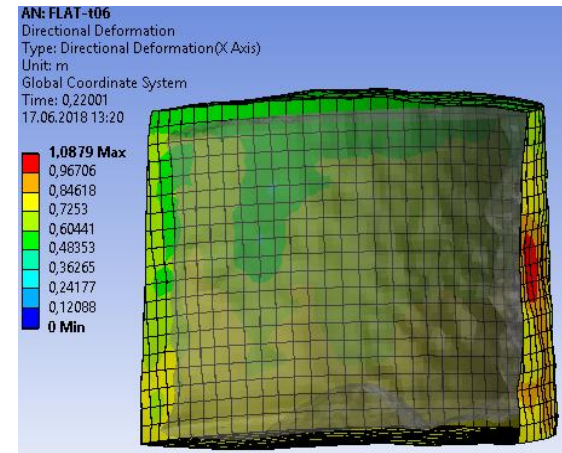
b) Half geometry of directional deformation

**Figure 7. 11** Directional deformation of open-top tank

In Figure 7.12 is shown flat-closed directional deformation. This closed model has lower directional deformation than open-top tank model. It is focused that on the half geometry, water level is increased top right side of the tank. It is probability cause of more deformation on shell of tank.



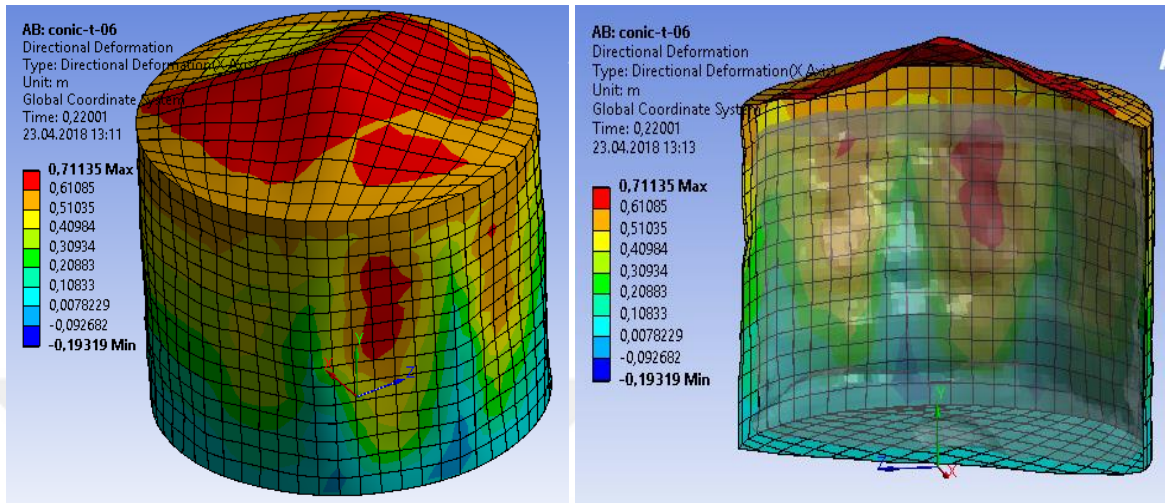
a) Directional deformation of flat-closed



b) Half geometry of flat-closed tank

**Figure 7. 12** Directional deformation of flat-closed tank

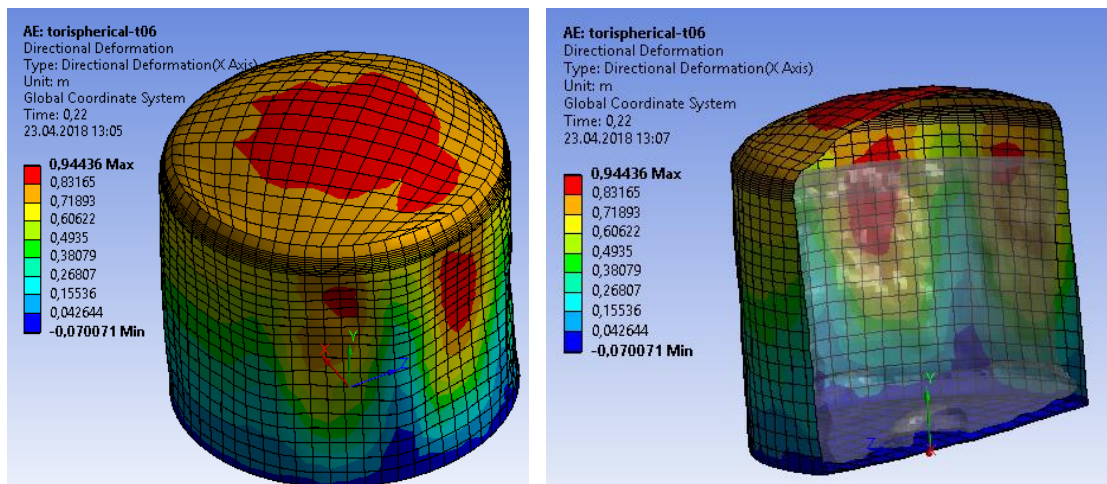
In Figure 7.13, tank is closed a conical shape. Directional deformation is decreased to 0.711 m thanks to conical roof type. In the conical-closed tank, it is understood that the maximum deformation showed better seismic performance compared to the open-top and flat-closed models.



a) Directional deformation of conical-closed b) Half geometry of conical-closed tank

**Figure 7. 13** Directional deformation of conical-closed tank

Figure 7.14 shows the directional deformation on the torispherical tank, maximum deformation is decreased in torispherical-closed tank than open and, flat closed tank models.



a) Directional deformation of torispherical-closed b) Half geometry

**Figure 7. 14** Directional deformation of torispherical-closed tank

An axial deformation graph is shown in Figure 7.15. Plastic deformation started after 0.02 seconds in all models, Maximum deformation is 1.233 m at the 0.12 second in the conical model, while it is 1.15 m in the torispherical-closed model. At 0.22 seconds, the conical and dome model is declining while the open model is 1.192 meters. The recent upswing suggests that the sloshing effect continues in the open-top and flat-closed model.

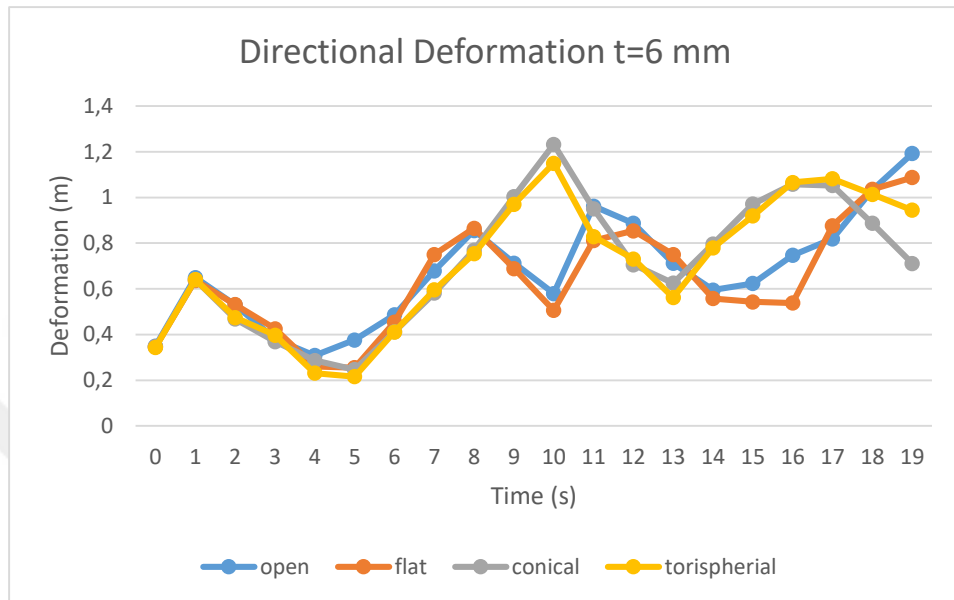


**Figure 7. 15** Directional deformation graphs t=6 mm

#### 7.4.1 Buckling Analysis of Cylindrical Steel Water Tanks

One of the most common causes of buckling in cylindrical steel tanks is the buckling of the upper side of tank due to excessive sloshing. Accordingly, the damage that has taken place and the collapse obtained by Explicit Dynamics analysis are shown in pictures 7.16. The result obtained by the finite element method shows similarities with the actual dent. In addition, there is a diamond-like buckling in the lower regions of the tank.

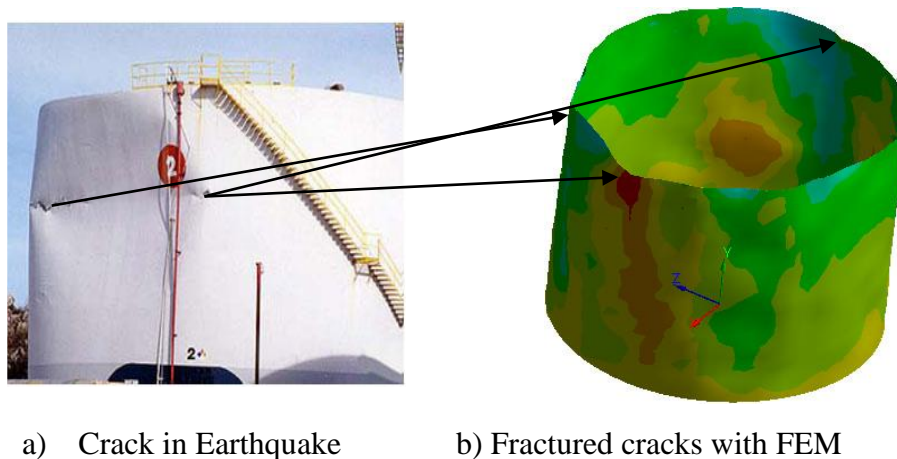
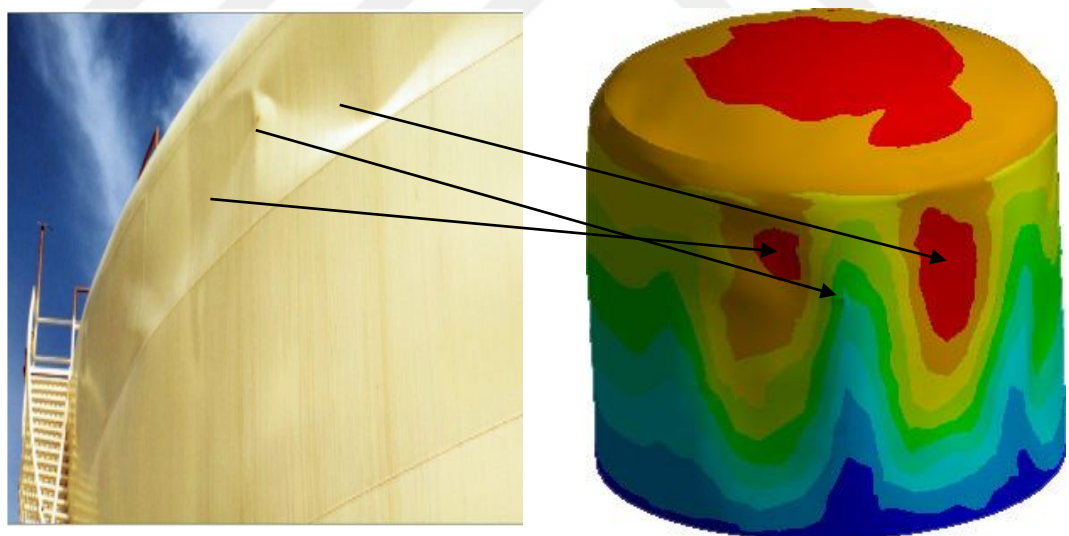


**Figure 7. 16** Buckling of shell tank



Depending on the duration of the earthquake, these buckles may increase further in cylindrical liquid tanks. One of the reasons is that the natural vibration periods of the tanks occur at intervals of 0.1 s – 0.5 s. If the maximum earthquake energy comes in this range, large deformations and cracks may occur in the tanks. To solve this problem, Malhotra, P., developed a seismic isolation method. With the seismic isolation created at the base of the tank, the natural vibration period was extended to remove it from the resonance range (Malhotra, 1997). The seismic isolation method is expensive and difficult to implement in existing construction, so it is not always a practical solution to prefer steel. Çelik and Akgül (2018) have wrapped the top of the open cylindrical steel tank with an epoxy-carbon composite material, reducing the buckles in the interior slightly (Çelik and Akgül, 2018). In this section, the effects on the buckling of the tank lid model are examined.

In the Figure 7.17 shows the true deformation and deformation of FEM results. This deformation shape occurs due to sloshing effect of liquid. In terms of the accuracy of the analysis, the real modelling analogy of the FEM model is an important study. This also indicates that the route is correct and that the model is installed correctly.



a) Crack in Earthquake

b) Fractured cracks with FEM

**Figure 7.17** Cracks in the shell of tanks

In Figure 18(a) is shown buckles of conical-closed tank. If a cylindrical tank is conically closed, buckling may occur only on one side. But there are some buckling due to excessive deformation in the roof. If a cylindrical steel tank is closed in the form of a torispherical dome shape in Figure 18(b), the buckling may also occur only one side of

the axis. As with the conical model in the torispherical model, the deformation is seen to increase in the roof, but in the combination of the roof and the wall there is little buckles.

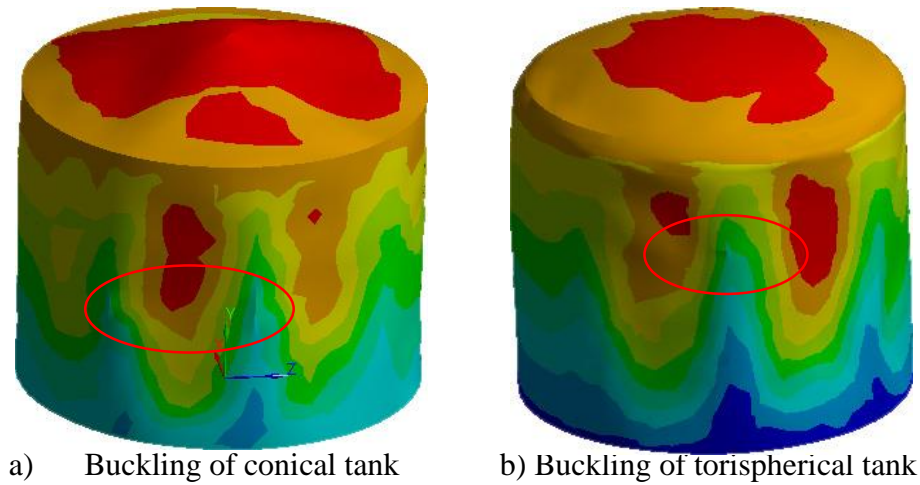
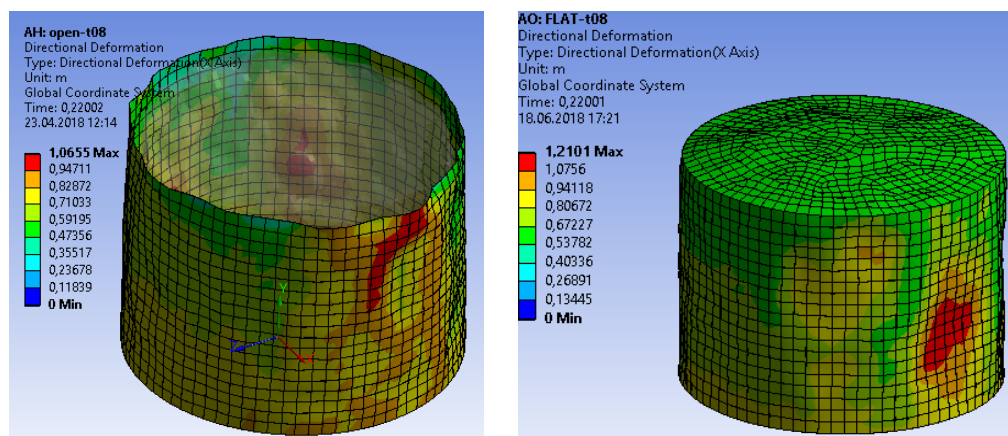


**Figure 7. 18** Buckling of shell tanks

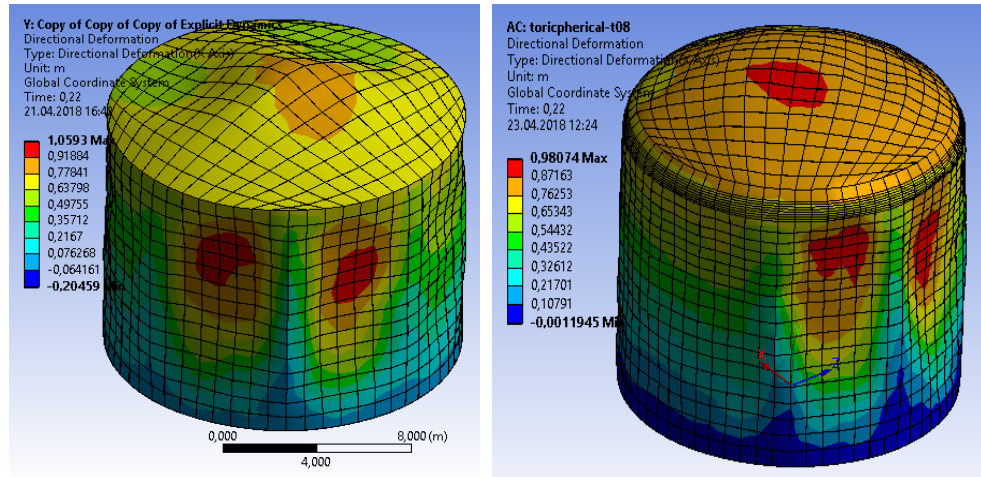
#### 7.4.1.1 Buckling analysis at different thicknesses

Shell thickness which is 6 mm used this study, it is suitable optimum tank wall thickness specified in API 650 standard. All analysis was repeated at 4mm and 8mm shell thickness for open-top, flat-closed, conical-closed and torispherical closed of tank's roof. It is aimed to see the effects on different types of tanks with a thickness of 2 mm below and 2 mm above the standard. In Figure 7.19 are shown directional deformation concern to open-top, flat-closed, conical-closed and torispherical-closed tanks. Maximum deformation occurs 1.0655 m in open-top tank model, while it is 1.059 m in conical-closed model. Torispherical-closed tank has lowest directional deformation with 0.98074 m. The highest directional deformation is 1.22 m in flat-closed tank.



a) Open-top tank

b) Flat-closed tank



a) Conical-closed tank                      d) Torispherical-closed tank  
**Figure 7. 19** Directional deformation of different tanks t=8 mm

Figure 7.20 summarized the directional deformation of at 8 mm shell thickness all tanks. Flat-closed tank demonstration is of interest. Normally, a rise in directional deformation is expected depending on the shell thickness, but maximum directional deformation increased is observed in flat-closed tank. In addition, it is observed that the sloshing effect towards the end of the simulation and the rise in the directional deformation in the flat-closed tank.

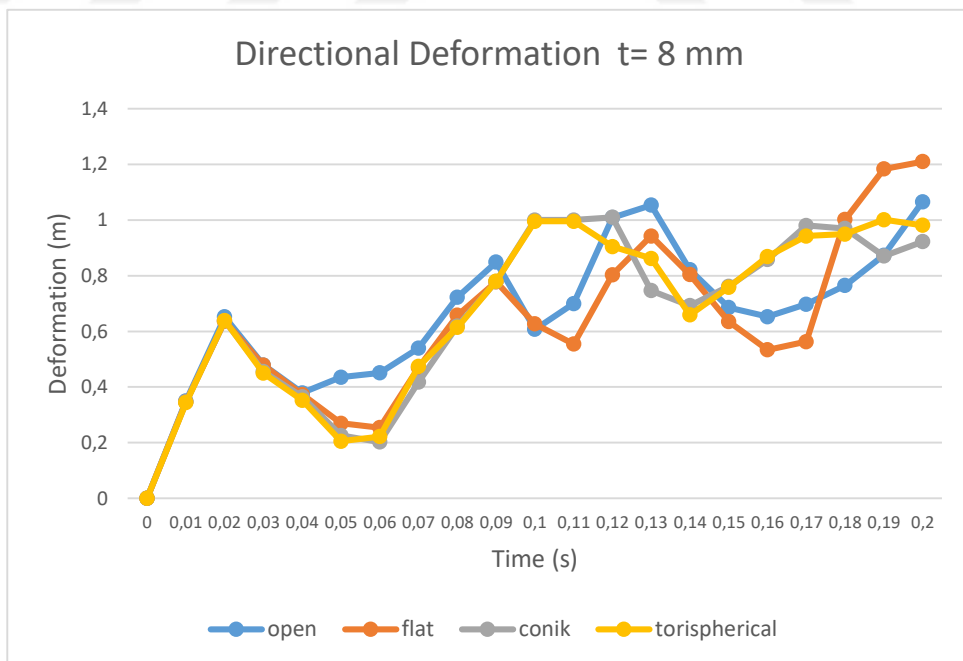
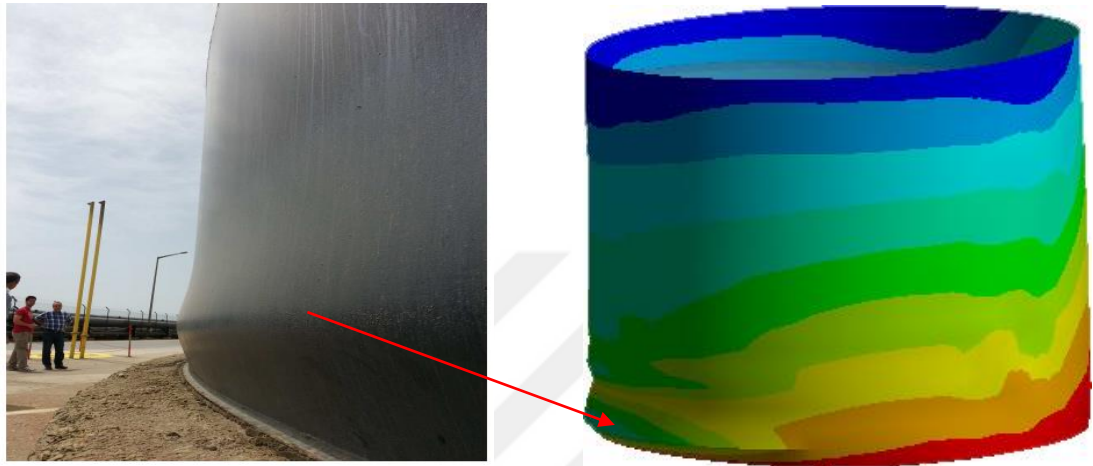


**Figure 7. 20** Directional deformation graphs t=8 mm

One of the most important buckling forms caused by earthquake effect in cylindrical steel tanks is elephant foot buckling. Figure 7.21(a) shows the elephant foot buckling that

formed during the Marmara earthquake of 1999 in TÜPRAŞ refinery. The thickness of the FEM model in Figure 7.21(b) is defined as 4 mm. It is attention that the bottom of the tank, the elephant foot sprain, similar to figure during an earthquake, it may be desirable for a structure to undergo some plastic deformation beyond the elastic shape limits, but important steel tanks used in the storage of flammable materials such as TÜPRAŞ should not be damaged.

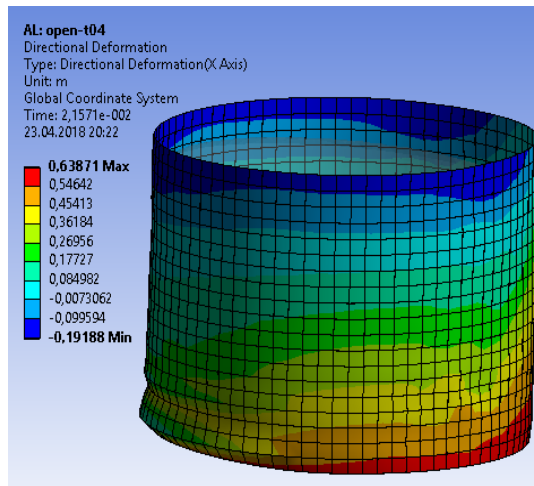


a) Elephant foot buckling in TÜPRAŞ 999 b) Elephant foot buckling FEM model

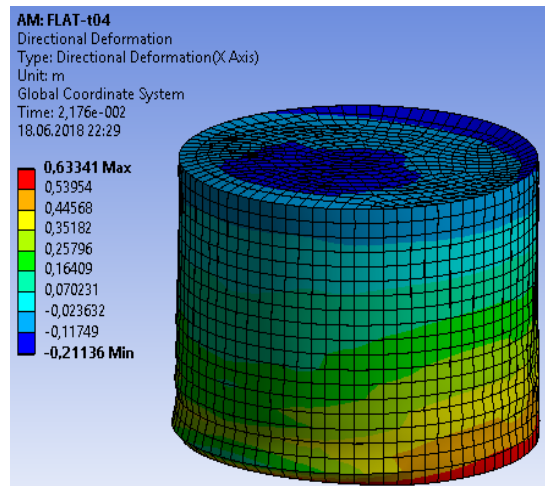
**Figure 7. 21** Occurred of elephant foot buckling

In Figure 7.21, the deformation values are less visible than in the previous models. However, since the wall thickness is low (4 mm.), Hydrostatic liquid pressurization is caused the permanent elephant foot buckling which is the overcome the elastic deformation limits in the bottom of the tank at the beginning of the seismic ground movement. In Figure 7.22, maximum directional deformation occurred in open-top tank model, and also flat-closed tank has a nearest maximum directional deformation. Figure 7.22 shows the maximum directional deformation distributions in all tanks. The maximum deformation occurred at 0.638 m in the open-top tank model, while at the very close value it was 0.633 m deformation in the flat-closed tank. The conical and torispherical-closed tanks have 0.514 m and 0.619 m maximum directional deformation respectively.

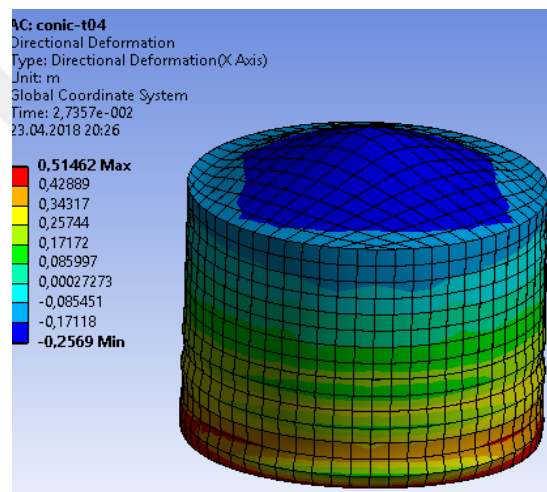




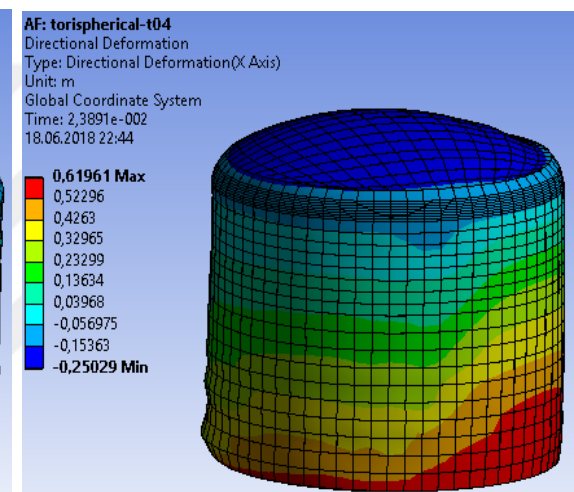
a) Open-top tank



b) Flat-closed tank



b) Conical-closed tank



d) Torispherical-closed tank

**Figure 7. 22** Directional deformation of different tanks  $t=4$  mm

## 7.5 Summary

Impact analysis was performed to see the plastic deformation on the tank. Euler body mesh provides a good interaction between water and shell. Since cylindrical steel water tanks are significant engineering structures, deformations under sudden and destructive forces due to earthquake are undesirable. Seismic analysis of these structures is very complicated due to the dynamic behaviour of the liquid they contain. Due to this complexity and the difficulty of dynamic and seismic analysis of CST is of interest to researchers. Studies previous chapters has been concerned with long-term time-series dynamic behaviour under seismic loading. Natural vibration periods of cylindrical steel

tanks are 0.1 sec. -0.5 sec. Because plastic deformation usually occurs in this short period, the El-Centro earthquake load of 0.22 seconds gave effective results in short time dynamic analyses. When performing analyses, the convective mass is neglected. The Explicit Dynamics finite element analysis revealed deformation and buckling zones on the tank that were not in previous finite element analyses. The most important findings of this study are listed below.

Analysis were carried out in the period of time during which the cylindrical steel tanks were being damaged and near-realistic deformation and buckling shapes were obtained.

In repeated simulations with different wall thickness (4 mm, 6 mm, 8 mm), it was observed that the plastic deformation in all models started after 0.02 seconds.

Deformation in the cylindrical steel water tank is caused by hydrodynamic pressures due to the water due to sudden earthquake movements. The fluctuation caused by the convective water mass from the upper side of the tank causes maximum deformation on the upper side.

Diamond-shaped buckling and elephant-foot buckling, which took place in cylindrical steel tanks, were obtained in a similar way with the finite element model and focused on the reasons for the buckling. 6 mm., the formation of buckles indicates the lack of standards. Also 4 mm. it is the most common type of damage that occurs in the earthquake.

Tanks subject to explosion under extreme earthquake loading by means of Explicit Dynamics analyses may take measures to prevent explosion as a result of analyzes simulated with the release of the liquid they contain.

## CHAPTER 8

### DISCUSSION AND CONCLUSION

#### 8.1 Introduction

The aim of this thesis is to assess the seismic analysis of the cylindrical ground support steel storage water tanks under the earthquake loads of El-Centro and Kobe by using the finite element method. Using this method fluid-structure interaction problem can be considered, including wall flexibility, impact motion and impulsive and convective terms, including FEM method and individual effects on a three-dimensional space. In this chapter, results of seismic analysis, buckling analysis, strengthening of tanks and impact analysis are evaluated. According the finite element method results directional deformation, Equivalent (von-mises) stress in base tank, interaction between liquid and wall with Eulerian body, stress and directional deformation resulting from depend on impact analysis, strengthening of tank with epoxy carbon are briefly discussed.

#### 8.2 Discussion and Conclusion

This thesis is the most extensive seismic analysis of cylindrical steel tanks under the El-Centro and Kobe earthquake loads with four different roof type shapes and 3 different shell thicknesses. In order to clarify the directional deformation to depend on time cylindrical steel open-top, flat-closed, conical-closed and torispherical-closed top a dome shape tank models simulated by 3D ANSYS Workbench. The thickness of the tank used in this study is 6 mm according to the API 650 standard. In addition, analyses were repeated at shell thicknesses of 4 mm and 8 mm in order to be able to see the effect of the wall thickness on the roof shape. The effect of shell thickness on the roof type were investigated of tanks via of the finite element method.

First of all, modal analysis was carried out to determine the natural impulsive and convective vibration modes. Impulsive first mode was 3.23 Hz. and convective first mode

was 0.24 Hz. It also these frequencies values calculated by API 650 formulation and model was verified.

Then linear-dynamic response spectrum analysis was performed to measure the contribution from each natural mode of vibration to indicate the likely maximum seismic response of an essentially elastic structure of tank in chapter 5. In order to observe the directional deformation, Equivalent (von-mises) stress and acceleration depend on time analysis of Transient Structure was performed under the both El-Centro and Kobe earthquake loads in workbench.

In chapter 6, buckling analysis was performed of cylindrical steel water tanks which are under the El-Centro and Kobe earthquake seismic loading. There are many types of buckling in cylindrical steel tanks such as elephant foot buckling, diamond shape buckling and cracks on the top side of tanks due to sloshing effect of liquid. It was focused on the buckling in different shell thickness and different roof types of cylindrical steel tanks. On the other hand, strengthening of existing vulnerable cylindrical steel liquid tanks are performed in this chapter. The tanks were covered with epoxy carbon material using the Workbench ACP tool to reduce deformation.

Impact analysis performed in chapter 7. The Explicit Dynamics expert tool was used to determine the dynamic response of the cylindrical steel tank due to stress wave propagation, impact or rapidly changing time-dependent loads. 0.22 second earthquake load values were used for Explicit Dynamic analysis. When performing analyses, the convective mass is neglected. Since Eulerian body formulation permits formation of large structural and fluid deformations without causing mesh distortion problems, a Eulerian mesh system for structure is combined with an Eulerian (virtual) mesh for fluid domain by merging nodes at the fluid-structure interface.

After all numerical simulations in ANSYS workbench modal analysis, response spectrum analysis depends on modal analysis, seismic analysis and impact analyses are main concluding remarks can be outlined as follows:

### **Results of modal analysis**

Initially, modal analysis was performed with ANSYS workbench for three different water levels for the open model. The impulsive value for the first mode is 3.24 and the

convective value 0.24. These are also validated by calculating API 650 standard formulas. Then the modal analysis was carried out in the enclosed top a shape dome tank model and the first 6 modes were shown in the table 5.8. The values close to each other, indicating that the interaction between shell and water element is correct.

### **Result of Response Spectrum Analysis**

Response-spectrum analysis is a linear-dynamic statistical analysis method which measures the contribution from each natural mode of vibration to indicate the likely maximum seismic response of an essentially elastic structure. The response-spectrum analysis was performed linked modal analysis, the maximum displacement value was  $2.1485 \times 10^{-6}$  m under the El-Centro earthquake and  $6.3523 \times 10^{-10}$  m under the Kobe earthquake loads for impulsive pressure. At same time, the maximum displacement value was  $2.9904 \times 10^{-5}$  m under the El-Centro earthquake and  $6.4452 \times 10^{-8}$  m.under the Kobe earthquake loads for convective pressure.

### **Results of Seismic Transient Structure Analysis**

Time-story analysis is a step-by-step analysis of the dynamic response of a structure to a specific load that may vary with time. First time history analysis using of the north-south component of the 1940 El Centro earthquake which had 6.9 magnitudes (magnitude 7.1 on the Richter scale) was performed. Second analysis was carried out under 1995 Kobe earthquake load which was measured 6.9 (7.3 on Reacher scale). The time history of the tanks was separated into impulsive and convective components in order to perform the time varying response characteristics of the tank models.

The maximum directional deformation occurred in the flat-closed tank and also the most buckling was occurred in flat-closed tank. One of the biggest reasons for this is that the pressure centre changes due to the flatness of roof tank. The deformation calculation was performed via transient structural analysis which was not exceeding the limit of the tank, so that the tank can be safe under the analysis condition.

The significant finding in this chapter is that if the top of the tank is in the shape of a torispherical dome, the deformation is majorly reduced. The flat-closed tank has a maximum directional deformation in both impulsive and convective periods. As a result, the flat-closed roof tank does not provide any advantage in directional deformation, if the

tank is flat-closed, the deformations and buckling will be more likely to occur even if the shell thickness is increased. However, the existing tanks can be prevented from being damaged by being closed in the shape of a torispherical dome so that they are not damaged by directional deformation during the earthquake.

To sum up, the equivalent stress in the unprotected tank is 81.92 MPa, while the maximum environmental stress is reduced to 63.40 MPa after it was coated with the epoxy-carbon in open-top tank. While maximum von-mises stress is occurred 108.23 MPa in cylindrical steel tank, it is decreased to 52.71 MPa in strengthening of tank with epoxy-carbon in flat-closed tank. While maximum stress is 108.03 MPa in the unprotected tank, it is 63.37 MPa in the protected tank with epoxy-carbon material in conical-closed tank. While maximum stress is 107.66 MPa in the unprotected tank, it is 50.036 MPa in the protected tank with epoxy-carbon material in torispherical-closed tank. Depending on the decrease in stress, there have been serious reductions in directional deformation and buckles of the open-top, flat-closed, conical-closed and torispherical-closed tanks respectively.

### **Result of Impact Analysis**

Impact analyses were carried out in the period of time during which the cylindrical steel tanks were being damaged and near-realistic deformation and buckling shapes were obtained.

In repeated simulations with different wall thickness (4 mm, 6 mm, 8 mm), it was observed that the plastic deformation in all models started after 0.02 seconds.

Explicit Dynamic analysis was performed to see the plastic deformation on the tank. Eulerian body mesh provides a good interaction between water and shell. Maximum deformation occurred upper side of tank. The effect of 0.22 seconds an earthquake load for explicit dynamic impact analysis was clearly observed. In repeated simulations with different wall thickness (4 mm, 6 mm, 8 mm), plastic deformation started after the 0.02 second in all models. The maximum deformations were 1.065 m in the open-top tank, 1.059 m in the conical-closed tank and 0.980 m in the torispherical-closed tank respectively. The open tank model shows more buckling than the closed model. Deformation in the roof of the closed models seems to be reduced, but some buckling occurs in both.

Deformation in the cylindrical steel water tank is caused by hydrodynamic pressures due to the water due to sudden earthquake movements. The fluctuation caused by the convective water mass from the upper side of the tank causes maximum deformation on the upper side.

Diamond-shaped buckling and elephant-foot buckling, which took place in cylindrical steel tanks, were obtained in a similar way with the finite element model and focused on the reasons for the buckling. Despite the tank thickness of 6 mm, the formation of buckling indicates the lack of standards. Moreover, the fact that the elephant foot buckle in the 4 mm wall thickness is the most common type of damage coming from the earthquake

Tanks subject to explosion under extreme earthquake loading by means of Explicit Dynamics analysis may take measures to prevent explosion as a result of analyses simulated with the release of the liquid they contain.

## REFERENCES

- Akkas, N. Akay, C. and Yilmaz, H. U. (1979) Applicability of general-purpose finite element program in solid-fluid interaction problems [Journal] // *J of Computers and Structures, Vol. 10, Computers & Structures, 3, - Issue 5, Pages 773-78 : Vol. Volume 10.*
- Altun, H. A. (2013), Sesimic Analysis of Steel Liquid Storage Tanks by API-650” // M.Sc. Thesis, *Department of Civil Engineering, Structural Engineering Programme, Istanbul Technical University, Graduate School of Science Engineering and Technology*
- ANSYS help, ANSYS company, (2018).
- Anumod, A.S. Harinarayanan, S. and Usha, S. (2014), “Finite Element Analysis of Steel Storage Tank Under Siesmic Load, *International Journal of Engineering Research and Applications, Trends and Recent Advances in Civil Engineering, ISSN: 2248-9622. - India 25th, - 47-54.*
- API650, Standards American Petroleum Institute (API) Standard, 650, (2013) Welded steel tanks for oil storage, *12th Ed., American Petroleum Institute, API Publishing Services.*
- Aquelet, N. and Souli, M. (2003) Damping Effect In Fluid-Structure Interaction: Appliction to Slamming Problem [Conference] // *SME 2003 Pressure Vessels and Piping Conference. USA : Copyright © 2003 by ASME, 2003. - Cilt Paper No. PVP2003-1968, pp. 233-242; 10 pages*
- Architectural Institute of Japan Design Recommendation for Storage Tanks and Their Supports with Emphasis on Seismic Design ( 2010), [Report]. Japon.
- Arnold, R. N. D. Sc. and Warburton, G. B. (1949) Flexural vibrations of the walls of thin cylindrical shells having freely supported ends [Journal]//*Downloaded from <http://rspa.royalsocietypublishing.org/> on January 7, 2018.*
- ASCE (2001) American Lifelines Alliance. Seismic fragility formulations for water systems.; [Report], USA.
- Bakalis, K., Vamvatsikos, D. and Fragiadakis, M. (2017) Seismic risk assessment of liquid storage tanks via a nonlinear [Journal] // *Earthquake Engng Struct Dyn.*46, pp. 2851–2868..
- Barton, D.C. and Parker, J.V. (1987) Finite element analysis of the seismic response of anchored and unanchored liquid storage tanks [Journal] // *Earthquake Engineering and Structural Dynamics, 15, 299-322. pp. 299-322..*
- Basler and Hofmann A.G.( 2015) Fluid damping of cylindrical liquid storage tanks [Journal] // DOI: 10.1186/s40064-015-1302-2 *SpringerPlus. Forchstrasse 395, 8032 Zurich, Switzerland*



- Bauer, H. F. (1964) Fluid oscillations in the containers of a space vehicle and their influence upon stability [Report] : *Technical., Washinton : NASA.*
- Bayraktar, A. Sevim, B., Altunürk, A. C. and Türker, T. (2010) Effect of the model updating on the earthquake behavior of steel storage tanks [Journal] // *Journal of Constructional Steel Research.*, pp. 462-468.
- Bonneau, D., Fatu, A. and Souchet, D. (2018) Thermo-hydrodynamic Lubrication in Hydrodynamic Bearings [Online] <https://leseprobe.buch.de/images-adb/46/3b/463b9a4a-b8da-44f7-9db6-38840557283f.pdf>.
- Buratti, N. and Tavano, M. (2014) Dynamic buckling and seismic fragility of anchored steel tanks by the added mass method [Journal] // *Earthq. Eng. Struct. Dyn.* 43 (1). pp. 1–21 .
- Chen, J. Z. and Kianousha, M. R. (2010) Generalized SDOF system for dynamic analysis of concrete rectangular liquid storage tanks // *Canadian Journal of Civil Engineering*, , 37(2): 262-272, <https://doi.org/10.1139/L09-132>, Department of Civil Engineering, Ryerson University, Toronto, ON, M5B 2K3 Canada.
- Cho, K. H., Kim, M. K., Lima, Y. M. and Cho, S. Y. (2004) Seismic response of base-isolated liquid storage tanks considering fluid–structure–soil interaction in time domain [Journal] // *Soil Dynamics and Earthquake Engineering*, Volume 24, Issue 11. pp. 839-852.
- CNG United USA. <http://www.cngschool.com>. tarih yok. [Online]. – 08.01.2018. - <http://www.cngschool.com/cng-tanks>.
- Crate, H., Lo, H. and Schwartz, E.B. (1951) Buckling of thin-walled cylinder under axial compression and internal pressure, [Journal] // *Natl. Advis. Comm. Aeronaut. Tech. Rep.* p. 1027.
- Çelik, A.İ and Akgül, T. (2018) Stress Analysis of Cylindrical Steel Storage Liquid Tanks During the [Conference] // *Proceedings of the 3rd World Congress on Civil, Structural, and Environmental Engineering (CSEE'18)*. - Budapest : CSEE. -Vol. ICSENM 128.
- He, Liu and Daniel Schubert, H. (2001) Effects of nonlinear geometric and material properties on the seismic response of Fluid/Tank system,” American water works association, D100,
- Daniel, I.M. and Ishai, O.S. (1994) Engineering Mechanics of Composite Material. [Book]. - New York: : Oxford University Press.
- Davidson, M. J . N., Priestley, J . H. and Wood, B. J. (1986) Seismic Desing of Storage Water Tanks [Journal] // *Bulletin of The New Zealand National Society For Earthquake Engineering*.
- Djermane, A. and Chikhi, M. (2017) Dynamic Buckling Of Cylindrical Storage Tanks During Earthquake Ex Citations [Journal] // *Asian Journal Of Civil Engineering (Bhrc)* Vol.18, No. 4. pp. 607-620.
- Douglas, S. C. and Lysle, A. (2009) [Online]. 01.11.2018.Wood Distinguished Professor <http://www.montana.edu/dcairns/documents/composites/MSUComposites2009.pdf>.

- Edwards N. A (1969) Procedure for the dynamic analysis of thin walled cylindrical liquid // *Ph.D. Thesis, University of Michigan, Ann Arbor, Michigan.*
- Eurocode 8, Design of Structures for Earthquake Resistance (2006), Part 4-Silos, Tanks and Pipelines. *European Committee for Standardization, Brussels, BS EN 1998-4.*
- Flügge, W. (1960) Stress in shells [Journal] // *Springer-Verlag Berlin.*
- Forsberg, K. (1966) A Review of analytical methods used to determine the modal characteristics of cylindrical shells [Report] : *Thechnical. - Washinton : NASA CR-613.*
- Galilei, G. (1948) Fundamantals of Vibration [Book]. - *New York : Dover publications.*
- Gemite, «<http://gemite.com>.» (2013). [Online]. - 08 01, 2018. - [http://gemite.com/wp-content/uploads/2013/04/Carbon\\_Structural\\_Strengthening.pdf](http://gemite.com/wp-content/uploads/2013/04/Carbon_Structural_Strengthening.pdf).
- Ghazvini, T., Hamid, R., Bahram, T., Navayi, N. and Sarokolay, L. K.(2013) Seismic response of aboveground steel storage tanks: comparative study of analyses by six and three correlated earthquake components [Journal] // *Latin American Journal of Solids and Structures.* pp. 1155-1176.
- Godoy, L.A. (2016) Buckling of vertical oil storage steel tanks: review of static buckling studies [Journal] // *Thin-Walled Struct.* 103. pp. 1–21.
- Hamdan, F.H. (2000) Seismic behaviour of cylindrical steel liquid storage tanks, [Journal] // *J. Constr. Steel Res.* 53 (3) *New York : Oxford University Press.*, pp. 307–333.
- Haroun, M. A. and Housner, G. W. (1981a) Earthquake Response of Deformable Liquid Storage Tanks [Journal] // *Journal of Applied Mechanics ASME*, Vol. 48, pp. 411-418.
- Haroun, M. A. and Housner, G. W. (1981b) Seismic Design of Liquid Storage Tanks [Journal] // *Journal of the Technical Councils of ASCE.*
- Haroun, M. A. and Housner, G. W. (1982) Complications in Free Vibration Analysis of Tanks [Journal] // *Journal of Engineering Mechnics* , ASCE, Vol. 108,. pp. 801-818.
- Haroun, M. A. and Tayel, M. A. (1985) Axisymmetrical Vibrations of Tanks-Numerical [Journal] // *Journal of Engineering Mechanics, ASCE*, Vol. 111, No. 3. pp. 329-345.
- Haroun, M. A. ( 1983) Behavior of Unanc hored Oil Storage Tanks: Imperial Valley Earthquake [Journal] // *Journal of Technical Topics in Civil Engineering*, Vol. 109. pp. 23-40.
- Haroun, M. A. (2007) Vibration studies and tests of liquid storage tanks [Journal] // Version of Record online: DOI: 10.1002/eqe.4290110204 *Earthquake Engineering & Structural Dynamics Volume 11, Issue 2.* - pp. 179–206, March/April 198.
- Héctor, C. S. and Carlos, S. S. (2008) Seismic Response of Cylindrical Storage Tanks For Oil [Conference] // *The 14th World Conference on Earthquake Engineering.* - Beijing, China
- Hosseini, M. and Mehdi, M. (2000) Effects of Foundation Geometry on the Natural Periods of Cylindrical Tank-Liquid-Soil Systems [Journal] // *JSEE: Fall* , Vol. 2, No. 4 / 43.

- Hosseinzadeh, N., Kazem, H. and Ghahremannejad, M. (2013) Comparison of API650-2008 provisions with FEM analyses for seismic assessment of existing steel oil storage tanks [Journal] // *Journal of Loss Prevention in the Process Industries* 26 666e675.
- Housner, G.W.( 1957) Dynamic pressures on accelerated fluid containers, [Journal] // *Bull. Seismol. Soc. Am Elsevier ltd. no. 685,.* - pp. 47 (1) 15–35..
- Housner, G.W.( 1955) Dynamic Prssure on Accelerated Fluid Containers [Report] : *Thechnic. - California : California Institue,.*
- Housner, G.W.( 1954) Earthquake Pressure With Fluid Containers [Report] : *Thecknic. - California : California Instuty of Thechonogy,.*
- Housner, G. W. (1963)The Dynamic Behaviour of Water Tank [Journal] // *Bulletin of the Seismological Society of America. Vol. 53, No. 2,.* - pp. pp. 381-387..
- Huddon, D. V. (2004) Fundamantals of Finite Element Analysis [Book]. - *USA : Higher Education,.*
- Hunt, B. and Priestley, N. (1978) Seismic water waves in a storage tank [Journal] // *Bulletin of the Seismological Society of America, 68(2).* - - p. 487.
- Jacobsen, L. S. (1949), "Impulsive Hydrodynamics of Fluid Inside a Cylindrical Tank and of a Fluid Surrounding a Cylindrical Pier," *Bull. Seism. Soc. Am., Vol. 39.*
- Jacobsen, Lydik S. and Ayre, Robert S. (1951) Hydrodynamic experiments with rigid cylindrical tanks subjected to transient motions [Journal] // *Bulletin of the Seismological Society of America. pp. 313-346.*
- Jaiswal, O. R., Durgesh, C. R., Eeri, M. and Sudhir, K. J. (2007) Review of Seismic Codes on Liquid Containing Tanks [Journal] // *Earthquake Spectra, Volume 23, No. 1, Earthquake Engineering Research Institute. pp. 239–260,.*
- Joseph, W. Tedesco and Kostem, Celal N. (1982) Vibrational Characteristics and Seismic Analysis of cylindrical Liquid Storage Tanks // *Report. -Pennsylvania : Fritz Engineering Laboratory, Department of Civil Engineering Lehigh University . Bethlehem.*
- Karim, A. A. (2008) Vibration Analysis Of Circular Cylindrical Liquid Storage Tanks Using Finite Element Technique // PhD Thesis. - Basrah : *The College Of Engineering Of The University Of Basrah In Partial Fulfillment of The Requirements For The Degreeof Doctor of Philosophy in Structural Engineering.*
- Kianoush, M.R., Mirzabozorg, H., and Ghaemian, M. (2006) Dynamic analysis of rectangular liquid containers in three-dimensional space [Journal] // *Canadian Journal of Civil Engineering. pp. 33, 501- 507.*
- Kim, N.S. and Lee, D.G. (1995) PseudDynamic Test for Evaluation of Earthquake Performance of Base Isolated Liquid Storage Tanks [Journal] // *Engineering Structures, 17(3).*pp. 198-208.
- Kuan, S. Y. (2009) Design Construction and Operation of the Floating Roof Tank // Course ENG 4111 and ENG 4112 Research Project towards the degree of Bachelor of Engineering (Mechanical Engineering). *University of Southern Queensland Faculty of Engineering and Surveying.*

- Lysmer, J., Ostadan, F., Tabatabaie, M., Tajirian, F. and Vahdani, S. (1999) A System for Analysis of Soil-Structure Interaction (SASSI2000)– User’s and Theoretical Manual [Report] : *Thechnic. - California : Department of Civil and Environmental Engineering, University of California.*
- Malhotra, K. P. (1997) Method for Seismic Base Isolation of Liquid Storage Tanks [Journal] // *Journal of Structural Engineering*, pp. 1,2.
- Manuel, G. and Akash, R. (2015)Effect of Flexible Wall Boundary in Seismic Design of Liquid Storage Tanks with Fluid Structure Interaction [Journal] // *International Journal of Engineering Research & Technology (IJERT)* ISSN: 2278-0181 Vol. 4 Issue 12, pp. 1,2.
- Marchaj, T. J. (1979) Importance of Vertical Acceleration in the Design of Liquid Containing Tanks [Journal] // *Proceedings of the Second U.S. National Conference on Earthquake Engineering Stanford, California.* August. pp. 146-155..
- Mark Baker, P.E. (2009) The Basics of API 650 [Conference] // *2009 Aboveground Storage Tank Management Conference and Trade Show.* Houston,Texas : Eleventh Edition,.
- Mehran, S. R. and Mohebbi, A. (2011) Predicting the Seismic Performance of Cylindrical Steel Tanks Using Artificial Neural Networks (ANN) [Journal] // *Acta Polytechnica Hungarica* Vol. 8, No. 2.
- Michell, R.S. and Wozniak, W. W. (1978) Basic of Seismic Design Provisions For Welded Steel Oil Storage Tank [Conference] // *MedYear Meting. - Toronto Canada : Iron company oak break,IL., -* pp. 1,2.
- Mirzabozorg, H., Khaloo, A.R. and Ghaemian, M. (2003) Staggered solution scheme for three dimensional analysis of dam reservoir interaction [Journal] // *Dam Engineering*, 14(3). pp. 147-179.
- Mohsen, M. and Ali, A. (2015) General considerations in the seismic analysis of steel storage tanks [Journal] // *Journal of Scientific Research and Development* 2 (6): pp. 151-156.
- Morris, T. B. (1938) A laboratory model study of the behavior of liquid filled cylindrical tanks in earthquakes // *Thesis, Stanford University.*
- Moslemi, M. (2005) Seismic Response of Ground Cylindrical and Elevated Conical Reinforced Concrete Tanks // *PhD Thesis. - Tehran, Iran, : Master of Applied Science.*
- Nakashima, M. and Naito, Y. (2010) Design Recommendation for Storage Tanks and Their Supports with Emphasis on Seismic Design [Report]. *Japan : Architectural Institute of Japan.*
- Nakayama, T. and Tanaka, H. A. (1991) Numerical Method for the Analysis of Nonlinear Sloshing in Circular Cylindrical Containers [Journal] // *L. Morino et al. (eds.), Boundary Integral Methods, Springer-Verlag Berlin, Heidelberg.* pp. 1,2,3.
- Nicolici, S. and Bilegan, R.M. (2013) Fluid structure interaction modeling of liquid sloshing phenomena in flexible tanks [Journal] // *Nuclear Engineering and Design* Volume 258,. pp. 51-56.

Niwa, A. and Clough, R.W. (1982) Buckling of cylindrical liquid-storage tanks under earthquake loading. [Journal] // *Earthq Struct Dyn*. pp. 10:107–22.

Ondrej, K. and Jessica, N. (2014) [Online] 01.11.2018. <https://wiki.csiamerica.com/display/kb/Response-spectrum+analysis>.

Özdemir, Zuhul(2010) Interaction Fluide Structure et Analyse sismique pour les déformations non linéaires de réservoirs // *PhD Thesis. Université des Sciences et Technologies de Lille*.

Balendra, T., Ang, K.K., Paramasivam, P. and Lee, S.L. (1981) Free vibration analysis of cylindrical liquid storage tanks, [Journal] // *Department of Civil Engineering, National University of Singapore*.

Prasad, K. J. and Prasad, C.S. (2017) Seismic Analysis And Design of Strengthening Techniques of Steel Storage Tank [Journal] // *International Journal of Advance Engineering and Research Development*, Volume 4, Issue 5, e-ISSN: 2348 - 4470, print-ISSN: 2348-6406. pp. 319-327.

Quizlet <https://quizlet.com> [Online]. 01.11.2018. - <https://quizlet.com/110694842/ch-9-flash-cards>.

SASIP inc. [Online] (01.11.2018) [https://www.sharcnet.ca/Software/Ansys/17.0/en-us/help/exd\\_ag/exp\\_dyn\\_theory\\_expl\\_flui\\_struct\\_582.html](https://www.sharcnet.ca/Software/Ansys/17.0/en-us/help/exd_ag/exp_dyn_theory_expl_flui_struct_582.html).

Scharf, K. (1990) Beiträge zur Erfassung des Verhaltens von erdbebenerregten, oberirdischen Tankbauwerken [Journal] // *Fortschritt-Berichte VDI, Reihe 4, Bauingenieurwesen*, Nr. 97, VDI, Verlag, Düsseldorf. .

Shaaban, S. H. and Nash, W.A. (1975) Finite Element Analysis of a Seismically Excited [Report]. - *Washington : Report, University of Massachusetts, Amherst*.

Sudhir, K. J. and Kanpur, IIT. ( 2006) E-Course on Seismic Design of Tanks/ January [Online] // <https://tr.scribd.com/doc/52085620/IS-1893-Tanks-Water-Retaining>. - *Tanks Water Retaining*. 01 11, 2018. - <https://tr.scribd.com/doc/52085620/IS-1893-Tanks-Water-Retaining>.

Sunitha, K. R. and Jacob, B. (2015) Dynamci Buckling of Steel Water Tank Under Seismic Loading [Journal] // *International Journal of Civil Engineering*. pp. 81-90.

Tosaka, N., Sugino, R. and Kawabata, H. (1990) Boundary Element-Lagrangian Solution Method [Journal] // *Boundary Element Methods in Engineering*. pp. 1,2.

Veletos, A.S. and Ahkok Kumar (1977) Dynamic Response of Vertical Excited Liquid Storage Tanks [Journal]. p. 101.

Veletos, A.S. (1977) Seismic Effect in Flexible Liquid Storage Tanks [Journal] // *Civil Engineering Rice University*.

Vasiliev, V. and Morozov, E. (2018) Composite materials and structure materials. [Book].

Veletsos, A.S. and Tang, Y. (1987) Roc king Response of Liquid Storage Tanks [Journal] // *Journal of Engineering Mechanics* ol. 113, No. 11. - November,. pp. 1774-1792.

Veletsos, A.S., and Tang, Y. (1990) Soil-structure interaction effects for laterally excited liquid storage tanks [Journal] // *Journal of Earthquake Engineering and Structural Dynamics*, Vol. 19, No. 4. pp. 473-496.

Víctor, F. C., Héctor, A., Sánchez, S., María, J., Pérez de la, C. and Carlos, C. S. (2009) Mechanical Behaviour of The Storage Water Tanks [Conference] // *7th EUROMECH Solid Mechanics Conference J. Ambrósio et.al. (eds.). - Lisbon, Portugal*

Virella, J. C., Godoy, L. A. and Soares, L. E. (2006a) Fundamental modes of tank-liquid systems under horizontal motions [Journal] // *J Engineering Structures*. Volume 28, Issue 10, Pages 1450-1461

Virella J.C., Godoy, L.A. and Suárez, L.E. (2006b) Dynamic buckling of anchored steel tanks subjected to horizontal earthquake excitation, [Journal] // *J. Constr. Steel Res.* 62 (6). pp. 521

Wakui, H. and Matsumoto, N. (1997) <http://www.jsce.or.jp> [Online]. – 08.01.2018. [http://www.jsce.or.jp/kokusai/civil\\_engineering/1997/Seismic\\_Strengthening/97jsce8.html](http://www.jsce.or.jp/kokusai/civil_engineering/1997/Seismic_Strengthening/97jsce8.html).

Warburton, G.B. (1976) *The Dynamical Behaviour of Structures* [Book]. Pergamon Press, 2nd edition.

Watkins, Cl. and Robert, R. (1965) *Vibrational Characteristics of Some Thin Walled* [Report]. - Washinton : NASA.

Xu, Costantino, J., Hofmayer, C.C. and Graves, H. (2006) Finite Element Models for Computing Seismic Induced Soil Pressures on Deeply Embedded Nuclear Power Plant Structures [Conference] // *ASME Pressure Vessels and Piping Division Conference*. - Vancouver : BNL-NUREG-76748-2006-CP R&D Project: JCN Y-6718; 56015113107; TRN: US0604280, USA

Xu, Costantino, J., Hofmayer, C.C. and Graves, H. (2007) Overview on BNL Assessment of Seismic Analysis Methods for Deeply Embedded NPP Structures [Conference] // *19th International Conference on Structural Mechanics In Reactor Technology (SMiRT 19)* Toronto

Yazdanian, M., Razavi S.V. and Mashal, M. (2016) Study on the dynamic behavior of cylindrical steel liquid storage tanks using finite element method [Journal] // *Journal of Theoretical and Applied Vibration and Acoustics* 2(2) 145-166.

Yoshio, O. and Nobuyuki K. (1977) Sloshing Experiment of a Cylindrical Storage Tank, [Journal] // *Ishikawajima-Harima Engineering Review*, Vol.17, :o. 6. pp. 607-615.

Zeiny Al. (2003) Factor Effecting The Nonlinear Seismic Response of Unanchored Tanks [Conference] // *16th ASCE Engineering Mechanic Conferance*. - Washinton : ASCE .

## CURRICULUM VITAE

### PERSONAL INFORMATION

Name and Surname: Ali İhsan ÇELİK  
Nationality: Republic of Turkey  
Birth place and date: 06.06.1972  
Phone number: +90 533 221 76 35  
Email: acelik@adiyaman.edu.tr

### EDUCATION

	<b>Graduate school</b>	<b>Year</b>
Ph.D.	Hasan Kalyoncu University	2018
Master	Gaziantep University	2012
Bachelor	Gazi University	1996

### WORK EXPERIENCE

	<b>Place</b>	<b>Enrollment</b>
2006-Present	Adiyaman University	Lecturer
1998-2006	Gaziantep University	Lecturer

### PUBLICATIONS

#### Articles:

Çelik A., İ., Akgül, T., Celal A., A., (2018). Plastic Deformation of Cylindrical Steel Tank both under the Kocaeli and El-Centro Earthquake, International Journal of Advance Engineering and Research Development, Volume 5, Issue 9, DOI:10.21090/IJAERD.14654, pp 27-35, September -2018

Çelik A., İ., Akgül, T., Celal A., A., Yurtsever, A., (2018) Sismik Yükleme Altında Silindirik Çelik Su Tanklarının Gerilme ve Burkulma Analizi, Sürdürülebilir Mühendislik Uygulamaları ve Teknolojik Gelişmeler Dergisi, Cilt 1 - Sayı 2 - Aralık 2018

#### Proceedings:

Çelik A., İ., Akgül, T., (2018). Stress Analysis of Cylindrical Steel Storage Liquid Tanks During the Instantaneous Loads, Proceedings of the 3rd World Congress on Civil, Structural, and Environmental Engineering (CSEE'18) Budapest, Hungary – April 8 - 10, 2018 Paper No. ICSENM 128 DOI: 10.11159/icsenm18.128

**Çelik A., İ., Akgül, T., Celal A., A., Yurtsever, A.,** (May 2018). Silindirik Çelik Su Tanklarının Sismik Analizinin Fem İle Gerçekleştirilmesi, 2nd International Symposium on Natural Hazards and Disaster Management, Sakarya University Culture and Congress Center, Sakarya - Turkey 04-06 May 2018

